A Mechanistic Understanding of Agglomeration in Agitated Filter Dryers Across Scales

By

Suruthi Gnanenthiran

A thesis submitted in partial fulfilment of the requirements for the degree of

DOCTOR OF PHILOSOPHY

The University of Sheffield

Faculty of Engineering

School of Chemical, Materials and Biological Engineering

September 2025

Declaration

I, the author, confirm that the Thesis is my own work. I am aware of the University's Guidance on the Use of Unfair Means (www.sheffield.ac.uk/ssid/unfair-means). This work has not previously been presented for an award at this, or any other, university.

Suruthi Gnanenthiran

List of Outputs

Publications

S. Gnanenthiran, C. Hewitt, P. Rao, K. Pitt, J. Litster and R. Smith, Undesired agglomeration in agitated filter dryers: A critical review, *Powder Technology* (2025), https://doi.org/10.1016/J.POWTEC.2025.121425.

Oral Presentations

11th International Granulation Conference	Hamburg University of Technology, June 2025
CMAC Open Days	University of Strathclyde, March 2025 and November 2023
10th Winter Process Chemistry Conference	Birmingham, December 2024
AstraZeneca CASE Symposium	AstraZeneca Cambridge, September 2024
AstraZeneca Pharm Sci/PT&D PhD Review Day	AstraZeneca Macclesfield, April 2024

Poster Presentations

ChemEngDayUK	University of Sheffield, April 2025
CMAC Open Days	University of Strathclyde, March 2025, November 2023 and March 2022
10th Winter Process Chemistry Conference	Birmingham, December 2024
Advances in Particle Technology	University of Sheffield, September 2024
CMAC Summer School	Dunblane, June 2024 and June 2023 and Crieff, June 2022
AstraZeneca Pharm Sci/PT&D PhD Review Day	AstraZeneca Macclesfield, April 2024
STEM for Britain	Houses of Parliament, March 2024
CBE Summer PGR Conference	University of Sheffield, June 2023
10th International Granulation Conference	Sheffield, June 2023

Dedicated to my அம்மா and அப்பா

Acknowledgements

I would like to thank my academic supervisors, Professor Rachel Smith and Professor Jim Litster, for giving me the opportunity to do this PhD and for their support throughout. Thank you, Rachel, for always challenging me to become a better researcher as well as giving me the opportunity to travel during my PhD. I am very grateful for the amazing experiences I have had during my PhD journey.

To my industrial supervisors from AstraZeneca, Christopher Hewitt and Pari Rao - thank you both for your continuous encouragement and advice throughout my PhD, and all the approvals you had to deal with every time I had to present! My placement would not have been nearly as productive or enjoyable without both your efforts. As we always say, teamwork makes the dream work!

My placement experience at AstraZeneca was truly special thanks to the incredible support and kindness of several individuals, to whom I am deeply grateful. Aatika, thank you for being my buddy and showing me the ropes when I started, and for your friendship throughout. Raquel, you were a brilliant manager, and I truly enjoyed my time in your team. I would also like to thank the Particle Engineering team, who welcomed me so warmly and taught me so much in just a few weeks. Special thanks go to Billy Hicks, Petros Neoptolemou, Amy Robertson, Helen Wheatcroft, Dean Murphy and Helen Blade for going above and beyond to help me get the most out of my placement - even when things were busy!

To Kate Pitt, thank you for always being there to lend a helping hand, even when you had a lot on your plate, and for always reminding me to just laugh about it all. I cannot express in words how grateful I am for your kindness and unwavering faith in me, even when I struggled to believe in myself. This PhD would not have been possible without you. I will always cherish our memories of laughing about filtration terminology, Charles Dickens quizzes on the radio and so much more.

To members of the Particle Technology group (both past and present), thank you for all the good times we have shared and the amazing support throughout the years. I never realised just how healing a few hours after work at the pub could be! Although there are too many names to mention here, I truly appreciate having had such great team members. I would also like to thank others outside the research group for their support, with a special mention for Mario Dorna from the workshop team. Mario, thank you for making my dream come true. Working together to get the agitated filter dryer up and running was more fun than I imagined, and I really appreciated all of our catch ups over coffee along the way.

My friends, although scattered across the globe, never fail to make me laugh or feel supported. Thank you for always providing a welcome distraction from my PhD and all the chaos that came with it. To those who met me for overdue catch ups when I came home to run away from Sheffield, thank you for keeping me sane! To James, Joe and Meg, thank you for making Sheffield feel like home. I cannot thank you three enough for all the meals, games nights and catch ups over the past four years and I feel

truly lucky to have such a supportive circle around me. I look forward to the inevitable evening of blind karaoke in the future.

My deepest gratitude, of course, goes to my family, who have never let me go a day without feeling their love and support. To my brother, Abishaik, I could not be more grateful to have such a supportive and caring brother. To my beloved parents, அம்மா and அப்பா, words are not enough to capture the depth of my gratitude for the countless sacrifices you have made. You were both forced to start from scratch in a new country and gave up your own dreams so that I could have the chance to chase mine. Thank you for supporting me throughout my many, *many* years of education. This achievement is as much yours as it is mine, and I dedicate it to you both with all my heart. I love you.

Above all, I thank God for giving me the strength to keep going and for supporting me throughout this journey.

Abstract

Agitated filter dryers (AFDs) are commonly used in many industries, however the mechanisms driving undesired agglomeration remain poorly understood. Undesired agglomeration can have several consequences including out of specification product, additional downstream processing and increased cycle times and cost.

This thesis proposes a novel mechanism consisting of three rate processes governing agglomeration during agitated drying: the formation of loosely bound agglomerates, consolidation and coalescence, and solidification of liquid bridges.

The influence of key material and process parameters such as agitation speed, agitation time, moisture content, temperature and fill level on the extent of agglomeration in an AFD were investigated. Higher agitation speeds resulted in a dynamic equilibrium between agglomerate growth and breakage. At lower speeds, breakage dominated behaviour shifted to agglomeration dominated over time. Moisture content played a critical role, with significant agglomeration observed even at low moisture contents. Increased fill levels promoted agglomeration due to reduced mixing efficiency, though this could be offset by using higher agitation speeds.

Different agglomerate growth dynamics of salicylic acid were identified by modifying primary particle size. The resulting agglomerate growth and breakage dynamics were categorised using a regime map, where agglomerate growth is described as a function of maximum pore saturation and Stokes deformation number. This is the first regime map of its kind developed specifically to describe agglomerate growth and breakage dynamics observed in an AFD.

The scale up of agglomeration behaviour using constant tip speed was investigated. In a larger AFD, scaling with constant tip speed while maintaining the geometric similarity captured agglomeration dynamics qualitatively but not quantitatively, likely due to the different shear profile in a larger AFD. Agglomeration dynamics observed in the conical dryer varied considerably, which was expected due to the very different mixing dynamics.

Overall, this work provides a mechanistic framework for understanding undesired agglomeration in AFDs.

Table of Contents

List of Figures

List of Tables

Nomenclature

D	Impeller diameter	[m]
d_{10}	Particle size below which 10 % of the material is contained	[m]
$d_{3,2}$	Surface area mean diameter	[m]
$d_{4,3}$	Volume moment mean diameter	[m]
d_{50}	Median particle size	[m]
d_{90}	Particle size below which 90 % of the material is contained	[m]
ε_{min}	Minimum porosity of formulation	[-]
m	Mass	[kg]
N	Stirrer speed	[min^{-1}]
ρ_{bulk}	Bulk density of wet granular material	[kgm^{-3}]
ρ_g	Granule density	[kgm^{-3}]
ρ_l	Liquid density	[kgm^{-3} or g/ml]
ρ_s	Density of solid particles	[kgm^{-3}]
s_{max}	Maximum pore saturation	[-]
St_{def}	Stokes deformation number	[-]
St^*	Critical Stokes number	[-]
τ	Torque	[Nm]
U_c	Representative collision velocity	[ms^{-1}]
μ	Viscosity of powder bed	[Pa.s]
V	Volume	[m^3]
w	Mass ratio of liquid to solid	[-]
Y_g	Dynamic yield stress	[Pa]

Abbreviations

ABI	Agglomerate Brittleness Index
AgD	Agglomeration Degree
AFD	Agitated Filter Dryer
API	Active Pharmaceutical Ingredient
ASD	Agglomerate Size Distribution
BFDH	Bravais-Friedel-Donnay-Harker
$CaCO_3$	Calcium Carbonate
CMC	Critical Moisture Content
CT	Computed Tomography
DEM	Discrete Element Method
FBD	Fluidised Bed Dryer
FIM	Full Interaction Map
LOD	Loss On Drying
MC	Moisture Content
MTR	Mixer Torque Rheometer
$NaHCO_3$	Sodium Hydrogencarbonate
PSD	Particle Size Distribution
PXRD	Powder X-Ray Diffraction
SEM	Scanning Electron Microscopy

Chapter 1 - Introduction

The manufacturing of active pharmaceutical ingredients (APIs) is a lengthy process with many downstream processing steps involved after crystallisation such as filtration, washing and drying (Figure 1.1). It is important to streamline these steps to avoid altering the API properties achieved during crystallisation. Drying is typically the last step in the manufacturing process and is required to lower the solvent content to acceptable levels but is often a bottleneck in the overall manufacturing process.[1]

To improve the efficiency of drying, agitated filter dryers (AFDs) are commonly used, and non-agitated drying is typically no longer used for large scale manufacture.[2] This is because AFDs have several advantages compared to non-agitated dryers such as improved drying rates and improved homogeneity in the powder bed. In contrast, non-agitated dryers such as tray dryers can lead to tray sized agglomerates that require further delumping and milling. However, these advantages need to be weighed against an increased potential for undesired agglomeration of primary particles during the drying stage. The formation of agglomerates and the resulting impact of final product properties are a common problem in many industries.[3]

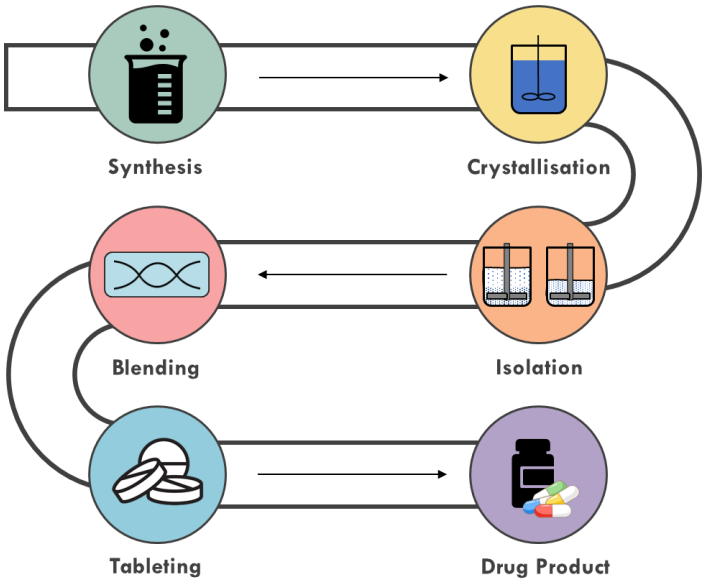

Figure 1.1: Typical pharmaceutical manufacturing process.

Filtration and drying can be carried out in separate units such as centrifuges for filtration followed by drying in dedicated equipment. However, AFDs can be used as an integrated solution, particularly in pharmaceutical manufacturing, allowing for filtration and drying within a single item of equipment. This integration eliminates the need for multiple handling steps, reducing product loss, and minimises the required floor space, resulting in a smaller physical footprint and reduced capital investment while also minimising contamination and protecting employees through improved containment.[4] Despite their widespread use, there remains a limited mechanistic understanding of the agglomeration processes occurring within AFDs which can impact final product properties.

Filter dryers are typically equipped with an agitator which can increase the efficiency of filtration, cake washing and drying by improving mass and heat transfer and enabling more homogeneous mixing. The agitator can be heated to allow particles to be periodically exposed to heated surfaces which further increases the rate of heat transfer and shortens drying times.[5] AFDs are commonly used in the pharmaceutical industry as they can operate under low pressure or vacuum conditions. Many APIs are heat sensitive and prone to degradation at high temperatures. While operating at lower temperatures typically results in prolonged drying times, working at low pressures allows for high levels of heat and mass transfer to be maintained at these temperatures.

Ideally, the API should be dried without altering the physical properties imparted during crystallisation to ensure better control and suitability for downstream formulation. However, intense agitation and rapid moisture loss can cause particle agglomeration, attrition, or other modifications that impact drug performance. Undesired agglomeration can lead to out of specification products due to deviations in particle size, appearance or residual solvent content, and may require further milling. It can also lead to difficulties in batch removal from equipment, longer cycle times and, in extreme cases, damage to the equipment due to the formation of hard agglomerates.[6]

Despite the need to control agglomeration in AFDs, existing research predominantly focuses on the influence of specific process parameters rather than identifying the underlying rate processes. As a result, current approaches for mitigating undesired agglomeration rely heavily on empirical knowledge and trial and error. The lack of a mechanistic framework to describe the processes driving undesired agglomeration has limited the development of predictive tools.

1.1 Research Objectives

The aim of this thesis is to develop a mechanistic understanding of the agglomeration occurring in AFDs. To achieve this, the following research objectives were identified:

- Propose a mechanism accounting for the rate processes that govern undesired agglomeration in AFDs.
- Design and conduct experiments to gain mechanistic insight into the effect of agitation input on resulting agglomeration behaviour.
- Investigate the effects of moisture content, drying temperature and fill level on the extent of agglomeration observed.
- Develop a regime map to describe different agglomerate growth and breakage behaviours observed experimentally in an AFD.
- Evaluate the suitability of constant tip speed as a scaling index for scaling up agglomeration behaviour in larger agitated dryers.

1.2 Thesis Structure

Chapter 2 provides a detailed review of the literature on drying theory and agitated filter dryers (AFDs). The chapter initially covers the fundamental principles of drying and common types of dryers, providing context for the widespread use of AFDs across various industries. The literature on material and process parameters influencing undesired agglomeration in AFDs is critically reviewed, highlighting knowledge gaps.

Chapter 3 describes the properties and preparation of materials used in the experimental work. The set up of the AFD and the experimental methodology are presented. Additionally, various characterisation techniques used to analyse the primary material and the agglomerates formed are described.

Chapter 4 presents a proposed mechanism for undesired agglomeration in AFDs. The results from experiments designed to investigate the mechanisms of agglomeration under varying agitation conditions are also presented. To gain mechanistic insight into the influence of agitation speed and time on agglomeration behaviour, experiments were conducted at constant temperature (and therefore moisture content), effectively decoupling the drying process. This chapter also explores the effect of moisture content, drying temperature and fill level on the extent of agglomeration observed.

Chapter 5 investigates the effect of modifying the primary material size on the extent of agglomeration and reports different agglomerate growth behaviours to those reported in Chapter 4. A novel regime map is proposed to describe different agglomerate growth and breakage behaviours observed experimentally in an AFD.

Chapter 6 presents the experimental work conducted during a placement at AstraZeneca (Macclesfield, UK). This work focuses on assessing the use of constant tip speed as a scaling index for scaling up the agglomeration observed in Chapter 4 in a larger AFD. The effect of scaling up using constant tip speed while also modifying the dryer geometry to a conical dryer is discussed. Additionally, characterisation techniques such as SEM and micro-CT are evaluated for their potential use in studying agglomerate morphology.

Chapter 7 concludes the thesis with a summary of key findings in each chapter and provides recommendations for future work.

A schematic representation of the thesis structure is provided in Figure 1.2.

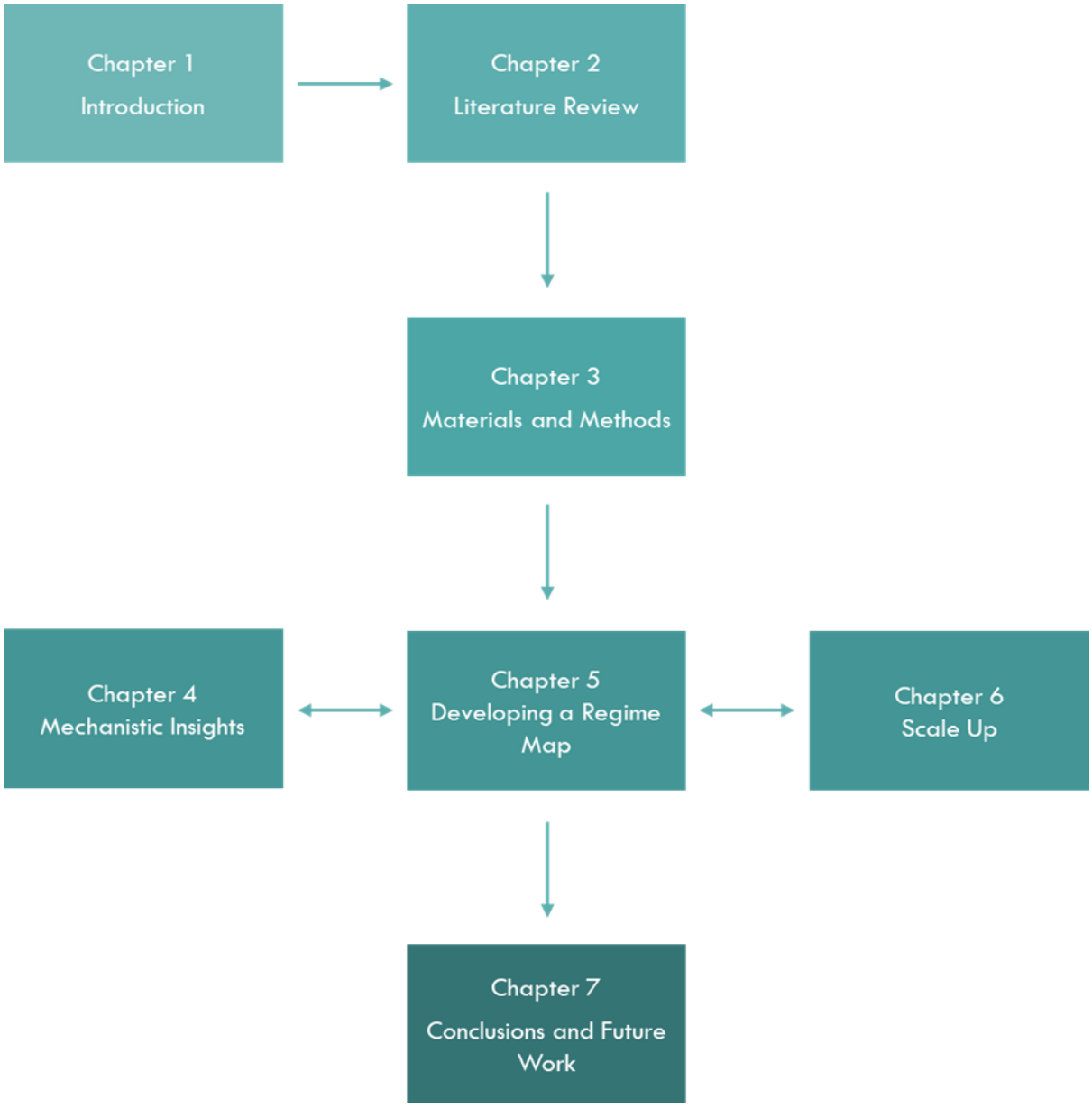

Figure 1.2: Schematic diagram of the thesis structure.

Chapter 2 - Literature Review

As discussed in Chapter 1, agitated filter dryers (AFDs) are commonly used in multiple industries and yet the mechanisms driving undesired agglomeration remain poorly understood. Drying as a unit operation is inherently complex due to simultaneous heat, mass and momentum transfer, and is also influenced by numerous solid, liquid and equipment parameters. This dynamic nature has limited the development of predictive tools for drying operations. This chapter reviews the theoretical concepts essential for understanding agglomeration behaviour during drying in AFDs.

This literature review is divided into two sections. The first section (Figure 2.1a) focuses on the theory of drying, methods of heat transfer and common types of dryers, providing context for the widespread use of AFDs. The second section (Figure 2.1b) covers the construction and operation of AFDs, the binding mechanisms of agglomeration and parallels between wet granulation and undesired agglomeration in AFDs. The proposed mechanism of undesired agglomeration is presented and key parameters affecting each underlying rate process are discussed. Finally, recent computational modelling efforts are reviewed. This chapter provides a comprehensive theoretical framework for the mechanistic studies and scale-up work presented in later chapters.

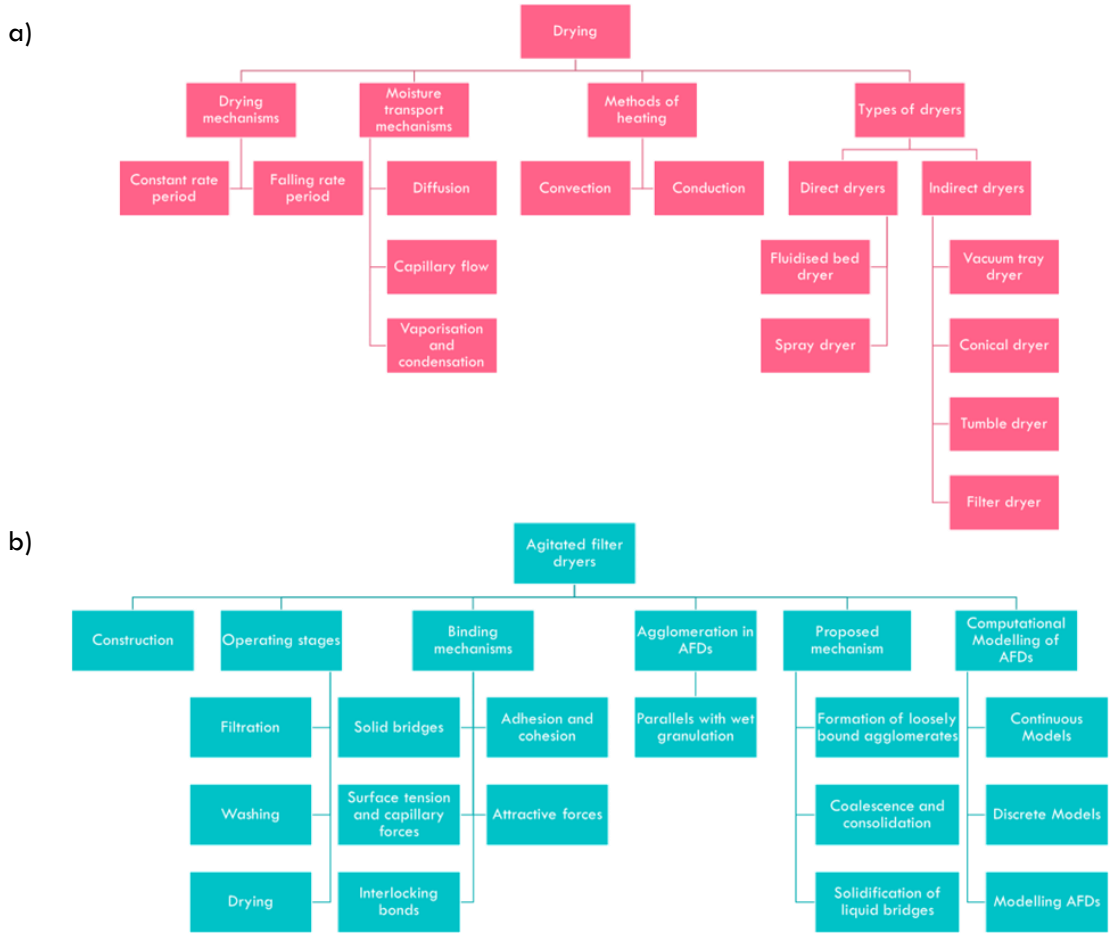

Figure 2.1: Schematic diagrams of topics covered in Chapter 2 on a) drying principles and b) agglomeration in AFDs.

2.1 Drying

The basic principles of drying and key concepts such as dryer types and design are covered in this section. Drying is the removal of solvent by evaporation from a wet heterogeneous substance consisting of solid, liquid and vapour. Despite drying seeming to be a relatively simple process that many encounter in day-to-day activities, it involves simultaneous heat and mass transfer and is rather complex. It is crucial to understand these mechanisms to predict drying curves and drying performance.

Drying is often the last stage of isolation after crystallisation of API and subsequent filtration. As filtration is not sufficient to remove solvent to acceptable levels, drying is a crucial stage in API manufacturing. Following filtration, a typical wet cake will have a moisture content anywhere in the range of 5-50 %, whereas a successful drying operation will reduce this to trace levels of moisture.[7] Any residual moisture may not only affect the formulation and performance of the end drug product but may also impact patient safety. Therefore, the residual solvent levels must be lowered to the limits outlined by ICH guidelines.[8]

The moisture content (MC) is defined as the mass of moisture (m_w) per unit of dry material (m_d):

$$MC = \frac{m_w}{m_d} \tag{2.1}$$

As a wet solid is swollen compared to the dry material, and the volume changes throughout the drying period, moisture content is conventionally expressed by mass, not volume. Another way of calculating the moisture content is through loss on drying (LOD) where:

$$LOD = \frac{initial\ sample\ mass - dry\ sample\ mass}{initial\ sample\ mass}\ x\ 100 \tag{2.2}$$

When discussing moisture content, it is important to also consider the various types of residual moisture, and these are illustrated in Figure 2.2. The total moisture content consists of both unbound and bound moisture. Moisture within the solid or trapped in the microstructure of the solid, with a vapour pressure less than that of the pure liquid, is the bound moisture. Any excess moisture is the unbound moisture. For non-hygroscopic materials, all moisture can be classed as unbound moisture. Pharmaceutical compounds are typically non-porous and do not show significant movement of moisture or solvent, unless they exist as hydrates or solvates. Solvates and hydrates are formed when solvent or water molecules are incorporated into the crystal lattice. Free moisture is the moisture that can be removed at a given temperature during drying and consists of both bound and unbound moisture. Another important parameter is the equilibrium moisture content. When a wet solid is dried, it reaches a stage where the moisture content is at equilibrium with the partial pressure of vapor in the gas. This is the equilibrium

moisture content and further drying will not result in any moisture loss as this is the lowest moisture content achievable under these conditions.[9]

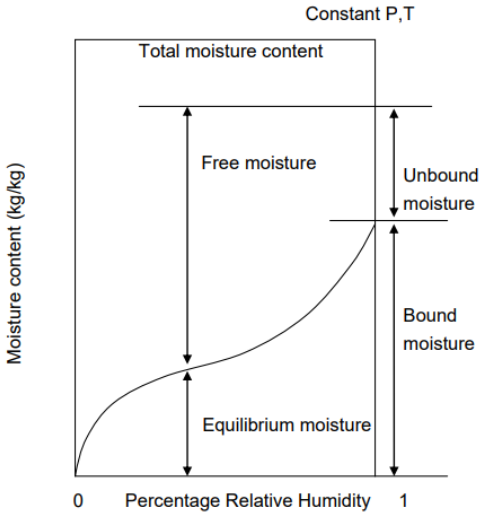

Figure 2.2: Types of moisture present when drying wet solids.[10]

There are two ways to remove unbound moisture, evaporation, and vaporisation. Evaporation occurs when the vapour pressure of the moisture present on the solid surface is equal to the atmospheric pressure. Evaporation is usually conducted at the boiling point of the solvent but if the material is heat sensitive, then vacuum evaporation is used which reduces the boiling point by lowering the pressure. Vaporisation involves a hot air, or a nitrogen blow through over the wet solids and direct heat is applied to remove moisture (drying by convection).[9] This provides the latent heat of vaporisation required for the liquid to undergo a phase change and form vapour. The air is cooled by the wet solids and the moisture is transferred to the air and carried away. The propensity for the moisture to be removed by the hot air is dependent on the temperature and humidity.

The absolute humidity (Y) can be defined as the mass of water vapour (m_w) per mass of dry air (m_g)[11]:

$$Y = \frac{m_w}{m_g} \tag{2.3}$$

The total mass can therefore be written as:

$$m_g + m_w = m_g(1 + Y) \tag{2.4}$$

Using the ideal gas law for both vapour and air fractions at a constant temperature and total volume:

$$m_g = \frac{P_g V}{RT} M_g \text{ and } m_W = \frac{P_w V}{RT} M_w \tag{2.5}$$

where P_x is the partial pressure, V is the volume, M_x is the moles, R is the universal gas constant and T is the temperature. By combining this equation with Dalton's law of partial pressures, Equation 2. 3 can be written as:

$$Y = \frac{M_w}{M_g} \frac{P_w}{P - P_w}$$

2. 6

The relative humidity (ψ) of a vapour-gas mixture is given by the ratio of the vapour partial pressure to the saturated vapour pressure (P_w^0) at the same temperature (Equation 2. 7). The gas is saturated with vapour when the partial pressure of vapour in the gas is equal to the vapour pressure of the liquid and an equilibrium is established.

$$\psi = \frac{P_w}{P_w^0}$$

2. 7

Therefore, for an air and water system, Equation 2. 3 can be written as:

$$Y = \frac{18\,\psi P_w^0}{29(P - \psi P_w^0)}$$

2. 8

2.1.1 Drying Mechanisms

To understand the drying behaviour of a given material system, the moisture content is measured as a function of time, and the derivative of this (the rate of drying) is plotted against time to give a drying curve (Figure 2.3). Drying curves are useful for understanding which mechanisms dominate the removal of moisture. For a given material, the drying rate curve usually has a similar shape over a range of conditions, and so if these curves are normalised with respect to the initial drying rate and average moisture content, this creates a 'characteristic drying curve' for the material.[9]

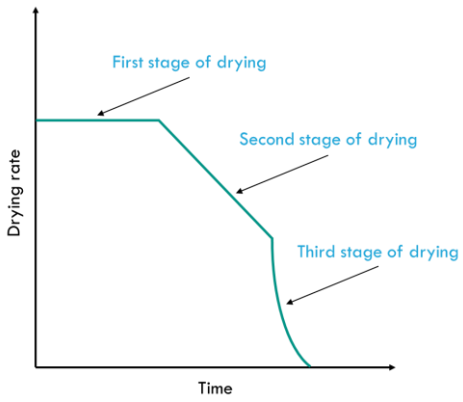

Figure 2.3: Typical drying rate curve reproduced.[12]

2.1.1.1 Constant rate period

Looking at a typical drying curve (Figure 2.3), it is evident that during the first stage of drying, the drying rate is constant. This initial constant rate period is where the solvent on the solid surface rapidly vaporises, and the drying rate is dominated by heat transfer. The driving force at this stage is the difference in temperature between the jacket of the dryer and the solvent being removed. Therefore, the drying rate can be increased by either increasing the jacket temperature or decreasing the pressure. However, the drying rate also depends on the surface area available for heat transfer and this area decreases as the cake dries. This highlights the benefits of agitated dryers, as agitation of the cake exposes wet material to the heated surface and increases the area available for heat transfer.[2] Even without agitation, the presence of a heated agitator benefits the constant rate period by providing an extra heat source.[13] Towards the end of this drying stage, solvent is transported from within the solid to the surface by capillary action.

2.1.1.2 Falling rate period

The second drying stage, also known as the first falling rate period, occurs where solvent is no longer saturating the surface and dry spots appear, and hence the drying rate declines. The constant and falling rate period are demarcated by a point termed the *critical moisture content* (CMC) which is the average moisture content at which the drying rate begins to fall due to insufficient moisture to saturate the surface. The CMC is unique to the material being dried but can also vary depending on the thickness of the cake, and these variations should be considered when scaling up drying processes. The limiting mechanism in this stage is no longer heat transfer and is instead dominated by mass transfer.[14] Therefore, using agitation is favourable as it can enhance mass transfer.[15] This drying stage continues until the surface film of solvent has completely evaporated.

Once the solvent present on the surface dries, some solvent will remain within the solid and this drying stage is the second falling rate period. The drying rate of this period depends on the movement of the internal solvent towards the surface and is often called the diffusion period. As the moisture content continues to fall until the equilibrium moisture content is reached, the rate of internal movement of solvent decreases and hence the drying rate declines more rapidly. However, this solvent migration is difficult to model and does not always appear on drying curves, and the transition between the first and second falling rate periods can be difficult to identify. The drying rate in this period may be extremely slow especially when low moisture contents are required. Therefore, using agitation can be beneficial.[2]

2.1.2 Mechanism of Moisture Movement

Understanding the exact mechanisms of moisture movement during the drying period, which consists of various stages as explained above, is crucial. Moisture transport can be controlled internally (by diffusion) or externally (by heat).

During the constant rate period, moisture is removed from the surface via evaporation. Drying in this period is controlled by external conditions such as the temperature difference between the wet surface and drying medium, the area of wet solid surface available, humidity and pressure.[14] The falling rate period depends on the rates of internal heat and mass transfer within the solid. The transport of moisture from within the solid to the surface can occur through one or more of the following mechanisms:

- Diffusion

Diffusion refers to the movement of molecules from an area of high concentration to low concentration to rectify the concentration gradient. When there is a moisture concentration gradient between the solid's core and surface, moisture diffusion takes place. Moisture diffusivity is proportional to the moisture content and hence decreases throughout the drying period.

- Capillary flow

Capillary flow describes the movement of liquid through capillaries, or over the surface of a solid as a result of molecular attraction between the liquid and solid. Schlichter first reported the effect of capillaries when studying moisture movement in soil.[16] Ceaglske and Hougen further supported this, suggesting that capillary flow dominates as the transport mechanism for water in granular material rather than diffusion.[17] They noted that water may also move from areas of low concentration to high concentration depending on the pore size. Capillary flow is driven by the wettability of the solvent and is determined by the contact angle, which is the angle between a liquid interface and a solid surface at the point of contact. A low contact angle (0 to 90°) suggests high wettability and strong capillary action.

- Vaporisation and condensation

This mechanism refers to the cycle of solvent evaporating and recondensing on colder surfaces and is often observed in indirect conduction dryers. It was first proposed by Henry that the temperature gradient creates a resulting vapour pressure gradient, and this allows liquid to evaporate and recondense.[18]

2.1.3 Methods of Heating

Drying is an integral step in not only API manufacturing but many other industries. When designing a drying process, various parameters are considered to optimise the process. The first consideration is the heat transfer mechanism, which can be conduction, convection or radiation. This review focuses on conduction and convection, as these are the most commonly used mechanisms in the pharmaceutical industry.

2.1.3.1 Convection

Convective drying is a method of direct heat transfer which typically involves passing heated air or gas over the surface of the wet solids. The evaporated moisture is removed by the medium used, often air or nitrogen gas. This proves useful for thermosensitive materials as it can be conducted at relatively low temperatures. These dryers also scale up relatively easily and are commonly used for drying particulate solids. Common examples of convective dryers include fluid bed, rotary and spray dryers.

2.1.3.2 Conduction

Conductive drying is an indirect drying method often used for very wet solids, where the wet solids are in contact with a heated surface to supply the heat for evaporation. Due to this mechanism, conductive dryers are also referred to as contact dryers and are the most commonly used dryer type in the pharmaceutical industry.[7] Vacuum can be used to remove evaporated moisture and is typically used for thermosensitive materials. The driving force is the temperature difference so high contact surface temperatures that approach the solvent boiling point typically exhibit faster drying rates. These dryers are typically more energy efficient than convective dryers and usually operated in batch mode.[7] Some examples of conductive dryers include filter dryers, conical dryers and tumble dryers.

2.1.4 Dryer Types and Classification

There are many types of dryers, and various classification systems are used, categorising them by heating method, feed type, batch or continuous operation etc. In the pharmaceutical industry, and for granular materials, the most commonly used dryers can be classified as direct (convective) or indirect (conductive) dryers. Some commonly used dryers for each subtype are presented in the following sections.

2.1.4.1 Direct dryers

Direct dryers are often less expensive as they do not require heating jackets or tubes to contain the heating medium. They also allow for very precise temperature control, hence their popularity with thermosensitive solids. However, they tend to have low thermal efficiency.

Fluidised bed dryers

Fluidised bed dryers (FBD) are commonly used in wet granulation and can dry products between 200 – 2000 μm in size. They operate by passing heated air through the powder bed, where at a certain gas velocity, the bed becomes fluidised. This is known as the minimum fluidisation velocity.[19] The contact between air and solids is considerably better than standard tray ovens, resulting in faster drying times and improved uniformity. FBDs can operate at various feed rates, ranging from just a few grams to tonnes per hour, and are designed for both batch and continuous operations. However, they can result in attrition and are avoided when handling friable products.

Spray dryers

Spray dryers are useful for drying solutions and slurries, which are dispersed as droplets into a stream of hot gas to be dried as individual particles. This results in fine powders, and good control of the final particle size. Spray dryers have short contact times so are suitable for drying at low temperatures and can be used for batch and continuous operations. Spray dryers are used in several industries, especially the dairy industry for drying milk powders. However, they must be carefully monitored for any dust formation within the vessel, especially when using air as the heating medium as this can be a fire risk.

2.1.4.2 Indirect dryers

Indirect dryers are widely used across many industries due to their increased efficiency and solvent recovery capabilities. This section highlights four commonly used dryers in the pharmaceutical industry.

Vacuum tray dryer

A tray dryer is essentially a larger oven where trays containing the wet solids are placed on heated shelves inside the dryer. Sometimes they are operated with vacuum and/or inert gas supply, however the bulk of the heat transfer occurs via conduction from the heated surfaces, allowing them to be categorised as indirect dryers.[7] Tray dryers are relatively simple to operate and can be useful for drying small quantities of materials to avoid any attrition occurring. They can also be used with vacuum for thermosensitive materials. However, this static mode of drying can result in severe agglomeration, necessitating further unit operations like milling. They do not feature sampling ports, so the vessel must be opened every time a sample needs to be retrieved. The drying time can also be quite lengthy (12 – 24 h) and so this method is not ideal for very wet solids.[20]

Conical dryer

A conical dryer, sometimes referred to as a rotary cone dryer, is a jacketed conically shaped vessel with a screw impeller. Its geometry provides a large surface area to volume ratio for contact drying, generally better than in filter dryers. They are often used for drying wet free-flowing APIs and fine chemicals and, hence, are usually operated under vacuum.[21] The internal screw impeller rotates on its own axis and around the entire circumference of the vessel, ensuring agitation is provided to the whole feed. It not only provides agitation but can function as an additional heat source. The ability to rotate around the entire vessel also makes it useful for cleaning. Conical dryers typically have a sample port to retrieve samples throughout the drying operation, as well as separate charge and discharge ports to load and unload the wet cake, minimising any contamination.

Tumble dryer

Tumble dryers consist of a rotating or tumbling double cone-shaped vessel with a heated jacket and a vacuum line. They are often used to dry wet granules, and the gentle tumbling action allows for efficient drying by exposing material to the heated surfaces without using high shear. Typical speeds are roughly 5 rpm for larger units and up to 30 rpm for smaller units.[21] However, this does limit its use for sticky materials as they may coat the vessel walls or agglomerate. To overcome this, they are sometimes fitted with a delumping bar or rotated slowly/intermittently when the material has a high moisture content.

Filter dryer

Filter dryers combine multiple unit operations in one jacketed vessel, which has many benefits from a safety and contamination perspective. They are very commonly used in the pharmaceutical industry and typically fitted with an agitator for improved heat and mass transfer. The construction and operation of agitated filter dryers will be discussed in further detail in Section 2.2 and Section 2.3.

2.1.5 Summary

Drying is arguably one of the oldest chemical engineering unit operations and remains a crucial stage of the API manufacturing process. In this section, key principles of drying mechanisms and kinetics are covered, and some relevant examples of direct and indirect dryers are given. When designing a drying process, it is important to consider the properties of the wet solid being dried as well as the desired product quality and operational costs. The following sections will elaborate on the operation and construction of AFDs and explain their prevalence in the pharmaceutical industry.

2.2 Construction of Agitated Filter Dryers

A schematic of an AFD is shown in Figure 2.4, and the agitator can be lowered or raised as needed, and accommodate low and high speed rotations.[2] The agitator can be heated to enhance heat transfer, and the heated agitator contributes to roughly 45 % of the total energy input, with the vessel walls and filter plate providing 30 % and 25 % respectively.[5] Agitation can also aid in cake washing by agitating in reverse to smooth out cracks in the wet cake, preventing the channelling of wash solvents. To avoid disturbing the filter cloth, there is an offset between this and the agitator base. However, this can cause residual cake build-up, which is known as the heel.[2]

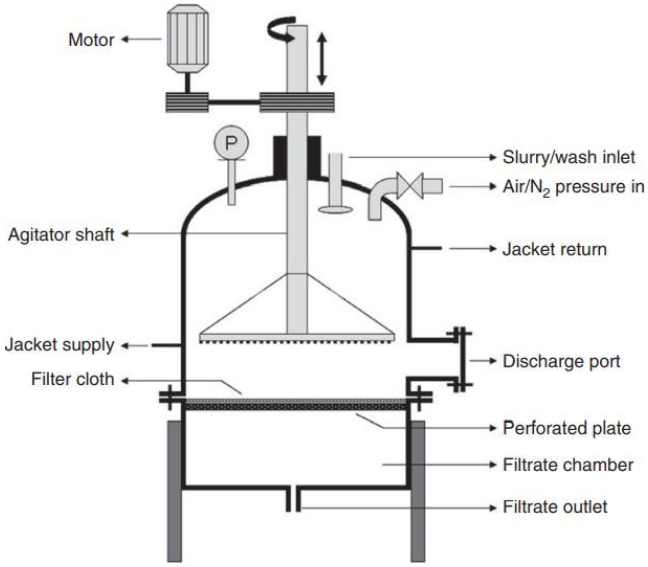

Figure 2.4: Cross-sectional representation of an agitated filter dryer (AFD).[7]

AFDs are fitted with a jacket to provide heat for drying. The jacket is also used to conduct filtration at various temperatures.[2] The heat is usually supplied by circulating heating fluid throughout the insulated jacket surrounding the vessel.[22]

The AFD base often has a filter plate which can be heated to direct heat energy to the cake from below. These are in an all-welded design which provides efficient heat transfer without contaminating the cake.[13] The slurry passes through the filter media above the filter plate and solids are retained. The most common filter media are filter cloths and sintered metal screens. Filter cloths are cheap, can be designed for specific pore sizes, may be discarded after use, and give very high retention. However, they are not very robust and require a greater clearance from the agitator compared to other filter media.[23] Sintered metal screens are usually multi-layered wire meshes that are rigid and more durable than standard wire meshes. Sintering offers a much stronger filter media which is less prone to deformation and using finer wires improves solid retention.[24] Sintered metal screens allow a tighter clearance between the filter and agitator, minimising the product heel.[13] These components can all be altered for specific functions, increasing the applicability of AFD's. Many functions such as agitator speed and height can be adjusted by the operator.

2.3 Operating Stages of Agitated Filter Dryers

An AFD tends to operate in three stages: filtration, washing and drying. These are discussed briefly in the following section.

2.3.1 Filtration

Filtration is the process of separating solids from a liquid suspension by passing the slurry through a filter medium and applying a pressure gradient across the medium. The slurry is transferred into the AFD and given time to settle and form the powder bed before filtration.[3] Filtration occurs by creating a pressure drop across the filter medium, either by applying pressure above the cake or vacuum below it. As previously mentioned in Section 2.2, it is important to choose a suitable filter medium for sufficient product retention.

2.3.2 Washing

Following filtration, cake washing is often conducted to displace or remove the crystallisation solution from the cake. This is to allow:

- Removal of any impurities, unreacted or excess materials.
- Removal of the crystallisation solvent to acceptable levels if increased solubility is expected at the drying temperature. By lowering the level of solvent, the redissolution of crystals in the solvent which can later form agglomerates is minimised.[25]

There are two primary types of cake washes: displacement and reslurry. Displacement washes pass a large volume of solvent through the wet cake to displace trapped crystallisation solvent and are preferred for insoluble contaminants. It is the most common wash and is very efficient, except when the cake cracks due to crystallisation solvent being substituted by a different liquid or solid impurities passing through the cake. Cake cracking is often caused by deliquoring before the washing stage. Cracking of the cake can sometimes be limited by using the agitator to smooth the cake throughout the wash and fill up the cracks.[2,26] Reslurry washes involve adding fresh wash solvent and agitating the wet cake to form a slurry which is filtered. This is preferred for soluble impurities and results in less cake cracking.[26]

AFDs can incorporate both displacement and reslurry washes. Using both displacement and reslurry washes gives the highest purity, and a washing sequence of displacement, reslurry, displacement is often used in agitated vessels.[2] Washing is crucial in AFDs to minimise the undesired agglomeration, often observed upon drying, by reducing the amount of crystallisation solvent present in the deliquored cake. This was shown in one study comparing the effect of different filtration methods on agglomeration behaviour. The washed filter cake had considerably less agglomerates forming compared to the unwashed filter cake, due to the crystallisation solvent being displaced by the wash solvent.[27] By preventing the formation of solid bridges, agglomeration can be reduced.

2.3.3 Drying

Following the filtration and washing steps, the cake can be dried within the same equipment. There is often a nitrogen or cold air blow through to reduce the moisture content of the wet cake before drying, also known as the deliquoring step.[6] Drying occurs primarily by contact drying where heat is transferred to wet solids from heated surfaces such as heated vessel walls, agitator and filter plate. Contact dryers are useful in pharmaceuticals where many API's and excipients are heat sensitive and prone to degradation.[28] They also operate under vacuum conditions which lower the boiling point of solvents.[6] Contact heating from heated surfaces coupled with agitation and vacuum produces dried solids with low moisture contents.

Once dried, the dry cake is discharged through the discharge port and the agitator is slowly lowered to facilitate this.[2] The agitator removes the majority of the dried product, but a thin heel can remain on the filter plate. This affects filtration in subsequent batches due to increased flow resistance, so must be removed, and this is often done after several batches.[29]

Agglomeration during drying is a widespread problem in AFDs. AFDs commonly use heated agitator blades, enhancing heat and mass transfer, resulting in more uniform drying.[30] However, this agitation contributes to agglomeration or attrition (breakage). Agglomeration during drying occurs when particles with residual solvent become bound during agitation. As the solvent evaporates, a viscous API solution film forms around the particles. Upon evaporation, the viscous film forms crystalline bridges, cementing the agglomerates.[31]

2.4 Binding Mechanisms of Agglomeration

Agglomeration can be defined as particles sticking together either due to short range physical forces between particles or the use of binders which form a material bridge between particles to form a larger entity.[32] To better understand the agglomeration phenomena observed during AFD operations, it is crucial to understand the different types of agglomeration based on the binding mechanisms. These are listed in Table 2.1 and discussed in the following sections.

Table 2.1: Binding mechanisms of agglomeration.[32]

I. Solid Bridges

- Sintering
- Partial melting
- Chemical reaction
- Hardening binders
- Recrystallisation
- During drying (recrystallisation of dissolved substances or deposition of colloidal particles)

II. Adhesion and cohesion forces

- Viscous binders
- Adsorption layers (< 3nm thickness)

III. Surface tension and capillary pressure

- Liquid bridges
- Capillary pressure

IV. Attraction forces between solid particles

- Molecular forces
  - Van der Waals forces
  - Free chemical bonds (valence forces)
  - Associations (non-valence); hydrogen bridges
- Electrostatic forces
- Magnetic forces

V. Interlocking bonds (form-closed bonds)

2.4.1 Solid Bridges

At elevated temperatures, diffusion of molecules from one particle to another at points of contact forms sinter bridges (Figure 2.5a). Solid bridges may also form because of partial melting of the contact between particles, chemical reactions or recrystallisation.

2.4.2 Adhesion and Cohesion Forces

Adhesion describes the forces causing particles to stick to other surfaces, such as vessel walls in dryers. Cohesion is the attractive forces in which particles stick to each other.

When using highly viscous binders, there are adhesion forces between the binder and solid particles, as well as cohesion within the viscous material, resulting in agglomeration. Fine particles often collect solvent molecules to form thin immobile adsorption layers which can penetrate each other and bond particles together.

2.4.3 Surface Tension and Capillary Forces

A common binding mechanism in wet agglomeration is liquid bridges holding together particles in an agglomerate (Figure 2.5f). Liquid bridges can form due to solvent present or capillary condensation. As the solvent fills the pores of the solids, a negative capillary pressure develops which strengthens the liquid bridge and holds particles together. Liquid bridges are often a precursor to solid bridges, and this is commonly seen in AFDs.

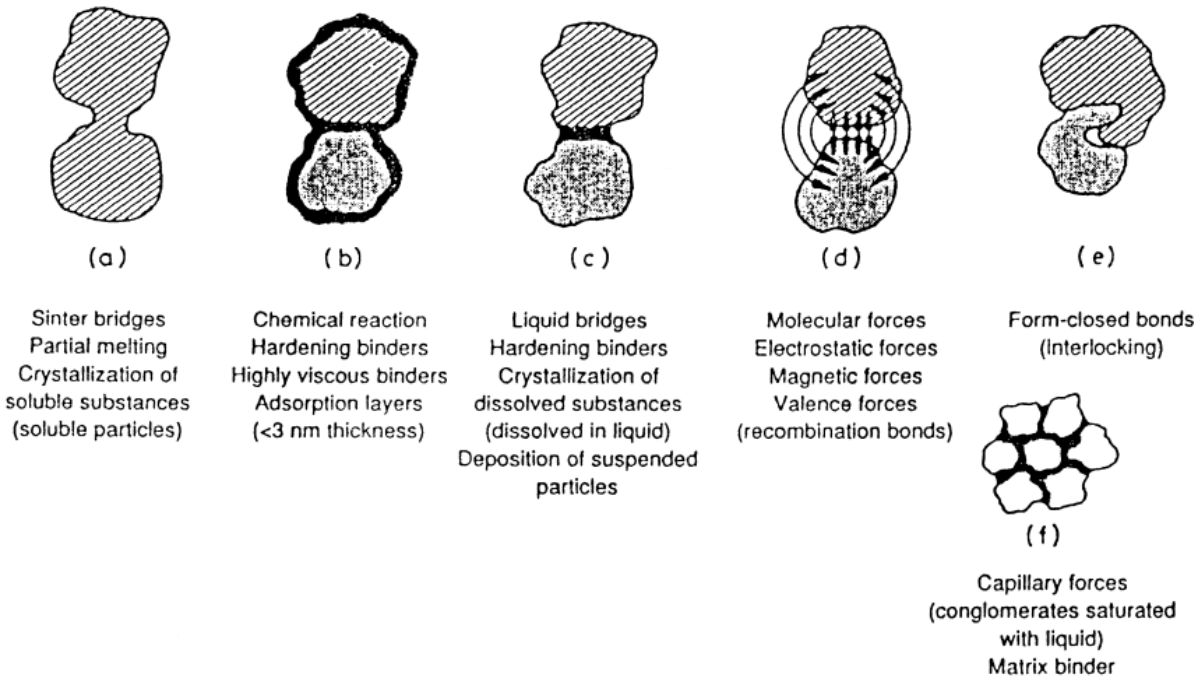

Figure 2.5: Illustrations of various binding mechanisms of agglomeration.[33]

2.4.4 Attraction Forces between Solid Particles

These are typically short-range forces such as van der Waals, electrostatic and magnetic forces and this is shown in Figure 2.5d. This mechanism is especially significant for fine particles, however if the distance between particles increases (above 0.2 nm), these forces become negligible.[33]

2.4.5 Interlocking Bonds

These are also referred to as form-closed bonds and are often seen if the solid particles have shapes such as fibres or platelets which can become tangled or interlock with each other to promote agglomerates. An example of this can be seen in Figure 2.5e.

2.5 Agglomeration in AFDs

Although agglomerates are only characterised after drying, there are many parameters in the filtration and washing regimes that may encourage agglomeration. The key parameters influencing agglomeration are shown in the Ishikawa diagram in Figure 2.6.

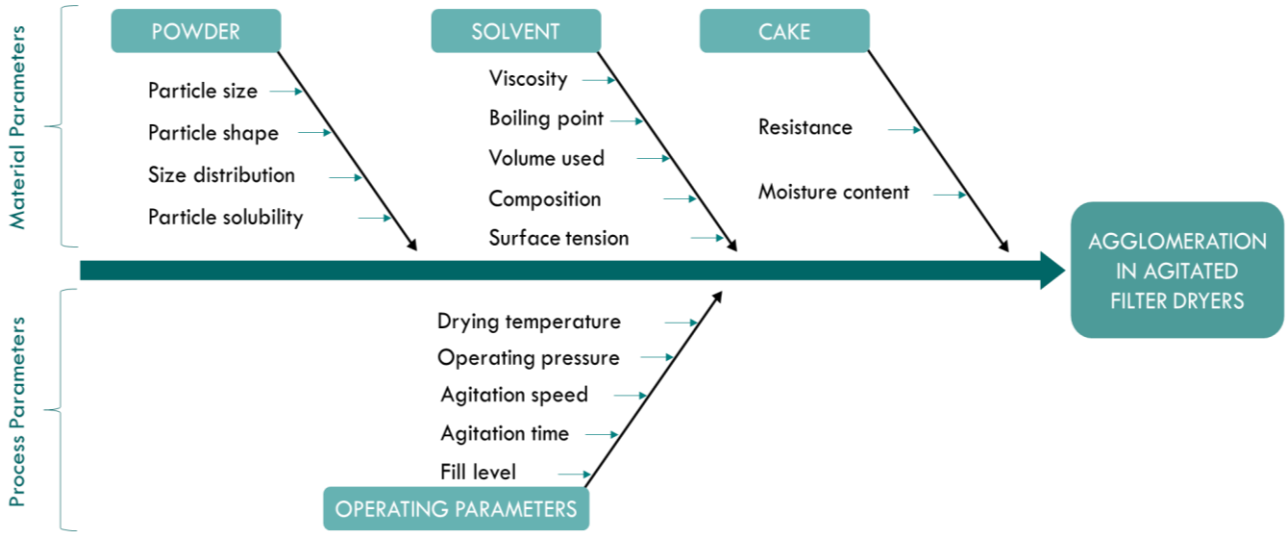

Figure 2.6: Ishikawa diagram of different parameters influencing agglomeration in agitated filter dryers - modified from Tamrakar *et al.*[30]

2.5.1 Parallels with Wet Granulation

Due to a lack of understanding of the rate processes involved, these studies mainly report correlations between experimental conditions and resulting agglomeration. In this thesis, a proposed mechanism is presented. To guide this, parallels were drawn between agglomeration in AFDs and wet granulation.

Wet granulation is a particle size enlargement technique that involves agglomerating particles into larger granules where the original particles are still distinguishable.[34] This is achieved by spraying particles with liquid binder over an agitated particle bed, where the liquid binds particles together through capillary and viscous forces. More permanent bonds are formed upon subsequent drying or sintering.[35] This is an important unit operation used in many industries including pharmaceuticals where the aim is to produce larger granules. Wet granulation is commonly described as a combination of three rate processes (Figure 2.7) and these are discussed in the following sections.

2.5.1.1 Wetting and nucleation

The liquid binder makes contact with dry powder allowing initial nuclei to form. Poor binder dispersion results in some nuclei being more saturated than others leading to preferential growth. Good binder dispersion leads to uniform wetting and controlled nucleation which gives a narrow size distribution. The nucleation mechanism is determined by the relative ratio of droplet to particle size. If the droplet is larger than the particles, nucleation occurs via the immersion mechanism where small particles

become immersed into the larger drop, producing nuclei with saturated pores. When the droplet is similar to or smaller than the particles, nucleation occurs via the distribution mechanism. Small droplets coat the outside of the solid particles which coalesce to form a nuclei granule.[36]

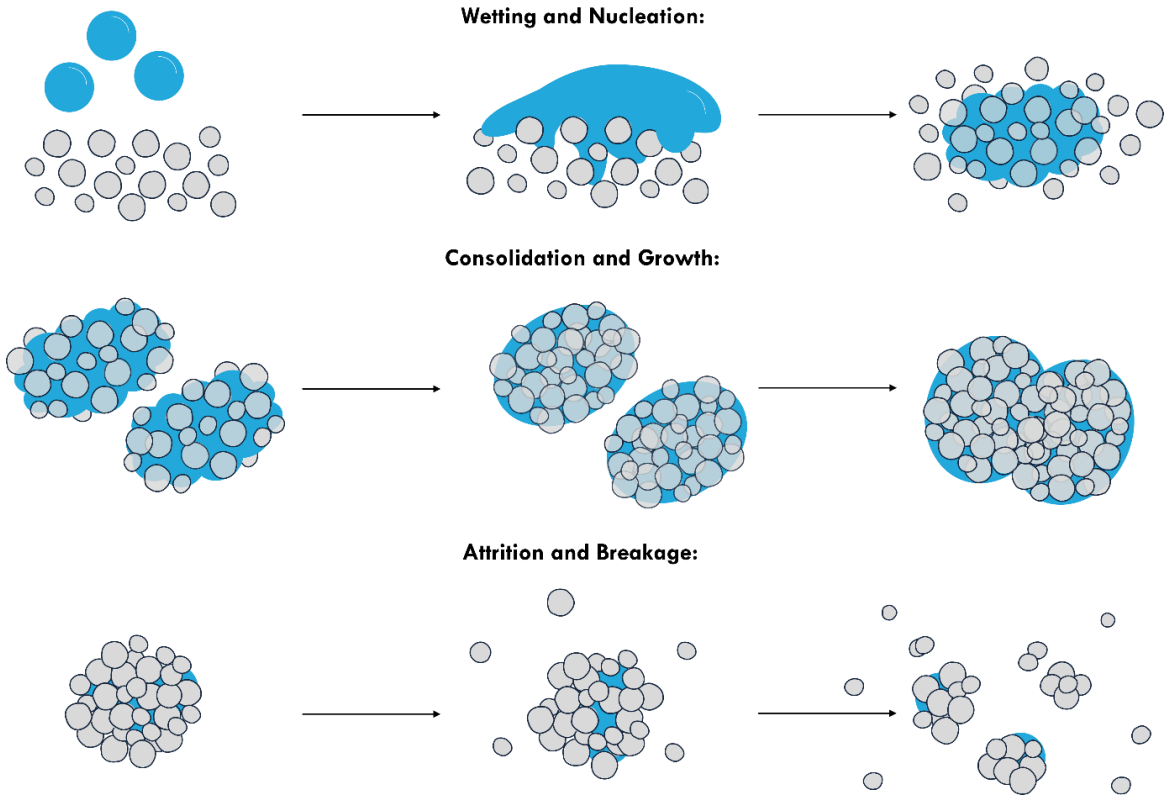

Figure 2.7: Wet granulation mechanism reproduced.[34]

2.5.1.2 Consolidation and growth

After nucleation, granules may increase in size and density. Granules collide with other granules and the granulator walls, resulting in consolidation. As they consolidate, particles move closer together and squeeze out trapped air and liquid binder to the surface, reducing their size and porosity. If there are many unwetted particles, granules grow by layering as particles adhere to the wet granule surface. If there is a lot of liquid binder present, granules grow by coalescence as the granules stick to other granules.

Granule growth can be classified into broad categories of steady and induction growth. Steady growth is seen with weak, deformable granules and the granule size increases linearly with time. Induction growth happens with strong particles which do not show sufficient deformation upon impact to coalesce. Once initial nuclei form, there is a period of little to no growth (the induction period), followed by rapid growth. The granules slowly consolidate and squeeze liquid binder to the surface which then allows them to quickly grow. By increasing the binder content, the induction period can be decreased.[37]

Other growth behaviours have been observed. Nucleation only growth refers to formation of granule nuclei where there is insufficient liquid binder for further growth.[38] Crumb behaviour refers to formulations too weak for permanent granules to form, so a loose crumb is observed which cushions larger granules that constantly break and reform.[39] Overwetting occurs in systems with an excess of liquid binder, forming a slurry.

A granule growth regime map (Figure 2.8) was designed on the basis that granule growth behaviour is a function of only the maximum pore liquid saturation and extent of granule deformation during impact.[37]

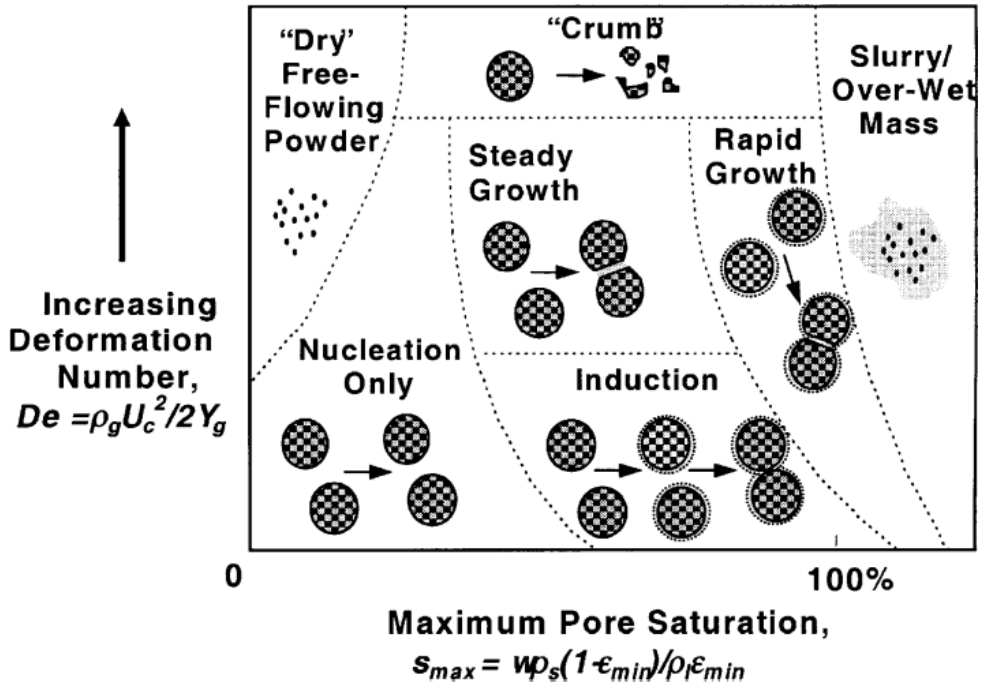

Figure 2.8: Granule growth regime map.[8]

As the pore liquid saturation varies during granulation as granules consolidate, the maximum granule pore saturation (s_{max}) was used:

$$s_{max} = \frac{w\rho_s(1 - \varepsilon_{min})}{\rho_l \varepsilon_{min}}$$

2. 9

where w is the mass ratio of liquid to solid, ρ_s is the solid particle density, ρ_l is the liquid density and ε_{min} is the minimum porosity of the formulation for specific operating conditions.

The deformation of granules during impact is quantified using Stokes deformation number:

$$St_{def} = \frac{\rho_g U_c^2}{2Y_g}$$

2. 10

where U_c is collision velocity in the granulator, ρ_g and Y_g are the granule density and dynamic yield stress, respectively. The Stokes deformation number is the ratio of impact kinetic energy to energy dissipated by the liquid bonds between particles.

The regime map is a useful descriptive tool to estimate the growth behaviour for different systems and has been extensively used in pharmaceutical industry to predict agglomeration in wet granulation.

2.5.1.3 Attrition and breakage

This rate process describes the breakage of wet or dried granules due to impact, wear or compaction in the granulator or during further handling. Attrition refers to a gradual wearing of a granule surface, resulting in fines, whereas breakage occurs when granules fracture into multiple fragments

Breakage of wet granules can be controlled by growing granules up to a breakage limit, potentially giving a narrow size distribution. The breakage is dependent on other factors such as the granulator used and is difficult to predict as granule strength depends on the final granule properties. Granulation processes either dry granules simultaneously or after granulation in a drier, which can lead to attrition or fracture of granules. Attrition of dried granules generates dusty fines which are undesirable.[34]

2.5.1.4 Comparison with agglomeration in AFDs

Wet granulation is a well-established field, and this existing knowledge can be used to guide AFD operations due to their similarities.[40] Wet granulation aims to take a dry solid, which is then wetted and agitated to form granules. In contrast, drying in AFDs starts with a damp solid, and solvent is removed while agitating the wet cake, but agglomeration is undesired in this process (Figure 2.9).

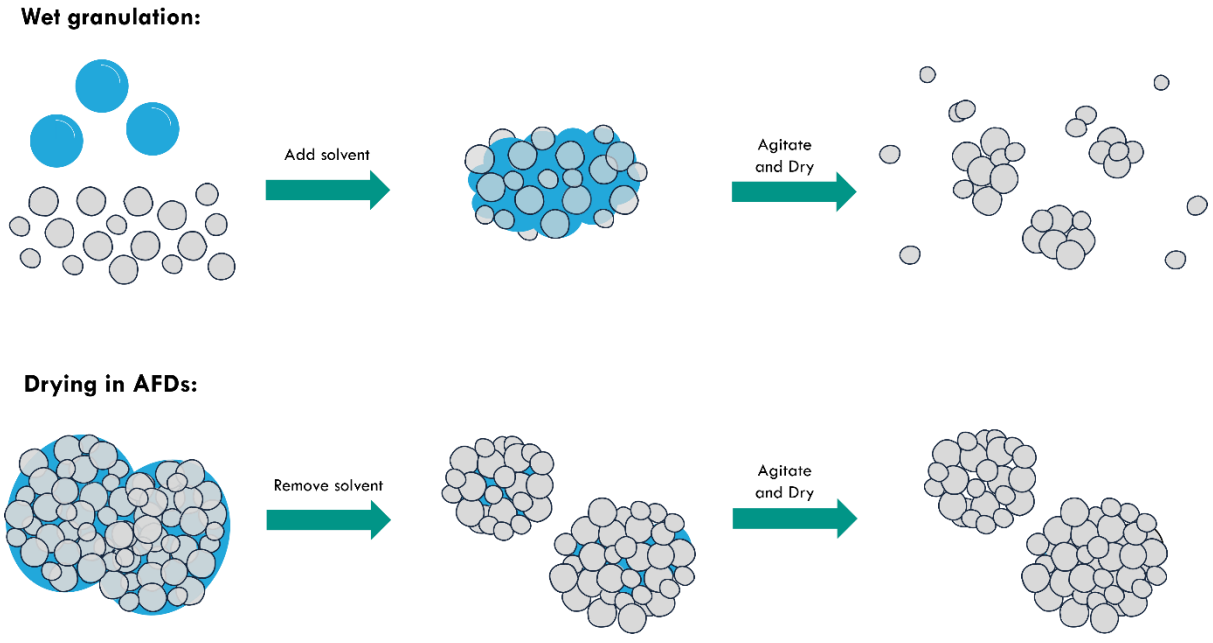

Figure 2.9: Contrasting wet granulation to drying in AFDs.

2.6 Proposed Mechanism

Using available literature on wet granulation and agglomeration in AFDs, a new mechanism for undesired agglomeration during agitated drying is proposed (Figure 2.10), as a function of three rate processes:

1) Formation of loosely bound agglomerates

The slurry achieved in crystallisation is filtered and often deliquored to form a wet cake (or filter cake). Within this wet cake, there are loosely bound agglomerates.

2) Consolidation and coalescence

Agitation of these wet solids encourages initial consolidation of agglomerates followed by growth by coalescence and/or layering.

3) Solidification of liquid bridges

Wet agglomerates are subjected to agitation during drying, and those able to withstand these shear forces will experience evaporation of solvent from these liquid bridges resulting in solid crystalline bridges cementing the agglomerates.

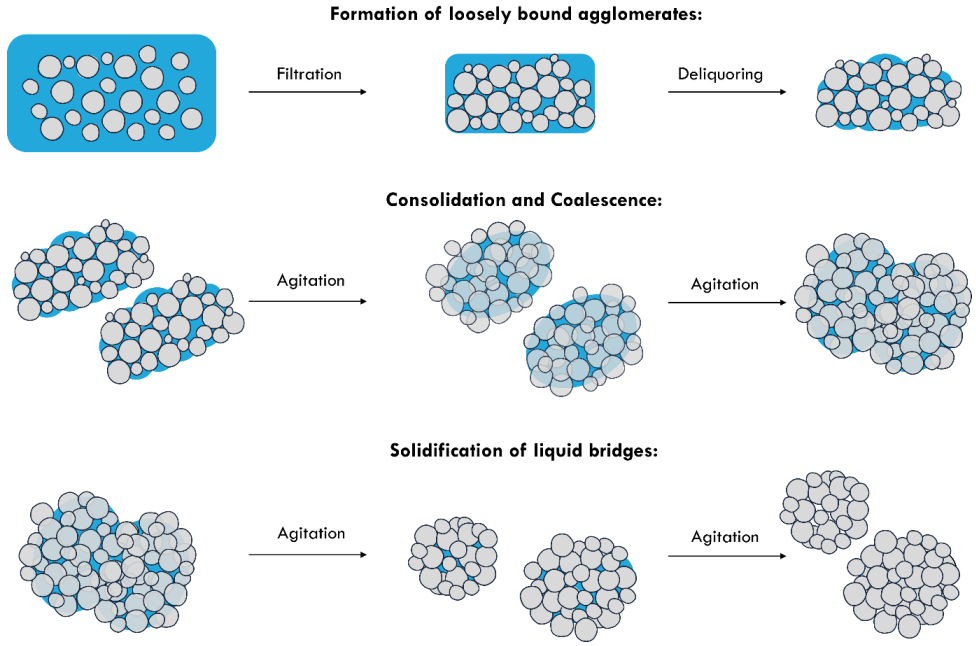

Figure 2.10: Proposed mechanism of undesired agglomeration.

The proposed mechanism will be covered in further detail in Chapter 4, Section 4.2, but for the purpose of this literature review, the key parameters affecting agglomeration in AFDs are organised according to the underlying rate processes they affect. The material and solvent properties available for the studies discussed in the following sections are summarised in Table 2.4, located at the end of Section 2.6.3.

2.6.1 Formation of Loosely Bound Agglomerates

The wet cake is initially formed during the filtration step but may be reformed after the washing step. It consists of loosely bound agglomerates. The wet cake properties are crucial as they influence the effect of subsequent agitated drying and the likelihood of agglomeration. Key parameters that influence the properties of the wet cake during both filtration and washing are discussed in the following sections.

2.6.1.1 Filtration rates

Filtration theory is well established and more in-depth explanations of the parameters affecting the filtration performance can be found in studies by Wakeman and others.[2,41,42] These studies are useful for designing AFD processes with efficient filtration where the filter cake is deliquored to low moisture contents, particularly in the absence of a washing procedure. The key parameters that influence filtration performance and properties of the resulting wet cake can be classified as particle and solvent properties and a brief overview is given in Table 2.2.

Table 2.2: Summary of effect of particle and solvent parameters on filtration rates.

Parameter	Effect on filtration rate
Particle size	By having larger particles, the solvent can readily flow through the openings in the cake, resulting in lower specific cake resistance and better filtration rates.[41,43]
Particle size distribution (PSD)	Having a narrow PSD is ideal for lower cake resistance and greater filtration rates as the filter cake has more open voids for solvent flow. When the PSD is wide, finer particles fill the gaps between larger particles, resulting in higher resistance to solvent flow.[44–46]
Particle shape	Particle shapes with greater aspect ratios such as needles result in high specific cake resistance and poor filtration rates.[41,46]
Solvent viscosity	Low viscosity crystallisation solutions will have less resistance passing through cake pores and this results in better filtration rates.[45,47]

The parameters given in Table 2.2 and their effect on filtration rate and cake resistance is significant due to the consequence of slow filtration rates. High cake resistance gives slow filtration rates which results in longer period of contact between the crystallisation solution and crystals. This can enable the formation of liquid bridges between particles in the wet cake, which solidify upon drying to give agglomerates.[40,45] Even though agglomeration occurring in AFDs is commonly attributed to the drying process, these findings indicate that agglomeration may be initiated much earlier during downstream

processing. This emphasises the need for more meticulous design of filtration processes to not only improve filtration times but reduce the possibility of agglomeration occurring.

2.6.1.2 Design of washing procedure

The reduction in agglomeration as a result of washing was clearly demonstrated in a study by Löbnitz *et al.* when looking at *L*-phenylalanine crystals washed with ethanol.[27] Figure 2.11 shows a clear reduction in the number of agglomerates when washed with ethanol, compared to the unwashed filter cake, due to the crystallisation solvent being replaced by ethanol. By preventing and/or reducing the formation of strong liquid bridges within the wet cake, agglomeration can be reduced. When designing an optimal washing procedure, various parameters must be considered to minimise the potential for agglomeration to occur, and these will be discussed in the following sections.

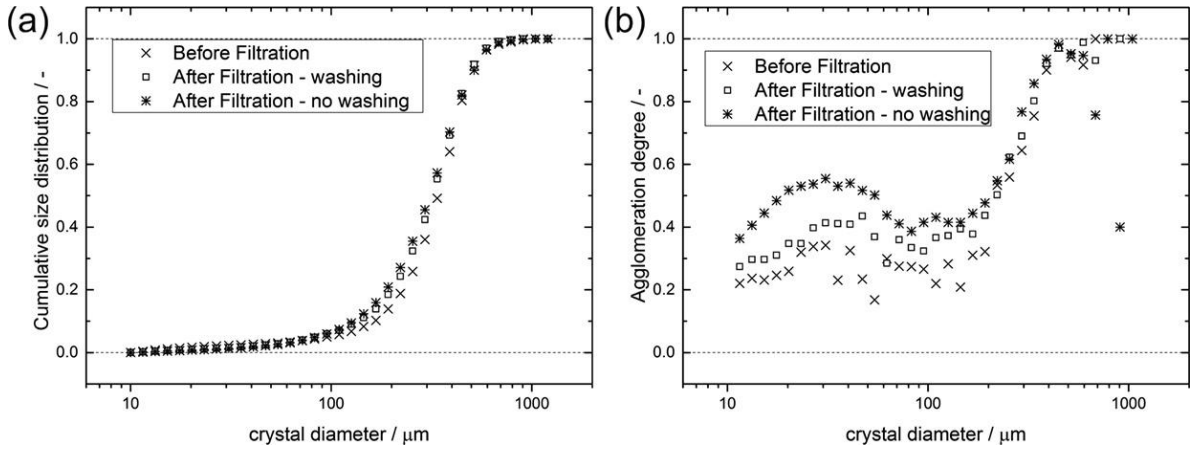

Figure 2.11: (a) PSD and (b) Agglomeration degree (AgD) of *L*-phenylalanine before and after filtration with ethanol wash.[27]

2.6.1.2.1 Solubility of API in the wash solvent

The solubility of the product in the solvent should be minimal to prevent dissolution of the crystals and product loss during washing.[2,48] High solubility of the API in the solvent promotes agglomerate formation and this was investigated by Birch and Marziano.[49] Compound A was washed with four solvent systems of varying solubility, and at lower solubilities, there was not only a reduced likelihood of agglomeration but agglomerates formed were also more friable. Ottoboni *et al.* also investigated the effect of various wash solvents on the extent of agglomeration and agglomerate brittleness index (ABI) for paracetamol (Table 2.3).[45] The greatest extent of agglomeration was seen for isopropyl acetate in which paracetamol has a very high solubility, whereas the least agglomeration was seen with cyclohexane in which paracetamol has a low solubility.

Figure 2.12 also highlights the striking difference between the two samples. The ABI was calculated which is a qualitative measure of agglomerate strength using successive cycles of sieving.[49] The highest API solubility was in acetonitrile, which produced the hardest agglomerates as shown by the ABI value in Table 2.3 and the images in Figure 2.12. The increased solubility allows for more liquid bridges with

dissolved API which solidify upon drying and give hard agglomerates. However, the solubility of impurities present should be sufficiently high to be removed efficiently. A low solubility may facilitate impurities crystallising with the product crystals.[25]

Table 2.3: Agglomerate characterisation for paracetamol with various wash solvents.[45]

Wash solvent	Extent of agglomeration (%)	ABI index
n-heptane,	91.42	**0.223**
Isopropyl acetate	**99.48**	0.113
Toluene	95.52	0.146
Anisole	95.33	0.19
Dodecane	94.59	0.111
TBME	92.57	0.127
Cyclohexane	**87.57**	0.218
4-methylpentan-2-one	95.47	0.197
Acetonitrile	98.29	**0.066**

Figure 2.12: Images of paracetamol agglomerates produced with different wash solvents.[45]

It is also crucial to minimise the solubility difference between the crystallisation and wash solvents, to avoid an anti-solvent effect. This can result in precipitation of both the product and impurities, which can also lead to extensive agglomeration.[50] Although this is a useful tool in anti-solvent crystallisation, controlling it during washing can be challenging, especially if a large volume of crystallisation solvent remains, potentially resulting in significant agglomeration. Shahid *et al.* compared paracetamol isolated from three different crystallisation solvents (ethanol, isopropyl alcohol and isoamyl alcohol) with three wash solvents (heptane, acetonitrile, and isopropyl acetate).[50] Paracetamol has the lowest solubility in heptane and using this as the wash solvent resulted in precipitation regardless of the crystallisation

solvent used. This anti-solvent effect is to be expected given the large solubility difference between heptane and the crystallisation solvents. One method to mitigate this is to use a mixture of the crystallisation solvent and wash solvent for the first wash.[51]

The effect of solvent solubility on agglomeration behaviour is not always clear. Lim *et al.* investigated two food-grade model powders and an API with four different wash solvents and observed significantly reduced agglomeration for sodium hydrogencarbonate ($NaHCO_3$) with reduced solubility.[3] The API intermediate investigated had 82 wt % agglomerates regardless of the solvent system. Both calcium carbonate ($CaCO_3$) and the API are only sparingly soluble in water, but extensive agglomeration was observed suggesting a different underlying agglomeration mechanism to liquid bridges forming. Agglomeration was reduced when washing $CaCO_3$ with binary solvents, possibly due to the reduced surface tension and modified wettability of the particle surfaces. Therefore, the solubility of the API in the solvent may not be the only solvent parameter influencing liquid bridge formation and subsequent agglomeration.

2.6.1.2.2 Viscosity of the wash solvent

Various approaches are used in the pharmaceutical industry for the washing procedure, with some using the same solvent from crystallisation. However, wash solvents often have a lower viscosity than the crystallisation solvent, allowing them to penetrate smaller capillaries within the cake more effectively and displace the crystallisation solvent.[52] To achieve effective displacement, the contact time with the wash solvent must be sufficient and low viscosity wash solvents tend to pass through the wet cake rapidly.[50] Additionally, if there is a large viscosity difference between crystallisation and wash solvents, the less viscous wash solvent would preferentially travel through any cracks or passages between particles as opposed to forcing out the crystallisation solvent.[51]

Tamrakar *et al.* suggested the wash solvent's effect on agglomeration may be due to solvent viscosity, contrasting previous literature which indicate that the solubility is the most influential factor.[6] Micronized acetaminophen (APAP) exhibited greater solubility in methanol but formed more agglomerates with ethanol, which were also more resistant to agitation. The authors attributed this to ethanol's higher heat of vaporisation and boiling point which allows it to remain at a higher moisture content, as well as its higher viscosity. This resulted in the formation of strong solid bridges, as demonstrated by the agglomerates' increased yield strength. Solvent viscosity can impact the deliquoring of wet cakes with more viscous solvents deliquoring less efficiently and resulting in solvent retention.[53] However, the viscosity difference is minimal (0.53 mPa.s for methanol and 1.06 mPa.s for ethanol), making it difficult to conclude that viscosity is the dominating factor for the agglomeration behaviour observed. The effect of viscosity was also highlighted by Zhang *et al.* when investigating Compound A, which was tested in two solvent systems of methanol/water and isobutyl acetate/heptane using mixer torque rheometry (MTR).[54] MTR gives torque measurements at various solvent contents,

indicating the resistance of the mixing blades to movement through the wet solid. Surprisingly, the results indicated a significantly higher agglomeration potential for Compound A in the methanol/water system, despite Compound A's solubility being approximately five times higher in isobutyl acetate/heptane. This could be due to the methanol/water system exhibiting not only a higher viscosity but increased surface tension.

As suggested by Tamrakar *et al.*, the properties of the wash solvent might be the most crucial and controllable parameter to reduce agglomeration during agitated drying.[6] However, the existing literature on the effect of solvents on agglomeration shows disparities and needs further research. This shows the need to move away from viewing agglomeration in AFDs as a function of various parameters and instead identify the underlying rate processes for a better understanding.

2.6.1.2.3 Particle size

The effect of particle size on washing performance is analogous to the effect on filtration. Larger particle sizes have lower cake resistance and allow a higher flow rate of wash solvent. Conversely, small particles have smaller pore networks, and the wash solvent has a much lower flow rate. This results in a prolonged period of contact between the API particles and the solvent, and these liquid bridges facilitate agglomeration upon drying.[41] However, Shahid *et al.* demonstrated that smaller particles also run the risk of being lost during washing. Compared to the granular paracetamol, the micronized and crystalline material have a larger surface area and more likely to dissolve during the washing process.[51]

2.6.2 Consolidation and Coalescence

As the wet cake is agitated during the drying process, the particles and agglomerates collide with each other, the vessel walls and the impeller allowing them to consolidate. This results in smaller, more dense agglomerates. In some cases, this can also squeeze solvent from within the agglomerate to the surface. The presence of wet surfaces then encourages coalescence of agglomerates. Coalescence is categorised as type I or type II. In type I coalescence, the granules coalesce through viscous dissipation in their liquid binder layers before surfaces touch. In this work, we consider type II coalescence, where colliding particles come into contact for a finite time, and a bond is formed. The coalescence is only permanent should the bond be able to resist the shear forces from collisions and agitation. Various parameters influencing the consolidation and coalescence of agglomerates are discussed in the following sections.

2.6.2.1 Moisture content of wet cake

Numerous studies have highlighted the relationship between the moisture content of the wet cake before agitation and the extent of agglomeration. This is due to agglomerates forming by liquid bridges, which is dependent on the amount of solvent. The moisture content defines the saturation state of the agglomerates, which transition through the various states with increasing moisture as shown in Figure 2.13.[34] In the pendular state, particles are held together by lens-shaped rings of liquid (i.e. liquid bridges). Increasing the moisture results in a more continuous network of liquid, which is the funicular state. When the particles are fully saturated and all pores are filled, the capillary state is reached. The droplet stage is when the particles are held within a liquid drop. Using MTR to investigate these saturation states has shown that the torque peaks when particles are within the capillary state.[49,55] This moisture content is known as the 'sticky point' at which agglomeration is most likely, and this varies for different solid/solvent systems. The combined effect of capillary forces peaks at the sticky point so agitation would promote agglomeration.[49]

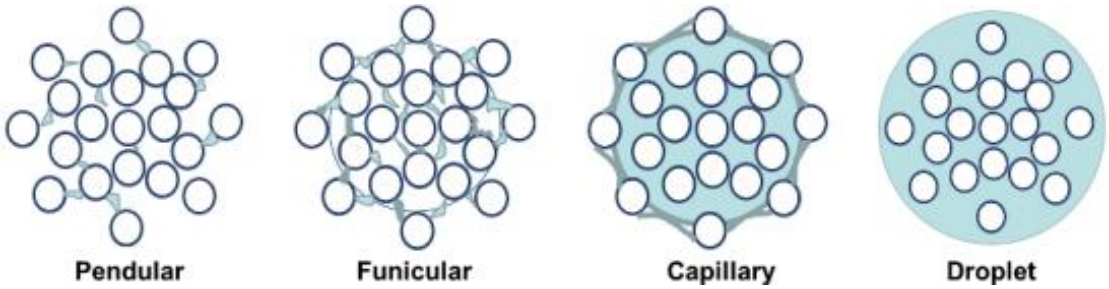

Figure 2.13: States of liquid saturation for agglomerates.[56]

As MTR gives a measure of torque at different solvent contents, it is often used to determine the sticky point so agitation can be avoided until the moisture content is lower than this value. This has been experimentally validated by various researchers who observed increased agglomeration when the wet solid was agitated at or beyond the sticky point.[40,55] Shin *et al.* used MTR to investigate an AbbVie compound (ABT-089) where torque readings at various moisture contents (using a 7:3 ethanol-

methanol mixture) were validated by characterisation of the dry agglomerates.[55] This allowed them to define a 'risky zone' for the compound, as shown in Figure 2.14, which describes moisture contents of the sticky point and higher, which also corresponds to a change in granule saturation from funicular to capillary state. The sticky point is not only important to assess optimal moisture content but also gives an indication of the hardness of agglomerates, relative to the maximum torque value. However, using a sieving method can be more accurate and straightforward. The percentage of the initial mass sieved that is retained by the sieve also indicates the extent of agglomeration.[49]

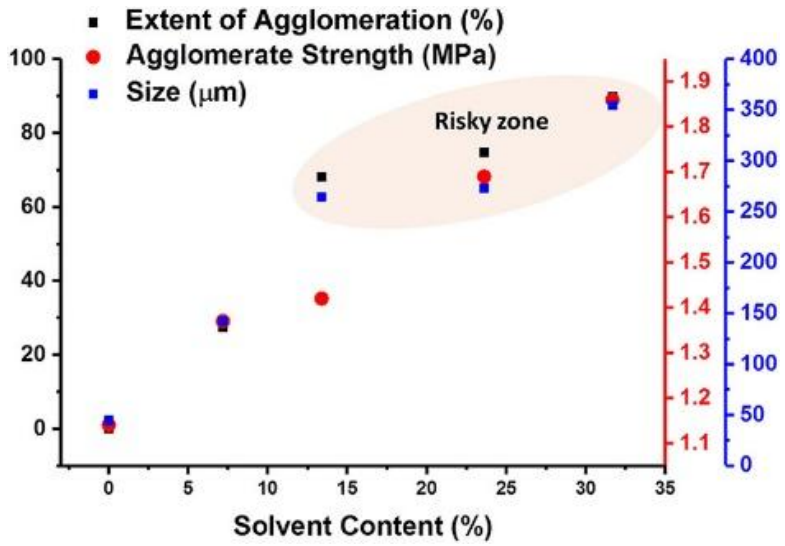

Figure 2.14: The variation in extent of agglomeration, agglomerate strength, and size as a function of the solvent content.[55]

Zhang and Lamberto probed the validity of MTR as a useful tool by using an acoustic mixer. The results from MTR were not only in agreement at lab-scale with the acoustic mixer but also pilot plant data.[54] In lab scale experiments, the torque was measured as increasing amounts of isopropanol were added to the powder bed (Compound B), but at pilot scale the torque was recorded as the wet cake dried. Despite this difference, the torque profiles for both showed good agreement, with both having a maximum torque at a loss on drying (LOD) of 38 %, validating the use of MTR. However, MTR experiments function as a guide but do not fully simulate agitated drying. It gives a measure of the potential to agglomerate when a wet mass is agitated but is not definitive. Some materials show a high propensity for agglomeration but are deliquored well and have a low moisture content before drying, showing little agglomeration upon scale-up. For better accuracy, MTR data should be used alongside the moisture content post-filtration to assess the risk of agglomeration, particularly upon scale-up.[40]

Birch and Marziano measured the sticky point of different particle sizes of Compound A using 2-methyl tetrahydrofuran/water and acetone/water washes and observed that smaller particles required larger amounts of solvent to reach the sticky point.[49] The capillary forces act on a larger surface area and smaller particles need more binder to achieve the same capillary forces as larger particles. This highlights the variance of the sticky point with different particle sizes, even in the same solid/liquid

system. However, the sticky point and the relationship between moisture content and extent of agglomeration have been well researched on both lab scale equipment and pilot plant AFDs.[40,57]

2.6.2.2 Solvent viscosity

Ottoboni *et al.* showed that the solvent viscosity has a knock-on effect on the residual moisture content prior to drying, with more viscous solvents resulting in greater solvent retention in the wet cake.[45] By having more wet surfaces, this not only increases particle mobility for consolidation but also facilitates coalescence of agglomerates. Viscous solvents are also effective in dissipating kinetic energy of collisions, which also promotes coalescence. The effect of solvent viscosity is a complex phenomenon as observed with Avicel, a microcrystalline cellulose, which was wetted with both water and isopropyl alcohol. Despite having a low solubility in both solvents, Avicel demonstrated a greater potential for agglomeration in water, the less viscous solvent, and this was confirmed experimentally.[40] However, this may not be due to the viscosity difference but rather the swelling behaviour often seen with Avicel in water. This polymeric compound can absorb large amounts of water and expand in volume (swell) as a result. The absorbed water is strongly bound within the polymer matrix and has much higher binding forces than the water loosely bound to the polymer chain (free water).[58] It should be noted that Avicel is used as a binder and is not representative of typical APIs. In contrast, most APIs are molecular substances that do not absorb water and swell but instead dissolve to various extents. More investigation is required for a more comprehensive understanding of the interplay between solvent properties such as solubility and viscosity to predict agglomeration accurately.

2.6.2.3 Solvent surface tension

Solvents with high surface tension, such as water, may encourage more and stronger liquid bridges due to their hydrogen bonding ability, leading to increased agglomeration. Lim *et al.* found that using a binary solvent mixture of 1-propanol with a lower surface tension reduced the agglomeration of $CaCO_3$.[3] The reduced surface tension can modify the critical moisture content (CMC) or 'sticky point' and reduce agglomeration, as well as agglomerate strength. The correlation between the surface tension of the solvent and agglomeration for $CaCO_3$ can be seen in Figure 2.15. This finding was further supported by Zhang and Lamberto who used MTR and observed that solvents with high surface tension resulted in higher torque readings, indicating a higher risk of agglomeration during drying.[54] This effect has also been reported in wet granulation literature, where although reducing the surface tension may increase the rate of consolidation, the extent of this is lower.[59]

A different study examining the effect of eight different solvents on a Takeda API showed no correlation between viscosity or surface tension and the agglomeration potential.[60] This may be due to the contrasting effects of reducing surface tension on consolidation and coalescence. Although it may increase the consolidation, it results in agglomerates with weaker bonds, which therefore reduces the chance of permanent coalescence.

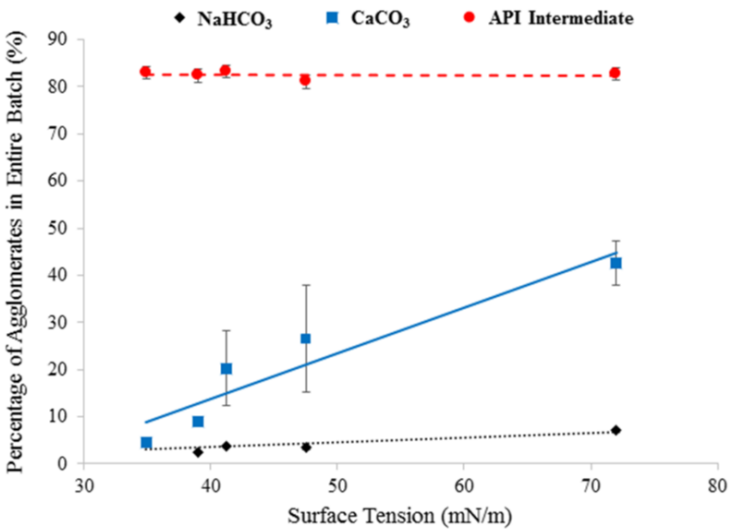

Figure 2.15: Effect of increasing surface tension on agglomeration of $NaHCO_3$, $CaCO_3$ and an API intermediate.[3]

2.6.2.4 Particle size

The effect of particle size on solvent retention was discussed previously in Section 2.6.1.2.3, and as a result of poor solvent removal, smaller particles tend to stay wetter which naturally facilitates both consolidation and coalescence. Smaller particles also tend to agglomerate due to a greater contact area with the solvent allowing liquid bridges to form.[61] This was observed by Papageorgiou *et al.* when coarse (d_{10} = 4.6 µm, d_{50} = 14.1 µm, d_{90} = 40.5 µm), fine (d_{10} = 2.5 µm, d_{50} = 6.2 µm, d_{90} = 13.8 µm) and micronized (d_{10} = 0.4 µm, d_{50} = 1.9 µm, d_{90} = 4.3 µm) grades of a Takeda API (TAK-117) in water were compared. As seen in Figure 2.16, the micronized API had the lowest friability and hence exhibited the highest potential for agglomeration. This behaviour has been reported in wet granulation literature where small particles produce very strong granules that do not deform and cannot coalesce with other granules unless there is solvent available at the surface.[37]

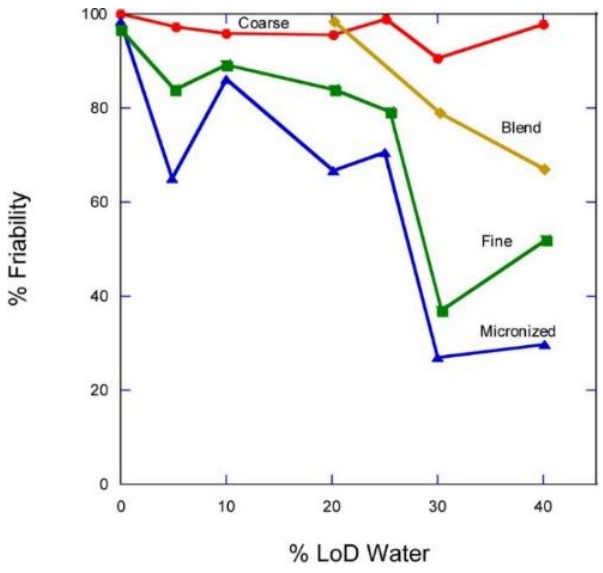

Figure 2.16: Effect of particle size on agglomerate friability for Takeda API TAK-117 with water.[60]

A blend of 75 % coarse API and 25 % micronized API was also investigated, and this showed a significantly higher agglomeration risk compared to the coarse API. This demonstrates how even a small number of fines can exacerbate agglomeration.[60] The presence of finer particles leads to less void space and higher compaction, resulting in higher cohesion between particles, and potentially cake hardening and heel formation. Therefore, wide PSDs are not ideal when aiming to minimise agglomeration.[40]

2.6.2.5 Particle shape

Agglomeration is greatly influenced by crystal properties including morphology, and it was shown by Schæfer that interlocking between plate or needle morphologies often results in weak agglomerates.[62] Irregularly shaped particles such as needles are sensitive to attrition and more likely to be broken down whereas spherical particles are less prone to attrition or breakage.[6,63] However, a mixture of needle or plate crystals with spherical crystals generates stronger agglomerates, with the strength increasing as a function of shape irregularity.[62] This is because coarse, irregular particles increase the internal friction of the packed bed and reduce the flowability, resulting in poor mixing. This leads to increased solvent retention which encourages consolidation and coalescence of agglomerates.[30]

2.6.2.6 Agitation time

Agitating the wet cake promotes the consolidation and coalescence of agglomerates. However, agitating for prolonged periods may result in breakage or fragmentation. This can be seen in the work by Tamrakar *et al.* where the median particle diameter reaches a peak at approximately 7 minutes into the 24-minute agitation period, for moisture contents of 5 %, 15 % and 25 %.[6] Further agitation results in the breakage of agglomerates. However, there may be an upper limit for this as reported for carbamazepine dihydrate, where there is an increase in breakage for up to 20 minutes agitation, but further agitation for 40 minutes shows no further breakage.[64] This may be due to smaller crystals being harder to break. This is also seen in the wet granulation literature where some authors report larger granules with increased wet massing times, whilst others observed a decrease in granule size.[65–67]

2.6.3 Solidification of Liquid Bridges

The drying stage in AFDs is most commonly associated with undesired agglomeration, as it is during the post-drying phase that agglomeration is typically characterised. Drying involves simultaneous heat and mass transfer and is influenced by a multitude of material and process parameters. This complex interplay of powder, solvent and equipment parameters has resulted in significant challenges in predicting drying performance. Kemp and Oakley have even gone as far to describe drying as 'the graveyard of academic theory' due to the lack of accurate, predictive models.[68] The reported effects of various material and process parameters on the solidification of liquid bridges are discussed in the following sections.

2.6.3.1 Particle solubility in solvent

Although the choice of crystallisation and wash solvents and the influence of the particle solubility have been discussed in the previous sections, it is essential to consider how solvent selection affects the drying process itself. The solubility of the solids in the solvent/solvent mixture influences agglomeration. When solvent is removed during drying, any compounds dissolved in the solvent will precipitate, potentially forming solid bridges that facilitate agglomeration. The greater the solubility of solids in the solvent, the more likely solid bridges will form.[6] When particles have a high solubility in the crystallisation solvent, the agglomerates formed also tend to be harder and difficult to break.[45]

2.6.3.2 Boiling point of solvent

The agglomeration of wet particles is usually facilitated when the residual solvent around the particles becomes more viscous during drying, and this viscous film binds particles together.[69] However, solvents with low vaporisation enthalpies and boiling points evaporate quickly and do not allow this to occur. This was seen by Tamrakar *et al.* when investigating the use of four different solvents (methanol, ethanol, water, and acetone) with APAP.[6] The lowest vaporisation enthalpy and boiling point was for acetone, and the APAP/acetone samples showed the least agglomerate growth. Solvents with higher boiling points require longer drying times which prolongs the time in which the wet cake is agitated. This promotes solid bridge formation and was observed in the drying of APAP with ethanol and methanol, where the APAP/ethanol system resulted in more agglomerates. Ethanol has a higher boiling point, and the system remained at a higher moisture content resulting in more agglomeration.[6] This highlights the need to consider solvent boiling points when designing optimal drying processes.

2.6.3.3 Solvent composition

Multicomponent solvents are used to reduce the surface tension and particle solubility and remove impurities more effectively in filtration. It is important for solvents to have similar boiling points to reduce agglomeration as otherwise, one solvent may become more enriched in drying. If the particles have a higher solubility in this solvent, this can lead to dissolution and recrystallisation and bridging of

crystals.[40] Also, if the wettability of the crystallisation solvent is high then the wash solvent needs a similar wettability to efficiently remove the crystallisation solvent and reduce agglomerate formation.[45]

Hydrophobic compounds have been shown to form agglomerates in aqueous systems due to hydrophobic interactions. In these systems, the water molecules preferentially form hydrogen bonds with each other, excluding the hydrophobic particles from the solvent.[70] This exclusion results in mutual attraction between hydrophobic compounds, forming agglomerates that are typically held together by relatively weak binding forces. Research has shown that the surface hydrophobicity of particles has a linear correlation with the potential energy for hydrophobic attraction and the extent of agglomeration.[71]

Lim *et al.* reported another interesting observation where alcohol washes not only reduced agglomeration but formed much weaker agglomerates. Alcohols such as ethanol form surface alcoholic functional groups such as ethoxy groups and this reduces hydrogen bonding between hydroxyl groups on the surface of the particle.[72] Hydrogen bonds cannot form between terminal ethoxy groups of different particles, unlike water. This results in a steric effect where individual particles are prevented from being attracted to each other which inhibits agglomerate formation as no chemical bonds form between particles.[3] This is different to the agglomerate formation in water washes, where although bridging water molecules are lost during drying, the terminal hydroxy groups of particles are in proximity and form hydrogen bonds. As drying continues, chemical bonds are formed between the powder particles, resulting in agglomerates.[72] This is illustrated in Figure 2.17, highlighting the contrasting bonding interactions between water and ethanol washes.

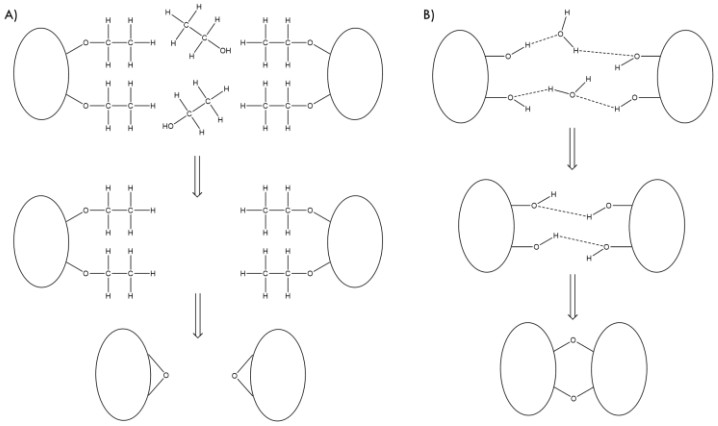

Figure 2.17: Proposed mechanism for agglomerate formation in a) ethanol and b) water washes.[72]

2.6.3.4 Particle shape

Lekhal *et al.* investigated the drying behaviour of *L*-threonine (needles) and potassium chloride (cubic) crystals in water and observed different relationships between the critical moisture content and agglomeration.[57,63] While the critical moisture content for potassium chloride (KCl) was consistent across batches, it showed variation for *L*-threonine with no single value for critical moisture content being established. This can be explained by the difference in particle shape and a wider PSD for *L*-

threonine. Particle shape and size will influence the amount of solvent retained during the drying process and hence facilitate agglomeration at various moisture contents. However, these findings are limited to only two potential crystal morphologies, and more work is needed to establish a more precise understanding of the relationship between particle shape and agglomeration during agitated drying.

2.6.3.5 Particle size

Experiments by Ottoboni *et al.* showed that not only do micronized materials show increased agglomeration compared to original and granular API, but the agglomerates formed are much harder.[45] The increased hardness of these agglomerates makes them less susceptible to breakage by the shearing action of the impeller, in contrast to the softer agglomerates formed with the original API. The enhanced agglomerate strength for micronized material may be related to the increased surface area available for solid bridge formation during drying. However, further investigation is necessary to establish a definitive link, as the agglomerate strength will also have been influenced by the different crystallisation and wash solvents used and the particle solubilities. Unless these factors are isolated, it is difficult to confirm the effect of particle size alone on agglomeration behaviour.

2.6.3.6 Agitation speed

Lekhal *et al.* measured the moisture content of KCl in water over time and found that drying times decreased at higher agitation speeds.[57] Similar drying rates were observed at lower agitation rates, whereas higher agitation speeds resulted in an increased drying rate. Agitation enhances heat and mass transfer by improving the mixing which increases the rate of drying.[63] The average diameter of particles decreased at higher agitation speeds. This suggests less agglomeration with increased agitation, due to greater shearing action and more particle collisions. At low agitation speeds, a higher fraction of larger particle sizes was observed after drying compared to before, as shown in Figure 2.18. This suggests that agglomeration is more prevalent at lower agitation rates as a result of the sample experiencing less shearing action from the impeller, and therefore solid bridges holding agglomerates together are less likely to break. Lower drying rates at lower agitation speeds allow prolonged periods of contact between crystals, further increasing the likelihood of agglomeration.

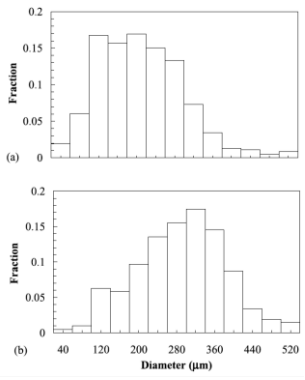

Figure 2.18: Particle size distribution of *L*-threonine (a) prior to drying and (b) after drying.[63]

Sahni *et al.* investigated the effect of agitation speed on the drying of lactose monohydrate in ethanol and observed a sharper decrease in solvent content at higher agitation speeds, along with a shift to the left in the PSD, indicating attrition had occurred.[4] Further analysis of the PSD suggested that more fines are generated at lower impeller speeds as attrition occurs. At higher agitation speeds, there are less fines produced, and fragmentation dominates. Several studies have reported a decrease in particle size with increased agitation. [63,73] Schæfer et al. proposed that the agglomeration behaviour is a function of the impeller speed and power input.[74]

The impact of increased agitation speeds on agglomeration shows variation between materials as demonstrated by Lim et al.[3] Increasing the agitation speed fivefold led to a threefold reduction in agglomerates for $NaHCO_3$ but had a negligible effect on $CaCO_3$. For $CaCO_3$, some snowballing was observed as soon as agitation began, and although greater agitation helped to break down agglomerates into smaller fragments, it was not possible to completely remove agglomerates. This was also seen with carbamazepine hydrate crystals where the effect of increasing the agitation speed on the PSD was minimal.[64] This contrasts other studies where there is a significant change in the PSD with increased agitation and shows the importance of considering material properties. Some materials are sensitive to strain rate and likely to show a greater change in their PSD. Therefore, it is crucial to consider the strength of materials when investigating the effect of increased agitation. If the liquid bridges can withstand the shear forces of agitation, they will solidify upon drying and result in agglomerates.

2.6.3.7 Agitation time

The agitation time can also impact the extent of agglomeration. Experiments conducted by Tamrakar *et al.* showed an interesting trend in PSD over the agitation period for various moisture contents.[6] Even at 0 % moisture content, due to the cohesive nature of the APAP powder used, agglomerates formed from the impeller agitation, and these agglomerates maintained their size throughout the agitation period. However, for 5 to 25 % moisture content, the agglomerates showed almost identical behaviour of alternating increase and decrease in PSD span over the drying period, as shown in Figure 2.19. The initial nuclei formed will grow by layering of fines to a certain size, but the free solvent will evaporate as the drying continues, and only weak agglomerates will remain. These weak agglomerates subsequently break, resulting in a continuous cycle of agglomeration and breakage. This cyclic behaviour is evident in the larger PSD spans observed at higher moisture contents.

These results show good agreement with previous studies that also investigated the effect of agitation time on agglomeration.[63,75] However, to determine the underlying mechanisms occurring and apply these observations to various powder/solvent systems and drying conditions, more work is needed.

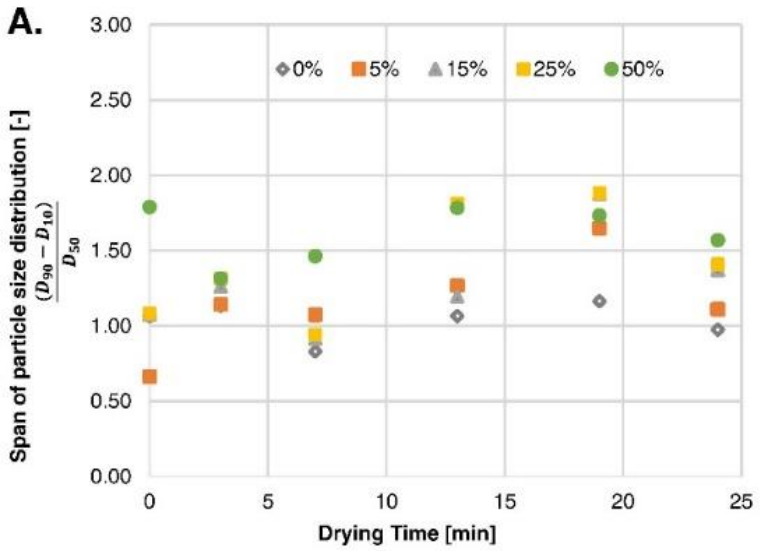

Figure 2.19: PSD span of APAP-methanol samples over time at different L/S ratios.[6]

2.6.3.8 Drying temperature

Lim *et al.* reported an increase in temperature resulted in more agglomerates in the drying of $NaHCO_3$ and $CaCO_3$.[3] Drying at higher temperatures reduces drying time and minimises the particles' exposure to the agitator, allowing more liquid bridges to solidify during drying.[63] Agglomerates produced at higher drying temperatures are often stronger and require intense milling, as seen with KCl in a study by Lekhal *et al*.[57] This is due to particles having a higher solubility at increased temperatures, allowing stronger solid bridges to form.

Contrasting effects were seen for $NaHCO_3$ where despite increased agglomeration at higher drying temperatures, the agglomerates formed were weaker.[3] This may be due to the surface crust formed on agglomerates being thicker and denser because of increased dissolution of solids. At higher drying temperatures, there will be significant stresses within agglomerates as they shrink due to moisture evaporation. A thick dense crust will be unable to shrink resulting in cracking of the agglomerates, hence reducing their strength.[63] There was also no significant change in the strength of $CaCO_3$ and API intermediate agglomerates investigated at higher temperatures.[3]

There is a vast amount of literature on the effect of drying temperature on agglomeration, both in agitated dryers and other systems.[4,69,76,77] However, additional studies are required for a more comprehensive understanding of how drying temperature can affect the agglomerate strength, which will also determine if agglomerates are likely to be broken during agitated drying.

2.6.3.9 Operating pressure

Lower pressures are used to reduce drying times, but this faster rate of drying means particles experience less shear and agglomeration occurs. Lekhal *et al.* investigated the change in average particle diameter of KCl in water with increasing temperature at three different pressures as shown in Figure 2.20.[57]

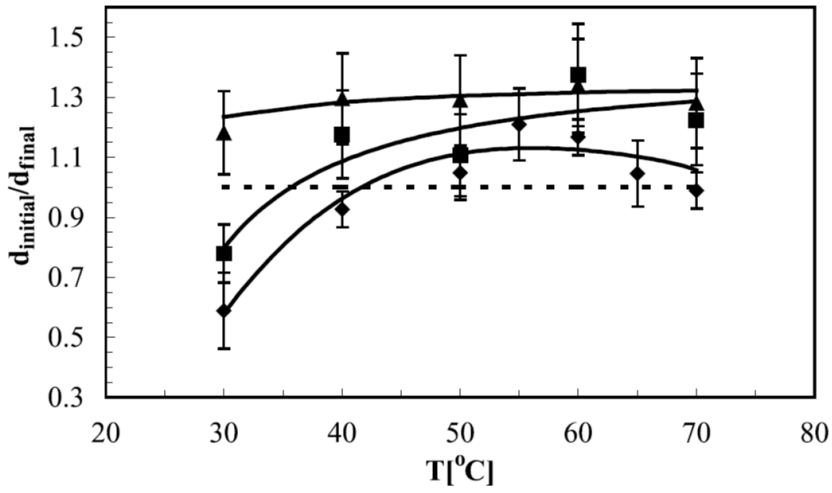

Figure 2.20: Change in average diameter with increasing temperature at different pressures (♦ P =1 atm, ■ P=200 Torr, ▲ P=80 Torr).[57]

It is evident that the average diameter experiences a general increase as the pressure is decreased, regardless of the temperature. However, this becomes less pronounced at higher temperatures (above 50 °C), where the drying rate is high and hence changing the pressure has minimal effects. However, at lower temperatures at approximately 30 °C, reducing the pressure switches the drying from a regime where attrition dominates to an agglomeration dominated regime. This transition can be attributed to the improved drying rates observed. As seen in Figure 2.20, when the pressure is very low (80 Torr), the average diameter has little variation with increasing temperatures. This phenomenon occurs as the low pressure means the liquid is boiling at any given temperature and the drying time is constant. Therefore, at very low pressures, the agglomerate size is independent of the drying temperature. Overall, the findings highlight the relationship between pressure, temperature, and average diameter. However, a significant limitation of this study is that it does not account for the potential variations in results based on different particle properties, such as hardness and crystal solubility. Therefore, further investigation is necessary to gain a more comprehensive understanding of the influence of pressure on drying processes.

2.6.3.10 Fill level

The fill volume of the dryer also affects agglomeration, and this was reported by Sahni *et al* when investigating lactose monohydrate in ethanol.[4] At lower fill levels, narrower PSDs were seen alongside smaller average particle sizes. Lower fill levels allow more particles to experience the shearing action of the impeller as well as more particle-particle collisions. At higher fill levels, fewer particles encounter the impeller blades and there is an increase in particle size and a wider PSD. There is also a greater resistance to heat transfer which results in longer drying times. Also, the PSD for the highest fill level was bimodal due to attrition occurring near the impeller and agglomeration occurring above the impeller. Similar observations were reported by other authors who also observed reduced agglomeration at lower fill levels.[3,78]

Table 2.4: Summary of particle and solvent properties for the studies discussed in Section 2.6.

Material	Crystallisation Solvent	Wash Solvent	Particle Shape	Particle Size	Reference
L-phenylalanine	Saturated solution of *L*-phenylalanine	Ethanol	-	-	Löbnitz *et al.*[27]
Compound A	2-MeTHF/Water	Acetone/water 1:1 v/v 2-MeTHF 2-MeTHF/water 99:1 v/v 2-MeTHF/water 96:4 v/v	-	-	Birch *et al.*[49]
Micronized Paracetamol	Ethanol Isopropanol Isoamyl alcohol	n-heptane Isopropyl acetate Toluene Anisole Dodecane TBME Cyclohexane 4-methylpentan-2-one Acetonitrile	-	d_{10} = 9.58 µm d_{50} = 24.55 µm d_{90} = 51.11 µm	Ottoboni *et al.*[45]
Crystalline Paracetamol				d_{10} = 23.85 µm d_{50} = 64.03 µm d_{90} = 179.14 µm	
Granular Paracetamol				d_{10} = 273.91 µm d_{50} = 363.58 µm d_{90} = 462.26 µm	
Crystalline Paracetamol		n-heptane Acetonitrile Isopropyl acetate	-	d_{10} = 12.48 µm d_{50} = 43.96 µm d_{90} = 101.30 µm	Shahid *et al.*[50]
Calcium Carbonate	Water	Ethanol 1-Propanol 2-Propanol Acetone	-	d_{50} = 9.5 µm	Lim *et al.*[3]
Sodium Hydrogencarbonate				d_{50} = 82.1 µm	
Model API				d_{50} = 13.2 µm	

Micronized Paracetamol	-	Water Methanol Ethanol Acetone	-	d_{50} = 30 µm	Tamrakar *et al.*[6]
Jet milled Compound A	-	Methanol/water 1:4 Isobutyl acetate/heptane 1:4		$d_{4,3}$ = 6.3 µm d_{90} = 11.6 µm	Zhang *et al.*[54]
AbbVie compound (ABT-089)	-	Ethanol/methanol 7:3	Needle-like	d_{10} = 13 µm d_{50} = 35 µm d_{90} = 81 µm	Shin *et al.*[55]
Avicel	-	Water Isopropyl Alcohol	-	-	Am Ende *et al.*[40]
Micronized Takeda API (TAK-117)	-	Water	Needles	d_{10} = 0.4 µm d_{50} = 1.9 µm d_{90} = 4.3 µm	Papageorgiou *et al.*[60]
Fine Takeda API (TAK-117)				d_{10} = 2.5 µm d_{50} = 6.2 µm d_{90} = 13.8 µm	
Coarse Takeda API (TAK-117)				d_{10} = 4.6 µm d_{50} = 14.1 µm d_{90} = 40.5 µm	
L-threonine	-	Water	Needles	-	Lekhal *et al.*[63]
Potassium Chloride	-		Cubic	-	Lekhal *et al.*[57]
Lactose Monohydrate	Ethanol	-	-	d_{90} = 189.83 µm	Sahni *et al.*[4]

2.7 Computational Modelling of AFDs

Simulating drying processes and the resulting agglomeration (or attrition) has long been a challenging task due to the simultaneous heat, mass and momentum transfer. There is no universal drying protocol for pharmaceutical compounds due to variations in the physicochemical properties of the wet cake.

The different approaches to modelling AFDs can be broadly categorised as continuous and discrete particle models and will be briefly discussed in the following sections. The limited modelling work on AFDs and gaps in the work will also be outlined.

2.7.1 Continuous Models

The continuous approach, developed by Schlünder and colleagues, is based on modelling heat penetration through a particle bed. This penetration model has significantly advanced our understanding of contact drying in mechanically agitated powder beds.[79–82] In this penetration model, the particle bed is considered as a quasi-continuous phase, and the mixing process is divided into a series of contact drying and mixing periods. During the hypothetical contact drying period (t_R), the agitated bed is assumed to be static, and a distinct drying front penetrates from the hot surface into the bulk. Any particles between the drying front and heated surface are considered dry whereas particles beyond the drying front are uniformly wet. The bed temperature is assumed to be uniform, and the bulk material is assumed to be perfectly mixed at the end of the contact time. The contact time (t_R) can be described as a function of the dimensionless mixing number (N_{mix}) and the inverse of rotational frequency (t_{mix}):

$$t_R = t_{mix} N_{mix} \tag{2. 11}$$

The mixing number is related to the Froude number and is also dependent on the agitator type.[82] The penetration model states that the overall heat transfer coefficient, α, can be expressed as the sum of the inverse of the wall to first layer heat transfer coefficient, α_{ws}, and the heat transfer coefficient of the dry bed, α_{bed}:

$$\frac{1}{\alpha} = \frac{1}{\alpha_{ws}} + \frac{1}{\alpha_{bed}} \tag{2. 12}$$

Extensive literature is available on the relevant equations and summaries of the penetration model developed by Schlünder and co-workers, so these will not be repeated here.[83,84] The widespread use of the penetration model can be attributed to its ability to be applied to various contact drying operations. It has been extended to various conditions such as vacuum drying, hygroscopic materials, drying under atmospheric pressure and drying paste-like materials, and is widely covered in literature.[80–82,85–87]

Despite the prevalent use of continuous models, which are also an industry standard, there are several limitations to be considered. One caveat is the key parameters of the model, contact time (t_R) and the mixing number (N_{mix}), are not based on theory and are empirical. Mollekopf addressed this by correlating N_{mix} to the Froude number (Fr) as shown in Equation 2. 13, where C and x are constants that vary for various dryer types.[82]

$$N_{mix} = CFr^{x}$$

2. 13

The values of C and x were experimentally determined, and these values can be found in the literature.[84] However, it is important to note that the data available to Mollekopf was limited and was based on two tray dryers, two paddle dryers and a rotary drum dryer. It is difficult to find values of N_{mix} for different applications as it will vary for different agitators and dryer type and size. The penetration model also does not account for the behaviour of particles and any inter-particle interactions and neglects the mechanics of particle motion.

2.7.2 Discrete Models

The weaknesses of the penetration model can be addressed by using discrete approaches such as the discrete element method (DEM). In DEM, individual particles within a dryer can be simulated and it can resolve the motion of each particle and calculate temperature changes as a result of collisions. The key assumption of DEM is that the time step chosen in the simulation is small enough for the interaction force to only apply to adjacent particles. By considering the properties of individual particles, DEM is a useful tool for modelling granular systems and discontinuous materials. A comprehensive review of DEM and its application in the pharmaceutical industry, published by Yeom *et al.*, can be consulted for further information.[88]

A key limitation of DEM is the computational time required for simulations, especially for systems like AFDs which contain trillions of particles. The time step (ΔT_{step}) between each iteration of the simulation is set to be less than the critical time step ($\Delta T_{critical}$) and can be calculated as:

$$\Delta T_{step} < \Delta T_{critical} = T_{Rayleigh} = \frac{\pi R\sqrt{\frac{\rho}{G}}}{0.1631\upsilon + 0.8766}$$

2. 14

where R is the particle radius, ρ is the particle density, G is the shear modulus and υ is Poisson's ratio.[89] The computational time required is directly related to particle properties such as density and size. Therefore, one common solution to reduce computational burden is to lessen the number of particles by using larger ones.[90] However, one caveat of this 'particle scaling' approach is that it can have significant effects on calculated particle velocities and often overestimates the degree of mixing. The other method

often mentioned in literature is to reduce the shear modulus value, as this can also reduce the simulation time.[91] It was shown by Lommen *et al.* that this approach is not always accurate and can lead to misleading simulation results.[92] Therefore, it is important to ensure that the effect of varying particle properties to reduce computational burden should be considered.

Researchers have applied DEM to simulate particles in various agitated vessels, such as rotary drums and bladed mixers, which share similarities with AFDs.[93,94] For example, Kwapinska *et al.* modelled heat transfer in agitated beds, with simulation results in good agreement with both experimental data and the penetration model. Although these results were limited to specific cases, it highlighted that DEM has the potential to not only simulate the heat and mass transfer in agitated beds but also provide more information than the penetration model, such as the thermal behaviour.[93] There has also been various work done in the field of wet granulation to look at the flow of wet granular materials.[95–98] Significant progress has been made in simulating particle velocities and size distributions, particularly in high shear granulators, fluidised beds, and twin-screw granulators.

In DEM, contact models can be used to calculate the forces experienced by colliding particles, and can be categorised as soft sphere or hard sphere approaches. In the hard sphere approach, particles are considered rigid, and collisions are instantaneous, with forces between particles not considered. This is usually best for highly agitated systems with rapid granular flow. Conversely, the soft sphere approach considers particles to deform when there are overlaps and assumes that multiple contacts between particles is possible.[99] This model is more commonly used for powder systems as particles tend to be deformable. Contact forces calculated are based on the normal and tangential force components. To calculate these forces, various models have been developed, and a detailed review of these can be found in a review paper by Zhu *et al.*[100]

2.7.3 Modelling AFDs

Table 2.5 provides an overview of modelling work on AFDs. Among these, a few notable studies are discussed in detail to highlight specific advancements and their implications.

Murru *et al.* modelled the drying of various pharmaceutical compounds to predict drying times at pilot plant scale using both static drying and intermittent agitation.[28] The model was validated using a small scale AFD. As it used scale-independent parameters, it proved suitable for scale-up prediction with the best agreement seen for static drying. Across all compounds and solvent systems, the average difference in predicted and actual drying times was 9 % and no greater than 12 %. However, this model still requires experimental input and also neglects any changes in particle size during drying as a result of either attrition or agglomeration.

Table 2.5: Comparison of modelling studies in AFDs.

Material	Solvent	Particle Shape	Type of Agitation	Drying Temperature (°C)	Drying Model	Reference
Paracetamol	-	Spherical	Continuous	-	DEM	Hare *et al.*[101]
Pharmaceutical compounds	Acetone, water, methanol, n-propanol, isopropyl acetate	Unknown	Intermittent	50-70	Penetration	Murru *et al.*[28]
Glass beads, lactose	Ethanol	Spherical	Continuous	45-80	DEM	Sahni *et al.*[102]
API bis-solvate	Ethanol	Unknown	Continuous	50-70	Penetration	Nere *et al.*[1]
Glass beads, lactose monohydrate	Ethanol	Spherical	Continuous	45-80	DEM	Sahni *et al.*[103]
Mono-sized material	Methanol, ethanol	Spherical. Square, Rod, Elongated rod	Continuous	92	DEM	Tamrakar *et al.*[30]
Pharmaceutical intermediate	Unknown	Spherical	Continuous	-	DEM	Sinha *et al.*[61]
Polydisperse cohesionless material	-	Spherical	Intermittent	50	DEM	Chaksmithanont *et al.*[104]

Later work by Sahni *et al.* used DEM to investigate differences between experimental findings and simulations of drying behaviour in an AFD with glass beads and lactose in ethanol. This was the first three-dimensional DEM model to study heat transfer in granular materials in an AFD.[102] The key variation was the decrease of solvent content over time during drying, which was greater in experiments. However, there were also disparities in the average bed temperature for different fill levels.

This was improved on in a later model by Sahni and Chaudhuri by incorporating heat transfer through liquid bridges in numerical simulations of contact drying in an AFD, with glass beads and lactose in ethanol.[103] This improved model was validated with experiments and indicated that vessel wall temperatures and impeller speeds have a considerable influence on the drying rate, due to increased drying temperatures. Another interesting observation was the greater impact of agitation speed on lactose compared to glass beads. For lactose, stable contact force chains form which results in deformation of the powder bed as heaps are formed, leading to recirculation zones. This was attributed to the high friction coefficient of lactose and has been reported by other researchers.[105,106] On the contrary, glass beads have low friction coefficients, allowing particles to slide past each other without forming heaps.

This work by Sahni and Chaudhuri further indicated that the drying performance should not only be considered as a function of process parameters but also material properties.[103] Some disparities between the simulation and experiments were observed and suggested to be due to the slight variations in particle properties and the assumption that particles were monodisperse. Sahni and Chaudhuri also highlighted that models often did not account for changes in particle size during drying due to agglomeration and/or attrition.[103]

Tamrakar *et al.* proposed a model that integrates both wet granular flow and heat transfer models to simulate the simultaneous processes occurring during the operation of an AFD and addresses both drying and agglomeration behaviour.[30] The model uses liquid bridge models for both capillary and viscous forces to calculate the cohesive forces between particles in contact but also calculates a critical separation distance for each contact. Exceeding this distance results in the liquid bridge being broken, reflecting the dynamic bonding occurring between wet granules. They also incorporated the capillary number, Ca, a dimensionless parameter that describes the ratio of viscous forces to capillary forces in a liquid bridge.[107] It is defined by the following equation:

$$Ca = \frac{\mu U}{\gamma} \qquad 2.15$$

where μ is the average viscosity of the fluid, U is the relative particle velocity and γ is the surface tension of liquid. To reflect the dynamic nature of the drying process where the viscosity of liquid is continuously changing, the model implements two conditions for liquid bridge formation. For low

capillary numbers ($Ca < 0.001$), capillary forces dominate and only the capillary force is used. For higher capillary forces ($Ca > 0.001$), both capillary and viscous force components are used. This novel model incorporates many of the phenomena occurring in AFDs and was used to investigate the effect of multiple material and process parameters on both drying and agglomeration behaviour. Although experimental validation is required, this is a great advancement in the modelling of agglomeration behaviour in AFDs.

As shown in Table 2.5, modelling of AFDs remains quite limited, with even fewer studies addressing changes in particle size during drying due to attrition, breakage, or agglomeration. Many models focus primarily on simpler systems such as basic agitated mixers. Although recent studies have made progress by investigating wet granular flow and agitation in heated vessels, significant gaps persist.

DEM has emerged as a promising tool to advance the understanding of agglomeration mechanisms and reduce experimental workload by providing detailed insights into particle interactions at the microscale. However, these models frequently rely on oversimplified assumptions to manage computational costs. As highlighted in Table 2.5, many studies only consider spherical particles or use unrealistically large particle sizes. These do not accurately reflect the irregular shapes and morphologies common in pharmaceutical materials, such as fine particles or needle-like APIs. These simplifications reduce the reliability and applicability of the models to real-world processes. However, the use of graphics processing units (GPUs) has shown promise for more realistic simulations of APIs with non-spherical particles.[108,109] This will allow models to better reflect typical industrial processes in AFDs.

Another key opportunity for this field is integrating wet granulation modelling approaches to improve AFD models. Incorporating both agglomeration and attrition would enable a more comprehensive understanding of the interplay between the two phenomena. There have been significant advances in modelling wet granulation and while not covered in detail here, the following references highlight some notable studies.[110–118] These models have also explored the challenges of scaling up, providing a foundation for developing more comprehensive models to understand and predict agglomeration behaviour in AFDs.

2.8 Conclusions

The widespread use of AFDs across various industries highlights the importance of developing a thorough understanding of undesired agglomeration. Multiple parameters influence agglomeration in AFDs, contributing to complex, simultaneous and often competing rate processes.

Future research should focus on moving away from empirical relationships to a mechanistic understanding, as this knowledge gap has long hindered the accuracy of models. Without a comprehensive understanding of the mechanisms and rate processes involved, any models developed will be significantly limited and unable to simulate the dynamic nature of agglomeration in AFDs, and the competing effects of various parameters.

It is also important for future models to account for the dynamic nature of drying in AFDs. Current computational tools such as DEM are often limited by the computational burden and this results in oversimplified assumptions, such as spherical monodisperse particles of unrealistic sizes. However, advancements such as GPUs provide an opportunity for models to incorporate more representative material properties while managing computational costs. It is also crucial to include attrition and agglomeration behaviour and the interplay between the two. Leveraging advancements in fields like wet granulation where this has been achieved offers an opportunity to address these gaps and refine AFD models.

While considerable progress has been made in recent decades, particularly in understanding the qualitative effects of key material and equipment parameters, a detailed mechanistic understanding remains essential for developing accurate predictive models. This will not only enhance our theoretical understanding but also improve the performance, scalability, and predictability of AFD processes, tackling the ongoing challenge of undesired agglomeration across industries.

Current studies on the effect of agitation speed on agglomeration have largely neglected the influence of material properties such as particle shape, size and cohesion. These properties directly affect how particles respond to shear forces, driving the balance between agglomeration and breakage and determining which mechanism dominates under given conditions. To bridge this gap, this research will investigate how material properties modulate the effects of agitation while highlighting that not all material systems exhibit increased breakage with higher agitation speeds. Additionally, further work will explore the interplay between agitation and other process parameters, such as drying temperature and fill level, and how they influence the extent of agglomeration. These findings will be used to develop a regime map for predicting agglomeration behaviour.

Chapter 3 - Materials and Methods

This chapter outlines the materials investigated and the methodology developed for AFD experiments. It also describes the characterisation methods used for the primary material and agglomerates.

3.1 Materials

Salicylic acid (≥ 98 %) was selected as the model API and obtained from VWR Chemicals. It was chosen due to its well-known properties: low solubility in water, propensity to agglomerate and similarity to a typical API. The salicylic acid powder consisted of very fine particles with a needle-like morphology. A size fraction below 106 µm was chosen as the primary material for the experiments. During the analysis of experimental results, any material exceeding 106 µm was classified as agglomerates. This approach was taken because sieving is less accurate for measuring particle sizes below 100 µm. Therefore, the agglomerate size distribution (ASD) was measured instead of analysing the full PSD. The powder was sieved to obtain a suitable size fraction for experiments, with the PSD data presented in Table 3.1. Further details of the sieving analysis are given in Section 3.6.1.

Table 3.1: Size analysis of salicylic acid as received and sieved.

Material	d_{10} (µm)	d_{50} (µm)	d_{90} (µm)
Salicylic acid (as received)	24.9	60.6	136
Salicylic acid primary material (sieved with 106 µm sieve)	22.3	52.3	111.0

Distilled water was chosen as the solvent due to the low solubility of salicylic acid at 25 °C. The distilled water was prepared using a Stuart D4000 Distinction water still.

3.2 Primary Material Characterisation

3.2.1 Sieving of Primary Material Size Fraction

Salicylic acid was sieved using a 106 µm mesh size sieve and a receiver pan at an amplitude of 0.85 mm/g for 12 minutes. Only material passing through the sieve was used in experiments, and this size fraction will be referred to as the primary material hereafter. This ensured the primary particle size is ≤ 106 µm, allowing particles larger than 106 µm to be classed as agglomerates. Although there is the possibility of agglomerates below this size, it was regarded as negligible. Further detail of the sieving technique is given in Section 3.6.1.

3.2.2 Laser Diffraction

Salicylic acid primary material was analysed using a Malvern Mastersizer 3000 PSA to obtain the PSD and characteristic particle sizes. This technique can measure sizes within the range of 10 nm to 2 mm.

The wet dispersion method was used with a wet sample unit (Hydro E.V.) and the solvent chosen was water. A saturated solution was initially achieved before adding excess salicylic acid. The measurements were conducted at a feed rate of 27 % and 3.6 barg air pressure to obtain a desirable obscuration of 14.33 %.

Laser diffraction is based on the scattering of a laser beam passing through a sample. Large particles have small scattering angles whereas small particles have large scattering angles.[119] The scattering patterns produced allow the particle sizes to be calculated. The output is often different size fractions and the corresponding volume of particles for each size fraction, which are plotted to give a standardised PSD showing the volume distribution. From the PSD, the surface area moment mean ($d_{3,2}$) and the volume moment mean diameter ($d_{4,3}$) can be found. The surface area means, or Sauter mean diameter, is the diameter of a particle with a volume to surface area ratio identical to the sample. The volume moment mean diameter (or De Brouckere mean diameter) denotes the size of the particles which constitute the bulk of the sample.[120]

The PSD of salicylic acid primary material was measured over ten laser diffraction experiments and the average was plotted (Figure 3.1). Average values for the d_{10}, d_{50} and d_{90} were also calculated (Table 3.1). The notation d_x relates to the particle size in which x % of particles are smaller than or equal to. For example, d_{10} gives the size below which 10 % of particles are found. The d_{50} is often referred to as the median particle size with 50 % of particles smaller and 50 % of particles larger.[121]

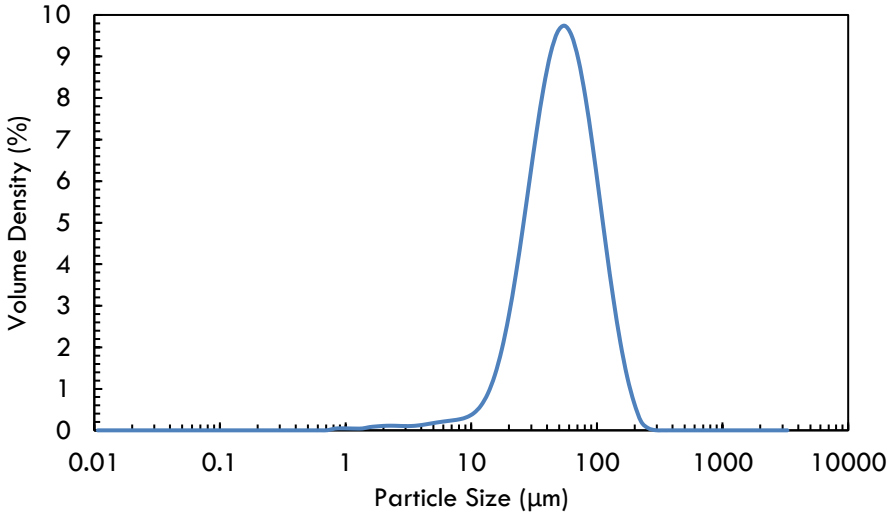

Figure 3.1: Particle size distribution of sieved salicylic acid fraction below 106 µm.

3.2.3 Scanning Electron Microscopy (SEM)

SEM was used to investigate the morphology and surfaces of the primary material in detail. In SEM, a highly focused electron beam is directed at the sample under vacuum, and the emitted secondary electrons are collected to generate images. Secondary electron (SE) emissions, which are sensitive to surface features, were used to study the topography of the material.

Images were acquired using an Inspect F scanning electron microscope. Samples were mounted onto SEM pin stubs using adhesive carbon tape and sputter coated with gold to minimise charging effects. The Inspect F was operated at an accelerating voltage of 10 kV, with a spot size of 3.0 (approximate working distance of 5 -7 mm), using a SE detector.

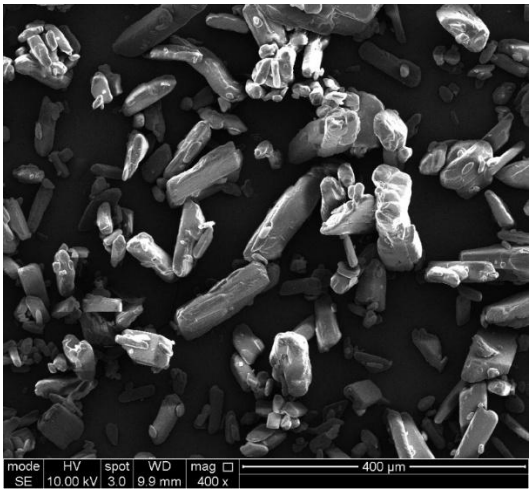

Figure 3.2: SEM image of sieved salicylic acid below 106 µm.

3.3 Agitated Filter Dryer Set Up

A benchtop agitated Nutsche glass filter dryer (GFD ® Lab 010 Series, Powder Systems Limited, UK) with a maximum vessel capacity of 0.3 L was used for experiments with salicylic acid and water. A schematic of the cross-section is shown in Figure 3.3. The overall dimensions of the vessel are 976 mm (H) x 540 mm (W) x 425 mm (D).

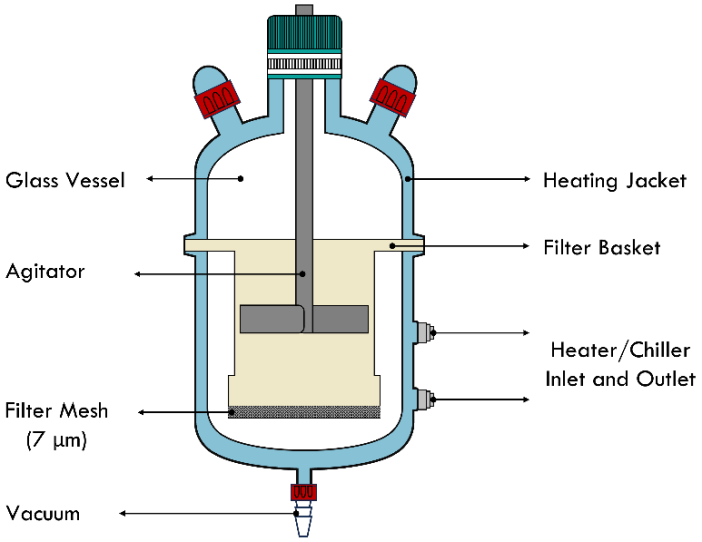

Figure 3.3: Cross-sectional diagram of the AFD.

The AFD was composed of a 3.3 borosilicate glass vessel with an internal polypropylene (PP) filter basket and a PP filter mesh with a mesh size of 7 µm. The filter basket was also fitted with an ethylene propylene diene monomer (EPDM) O-ring. The stainless-steel agitator was secured to the glass vessel

using a polytetrafluoroethylene-polyetheretherketone (PTFE-PEEK) composite seal. The agitation direction can either be forward (ploughing) or backwards (smoothing). The agitator blade had a 45° pitch blade geometry and the relative dimensions of the agitator blade, and the internal filter basket can be seen in Figure 3.4. Table 3.2 also lists relevant dimensions and properties of the AFD.

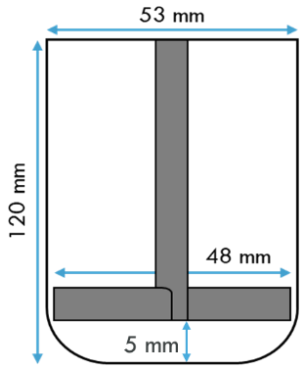

Figure 3.4: 2D schematic of agitator inside the filter basket.

Table 3.2: Important properties and dimensions of the AFD.

Basket Volume (L)	0.3
Internal Filter Basket Diameter (mm)	53
Filter Cake Volume max (L)	0.1
Filtration Area (m^2)	0.002
Agitator Diameter (mm)	48
Agitator Geometry	45° pitch blade
Agitator Speed (rpm)	5 - 100
Sweep Ratio D/T	0.91
Vessel Operating Temperature (°C)	-25 - 150

3.3.1 Modifications and Connections

A premade safety guard fitted with a plastic spacer was added to prevent any possible injury from the exposed rotating shaft.

The jacketed vessel was connected to a Huber Ministat125 heater/chiller, operated at 25 °C. The vessel was also connected to an ME 4C vacuum pump (Vacuubrand) to facilitate the filtration, and this diaphragm pump has a maximum pumping speed of 3.9 m^3/hour and ultimate vacuum of 70 mbar. A gauge (Vacuubrand) was also connected between the AFD and vacuum pump to control and measure the level of vacuum required for deliquoring the wet cake. A control panel was designed to fit the gauge. The experimental set up and control panel is shown in Figure 3.5. A modified Duran bottle was

connected between the AFD vacuum hose tail and the control panel to collect the filtrate. A full image of the AFD setup including all modifications and connections can be seen in Figure 3.6.

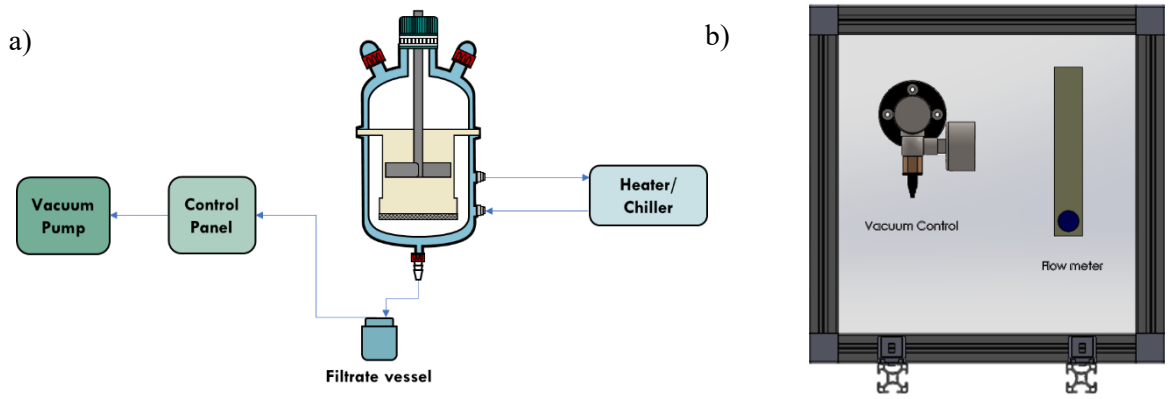

Figure 3.5: Schematic diagram of a) equipment set up and b) vacuum control panel.

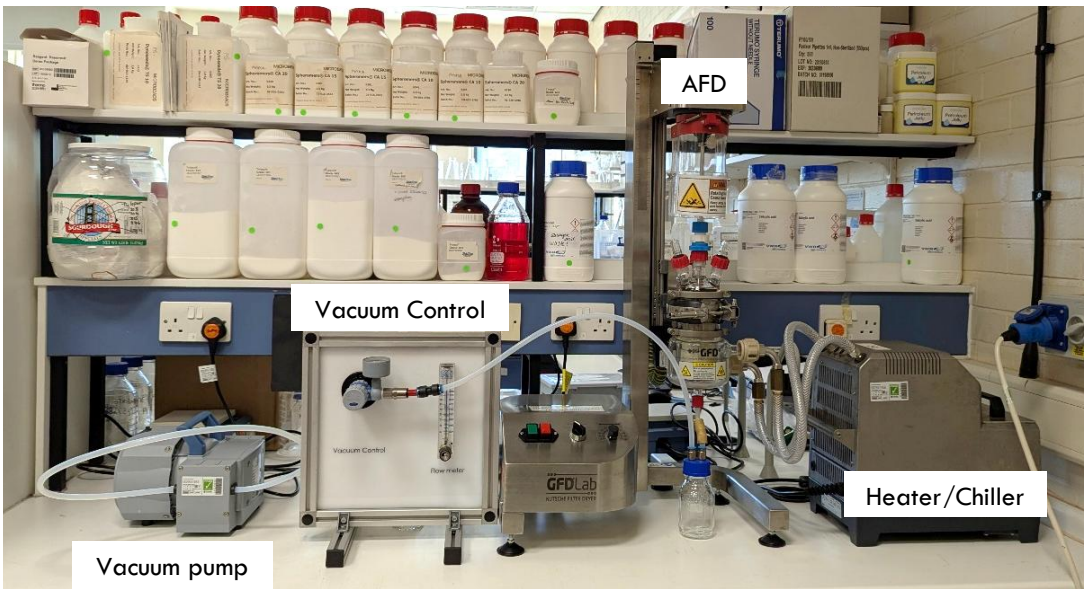

Figure 3.6: AFD set up.

3.4 Experimental Methodology

All experiments were conducted following a specific method to reduce variability in results. A general overview of this is given here but will be described in more detail in the relevant experimental chapters.

The salicylic acid primary material (< 106 μm size fraction) and distilled water were measured into the filter basket. The mixture was gently agitated at 25 rpm for 5 minutes to form a slurry, followed by 5 minutes of settling to form a powder bed. Vacuum was applied for the required deliquoring time to produce a wet cake of the desired moisture content. A schematic of this process is shown in Figure 3.7. The moisture content of the wet cake was then measured using a moisture analyser (Section 3.6.2). Samples are taken from various regions of the filter cake and combined to minimise sampling error.

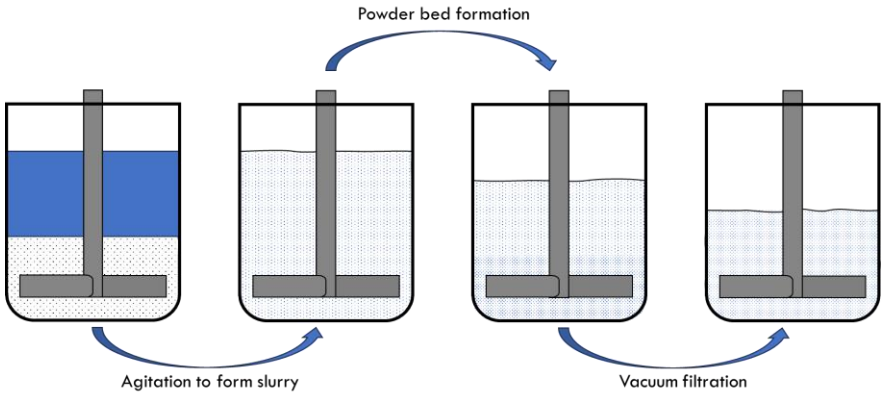

Figure 3.7: Schematic of experimental steps for wet cake formation.

After filtration, the wet cake was agitated under vacuum at 25 °C for the required agitation input, defined by both the agitation speed and time. Following this, the internal filter basket was removed and gently inverted to remove the sample. The sample was then statically dried overnight at 40 °C on a flat tray (215 mm diameter) in a BINDER convection drying oven. Once dried, the samples were characterised as explained in Section 3.6.

3.5 Scale-up Experiments

An industrial placement at the AstraZeneca Macclesfield site in Chemical development provided the opportunity to conduct scale-up experiments. Details of the equipment and characterisation methods are presented in Chapter 6.

3.6 Agglomerate Characterisation

3.6.1 Sieving

For samples with particle sizes exceeding 2 mm, the laser diffraction cannot be used due to size limitations of this technique, and sieving was used to measure agglomerates. Due to the low accuracy of sieving for particle sizes below 100 μm, the ASD was measured instead of the PSD. To minimise sampling errors, the entire batch was sieved for each experiment.

Sieving is used to determine the ASD by vibrating the sample in a sieve shaker through a column of sieves arranged in decreasing mesh sizes from top to bottom. The sample is separated into size fractions retained by each sieve. The weight of sample retained by each sieve is measured and used to calculate the ASD.[122] A Retsch AS 200 Sieve Shaker was used with 200 mm diameter sieves of mesh sizes from 106 μm to 53 mm (increasing by a magnitude of $\sqrt{2}$ per sieve) in order of decreasing aperture size from top to bottom. Samples were sieved for 2 minutes at an amplitude of 0.2 mm/g. This amplitude was carefully selected after testing some agglomerates to see the effect of amplitude on breakage, with no breakage seen until an amplitude of 0.3 mm/g. The sieving time was derived using DIN 66165 which states the optimal sieving time is achieved where after one minute of sieving, less than 0.1 % of the feed quantity passes the sieve. If this value is exceeded, the sieve time should be longer.

In order to obtain the size distribution, each sieve is weighed with and without sample to determine the respective particle masses. These masses are used to calculate the frequency f_i and the log frequency $f_i(\ln x)$ as shown[123]:

$$f_i = \frac{\Delta m_i}{\sum_{j=1}^{n} \Delta m_j} \frac{1}{x_i - x_{i-1}} \tag{3.1}$$

$$f_i(\ln x) = \frac{\Delta m_i}{\sum_{j=1}^{n} \Delta m_j} \frac{1}{\log_{10}(x_i / x_{i-1})} \tag{3.2}$$

where Δm_i is the respective particle mass of a given sieve fraction and x_i is the maximum size of the sieve fraction i. The cumulative frequency F_i is then calculated:

$$F_i = \frac{\sum_{j=1}^{i} \Delta m}{\sum_{j=1}^{n} \Delta m_j} \tag{3.3}$$

Sieving was also used to determine the extent of agglomeration. The methodology set out by Birch and Marziano was employed.[49] Agglomerates were defined as being 106 μm or greater in size and the extent of agglomeration was calculated using the equation below.

$$Extent\ of\ agglomeration = \frac{mass\ of\ agglomerates\ retained\ by\ 106\ \mu m\ sieve}{mass\ of\ total\ cake} \tag{3.4}$$

Samples were passed through a 106 μm sieve with a lid and receiver pan, which was gently shaken by hand for 1 minute to avoid breakage of agglomerates.[45]

3.6.2 Moisture Content Analysis

The moisture content of agglomerated samples was measured using a Ohaus MB90 Moisture Analyser with a halogen lamp and precision up to 0.01 % for moisture content readings. This was operated with a standard drying program which allowed the sample to be heated to 90 °C and held at this temperature. This temperature was chosen to be well below the melting point of salicylic acid (159 °C) to prevent any sample degradation occurring during the measurement.[124] The auto switch off criteria was chosen where the measurement is stopped once there is less than 1 mg loss in weight in 60 seconds.

3.6.3 Imaging

The agglomerated samples, placed in pie dishes with an approximate diameter of 227 mm, were imaged using a Canon EOS 2000D camera for qualitative comparison between different conditions investigated.

3.6.4 Scanning Electron Microscopy (SEM)

Representative samples were chosen for SEM analysis to investigate the morphology and surfaces of agglomerates, and the details of this technique can be found in Section 3.2.3.

Chapter 4 - Mechanistic Insights into Agglomeration in Agitated Filter Dryers: The Influence of Process and Material Parameters

Agglomeration in agitated filter dryers (AFDs) is influenced by a multitude of interacting parameters, as discussed in Chapter 2. Most existing research is based on empirical relationships, but there is a lack of mechanistic understanding of the agglomeration phenomena. Drying in AFDs is an inherently dynamic process, with simultaneous agitation and heat transfer. Although the effects of drying temperature and the subsequent effect on moisture content and solvent solubility are relatively well understood, the impact of agitation input alone remains underexplored.

In this chapter, a new mechanism is proposed, consisting of three rate processes that govern agglomeration during agitated drying. This chapter also investigates the mechanisms of agglomeration under varying agitation conditions, whilst maintaining constant temperature and therefore moisture content. By decoupling the thermal effect, this work aims to provide mechanistic insights into how agitation input alone influences agglomeration behaviour. Existing literature commonly suggests that the effect of agitation on the extent of agglomeration is linear, with higher agitation speeds facilitating increased levels of breakage and therefore fewer agglomerates.[4,57,63,125] However, this work highlights the significance of considering material properties when designing agitated drying processes.

4.1 Experimental Design and Methodology

4.1.1 Experimental Design

To understand the effect of agitation on agglomeration behaviour, a series of experiments were designed and conducted with the following aims:

- Investigate the relationship between agitation speed and time on the dynamic extent of agglomeration.
- Understand the effect of moisture content and drying temperature on liquid saturation and the resulting extent of agglomeration.
- Evaluate the impact of fill level and mixing efficiency to determine their contribution to the agglomeration dynamics.

4.1.2 Materials

Salicylic acid (≥ 98 %) was obtained from VWR Chemicals and sieved to obtain a size fraction below 106 µm to be used as a moisture sensitive model API. The solvent used was distilled water, prepared using a D4000 Distinction water still.

4.1.3 Experimental Methodology

This section describes in detail the experimental procedure for investigating the effect of agitation on wet cakes of various moisture contents. Experiments were conducted in a PSL GFD Lab 010 series AFD, with the jacket temperature maintained at 25 °C throughout each experiment. The solubility of salicylic acid in water at 25 °C is 2.2 g/L.[126]

4.1.3.1 Wet cake formation

Pre-sieved salicylic acid and distilled water were measured into the filter basket in the required quantities. The mixture is gently agitated at 25 rpm for 5 minutes to form a slurry and left to settle for 5 minutes to form a powder bed. Vacuum is applied at 200 mbar for the required deliquoring time to produce a wet cake of the desired moisture content. All experimental conditions for wet cake formation are summarised in Table 4.1.

Table 4.1: Summary of experimental conditions for wet cake formation.

Moisture Content (%)	Fill Level (cm)	Mass of Salicylic Acid (g)	Mass of Water (g)	Vacuum Time (min)
20	High (6 cm)	75	75	0.5
20	Low (3 cm)	37.5	37.5	0.25
5	High (6 cm)	75	37.5	2
0	High (6 cm)	75	0	-

4.1.3.2 Agitated drying

After filtration, the wet cake was agitated under vacuum at 25 °C at various agitation speeds and times. All experimental conditions are summarised in Table 4.2. The wet powder was carefully removed from the AFD filter basket and dried overnight at 40 °C on a flat tray in a convection drying oven. The drying temperature of 40 °C was chosen to minimise dissolution and recrystallisation, as the solubility of salicylic acid in water only increases slightly from 2.2 g/L at 25 °C to 4.14 g/L at 40 °C. This was to minimise any further agglomeration during drying and prevent changes to the agglomerate sizes achieved during the experiments.

Due to time constraints, it was not feasible to perform repeat experiments for every single run. However, a set of three replicate experiments were conducted at two select time points for each agitation speed. The repeated measurements are denoted with * in Table 4.2. The repeats data was used to calculate the average minimum and maximum errors for each agitation speed, which are represented as error bars in the corresponding figures in Section 4.3.

Table 4.2: Agitation conditions and moisture contents investigated at high fill.

Moisture Content (%)	Agitation Speed (rpm)	Tip Speed (m/s)	Agitation Time (min)
0, 5, 20	0	0	0
0, 5, 20	50	0.126	0.5
			2*
			4
			6
			8
			10*
			12
			14
			30
			60
20	75	0.188	0.5
			2
			4*
			6
			8
			10
			12*
			14
			30
			60
5, 20	100	0.251	0.5
			2
			4
			6*
			8
			10
			12
			14*
			30
			60

4.1.3.3 Effect of temperature

Selected runs were conducted at an increased jacket temperature of 75 °C, shown in Table 4.3. These experiments were performed to investigate the effect of increased solvent solubility on agglomeration, as the solubility of salicylic acid in water increases from 2.2 g/L at 25 °C to 17.1 g/L at 75 °C.[126]

Table 4.3: Agitation conditions investigated for experiments conducted at 75 °C.

Moisture Content (%)	Temperature (°C)	Agitation Speed (rpm)	Agitation Time (min)
20	75	50	10
			60

4.1.3.4 Effect of fill level and clearance

A few runs were completed with a lower fill level and different clearances at 20 % moisture content and are shown in Table 4.4. This was to study the effect of mixing efficiency on the extent of agglomeration.

Table 4.4: Agitation conditions and clearances investigated for low fill experiments.

Fill Level	Clearance (mm)	Agitation Speed (rpm)	Agitation Time (min)
LOW	10	50	10
	5	50	0
			10
			30
			60
		100	0
			10
			30
			60

4.1.4 Product Characterisation

Samples of wet cake were taken from the vessel prior to agitation to determine the moisture content using an Ohaus MB90 Moisture Analyser. The ASDs of the final dried samples were characterised by sieving using a Retsch AS 200 Sieve Shaker with sieve mesh sizes from 106 µm to 53 mm (increasing by a magnitude of $\sqrt{2}$ per sieve). The entire sample was analysed when sieving to minimise any potential sampling error. The amplitude and sieving time were carefully designed to avoid any breakage of agglomerates during the size analysis (see Chapter 3, Section 3.6.1 for further information). Selected samples were analysed using SEM to explore the structure of agglomerates.

4.2 Proposed Mechanism of Agglomeration

A mechanism for undesired agglomeration is proposed in this work, as shown in Figure 4.1, based on a comprehensive review of the literature and initial experimental findings. The governing rate processes for undesired agglomeration during agitated drying are discussed in the following section.

- Formation of loosely bound agglomerates

The slurry produced during crystallisation is filtered and typically deliquored to form a wet cake (or filter cake). Within this wet cake, there are loosely bound agglomerates, and the extent of their formation depends on the efficiency of the filtration and washing procedures. Poor filtration and washing lead to wet cakes with a higher moisture content, increasing contact between the crystallisation solvent and crystals, and promoting the formation of liquid bridges. These liquid bridges between particles result in small clusters of loosely bound agglomerates that act as nuclei for further agglomerate growth. The size of these agglomerates and the strength of the liquid bridges determine the likelihood of agglomerate growth and resistance to shear forces from agitation. Therefore, the properties of these initial agglomerates can influence the overall agglomeration observed at the end of the drying process.

- Consolidation and coalescence

Agitation of the wet cake encourages initial consolidation of agglomerates followed by growth via coalescence and/or layering. During the agitated drying process, particles and agglomerates collide with each other, vessel walls and the impeller, allowing them to consolidate into smaller, denser agglomerates. This makes them more resistant to crushing and breakage. In some cases, this can also squeeze solvent from within the agglomerate to the surface. The presence of wet surfaces can promote coalescence, specifically type II coalescence, where colliding particles remain in contact for a finite time, forming a bond. The coalescence only becomes permanent if the bond withstands the shear forces generated by collisions and agitation. Growth by layering occurs when fines stick to wet agglomerates. These fines can either be present in the starting material or produced by breakage.

- Solidification of liquid bridges

Wet agglomerates are subjected to agitation during drying, and those able to withstand these shear forces will undergo evaporation of solvent from the liquid bridges, resulting in solid crystalline bridges that strengthen the agglomerates. The level of agitation can vary depending on drying times, and therefore, the drying protocol, including temperature, equipment and fill level, will all influence the degree of agglomerate breakage.

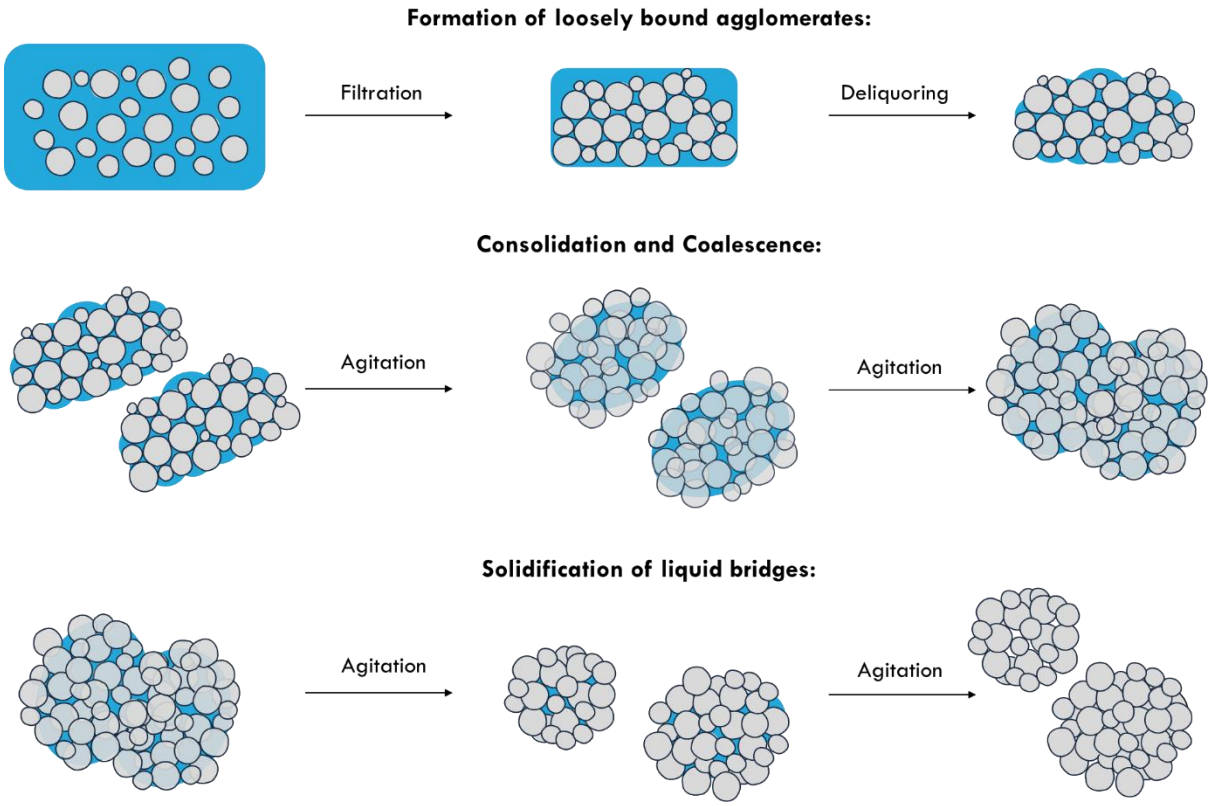

Figure 4.1: Proposed mechanism of undesired agglomeration.

The results in Section 4.3 will be used to verify the proposed mechanism by examining the trends in agglomeration behaviour over time under various conditions. The agglomerate size data along with characterisation techniques such as SEM will provide evidence to support and refine this mechanism. By contrasting these findings with expected trends, any limitations of the proposed mechanism can be identified. Additionally, investigating different conditions will provide insight into factors influencing the rates of key processes within this mechanism.

4.3 Results and Discussion

The primary aim of these experiments is to test the hypothesis that the agglomeration behaviour is a function of the agitation input, i.e. agitation speed and time. There are expected to be specific conditions under which either agglomeration or breakage regimes will dominate. As previously mentioned, the thermal effects during a typical drying process in AFDs are removed to be able to isolate the effect of agitation alone. The effect of moisture content and fill level on the observed agglomeration behaviour is also explored, with findings evaluated against the proposed mechanism.

Agglomeration trends are analysed by plotting d_{50} and d_{90} values as a function of time. Given the focus on agglomeration, the d_{50} is important as it represents the typical agglomerate size and reflects whether breakage or agglomeration behaviour is dominating. The d_{90} is also valuable for understanding the behaviour of the largest agglomerates which are more prone to growth or breakage over time. To give a comprehensive understanding of the full agglomerate size distribution (ASD), d_{10}, d_{50} and d_{90} values and ASD spans will also be provided.

4.3.1 Effect of Agitation Speed and Time on Agglomeration Rates

Wet cakes of salicylic acid and water were agitated at three speeds (50, 75 and 100 rpm) for agitation periods of 2 to 14 minutes in 2 minute increments. All experiments were conducted at an average moisture content (MC) of 20.3 ± 1 % to minimise any variability in agglomeration behaviour due to MC and liquid saturation levels. The d_{50} values as a function on time for all agitation speeds are shown in Figure 4.2. All other corresponding d values and ASD spans can be found in Table 4.5.

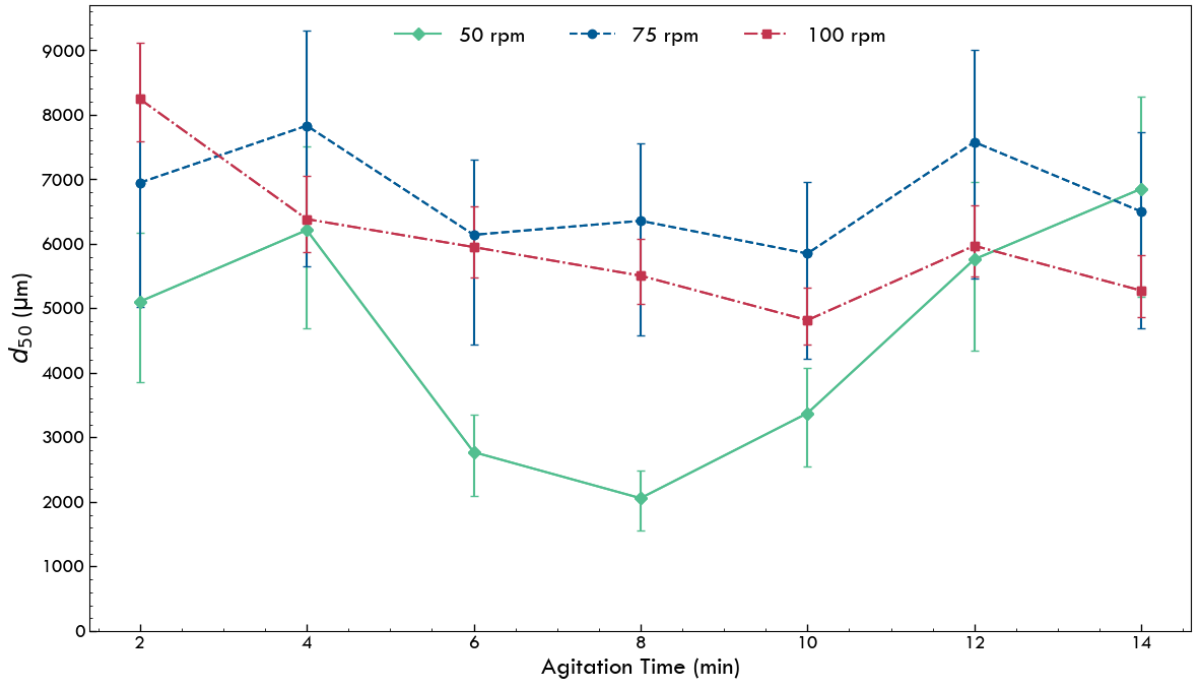

Figure 4.2: d_{50} values of samples with 20 % MC at various agitation speeds over time. Error bars represent the minimum and maximum error based on 3 repeat experiments at each speed.

Interestingly, the d_{50} values observed in this initial agitation period are larger at the higher speeds of 75 and 100 rpm. Between 6 to 10 minutes of agitation, it is clear that the d_{50} values are significantly lower for the lowest agitation speed of 50 rpm, and outside the bounds of error. This is contrary to literature reports that higher agitation speeds will facilitate greater levels of breakage.[4,57,125] At 50 rpm, there is an initial breakage dominated regime, as highlighted by the dip in d_{50} values, followed by a transition towards an agglomeration dominated regime. At the higher speeds however, there is a consistent balance between the agglomeration and breakage, resulting in stable d_{50} values. This can be attributed to liquid bridge strength, where if the liquid bridges are strong enough to withstand the shear forces experienced at higher agitation speeds, increased agitation facilitates more frequent contact between particles, promoting agglomerate growth. Any breakage occurring may produce fines that subsequently layer onto existing wet agglomerates, allowing them to be reincorporated. This mechanism of growth is referred to hereafter as snowballing. To highlight the contrast in agglomeration, the difference between runs at 50 rpm and 100 rpm after 8 minutes of agitation is shown in Figure 4.3. This time point is specifically chosen as it corresponds to the lowest d_{50} value at 50 rpm. The images clearly show a greater number of agglomerates at 100 rpm.

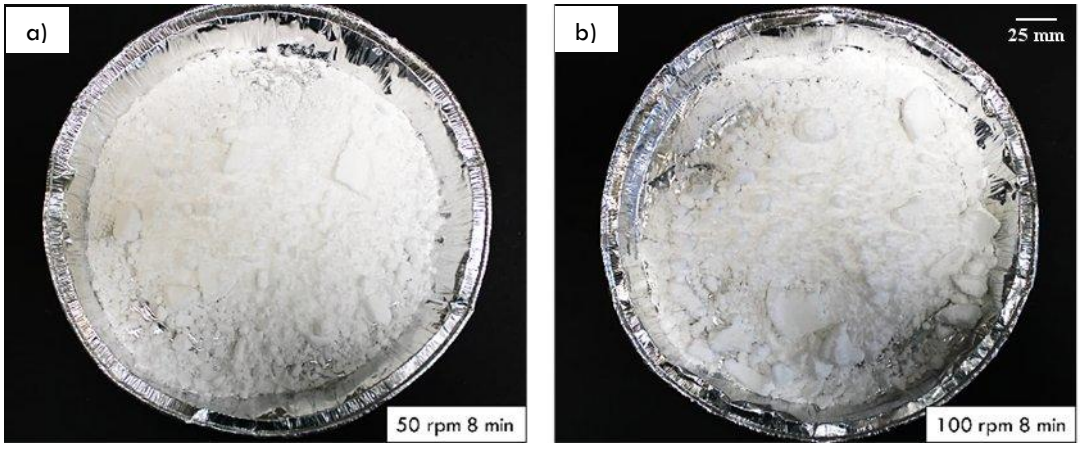

Figure 4.3: Wet samples at 20 % MC agitated for 8 mins at a) 50 and b) 100 rpm.

Referring to the proposed mechanism of undesired agglomeration in Figure 4.1, higher agitation speeds increase both the rate and extent of consolidation and coalescence. Breakage of large agglomerates may occur via fragmentation, and the resulting fragments are more likely to re-coalesce at higher speeds due to the greater energy of collisions. In contrast, at 50 rpm, not only is the rate of consolidation and coalescence slower, but the lower energy input also results in weaker, less consolidated agglomerates. This explains the initial breakage dominated behaviour, where the loose, poorly consolidated agglomerates are prone to fragmentation and attrition.

Another way to analyse this data is using the ASD span ($\frac{d_{90}- d_{10}}{d_{50}}$), to ensure the spread of particle sizes present in samples is considered, as the d_{50} only represents the midpoint of the ASD. The ASD spans for these experiments are shown in Figure 4.4, highlighting minimal fluctuations at 75 and 100 rpm

during this agitation period. This further supports the balance between simultaneous agglomerate growth and breakage observed at these higher speeds. The mixing efficiency is also improved at higher speeds, minimising any inhomogeneity in the moisture distribution, which can result in agglomeration dominating over breakage. In contrast, the ASD span for 50 rpm shows significant variation, aligning with the transition observed previously from breakage dominated towards agglomeration dominated behaviour. This may be a result of reduced contact frequency and inadequate mixing at lower speeds. At 50 rpm, there is also reduced consolidation of agglomerates which initially results in breakage, but with continued agitation, there is agglomerate growth via the snowballing mechanism. The effect of agitation speed on mixing efficiency will be explored further in Section 4.2.3.

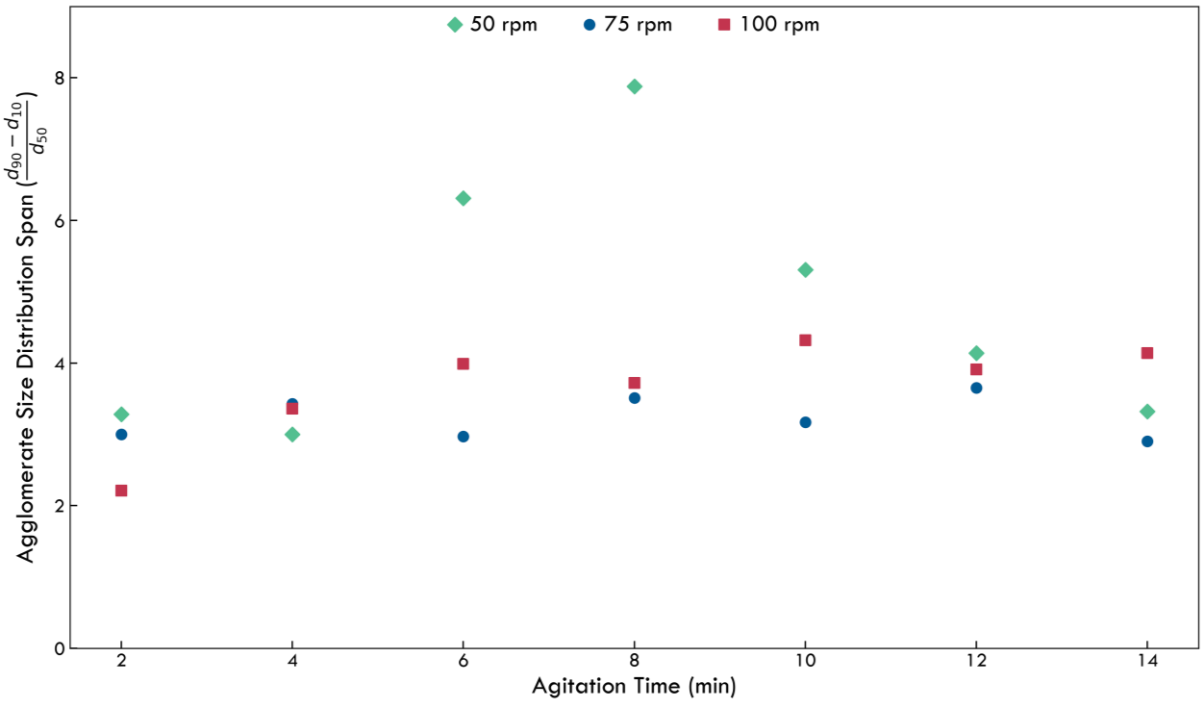

Figure 4.4: Change in ASD span over time at various agitation speeds for 20 % MC.

Based on initial experiments, longer agitation periods were investigated for all speeds to see if these trends continue. All relevant *d* values and ASD spans are given in Table 4.5. As seen in Figure 4.5, the balance between agglomeration and breakage at 75 and 100 rpm is sustained over a 60 minute agitation period. At high speeds, there is sufficient energy for successful collisions, promoting agglomeration via coalescence. Some degree of breakage also occurs, likely through both fragmentation and attrition. However, higher collision energies will favour fracture, making fragmentation the dominant breakage mechanism.[127] Sahni *et al.* observed a similar trend when studying the effect of impeller speed on lactose in an AFD, reporting increased fragmentation at higher speeds.[4] Due to increased contact frequency and energetic collisions, any fines or fragments from breakage are more likely to be reincorporated into wet agglomerates, especially fines which facilitate agglomerate growth via snowballing. This simultaneous breakage and agglomeration results in steady d_{50} values over time.

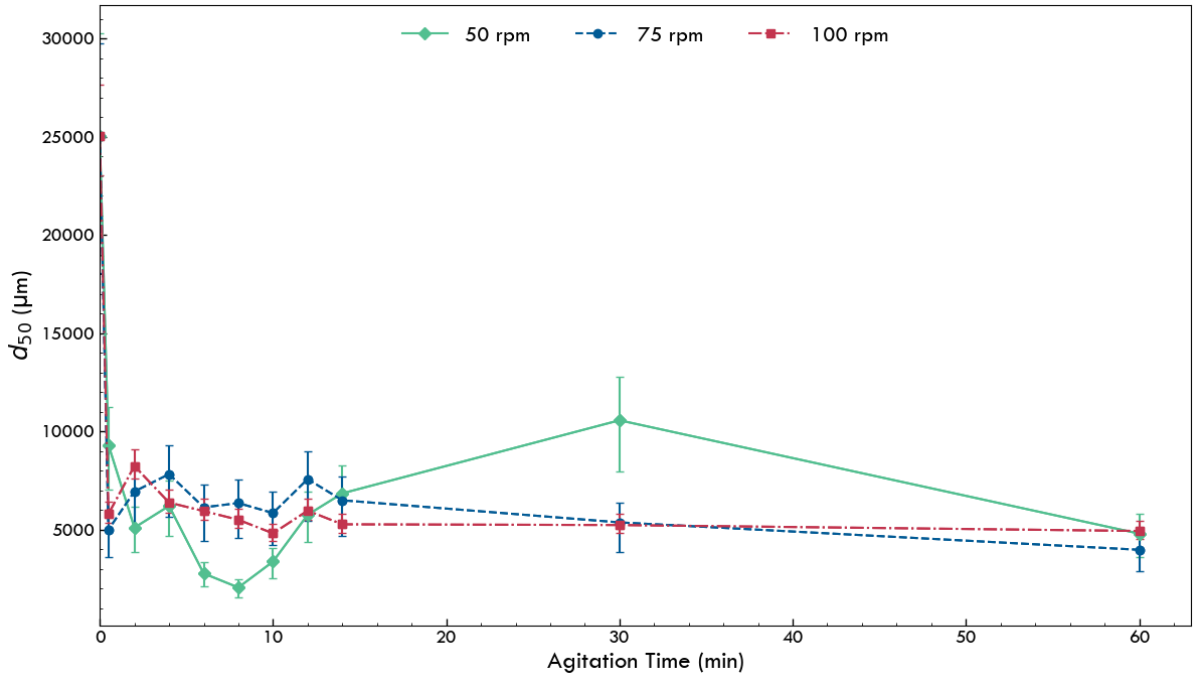

Figure 4.5: d_{50} values of samples with 20 % MC at various agitation speeds over time. Error bars represent the minimum and maximum error based on 3 repeat experiments at each speed.

At 50 rpm, however, the initially breakage dominated regime noticeably transitions to an agglomeration dominated regime. The increase in d_{50} observed may be due to longer agitation times required for sufficient contact between particles to facilitate agglomeration and agglomerate growth. At this lower speed, the collision energy is likely only sufficient for abrasion and attrition of agglomerates, producing fines. As the moisture content is kept constant, these fines will eventually layer onto the wet agglomerates via the snowballing mechanism, resulting in agglomeration dominating until the 30-minute mark. After this, some breakage is observed, which is likely driven by the weaker nature of agglomerates that are unable to withstand the shear forces of continued agitation. The extent of consolidation at 50 rpm is reduced compared to the higher speeds, resulting in weaker agglomerates.

Figure 4.5 also includes a control run with no agitation, as well as 0.5 minute agitation data points for all speeds. This highlights that, despite undesired agglomeration being a common issue in AFDs, agitation provides significant benefits over static drying. The sharp decline in d_{50} from 25044 µm to 9324 µm after just 30 seconds of agitation demonstrates the rapid initial breakage of loosely bound agglomerates. This observation also supports the proposed mechanism where the wet cake initially consists of loose agglomerates that are broken up.

The different rates of consolidation and coalescence at low and high speeds, along with the dominant breakage mechanisms, are highlighted in Figure 4.6. At 50 rpm, the initial breakage appears to be primarily driven by attrition, generating fines, which may contribute to subsequent agglomeration. Depending on the extent of fines produced, agglomerate growth may occur via the snowballing mechanism where fines adhere to wet agglomerates, or through the coalescence of smaller agglomerates

during collisions. At higher speeds, agglomeration and breakage likely occur simultaneously, with fragmentation as the primary breakage mechanism. Interestingly, despite the transitions between different regimes observed at 50 rpm, all systems reach equilibrium after 60 minutes. This suggests that, regardless of agitation speed, agglomerates may be unable to grow beyond a certain size limit, indicating that the underlying agglomeration mechanisms remain consistent for all speeds.

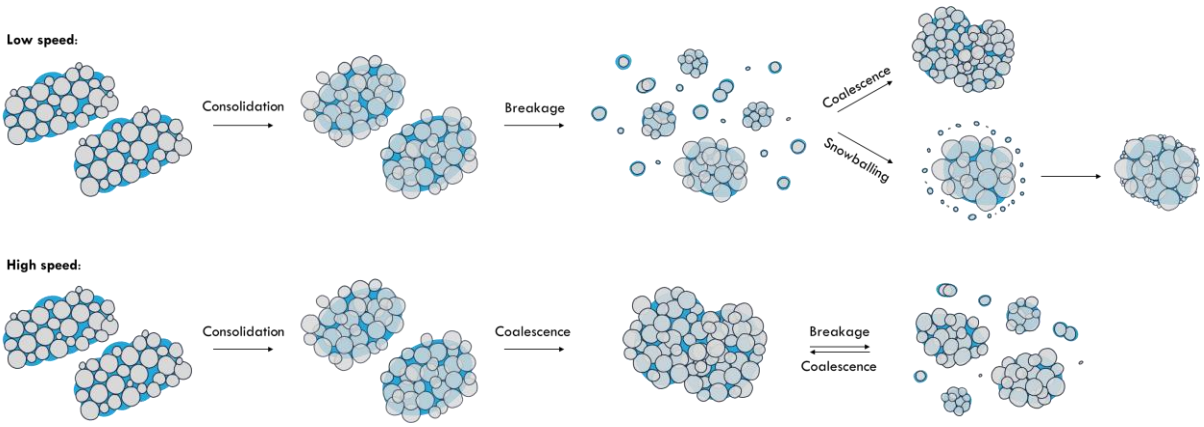

Figure 4.6: Comparison of consolidation, coalescence, and breakage mechanisms at low and high agitation speeds.

Table 4.5: *d* values and ASD spans for all agitation speeds and times investigated at 20 % MC.

Agitation Speed (rpm)	Agitation Time (min)	d_{10} (µm)	d_{50} (µm)	d_{90} (µm)	ASD Span
0	0	218	25044	49173	2.0
50	0.5	152	9324	22301	2.4
	2	146	5105	16907	3.3
	4	144	6213	18798	3.0
	6	224	2773	17718	6.3
	8	281	2059	16493	7.9
	10	181	3376	18095	5.3
	12	197	5760	24041	4.1
	14	168	6853	22930	3.3
	30	156	10573	24616	2.3
	60	136	4802	17203	3.6
75	0.5	138	5004	15635	3.1
	2	289	6947	21135	3.0
	4	222	7831	27100	3.4
	6	141	6140	18363	3.0
	8	141	6357	22473	3.5
	10	251	5850	18797	3.2
	12	179	7577	27823	3.7
	14	135	6500	18962	2.9
	30	168	5374	18570	3.4
	60	153	3979	17290	4.3
100	0.5	141	5805	20892	3.6
	2	224	8244	18411	2.2
	4	227	6383	21673	3.4
	6	191	5950	23938	4.0
	8	135	5507	20621	3.7
	10	172	4817	20995	4.3
	12	144	5971	23469	3.9
	14	148	5276	21996	4.1
	30	132	5239	17429	3.3
	60	179	4937	24868	5.0

4.3.2 Effect of Liquid Saturation and Temperature on Extent of Agglomeration

To investigate the effect of liquid saturation on agglomerate strength, experiments were conducted at a reduced average MC of 5.4 % ± 0.7 % for the two extreme agitation speeds: 50 and 100 rpm. As salicylic acid is an inherently cohesive material, a dry run was also conducted at 50 rpm for comparison. The d_{50} and d_{90} values as a function of time for 0, 5 and 20 % MC at 50 rpm are shown in Figure 4.7a and 4.7b respectively, with all d values and ASD spans given in Table 4.6.

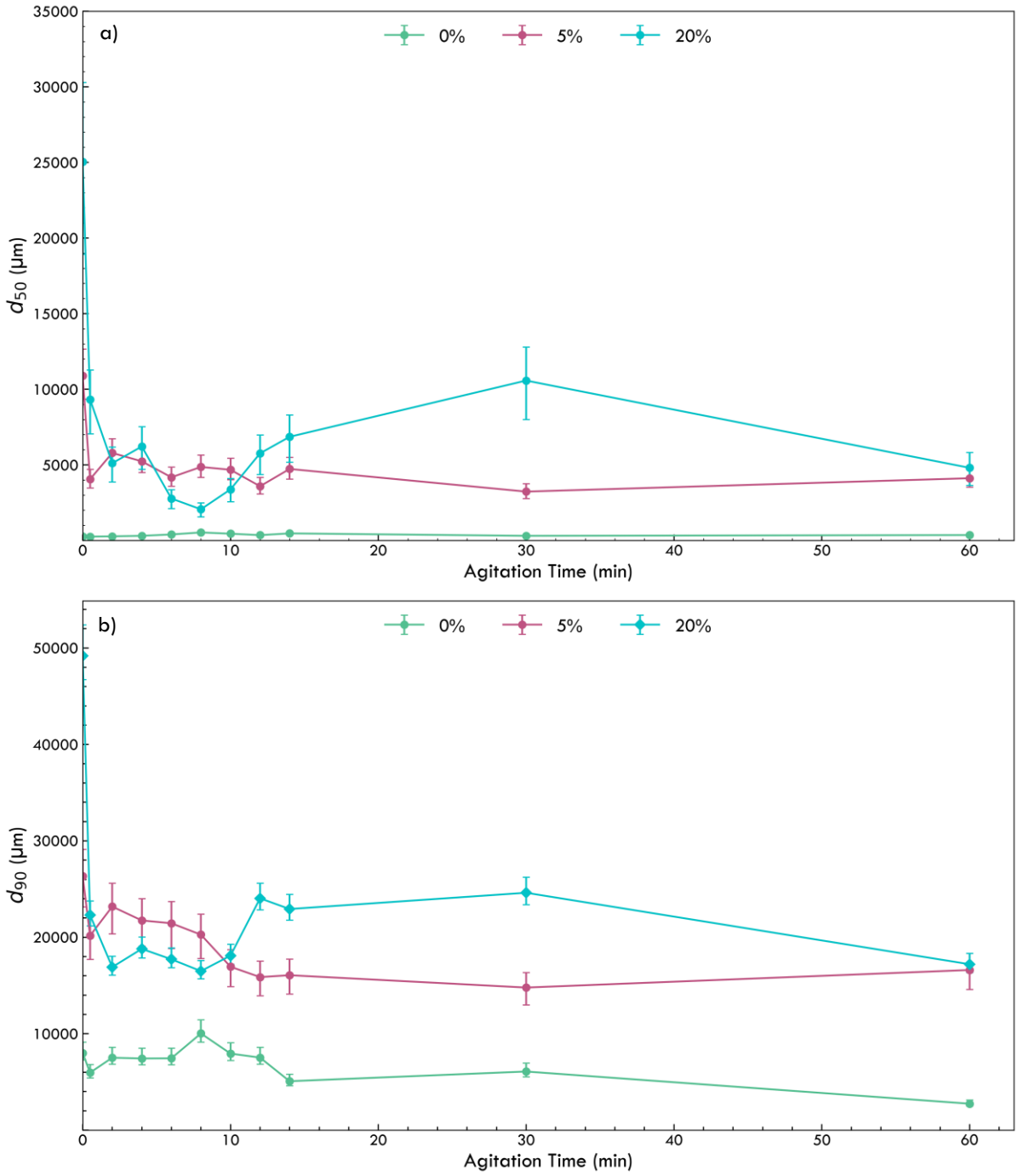

Figure 4.7: a) d_{50} and b) d_{90} values at various moisture contents agitated at 50 rpm over time. Error bars represent the minimum and maximum error based on 3 repeat experiments at 50 rpm for each moisture content.

Figure 4.7a shows a general increase in agglomeration with increasing moisture, which is expected as more solvent leads to greater liquid saturation of particles and more liquid bridges. This not only promotes agglomeration through increased coalescence but also enhances agglomerate strength. At 20 % MC, the agglomerates are likely in the capillary state where all pores are filled with liquid and agglomerate strength peaks. Increased moisture also improves particle mobility, allowing them to rearrange into more compact arrangements, and increasing the rate of consolidation.[128]

For the dry run (0 % MC), although some agglomeration of the starting material occurs, it is minimal compared to the other experiments, reflecting the absence of liquid bridges. This is also evident in the d_{90} values as shown in Figure 4.7b, where despite initial agglomerate growth up to 8 minutes, a limiting size is reached before the larger agglomerates break. Without any liquid present, the agglomeration likely results from particle cohesion and mechanical compression rather than liquid bridges.

The different agglomeration mechanisms between 20 % and 0 % MC were analysed using SEM, as shown in Figure 4.8. At 20 % MC, solid bridges between particles are visible. These are distinguishable from other binding mechanisms as their edges are fused with no distinct boundaries. The fusion likely indicates that there has been dissolution and recrystallisation of material to form a solid bridge. While not explicitly stated in the literature, this observation aligns with how solid bridges have previously been identified in agglomerates.[50,129,130] In contrast, the SEM image for dry agglomerates reveals distinct particle edges, indicating no recrystallisation or solid bridge formation. The binding mechanism for dry agglomerates is likely weak van der Waals forces and mechanical interlocking.

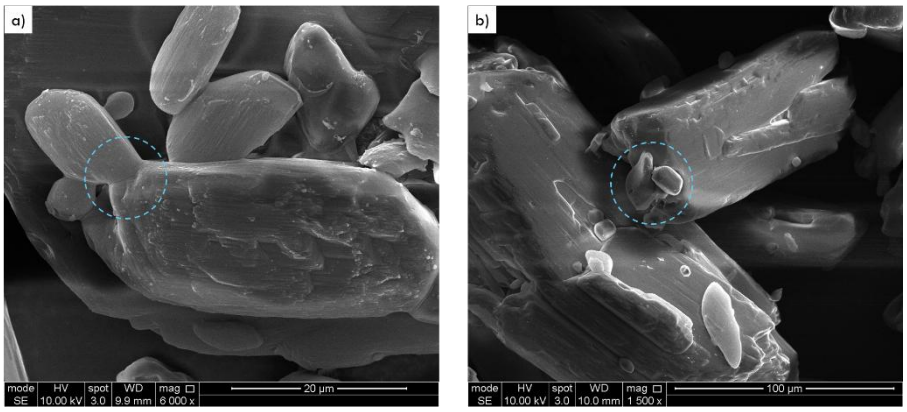

Figure 4.8: SEM images of agglomerates at a) 20 % MC and b) 0 % MC.

At 5 % MC, the initial wet cake prior to agitation has a d_{50} of 10887 µm and d_{90} of 26353 µm, which is significantly smaller than at 20 % MC where the d_{50} and d_{90} are 25044 µm and 49173 µm, respectively. This highlights how reduced liquid bridge availability at lower moisture levels can limit the extent of agglomeration, as weaker capillary forces result in smaller and less consolidated agglomerates. Nevertheless, there is still a significant level of agglomeration at 5 % MC, with a d_{50} of 4114 µm after 60 minutes of agitation, comparable to a d_{50} of 4802 µm at 20 % MC. This suggests the critical moisture content (CMC) for this material system may be quite low.

The d_{50} values at 5 % MC between 6 and 10 minutes are surprisingly higher than those at 20 % MC, and this is also reflected in the d_{90} values. This likely stems from localised wet spots facilitating excessive agglomeration. However, this effect is short lived as seen by the dip in d_{50} and d_{90} at approximately 10 to 12 minutes, where these weak agglomerates break up with continued agitation. Overall, the d_{50} values at 5 % MC are much more stable over time compared to the 20 % MC, likely due to the presence of fewer liquid bridges. This results in less dramatic changes in agglomerate size in the system, and a more consistent balance between agglomeration and breakage over time. The d_{90} values in Figure 4.8b further support this, with an initial increase followed by some gradual breakage, and then a steady d_{90} from 10 minutes onwards. At 20 % MC, the consequences of inhomogeneous moisture distribution and localised wet spots are more pronounced, as highlighted by the fall and rise in d_{50} and d_{90} values over time. This data highlights the critical role of moisture in agglomerate formation.

Table 4.6: *d* values and ASD spans for all agitation times investigated at 50 rpm for 0 % and 5 % MC.

Moisture Content (%)	Agitation Time (min)	d_{10} (µm)	d_{50} (µm)	d_{90} (µm)	ASD Span
0	0	134	270	7996	29.2
	0.5	135	252	5960	23.1
	2	130	271	7511	27.2
	4	146	305	7434	23.9
	6	152	395	7449	18.5
	8	188	528	10025	18.7
	10	169	445	7939	17.5
	12	152	350	7521	21.1
	14	163	466	5072	10.5
	30	146	304	6078	19.5
	60	167	355	2741	7.3
5	0	138	10887	26353	2.4
	0.5	129	4049	20164	5.0
	2	137	5786	23183	4.0
	4	124	5231	21746	4.1
	6	147	4175	21454	5.1
	8	134	4860	20271	4.1
	10	128	4673	16945	3.6
	12	113	3584	15869	4.4
	14	139	4727	16066	3.4
	30	131	3229	14786	4.5
	60	125	4114	16606	4.0

The effect of reduced MC on agglomeration was also investigated at 100 rpm, with the d_{50} and d_{90} values over time for 5 % and 20 % MC shown in Figure 4.9a and 4.9b. All *d* values and ASD spans are provided in Table 4.7. As expected, smaller d_{50} and d_{90} values are seen for the 5 % MC run compared to the 20 % MC run due to reduced opportunities for liquid bridge formation. Despite this, the extent of agglomeration at 100 rpm remains comparable between the two moisture contents, as seen previously at 50 rpm, particularly in the d_{50} values from 10 to 60 minutes of agitation. However, more pronounced differences are seen in the d_{90} values. For example, a d_{90} of 16861 µm at 5 % MC compared to 23469 µm at 20 % MC after 12 minutes of agitation. This suggests that while the d_{50} values may be similar, the formation of the larger agglomerates in the population is heavily influenced by the moisture. The lower d_{90} values at 5 % MC indicate that reduced solvent availability limits both the formation and survival of larger agglomerates.

At 100 rpm, both d_{50} and d_{90} values are much more stable over time compared to those at 50 rpm for both 5 % and 20 % MC. This is likely due to the higher agitation intensity promoting better mixing, which enables an equilibrium between breakage and agglomeration to be achieved sooner. The reduced variability in size at 5 % MC compared to 20 % MC, especially the d_{90} values, suggests fewer localised wet spots, leading to a more uniform agglomeration process.

Table 4.7: *d* values and ASD spans for all agitation times investigated at 100 rpm and 5 % MC.

Moisture Content (%)	Agitation Time (min)	d_{10} (µm)	d_{50} (µm)	d_{90} (µm)	ASD Span
5	0	138	10887	26353	2.4
	0.5	128	6314	22347	3.5
	2	153	4334	18430	4.2
	4	118	3131	19435	6.2
	6	135	3345	18967	5.6
	8	118	3784	18182	4.8
	10	121	3853	20521	5.3
	12	130	4423	16861	3.8
	14	125	4457	17652	3.9
	30	117	3975	16698	4.2
	60	118	3079	16507	5.3

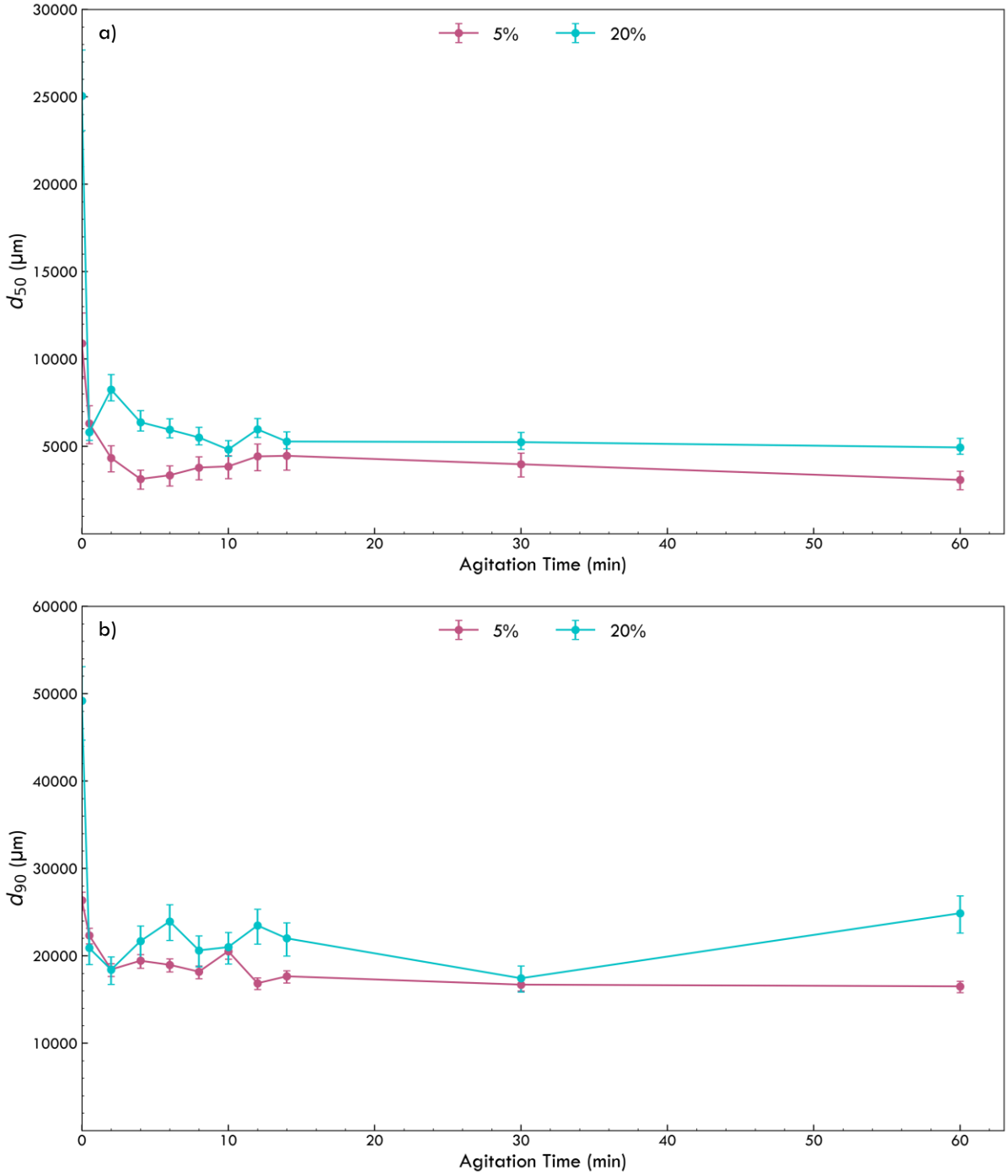

Figure 4.9: a) d_{50} and b) d_{90} values at various moisture contents agitated at 100 rpm over time. Error bars represent the minimum and maximum error based on 3 repeat experiments at 100 rpm for each moisture content.

To further understand the role of liquid bridges, the focus shifted from the effect of liquid saturation and availability of liquid bridges to investigating the effect of temperature on liquid bridge strength and the extent of agglomeration. Select experiments were conducted at an increased jacket temperature of 75 °C, increasing the solubility of salicylic acid from 2.2 g/L at 25 °C to 17.1 g/L at 75 °C. The ASDs of experiments conducted at 20 % MC and agitated at 50 rpm for 10 minutes at 25 °C and 75 °C are shown in Figure 4.10, with the *d* values and ASD spans provided in Table 4.8.

Table 4.8: *d* values for 20 % MC 50 rpm 10 min runs at 25 °C and 75 °C.

Agitation Time (min)	Temperature (°C)	d_{10} (µm)	d_{50} (µm)	d_{90} (µm)	ASD Span
10	25	181	3376	18095	5.3
	75	134	5464	21886	4.0

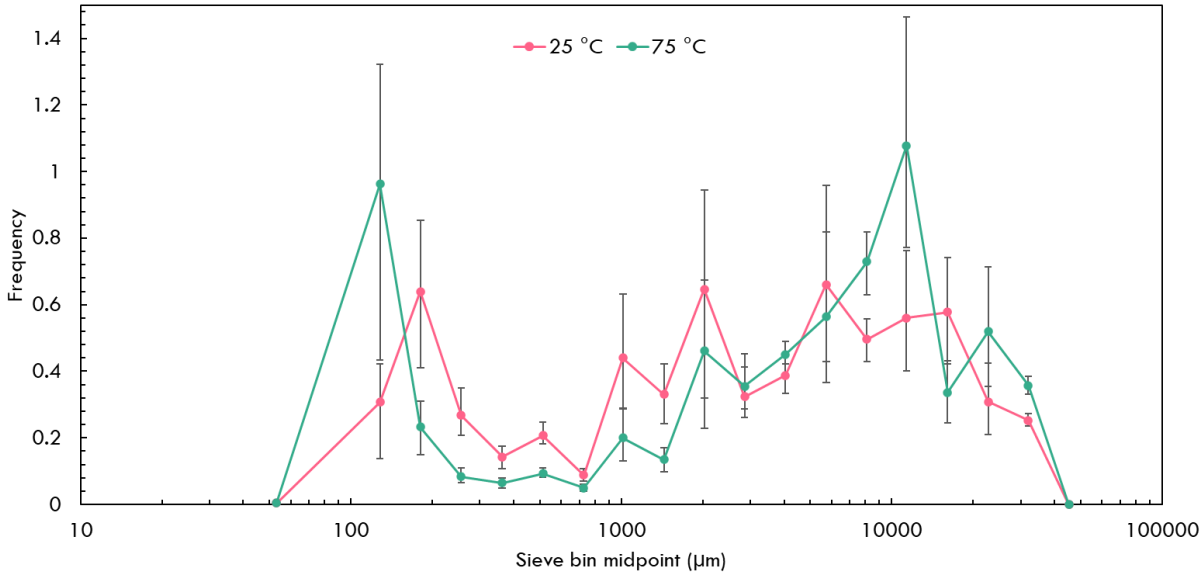

Figure 4.10: Agglomerate size distribution for 20 % MC 50 rpm 10 min runs at 25 °C and 75 °C. Error bars represent the minimum and maximum error based on 3 repeat experiments at 50 rpm.

In Figure 4.10, the ASD at 75 °C is much broader than at 25 °C, with an increased frequency of both smaller and larger particles sizes. The formation of larger agglomerates at higher temperatures is expected, as increased solubility results in more dissolved material. This not only increases the number of liquid bridges but also increases their strength.[3,57,131] This is highlighted by the noticeable increase in d_{50} and d_{90} at 75 °C, where stronger liquid bridges promote the formation of large agglomerates that are more resistant to breakage. This promotion of agglomeration at higher temperatures is due to the faster rate of consolidation and coalescence, as well as increased solidification of liquid bridges. This trend is also clear from the images in Figure 4.11, where the 75 °C run has a much more granular appearance due to an increase in agglomeration. However, the slight decrease in the d_{10} at 75 °C due to more fine

particles present suggests that higher drying temperatures may also promote breakage. As the agglomerates begin to dry, they shrink in size, becoming more prone to breakage and attrition.[63]

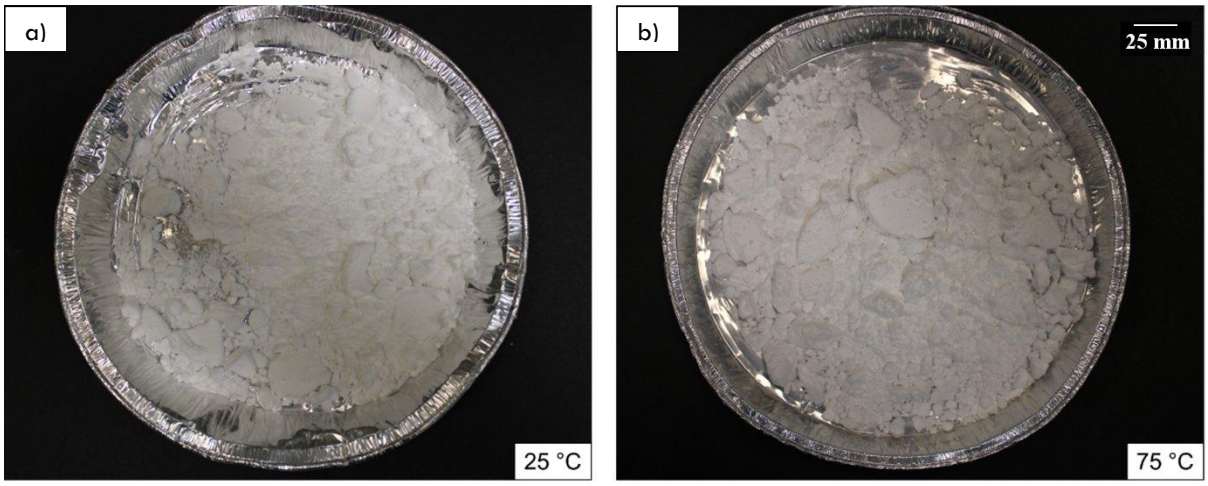

Figure 4.11: Wet samples at 20 % MC agitated at 50 rpm for 10 mins at a) 25 °C and b) 75 °C.

To further understand the relationship between drying temperature and agitation time, another experiment was conducted with 60 minutes of agitation. The ASDs for experiments at 20 % MC with 60 minutes of agitation at 50 rpm and jacket temperatures of 25 °C and 75 °C are shown in Figure 4.12, with the corresponding *d* values and ASD spans provided in Table 4.9.

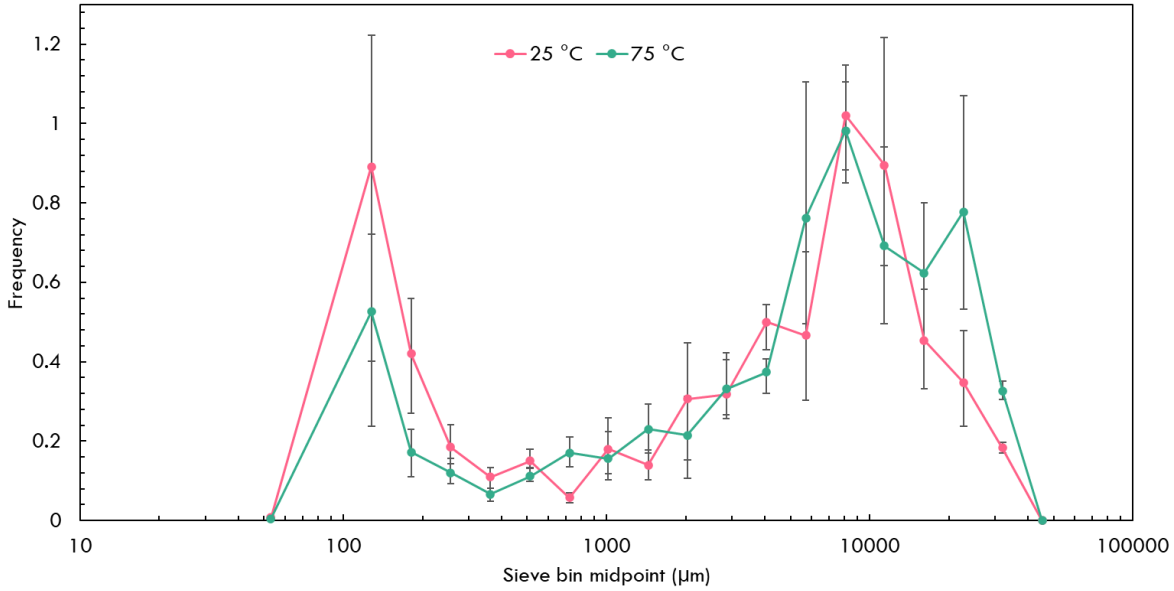

Figure 4.12: Agglomerate size distribution for 20 % MC 50 rpm 60 min runs at 25 °C and 75 °C. Error bars represent the minimum and maximum error based on 3 repeat experiments at 50 rpm.

Table 4.9: *d* values for 20 % MC, 50 rpm 60 min runs at 25 °C and 75 °C.

Agitation Time (min)	Temperature (°C)	d_{10} (µm)	d_{50} (µm)	d_{90} (µm)	ASD Span
60	25	136	4802	17203	3.6
	75	185	6849	23112	3.4

There is a clear increase in agglomeration at 75 °C, as evidenced by the ASD in Figure 4.12 and *d* values in Table 4.9. This behaviour is expected due to increased solubility and stronger liquid bridges at higher temperatures. However, most differences in the ASD for 75 °C fall within the bounds of error, with the only significant variation occurring at the largest sizes in the distribution. While higher temperatures promote agglomeration, they also result in faster drying rates, as evidenced by a final MC of 18.97 % at 25 °C compared to 8.65 % at 75 °C. With less solvent present to act as a lubricant, continued agitation can result in breakage of agglomerates, making the significant increase in d_{90} at 75 °C initially unexpected. However, some condensation was seen inside the vessel for the 60 minute run (Figure 4.13), but not at 10 minutes. The longer drying time generated more vapour which condensed on the unjacketed headspace of the vessel, which acts as a cold surface. This aligns with the final MC at 75 °C, which dropped from 16.74 % after 10 minutes to 8.65 % after 60 minutes. This condensation may contribute to the increased agglomeration at 75 °C, as the condensate drips down into the powder bed, inducing nucleation.[3] However, if the condensate dripping was significant, a higher final MC would be expected after 60 minutes, suggesting this had a limited effect. Condensate drips have a more substantial impact at lower MCs, whereas at higher MCs, they are dispersed into the wet powder bed and unlikely to result in nucleation. The formation of wet agglomerate nuclei allows fines from breakage to layer on, further promoting growth via the snowballing mechanism.

Figure 4.13: Condensation seen in the headspace of the AFD vessel during a 60 min run at 75 °C.

Although this was a small-scale study, it provided valuable insights into the influence of drying temperature on various rate processes of the proposed agglomeration mechanism. At higher drying temperatures, the solubility increases and results in stronger agglomerates. However, faster drying rates can also lead to breakage while condensate drips can introduce additional nucleation, highlighting the complex balance of parameters influencing agglomeration.

4.3.3 Effect of Fill Level and Mixing Efficiency on the balance between Agglomeration and Breakage

As discussed in Section 4.2.1, higher agitation speeds exhibited more consistent behaviour with a balance of agglomeration and breakage over time. In contrast, the lowest speed (50 rpm) showed clear transitions from breakage dominated to agglomeration dominated regimes. This may stem from reduced mixing efficiency at lower agitation speeds. To investigate this, additional experiments were conducted at half the previous fill level. The aim of these experiments was to see if the trends previously observed would continue with improved mixing.

Initially, the bed height was halved from 6 cm to 3 cm, but a clearance of 10 mm was maintained. The ASDs for 50 rpm runs agitated for 10 minutes at both bed heights are shown in Figure 4.14. The corresponding *d* values and ASD spans are also provided in Table 4.10. The ASDs show a decrease in agglomeration at a lower fill level, and this is supported by the *d* values in Table 4.10. Reducing the height of the powder bed and consequently the fill level increases the frequency of collisions and allows more agglomerates to be broken down by the shearing action of the impeller. This is seen by the increased frequency in smaller particle sizes (106 - 212 µm) at lower fill levels, and the absence of any large agglomerates at sieve sizes 26.5 mm and above.

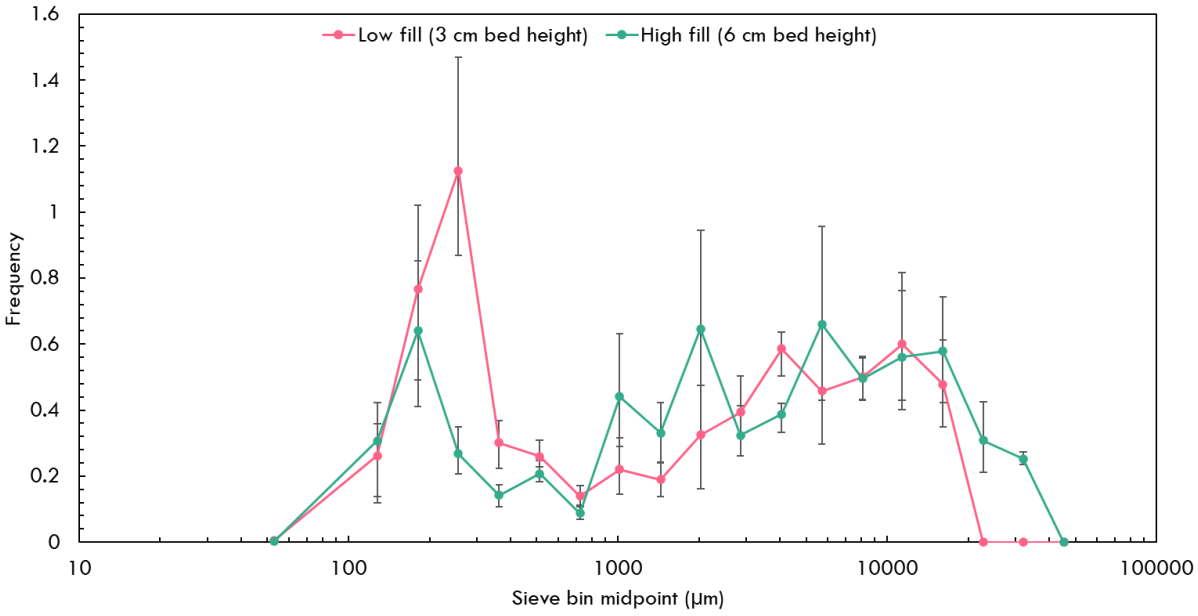

Figure 4.14: Agglomerate size distribution for 20 % MC 50 rpm 10 min runs at low and high fill. Error bars represent the minimum and maximum error based on 3 repeat experiments at 50 rpm.

Table 4.10: *d* values and ASD spans for 20 % MC 50 rpm 10 min runs at low and high fill.

Agitation Time (min)	Bed Height (cm)	d_{10} (µm)	d_{50} (µm)	d_{90} (µm)	ASD Span
10	3	178	1710	12143	7.0
	6	181	3376	18095	5.3

The extent of agglomeration is reduced at a lower fill level, however significant agglomeration compared to the starting material is still observed. To ensure a fair comparison and to further understand the impact of mixing efficiency, the low fill experiment was repeated with the clearance also halved to 5 mm. The ASDs for a low fill 50 rpm run agitated for 10 minutes at clearances of 5 mm and 10 mm are shown in Figure 4.15, with the *d* values and ASD spans provided in Table 4.11. The ASD shifts to the left when the clearance is decreased to 5 mm, and the *d* values also confirm a substantial decrease in agglomeration. The d_{50} shows a significant reduction from 1710 µm to 266 µm, indicating that coalescence and consolidation of agglomerates is greatly inhibited under these conditions. Reducing the clearance improves the mixing in the bulk of the material. The reduction in d_{10} from 178 µm to 122 µm falls outside the bounds of error, suggesting not only increased breakage but also reduced fines layering onto wet agglomerates, thereby limiting growth via the snowballing mechanism.

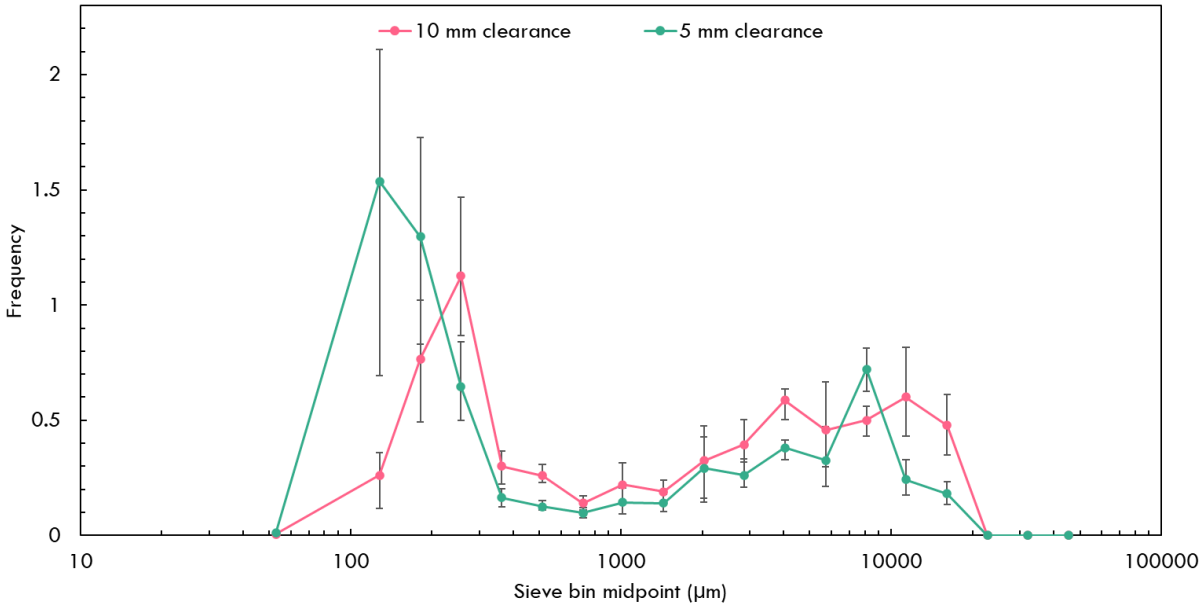

Figure 4.15: Agglomerate size distribution for low fill 20 % MC 50 rpm 10 min runs at 5 and 10 mm clearances. Error bars represent the minimum and maximum error based on 3 repeat experiments at 50 rpm.

Table 4.11: *d* values for low fill 20 % MC 50 rpm 10 min runs at 5 mm and 10 mm clearances.

Agitation Time (min)	Clearance (mm)	d_{10} (µm)	d_{50} (µm)	d_{90} (µm)	ASD Span
10	10	178	1710	12143	7.0
	5	122	266	8566	31.8

The findings indicate that the material below the base of the impeller (the heel) may significantly contribute to agglomeration. At high fill, the increased clearance results in a taller heel, leading to larger broken heel fragments compared to a 5 mm clearance. This is shown in Figure 4.16, where the high fill sample contains more agglomerates, including irregularly shaped agglomerates likely from the heel.

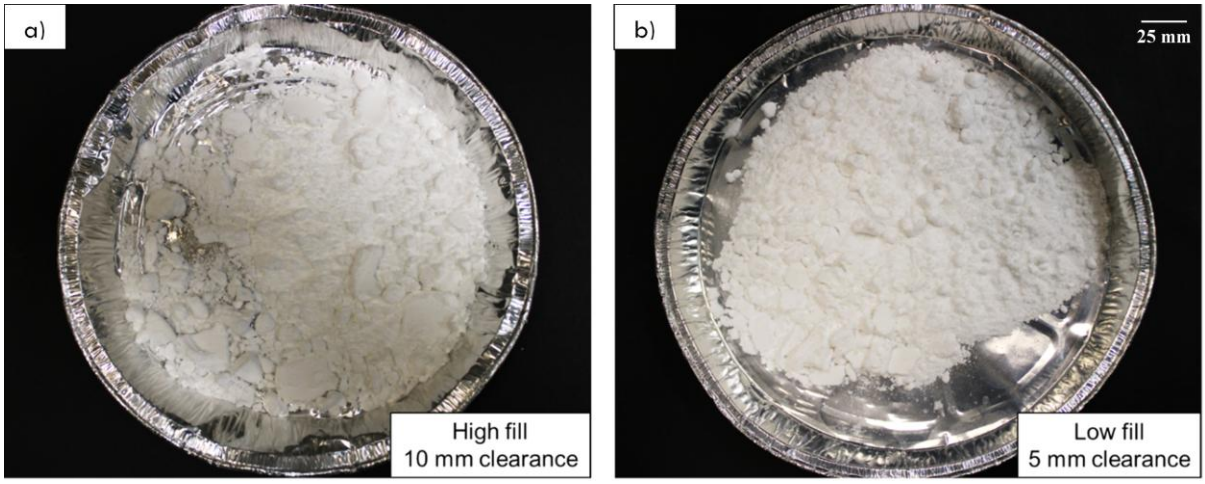

Figure 4.16: 50 rpm 10 min runs at a) high fill and 10 mm clearance and b) low fill and 5 mm clearance.

To further investigate whether the trends in agglomeration previously observed at 50 rpm can be attributed to poor mixing, additional low fill experiments were conducted at 20 % MC with a bed height of 3 cm and a clearance of 5 mm (halved bed height and clearance compared to high fill experiments). These conditions were tested at both 50 and 100 rpm. A comparison of d_{50} values for 50 rpm at both fill levels over time is shown in Figure 4.17, with all d values and ASD spans given in Table 4.12.

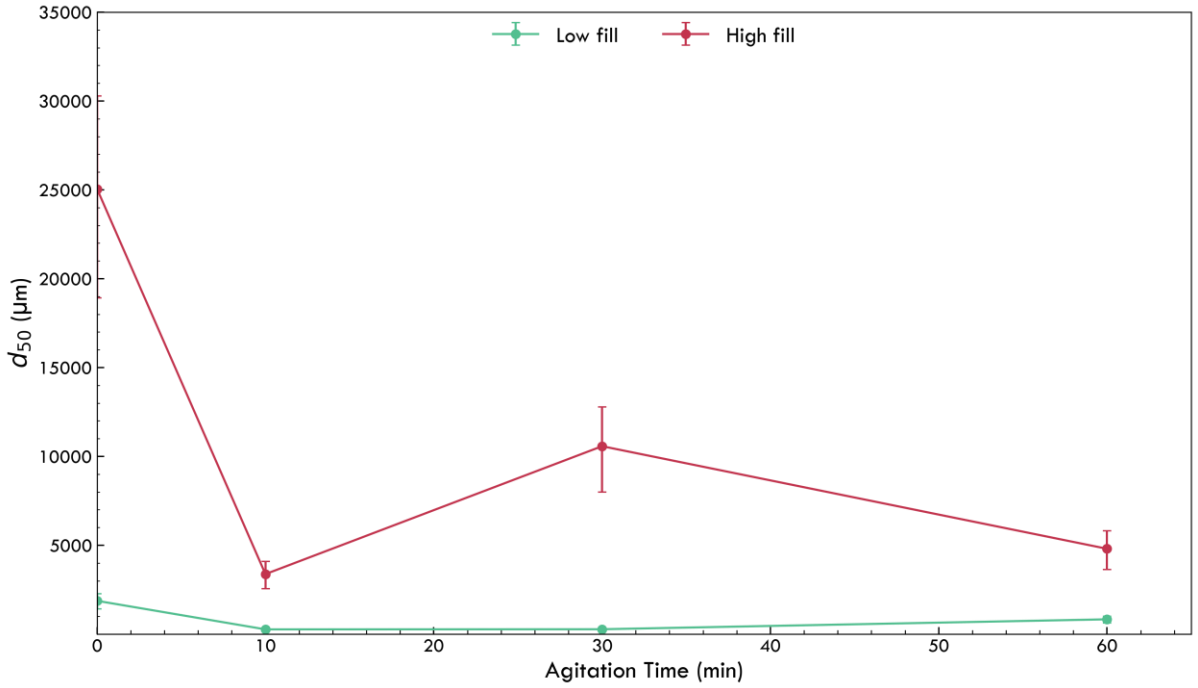

Figure 4.17: d_{50} values of 20 % MC low and high fill experiments at 50 rpm over time. Error bars represent the minimum and maximum error based on 3 repeat experiments at 50 rpm.

Table 4.12: *d* values and ASD spans for 20 % MC low and high fill experiments at 50 rpm.

Agitation Time (min)	Fill Level	d_{10} (µm)	d_{50} (µm)	d_{90} (µm)	ASD Span
0	LOW	114	1872	9834	5.2
10		122	266	8566	31.8
30		123	273	7916	28.5
60		127	832	8805	10.4
0	HIGH	218	25044	49173	2.0
10		181	3376	18095	5.3
30		156	10573	24616	2.3
60		136	4802	17203	3.6

Figure 4.17 shows fluctuations in average agglomerate size and transitions between breakage dominated and agglomeration dominated regimes observed in the high fill system do not occur at a lower fill level. Instead, there is initial breakage due to dispersion of the wet cake, followed by a sustained balance between agglomeration and breakage. This further supports the hypothesis that the fluctuations observed at high fill levels were due to poor mixing, which can lead to localised wet spots. Also, higher fill levels result in less particles being exposed to the shearing action of the impeller, resulting in both attrition near the impeller and agglomeration in less agitated parts of the powder bed.

By comparing the *d* values in Table 4.12, it is clear that the extent of agglomeration is significantly reduced at lower fill levels. This is expected due to the increase in particle collisions with other particles, the impeller and vessel walls. The d_{10} values exhibit minimal variation between the two fill levels, but there are significant differences in d_{50} and d_{90} values, indicating that higher fill levels promote agglomeration and agglomerate growth. Even after 60 minutes of agitation, while the low fill system has a d_{50} of 832 µm and a d_{90} of 8805 µm, the high fill system has a significantly larger d_{50} of 4802 µm and a d_{90} of 17203 µm for the same agitation period. With reduced collisions, large agglomerates are more likely to survive throughout the agitation period, but also able to grow via snowballing. There may also be a degree of the 'Brazil nut effect' where in an agitated system, large agglomerates may segregate towards the top of the bulk and avoid the shearing action of the impeller.[132]

Although all experiments were conducted at an initial MC of 20 %, the size of the wet cake prior to agitation differed significantly. In the high fill system, d_{50} and d_{90} values were 25044 µm and 49173 µm, respectively, but significantly smaller in the low fill system at 1872 µm and 9834 µm. Given that the wet cake volume was halved, a proportional reduction in agglomerate size may be expected, yet the observed difference is much larger (Figure 4.18). This can be attributed to the filtration where higher solid loadings will increase the cake resistance.[45] High fill experiments required a longer filtration time (Table 4.1) to achieve the same MC, which prolonged contact between salicylic acid and water,

potentially forming more liquid bridges. Both the increased filtration time and the larger quantity of material may have contributed to the formation of more and larger loosely bound agglomerates, explaining the observed differences in wet cake structure.

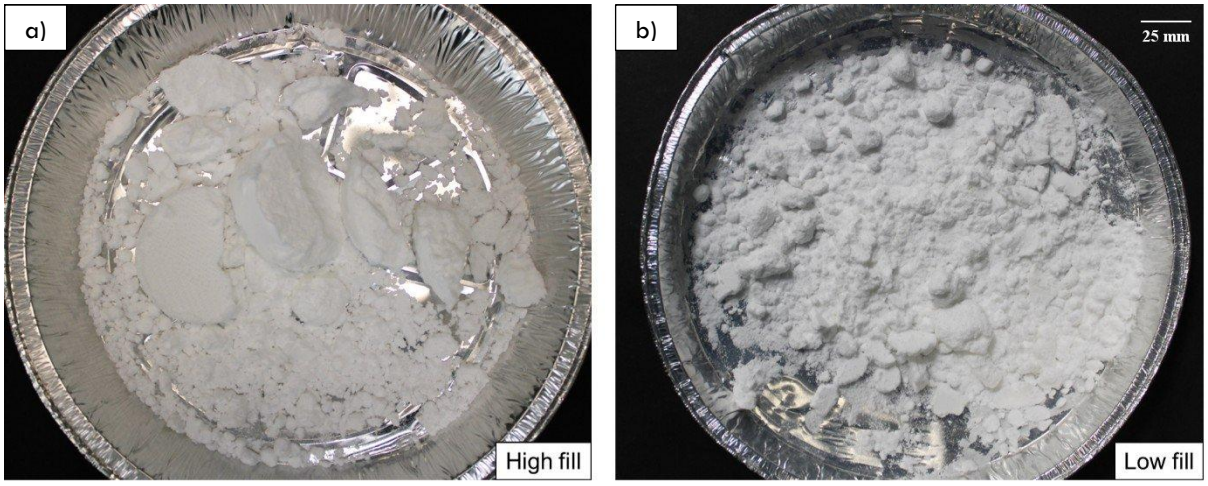

Figure 4.18: The initial wet cake prior to agitation at a) high fill and b) low fill.

The effect of fill level on agglomeration rate over time was also investigated at 100 rpm. The d_{50} values over time for both fill levels are shown in Figure 4.19, and all d values and ASD spans provided in Table 4.13. As expected, agglomeration is reduced at lower fill levels due to less material being present. Interestingly, the data reveals that the agglomeration behaviour over time is consistent for both low and high fill levels at 100 rpm. Both systems exhibit initial breakage of the wet cake, followed by a steady increase in agglomeration, suggesting a dynamic equilibrium between agglomerate growth and breakage, facilitated by the higher agitation speed.

Table 4.13: d values and ASD spans for 20 % MC low and high fill experiments at 100 rpm.

Agitation Time (min)	Fill Level	d_{10} (µm)	d_{50} (µm)	d_{90} (µm)	ASD Span
0	LOW	114	1872	9834	5.2
10		126	294	7820	26.2
30		124	482	7962	16.3
60		135	919	9105	9.8
0	HIGH	218	25044	49173	2.0
10		172	4817	20995	4.3
30		132	5239	17429	3.3
60		179	4937	24868	5.0

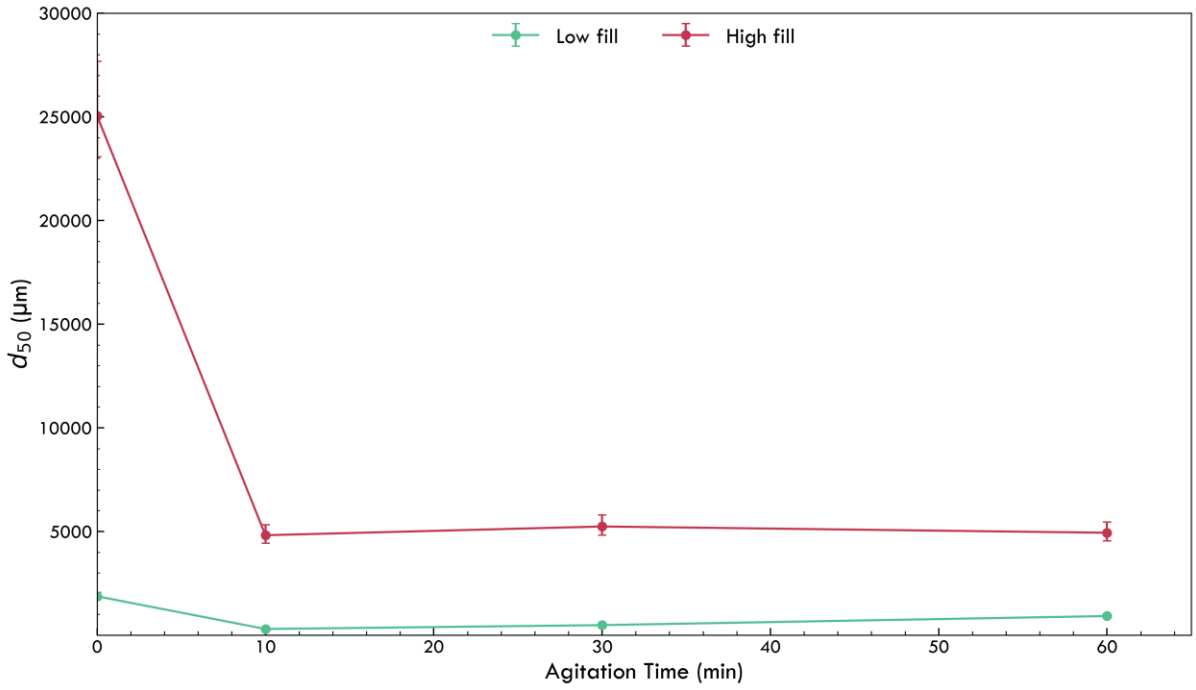

Figure 4.19: d_{50} values of 20 % MC low and high fill experiments at 100 rpm over time. Error bars represent the minimum and maximum error based on 3 repeat experiments at 100 rpm.

At low fill, the d_{50} and d_{90} values steadily increase over time (following the initial breakage of the wet cake), while the ASD span decreases from 26.2 at 10 minutes to 9.8 at 60 minutes. This suggests the ASD becomes more uniform as larger agglomerates grow while smaller fragments are reincorporated into agglomerates. However, the overall extent of agglomeration remains limited compared to high fill. The consistently larger d_{10}, d_{50}, and d_{90} values at all time points for high fill indicate a greater extent of agglomeration due to the higher frequency of particle contact.

Interestingly, while the trend in d_{50} over time is similar for both fill levels at 100 rpm, the d_{90} values differ, indicating distinct dynamics for the largest agglomerates in the population. At low fill, the d_{90} trend aligns with the d_{50}, showing a steady increase from 7820 µm to 9105 µm over time. However, at high fill, the d_{90} values initially decrease significantly, indicating continued breakage from 49173 µm at 0 minutes to 17429 µm at 30 minutes. This is followed by an increase in agglomeration, resulting in a d_{90} of 24868 µm after 60 minutes of agitation. The broken agglomerate fragments likely regrow over time as the system is at a constant MC of 20 %. The increased contact frequency may facilitate any agglomerate fragments or fines to be reincorporated into larger agglomerates, despite the initial breakage. These findings demonstrate how fill level influences the balance between agglomeration and breakage, even at a constant agitation speed.

To provide a comprehensive comparison of the effect of agitation speed on agglomeration across different fill levels, Figure 4.20 combines data from Figures 4.17 and 4.19. This graph highlights the reduced sensitivity to agitation speed at low fill levels and the pronounced impact of speed on high fill levels. While a similar extent of agglomeration is observed at low fill levels for both speeds, the high

fill system appears to be more sensitive to the effect of agitation speed. This indicates that the reduced mixing efficiency typically associated with higher fill levels can be partially offset by increasing the agitation speed, resulting in more steady agglomeration over time.

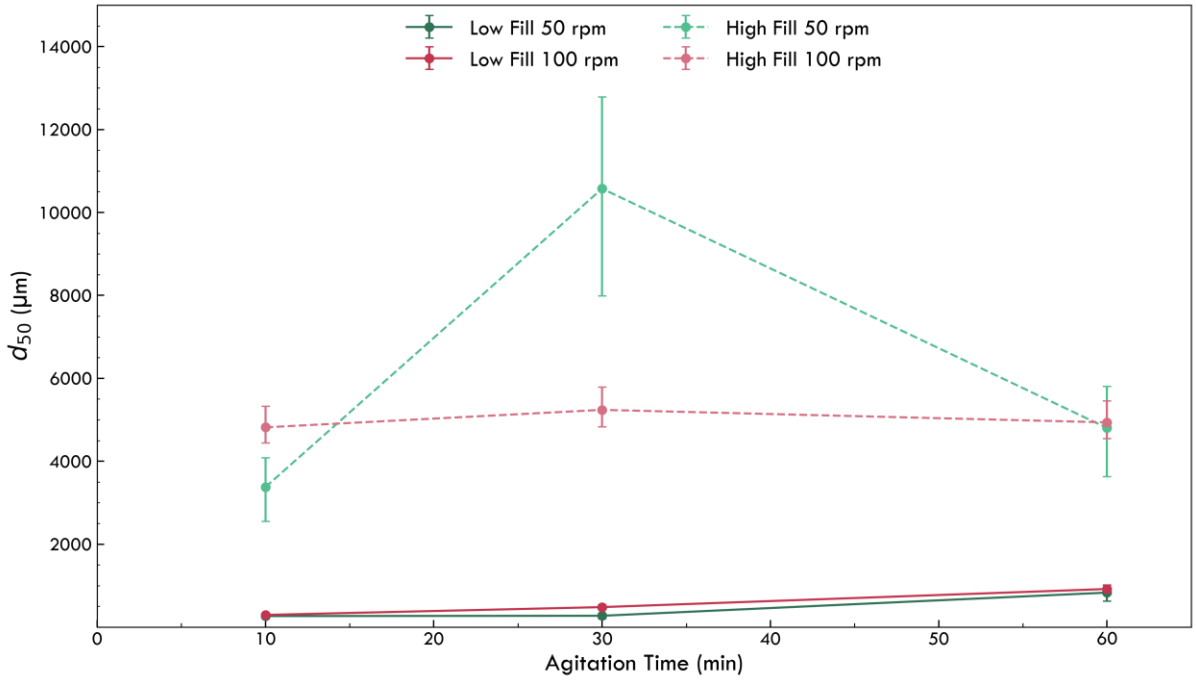

Figure 4.20: d_{50} values of 20 % MC low and high fill experiments at 50 and 100 rpm over time. Error bars represent the minimum and maximum error based on 3 repeat experiments at each speed.

Furthermore, as observed in the high fill experiments discussed in Section 4.3.1, higher agitation speeds continue to result in more agglomeration for this material system, even at a lower fill. At high fill, this effect was only seen during the initial agitation period until about 10 minutes. However, at low fill, this trend is consistent over the whole agitation period of 60 minutes. The effect is less pronounced, likely due to the reduced material available for agglomerate growth. Also, the improved mixing at lower fill level minimises the 'Brazil nut effect' which reduces the opportunity for agglomerates to continue growing by avoiding the shearing of the impeller.

4.3.4 Reflecting on the Proposed Mechanism

These experiments have refined the mechanism proposed in Section 4.2, incorporating the snowballing growth behaviour observed (Figure 4.6). Agglomeration dynamics varied with agitation speed and time, revealing different rates of consolidation and coalescence. At 50 rpm, initial breakage generated fines that promoted subsequent agglomeration. In contrast, higher speeds resulted in simultaneous agglomeration and breakage, as reflected in the relatively consistent d_{50} values over time.

Experiments conducted at 0 and 5 % MC highlighted the critical role of moisture in forming loosely bound agglomerates in the wet cake, and subsequent consolidation and coalescence. The fill level significantly influenced the extent of agglomeration at different agitation speeds, with both 50 and 100 rpm experiments showing consistent agglomeration and breakage over time at low fill. Lower fill levels also reduced the formation of loosely bound agglomerates in the wet cake, likely due to shorter filtration times (15 seconds for low fill compared to 30 seconds for high fill) and less material present.

Overall, these findings support the proposed mechanism while demonstrating how key material and process parameters interact to influence the extent of agglomeration. The results emphasise the significance of the wet cake structure and how the presence of loosely bound agglomerates can influence agglomeration dynamics during agitation. The proposed mechanism has also been refined to include the snowballing growth behaviour observed under certain conditions. This improves the mechanistic understanding of undesired agglomeration in AFDs and provides a foundation for predicting how different material and process parameters influence agglomeration dynamics.

4.4 Conclusions

In this work, a novel mechanism for undesired agglomeration is proposed, offering the first mechanistic framework for understanding this phenomenon in agitated dryers. Unlike previous studies that focus on individual parameters in isolation, this work highlights the limitations of a 'one-size-fits-all' approach. By capturing the rate processes driving agglomeration, the proposed mechanism provides a foundation for predictive models that can improve process design and scale up. This chapter has systematically investigated the influence of key material and process parameters such as agitation speed, agitation time, moisture content, temperature and fill level on the extent of agglomeration observed in an AFD.

Agitation speed and time were shown to have a significant influence on the rate and extent of agglomeration. Higher agitation speeds promoted a dynamic equilibrium between breakage and agglomerate growth, where fines generated were continuously reincorporated into wet agglomerates through snowballing. At lower speeds, a transition from breakage dominated to agglomeration dominated behaviour was observed, emphasising the role of shear forces in facilitating coalescence. Regardless of agitation speed, all systems reached an equilibrium state within 60 minutes, which is consistent with the fact that 60 minutes at 50 rpm corresponds to the same number of rotations as 30 minutes at 100 rpm, reinforcing that the same underlying mechanism governs agglomeration, albeit at different rates.

Moisture content played a critical role, with significant agglomeration observed even at 5 % MC, suggesting a low critical moisture content for this material system. The binding mechanisms of dry particles were also examined, demonstrating a smaller limiting agglomerate size in the absence of liquid bridges. Temperature effects further reinforced the role of liquid bridge strength, as increased dissolution at higher temperatures likely increased liquid bridge strength and the resulting extent of agglomeration.

Fill level was also shown to have a major influence on agglomeration behaviour. Both increased particle contact frequency and reduced shearing effects from the impeller at high fill levels resulted in increased agglomeration. Higher speeds were also shown to offset the reduced mixing efficiency observed with increased fill levels. The dynamic between fill level and clearance height further highlighted its impact on particle mobility and shear forces within the dryer.

These findings provide key mechanistic insight into the balance between agglomerate growth and breakage during agitated drying. The experimental results support the proposed mechanism, offering a more comprehensive understanding of how material properties and process conditions interact to drive agglomeration dynamics. Further work will develop the understanding of agglomeration dynamics in this chapter by investigating different process conditions and size fractions of salicylic acid. In the following chapter, distinct growth behaviours under various conditions will be identified.

Chapter 5 - Development of a Regime Map for Agglomeration Behaviour in Agitated Filter Dryers

Building on the mechanistic understanding developed in Chapter 4, this chapter presents a regime map to identify different agglomerate growth and breakage behaviours observed in an AFD. The aim is to link key input parameters (such as primary particle size, agitation speed and moisture content) to the resulting agglomeration behaviours observed experimentally.

In this chapter, different agglomerate growth behaviours of salicylic acid are identified by modifying the primary particle size. To compare different experimental conditions, the traditional Stokes deformation number is adapted to AFD applications by incorporating torque measurements to reflect the energy required for deformation. The Stokes deformation number is used in conjunction with the maximum pore saturation to construct a regime map that captures the range of agglomeration dynamics observed across this chapter and Chapter 4.

5.1 Experimental Design and Methodology

5.1.1 Experimental Design

To explore different agglomeration behaviours beyond those previously observed in Chapter 4, a series of experiments were conducted using a coarser size fraction of salicylic acid (212 – 300 μm). The aims of these experiments were to:

- Investigate the influence of primary particle size on the extent of agglomeration and the agglomeration dynamics.
- Characterise and compare the strength of agglomerates formed under different experimental conditions.
- Develop a regime map to identify different agglomerate growth and breakage behaviours of salicylic acid under various process conditions.

5.1.2 Materials

Salicylic acid (≥ 98 %) was obtained from VWR Chemicals and sieved to obtain a size fraction of 212 – 300 μm to be used as a moisture sensitive model API. Distilled water prepared using a Stuart D4000 Distinction water still was used as the solvent.

5.1.3 Experimental Methodology

This section outlines the experimental procedure used for investigating agglomerate growth behaviours of salicylic acid when using a larger size fraction of primary material at various agitation times and speeds. All experiments were conducted in a PSL GFD Lab 010 series AFD, with the jacket temperature maintained at 25 °C throughout each experiment.

5.1.3.1 Effect of primary material size fraction on agglomeration

To investigate how the primary material size affects the extent of agglomeration, experiments were conducted at 20 % moisture content (MC) using the 212 – 300 μm fraction of salicylic acid. These followed the methodology outlined in Chapter 4, Section 4.1.3. The experiments were conducted at a low fill level (bed height of 3 cm) with a 10 mm clearance at 20 % MC, as outlined in Table 5.1.

Table 5.1: Agitation conditions investigated for low fill experiments with salicylic acid (212–300 μm size fraction) at a 10 mm clearance.

Fill Level	Clearance (mm)	Agitation Speed (rpm)	Agitation Time (min)
LOW	10	50	0.5
			10

5.1.3.2 Effect of clearance

Following these experiments, the agitator clearance was lowered to 5 mm to further reduce the agglomeration. Table 5.2 presents the various agitation conditions investigated at 20 % MC and a 5 mm clearance.

Table 5.2: Agitation conditions investigated for low fill experiments with salicylic acid (212 – 300 μm size fraction) at a 5 mm clearance.

Fill Level	Clearance (mm)	Agitation Speed (rpm)	Agitation Time (min)
LOW	5	50	0
			0.5
			10
			30
			60
		100	0
			0.5
			10
			30
			60

For the experiments in Table 5.2, the heel was separated from the bulk material at the end of each experiment. The bulk material flowed easily and was primarily obtained by tilting the filter basket, whereas the heel adhered to the base of the filter basket and was removed by manually scraping with a spatula. Wet and dry masses of the bulk and the heel were recorded to calculate the percentage of the wet cake that consists of the heel.

5.1.4 Characterisation

The various methods used for primary material and product characterisation are summarised in the following sections.

5.1.4.1 Sieving

Salicylic acid was sieved using 212 μm and 300 μm mesh size sieves and a receiver pan at an amplitude of 0.85 mm/g for 12 minutes. Rationale for the amplitude and sieving time can be found in Chapter 3, Section 3.2.1. The agglomerated samples were also sieved to give the agglomerate size distribution (ASD), with the detailed method outlined in Chapter 3, Section 3.6.1.

5.1.4.2 Moisture content analysis

The moisture content of agglomerated samples was measured using a Ohaus MB90 Moisture Analyser, and more details on the technique can be found in Chapter 3, Section 3.6.2.

5.1.4.3 Envelope density

The envelope density of a material is defined as the mass per unit volume including all pores and was measured using a Micrometrics GeoPyc 1365 Envelope Density Analyser. This technique relies on the displacement of DryFlo powder to measure the volume and envelope density of the sample, assuming that the DryFlo powder is unable to enter any pores within the sample. DryFlo powder has a d_{50} of approximately 130 μm.[133] A 25.4 mm sample chamber was filled with DryFlo powder, ensuring that the sample occupied a minimum of 25 % of the chamber volume. The bed was compressed with a piston, applying a force of 51 N, and the volume of the powder was measured. The sample was then added and the volume of powder displaced by the sample was calculated. For the measurements, agglomerates were sieved to obtain those with a size between 2000 – 3350 μm and weighed to obtain approximately 3 g of sample. Each measurement was repeated three times to obtain an average volume and corresponding envelope density.

5.1.4.4 True density

True density refers to the mass per unit volume for a given material, excluding any internal porosity. Helium pycnometry was used for measuring the true density with a Micrometrics Accupyc 1340 pycnometer. A known mass of sample was placed in a 1 cm^3 sample cell, filled to between half and two-thirds of its capacity. The cell was then loaded into the instrument, sealed and pressurised. The chamber was purged before injecting helium until the desired pressure of 19 psi was achieved. As the helium penetrates any pores in the sample, the instrument uses the initial and equilibrium pressure to calculate the sample volume. The process involved five purge and fill cycles, after which an average true volume is calculated. The average true volume and the sample mass were used to determine the true density.

5.1.4.5 Compression testing

To determine the yield stress of agglomerates, a series of quasi-static compression tests were performed using an Instron ElectroPuls® E1000 testing machine equipped with a 1 kN load cell (Figure 5.1). Agglomerates from different experimental conditions were separated by size fractions and 12 measurements were conducted for each condition, which are outlined in Table 5.3. Size fractions were chosen to ensure sufficient agglomerates were available for testing. Each agglomerate was positioned axially between the two platens and quasi-static compression tests were performed at a speed of 2 mm/min, with the bottom platen fixed throughout. Force-displacement data were recorded by the Instron WaveMatrix software and exported for analysis.

Figure 5.1: Instron ElectroPuls® E1000 testing machine.

The force and displacement data obtained from quasi-static compression tests was converted into a stress-strain curve to identify the yield stress. The point of contact between the top platen and agglomerate was determined by a detectable increase in force. The initial height is subtracted from each of the platen position values after contact resulting in a starting position of 0 mm. The platen position after contact was subtracted from the initial agglomerate height to give the instantaneous height of the agglomerate. Based on these calculations, the natural strain (ε_a) for can be calculated using:

$$\varepsilon_a = \ln\left(\frac{H}{h}\right) \tag{5. 1}$$

where H is the initial height of the agglomerate and h is the platen separation distance at any time. The zeroed force was calculated by subtracting the average pre-contact force from each of the force values.

Assuming the agglomerates are spherical, the cross-sectional area of the agglomerate (A) at each point can be calculated using:

$$A = \frac{H}{h}\frac{\pi D^2}{4} \tag{5.2}$$

where D is the original diameter of the agglomerate. The stress (σ) at any given time was therefore:

$$\sigma = \frac{F}{A} \tag{5.3}$$

where F is the applied force. From the resulting stress-strain graph for each agglomerate, the peak yield stress value was identified as the stress value above which the agglomerate undergoes permanent deformation. An average of 12 yield stress values was calculated for each agglomerate condition and size fraction.

Table 5.3: Experimental conditions and size fractions of agglomerates used for quasi-static compression tests.

Moisture Content (%)	Agitation Speed (rpm)	Agitation Time (min)	Size Fraction (mm)
5	50	2	9.5 – 6.7
			4.75 –3.35
		60	9.5 – 6.7
			4.75 – 3.35
	100	10	9.5 – 6.7
			4.75 – 3.35
		60	9.5 – 6.7
			4.75 – 3.35
20	50	14	9.5 – 6.7
			4.75 – 3.35
		60	9.5 – 6.7
			4.75 – 3.35
	100	10	9.5 – 6.7
			4.75 – 3.35
		60	9.5 – 6.7
			4.75 – 3.35

5.1.4.6 Porosity measurements

The porosity of agglomerates was calculated using image analysis, using a Canon EOS 2000D camera and Lumenera Infinity Analyze software. Agglomerates from experiments conducted at various moisture contents were separated into two size fractions, with all conditions tested shown in Table 5.4.

Table 5.4: Experimental conditions and size fractions of agglomerates used for porosity calculations.

Moisture Content (%)	Size Fraction (mm)
0	9.5 – 6.7
	4.75 – 3.35
5	9.5 – 6.7
	4.75 – 3.35
20	9.5 – 6.7
	4.75 – 3.35

Individual dry agglomerates were weighed using a Mettler Toledo UMT2 microbalance (readability of 0.1µg). Image analysis was used to determine the average agglomerate diameter, which was then used to approximate the volume of the agglomerate, assuming a spherical geometry. The individual agglomerate density was calculated from the mass and volume, with twenty agglomerates measured for each condition to find the mean density. The porosity (ε) of the agglomerate can then be found using:

$$\varepsilon = 1 - \left(\frac{\rho_e}{\rho_t}\right) \qquad 5.4$$

where ρ_e is the envelope density and ρ_t is the true density of salicylic acid.

5.1.4.7 Mixer torque rheometry

A mixer torque rheometer (Caleva MTR 3) was used to obtain torque measurements of salicylic acid and water using the multiple addition method. The MTR was used with the reduced fill stainless steel bowl, which was fitted with two horizontal, contra-rotating mixing blades (33 mm diameter). The load cell features a torque arm to directly measure the torque of the wet solids. The torque of the empty bowl was measured for 20 seconds and used to normalise all subsequent measurements. The sample bowl was then filled with 10 g powder and mixed for 20 seconds before the torque of the dry powder was measured for a further 20 seconds. Distilled water was added sequentially in 0.5 mL aliquots using a micropipette. After each aliquot addition, the wet solids were mixed for 60 seconds before the torque was measured for 20 seconds. This was continued until 20 aliquots were added to achieve a 1:1 slurry and the mean torque at each aliquot was obtained. This was conducted using both size fractions of salicylic acid (< 106 µm and 212 – 300 µm) investigated in this chapter.

5.2 Results and Discussion

The aim of these experiments is to identify different agglomerate growth dynamics to those observed in Chapter 4 when using a larger size fraction of salicylic acid. By using the same material, the surface chemistry remains constant and differences in agglomeration growth dynamics can be attributed to changing the primary particle size. This ensures that the regime map later developed captures a range of different growth behaviours under different conditions. The data is presented using agglomerate size distributions (ASDs) or graphs of d_{50} values over time. To give a thorough understanding of the ASD, all d values and ASD spans are provided. Characterisation data from Instron compression tests, image analysis porosity approximations and MTR experiments were assessed for their ability to distinguish different strengths of agglomerates produced under varying conditions. The measurements were used to develop dimensionless numbers that describe the agglomerate growth behaviours observed. Using these, a regime map is developed where agglomerate growth is plotted as a function of these numbers.

5.2.1 Effect of Primary Particle Size Fraction on Agglomeration Rates

The particle size influences cohesion with fine particles often resulting in more agglomerates. This can be due to the greater contact area with the solvent, enabling liquid bridge formation.[61] To investigate the effect of using a larger particle size fraction of salicylic acid on the resulting agglomeration, a low fill experiment was conducted using the 212 – 300 µm fraction at 50 rpm for a 10 minute agitation period. The ASD for this experiment is plotted and compared against experiments conducted at the same MC, agitation speed and time using the < 106 µm size fraction at both low and high fill levels in Figure 5.2. The corresponding d values and ASD spans are given in Table 5.5.

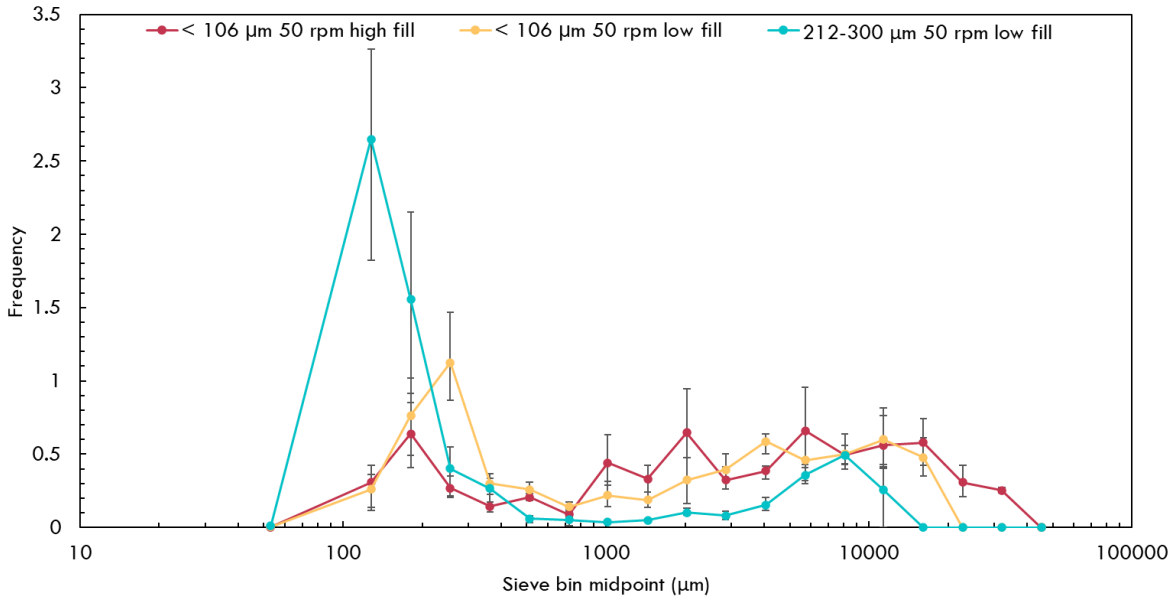

Figure 5.2: Agglomerate size distributions for 50 rpm 10 min runs at various fill levels using different size fractions of salicylic acid. Error bars represent the minimum and maximum error based on 3 repeat experiments for each size fraction.

It is evident from Figure 5.2 and Table 5.5 that both a lower fill level and a larger size fraction of primary material reduce the extent of agglomeration. Using the 212 – 300 µm size fraction of salicylic acid results in a shift in the ASD towards the left, indicating a reduced extent of agglomeration. The frequency of smaller particle sizes is also much higher for the coarser size fraction. Although the surface chemistry remains constant across size fractions, larger particles have a lower surface area to volume ratio, reducing the extent of liquid bridge formation. The d_{10} and d_{50} values for the 212 – 300 µm size fraction (115 µm and 171 µm, respectively) also suggest some breakage is occurring. This is likely because the agglomerates formed are weaker than those produced from the < 106 µm fraction, due to less liquid bridges binding the particles together and fewer points of contact for a given mass.

Table 5.5: *d* values and ASD spans for 20 % MC 50 rpm 10 min runs with various size fractions of salicylic acid.

Material Grade (µm)	Fill Level	d_{10} (µm)	d_{50} (µm)	d_{90} (µm)	ASD Span
< 106	High	181	3376	18095	5.3
< 106	Low	178	1710	12143	7.0
212 – 300	Low	115	171	7133	41.0

Although the extent of agglomeration is reduced with the 212 – 300 µm size fraction, there is still considerable agglomeration of the starting material, with some large agglomerates persisting as indicated by the d_{90} value of 7133 µm after just 10 minutes of agitation. This may be due to the 212 – 300 µm low fill experiment being conducted with a 10 mm clearance, whereas the < 106 µm low fill experiment had a 5 mm clearance. For a fair comparison, the 212 – 300 µm low fill experiment was repeated with the clearance also reduced to 5 mm. The ASDs for both clearances at 50 rpm for a 10 min agitation period are illustrated in Figure 5.3, with *d* values and ASD spans given in Table 5.6.

Table 5.6: *d* values for low fill 50 rpm 10 min runs at 5 mm and 10 mm clearances using the 212 – 300 µm size fraction of salicylic acid.

Agitation Time (min)	Clearance (mm)	d_{10} (µm)	d_{50} (µm)	d_{90} (µm)	ASD Span
10	10	115	171	7133	41.0
	5	121	197	3189	15.6

The ASDs in Figure 5.3 highlight that the most significant difference in the size distributions is the reduction in large agglomerates when the clearance is halved from 10 mm to 5 mm. This is further reinforced by the reduction in d_{90} from 7133 µm to 3189 µm. The d_{10} and d_{50} values are quite similar, with only the d_{90} showing a noticeable difference. The heel is subjected to different shear forces compared to the bulk of the vessel. The compression exerted by the agitator likely enables particles to

agglomerate and form large chunks below the agitator. With a larger clearance, there is more material present below the agitator and thus, this effect is exacerbated.

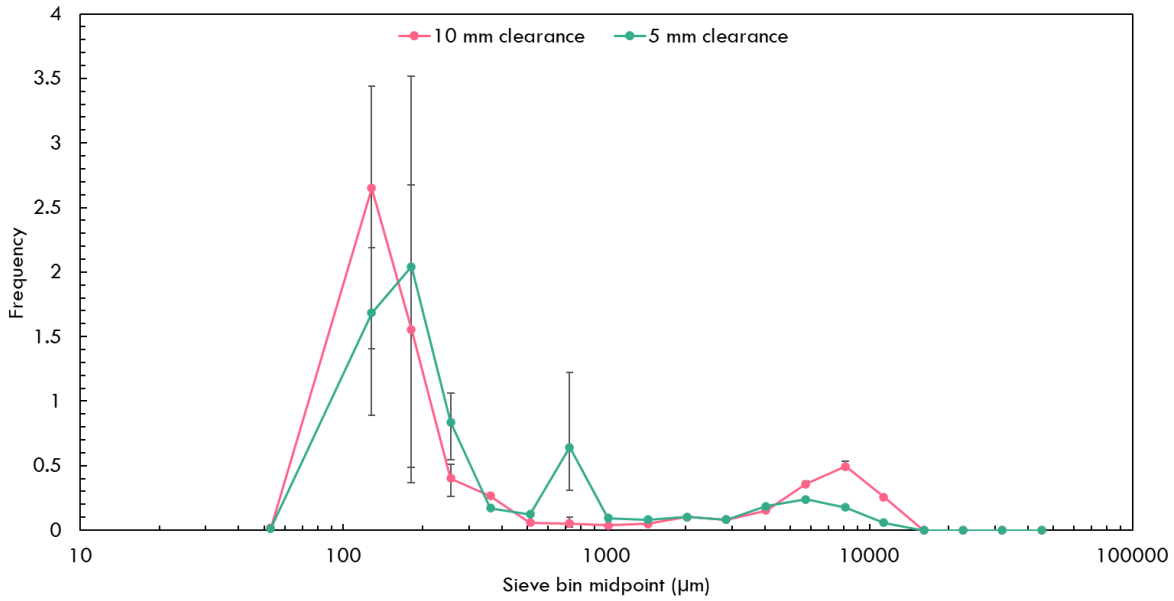

Figure 5.3: Agglomerate size distributions for low fill 50 rpm 10 min runs at 5 and 10 mm clearances using the 212 – 300 µm size fraction of salicylic acid. Error bars represent the minimum and maximum error based on 3 repeat experiments.

This difference was also observed visually, with images of the material from low fill 50 rpm runs for a 10 minute agitation period at both 10 mm and 5 mm clearances shown in Figure 5.4a and Figure 5.4b, respectively. Although agglomerates are present at both clearances, there are noticeably fewer large lumps in Figure 5.4b where the clearance has been lowered to 5 mm. This was also observed in Chapter 4, Section 4.3.3, and can be attributed to more material being agitated and experiencing the shear forces of the impeller at lower clearances. As these experiments were conducted with the aim of finding different growth behaviours of salicylic acid and conditions that reduce the extent of agglomeration, all subsequent experiments were conducted at a low fill with a 5 mm clearance.

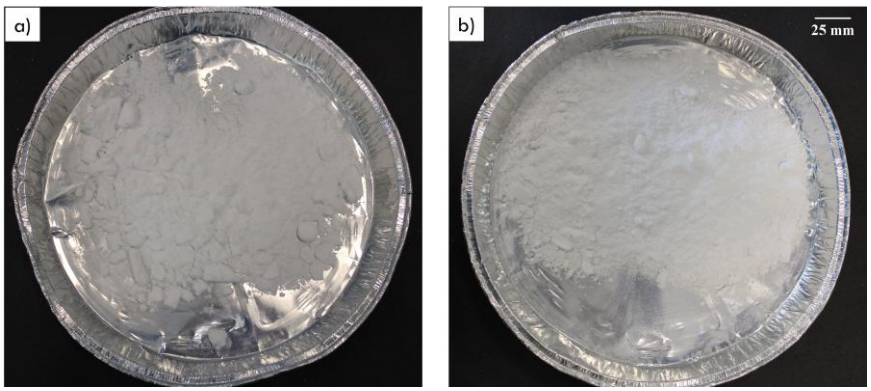

Figure 5.4: Low fill 50 rpm 10 min runs with a clearance of a) 10 mm and b) 5 mm.

In the low fill experiments conducted with a 5 mm clearance, the heel was separated from the bulk of the sample. The bulk was easily removed by tipping the filter basket, whereas the heel adhered to the

base and required manual scraping. Heel formation was only observed after longer agitation times of 30 and 60 minutes. An example of the heel remaining after isolating the bulk of the material from a 30 min run at 50 rpm is shown in Figure 5.5.

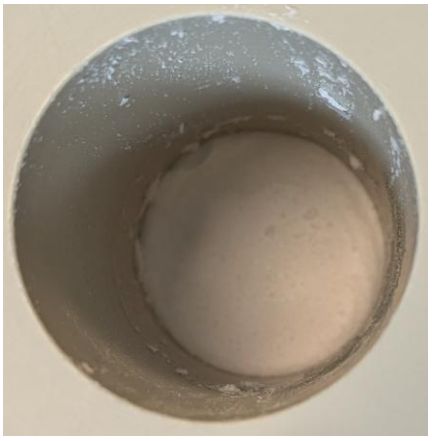

Figure 5.5: Heel remaining after isolating the bulk material from a 20 % MC 50 rpm 30 minute run.

To assess the heel's contribution to the extent of agglomeration, the masses of the bulk and heel were recorded. For a 60 minute run at 50 rpm, both the bulk and heel were characterised, with the ASDs shown in Figure 5.6. Care was taken to minimise any breakage of the heel when removing from the vessel. The corresponding *d* values, ASD spans and weight percentages are presented in Table 5.7.

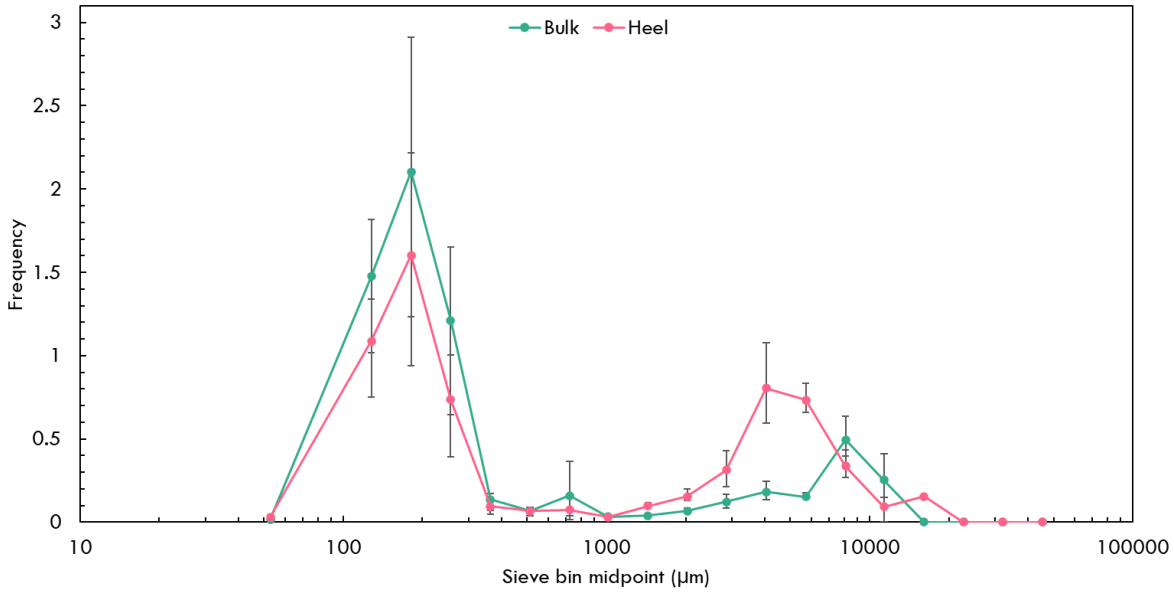

Figure 5.6: Agglomerate size distributions for the bulk and heel from a 20 % MC 50 rpm 60 minute run using the 212 – 300 µm size fraction of salicylic acid. Error bars represent the minimum and maximum error based on 3 repeat experiments.

The ASDs in Figure 5.6 indicate that although the heel contains large agglomerates, removing the heel does not necessarily result in less agglomeration, as the bulk material still has a d_{90} of 7118 µm. Large agglomerates clearly persist regardless of the heel. This approach was to ensure that agglomerate sizes determined by sieving were not artificially inflated by including the heel. At shorter agitation times, no

distinct heel was observed. For 30 and 60 minute runs where the heel was present, it was separated but not always characterised, as scraping the vessel to remove the heel would break apart agglomerates and affect the measured size distribution.

Table 5.7: *d* values, ASD spans and weight percentages of the bulk and heel from a 20 % MC 50 rpm 60 minute run using the 212 – 300 µm size fraction of salicylic acid.

Component	d_{10} (µm)	d_{50} (µm)	d_{90} (µm)	ASD Span	Weight (%)
Bulk	121	200	7118	35.0	73.4
Heel	122	257	6499	24.8	26.6

Once the experimental procedure was established, further 20 % MC low fill experiments using 212 – 300 µm salicylic acid were conducted at 50 and 100 rpm for various agitation periods. The d_{50} values for these experiments are plotted over time in Figure 5.7 and compared with analogous experiments using the < 106 µm size fraction of salicylic acid. The corresponding *d* values, ASD spans and heel weight percentages are given in Table 5.8.

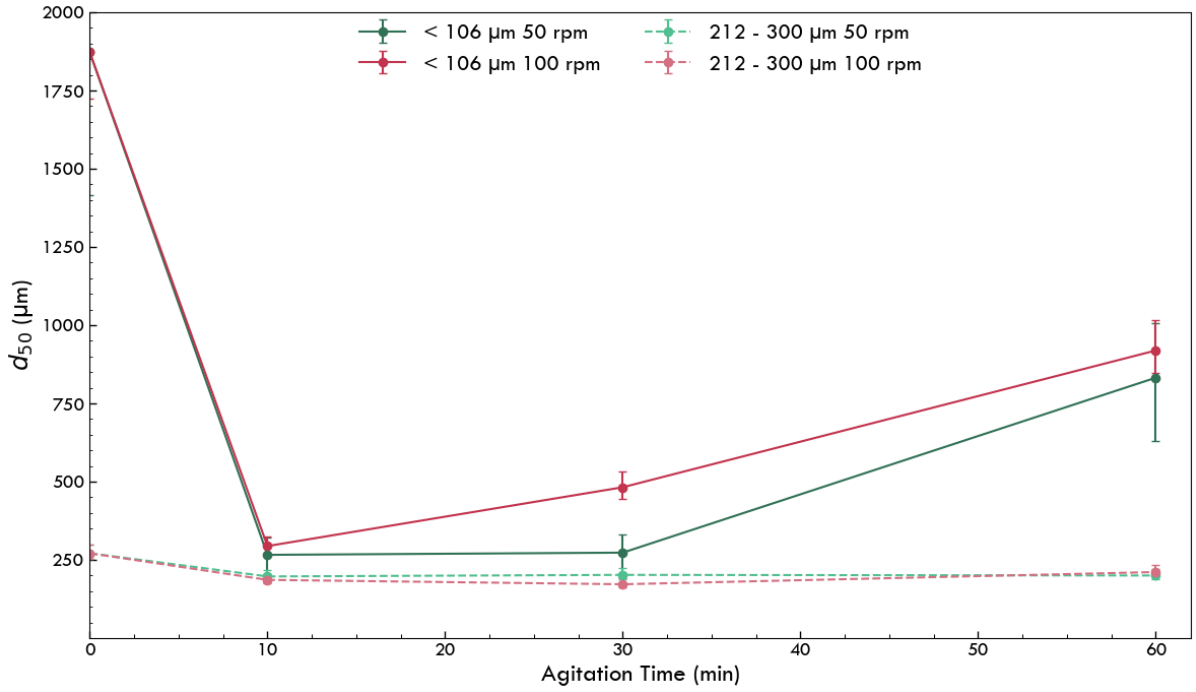

Figure 5.7: d_{50} values of 20 % MC low fill experiments at 50 and 100 rpm over time using various size fractions of salicylic acid. Error bars represent the minimum and maximum error based on 3 repeat experiments for each size fraction.

From Figure 5.7, it is evident that the d_{50} values remain lower throughout the time period investigated when using the 212 – 300 µm size fraction, regardless of agitation speed. This trend has been reported in the literature for experiments conducted using different grades of lactose, where smaller size fractions produced larger granules.[134] The authors attributed this to more efficient nucleation and coalescence of

particles. Analogous results have been reported in studies investigating the effect of drug substance particle size on granulation in a high shear mixer, where the final granule size was inversely proportional to the primary particle size of the drug substance.[135,136] Agglomerates composed of smaller particles also tend to be stronger and more likely to resist the shear forces exerted by the agitator, which explains the larger d_{50} values observed with the smaller size fraction.[137]

Table 5.8: *d* values, ASD spans and heel contributions for all agitation speeds and times investigated at 20 % MC using the 212 – 300 µm size fraction of salicylic acid.

Agitation Speed (rpm)	Agitation Time (min)	d_{10} (µm)	d_{50} (µm)	d_{90} (µm)	ASD Span	Heel Weight (%)
0	0	120	271	6335	22.9	-
50	10	121	197	3189	15.6	-
	30	125	202	5284	25.6	21.7
	60	121	200	7118	35.0	26.6
100	10	123	186	7543	39.8	-
	30	116	172	4718	26.7	26.0
	60	123	211	6972	32.5	26.7

The reduced agglomeration with the larger size fraction is reflected even before agitation, with the initial wet cake having a d_{50} of 271 µm. In comparison, the < 106 µm size fraction wet cake had a d_{50} of 1872 µm. This phenomenon has been observed in the literature, where smaller particles tend to have a higher cake resistance and therefore longer filtration times. This prolonged contact between the particles can enable liquid bridges to form.[43,45] Wakeman reported that doubling the particle size resulted in an almost 50 % increase in filtrate volume produced at any time.[41] Although the wet cakes for both size fractions were filtered to reach 20 % MC, the 212 – 300 µm fraction only required a filtration time of 20 seconds, compared to 30 seconds for the < 106 µm size fraction. However, this small difference in filtration time is unlikely to account for the significant variation in d_{50} values. It is more likely attributable to the reduced surface area for liquid bridge formation for the 212 – 300 µm fraction.

Once agitation begins, there is some initial breakage of the wet cake for both size fractions. For the larger size fraction, this breakage appears to be quite minimal in comparison, with the d_{50} values after 10 minutes of agitation being comparable to the < 106 µm size fraction. This is likely due to the wet cake containing fewer and smaller loosely bound agglomerates when using the larger size fraction. With continued agitation beyond 10 minutes, the d_{50} values remain fairly consistent up to 60 minutes at both 50 and 100 rpm. This reflects the limited agglomerate growth when using a coarser size fraction with reduced cohesivity.

It is also interesting to note that the heel weight percentages in Table 5.8 were similar at both speeds, in the range of 21.7 – 26.7 %. A distinct heel that could be separated from the bulk sample was only

observed after longer agitation periods of 30 and 60 minutes. The agitator clearance was set at 5 mm, with a cake height of 3 cm, so the heel would be expected to constitute 16.7 % of the wet cake volume. However, the higher heel weight percentages observed indicate that the heel is denser than the bulk material. This supports the hypothesis that agglomeration in the heel is driven by a different mechanism and is likely the result of compaction under the agitator. The morphology of the heel is analysed and compared with bulk agglomerates later in Chapter 6, Section 6.3.2.

Overall, these experiments demonstrate that different agglomeration behaviours of salicylic acid can be observed by changing the primary particle size. Using a larger size fraction with inherently lower cohesivity lowered the extent of agglomeration. Although limited to a small data set, this work highlights the importance of considering particle size when designing agitated drying processes.

5.2.2 Compression Testing

In order to characterise the strength of agglomerates produced from different experimental conditions, compression testing was performed using an Instron ElectroPuls® E1000 testing machine. For each experimental condition, 12 agglomerates were tested per size fraction. The average peak yield stress values for each size fraction and the overall averages for 5 % and 20 % MC are presented in Table 5.9. Agglomerates produced at 0 % MC were unsuitable for this analysis as they were too friable to be analysed with the 1 kN load cell.

Table 5.9: Peak yield stress values for agglomerates from all experimental conditions investigated.

Moisture Content (%)	Agitation Speed (rpm)	Agitation Time (min)	Size Fraction (mm)	Peak Yield Stress (Pa)	Average Peak Yield Stress (Pa)
5	50	2	9.5 – 6.7	25081	37405
			4.75 – 3.35	43470	
		60	9.5 – 6.7	32090	
			4.75 – 3.35	40846	
	100	10	9.5 – 6.7	26234	
			4.75 – 3.35	40411	
		60	9.5 – 6.7	29493	
			4.75 – 3.35	61612	
20	50	14	9.5 – 6.7	38681	41053
			4.75 – 3.35	55938	
		60	9.5 – 6.7	27796	
			4.75 – 3.35	46119	
	100	10	9.5 – 6.7	33886	
			4.75 – 3.35	47937	
		60	9.5 – 6.7	28466	
			4.75 – 3.35	49605	

From the peak stress values in Table 5.9, it is evident that there is no clear distinction in peak stress values between agitation times, speeds or MC. The only consistent trend is that the smaller size fraction (4.75 – 3.35 mm) generally exhibited higher yield stress values, which is expected as smaller agglomerates tend to be mechanically stronger.[45]

Considerable fluctuation was observed across the 12 data points used to calculate an average for each experimental condition. An example is shown in Figure 5.8, which plots all peak stress values for agglomerates from a 5 % MC 50 rpm 60 minute run in the 4.75 – 3.35 mm size fraction. Although the average peak stress was 40846 Pa, the recorded values ranged from 24464 to 60040 Pa. A trendline was added to Figure 5.8 to highlight that despite the variation in values, no clear outliers were present. This confirms the natural variation in the data set, likely due to the irregular shape of the agglomerates.

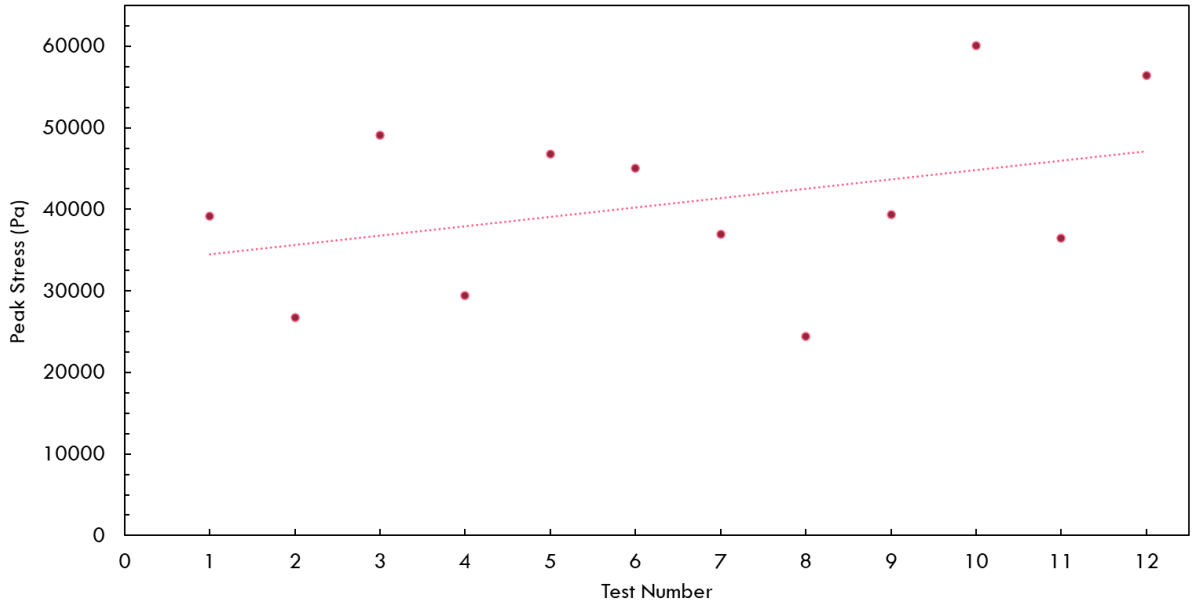

Figure 5.8: Peak stress values for agglomerates tested from a 5 % MC 50 rpm 60 minute run in the 4.75 – 3.35 mm size fraction.

For the data analysis, agglomerates were assumed to be spherical, as calculating the exact cross-sectional area of irregularly shaped particles is challenging. However, as the agglomerates varied in shape and were not perfectly spherical, this assumption may contribute to the fluctuations observed in the data. An example of agglomerates tested is shown in Figure 5.9, highlighting the extent of irregularity in shape.

One method commonly used for measuring agglomerate strength involves forming pellets rather than using actual agglomerates. The pellets can be prepared with defined size, porosity and MC, and they provide a uniform surface area for compression testing. Numerous studies have reported using pellets that act as pseudo-granules to measure the dynamic yield stress of granules and to investigate the deformation and breakage behaviour of granules.[6,37,138]

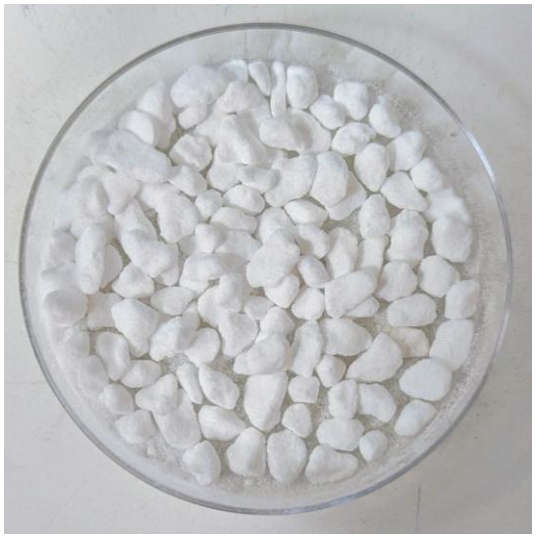

Figure 5.9: Example of agglomerates tested using the Instron.

While wet pellets are useful for understanding the deformation of wet agglomerates, it was essential for this work to study the dry agglomerates produced in experiments. In this study, the focus is on undesired agglomeration in AFDs and how material and process parameters impact the final agglomerate strength, as opposed to the deformation behaviour under impact. Measuring the dynamic yield stress of dry agglomerates provides more relevant insight into their mechanical strength and indicates whether additional processing steps such as milling may be required prior to tabletting.

It is also important to note that the experiments conducted at 5 and 20 % MC in Chapter 4, Section 4.3.2, highlighted that the extent of agglomeration was not significantly different, with comparable d_{50} values observed. However, a clearer difference was evident in the d_{90} values. As the MC influences the extent of liquid bridge formation, it is expected that the mechanical strengths of agglomerates would differ.

Compression testing is a valuable tool for characterising mechanical properties. However, this work was limited by the irregularity of the agglomerates. To investigate and quantify the structural differences between agglomerates from different MCs, porosity measurements were conducted, as porosity is inversely proportional to granule strength.[128]

5.2.3 Porosity Measurements

To evaluate the porosities of agglomerates formed under different experimental conditions, image analysis was used to approximate the porosity. Agglomerates produced at 0, 5 and 20 % MC were analysed using two size fractions for each experimental condition, and 20 agglomerates per size fraction. The average porosity values for each size fraction and the overall averages for 0, 5 and 20 % MC are presented in Table 5.10.

Table 5.10: Porosity values for agglomerates from all experimental conditions investigated.

Moisture Content (%)	Size Fraction (mm)	Porosity (%)	Average Porosity (%)
0	9.5 – 6.7	79.6	79.1
	4.75 – 3.35	78.7	
5	9.5 – 6.7	70.5	72.9
	4.75 – 3.35	75.2	
20	9.5 – 6.7	70.5	72.5
	4.75 – 3.35	74.5	

Similar to the compression test measurements, there is little difference in porosity values between 5 % and 20 % MC, with average values of 72.9 % and 72.5 %, respectively. One caveat is that this technique also assumes a spherical geometry. Although the average diameter was calculated using two diameter measurements for each agglomerate, and 20 agglomerates were tested for each size fraction to account for variations in shape, these differences may still introduce some error in the calculated porosity values.

One advantage of this technique compared to compression testing is that agglomerates produced at 0 % MC could also be analysed. Interestingly, these agglomerates clearly showed a higher porosity compared to those produced at 5 % and 20 % MC, with an average porosity of 79.1 %. This is expected as increasing the solvent content increases the deformability of agglomerates, which facilitates coalescence and consolidation and reduces the porosity. In the absence of solvent, agglomerates formed at 0 % MC have less opportunity to coalesce and consolidate. They are also mechanically weaker without solid bridges cementing the agglomerates together, which is reflected in the higher porosity value.

The difference in porosity between agglomerates at 0 % MC and agglomerates formed at 5 and 20 % MC is statistically significant. While the spherical assumption introduces some error, these measurements provide a useful comparison for understanding the effect of MC on agglomerate porosity. To further explore the difference in agglomerate strength between different MCs, mixer torque rheometer (MTR) results are discussed in the following section.

5.2.4 Rheometry Measurements

Mixer torque rheometry (MTR) is a useful technique for understanding the behaviour of material systems under agitation. In this work, MTR data were correlated with agglomeration rates and agglomerate strength. In the multiple addition method, the torque required to mix the wet powder at various liquid to solid (L/S) ratios is recorded. These readings can be used to evaluate the shear stress. As the rheology of wet powders dictates agglomerate growth, MTRs have been widely used to study the granulation process of different formulations.[139–141] It is efficient as it only requires a few grams of

material to generate a torque profile, and the amount of drug available for early stage formulation studies is often limited. As discussed in Chapter 2, Section 2.6.2.1, MTR has also proved to be a useful tool for designing drying processes in AFDs by predicting the moisture content above which agitation should be avoided to minimise undesired agglomeration.[49,54]

The torque measurements directly reflect the consistency of the wet powder, and indicate the resistance encountered by the blades during mixing. For this work, MTR measurements with salicylic acid (< 106 µm) and water were used to generate a torque profile across increasing L/S ratios and identify the various states of liquid saturation (Figure 5.10).

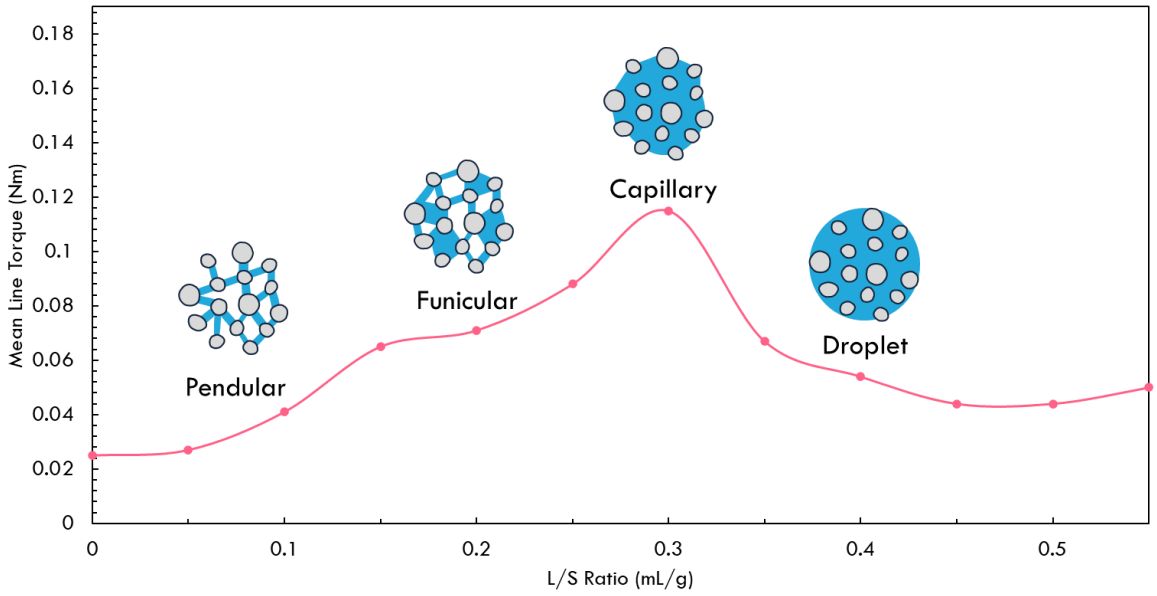

Figure 5.10: MTR curve showing the relationship between liquid to solid ratio (mL/g) and mean line torque (Nm) for salicylic acid and water, highlighting the various stages of liquid saturation (pendular, funicular, capillary and droplet).

In Figure 5.10, the particles are initially in the pendular state at low L/S ratios. As the L/S ratio increases, the torque rises, indicating a transition to the funicular state. When the pores are fully saturated with liquid, the capillary state is reached, which corresponds to the peak torque reading. Further addition of liquid results in a slurry forming and a subsequent drop in torque.

In this study, the capillary state for the < 106 µm size fraction was reached at a L/S ratio of 0.3 mL/g, which corresponds to a wet basis MC of 23.1 %. This aligns with the agglomerate size data presented in Chapter 4, Section 4.3.2 where experiments at 20 % MC resulted in extensive agglomeration. Given the critical moisture content (CMC) is approximately 23.1 %, the extent of agglomeration at 20 % MC is consistent with the system approaching the capillary state.

These results also highlight the effect of increasing MC on the extent of agglomeration. A MC of 5 % corresponds to a torque value of 0.027 Nm, whereas a 20 % MC results in a significantly higher torque reading of 0.088 Nm. The higher torque at 20 % MC reflects an increase in liquid bridges between

particles, making them more resistant to deformation. This difference in torque between 5 % and 20 % MC aligns with the experimental observations presented in Chapter 4, Section 4.3.2. Although the d_{50} values were similar, much larger d_{90} values were observed at 20 % MC, indicating the formation and survival of larger agglomerates.

To assess the impact of modifying the primary particle size on resulting agglomeration, an additional MTR experiment was performed using the 212 – 300 µm size fraction of salicylic acid with water. The resulting MTR curve is plotted alongside the results for the < 106 µm size fraction in Figure 5.11. Using a larger size fraction of salicylic acid (212 – 300 µm) resulted in a very different torque profile. The torque values for this size fraction were consistently lower than those for the < 106 µm size fraction which corresponds with the significantly lower levels of agglomeration observed in Section 5.2.1. These lower torque readings indicate reduced cohesiveness of the wet powder when using the larger size fraction, which implies that the blades encountered less resistance during mixing.

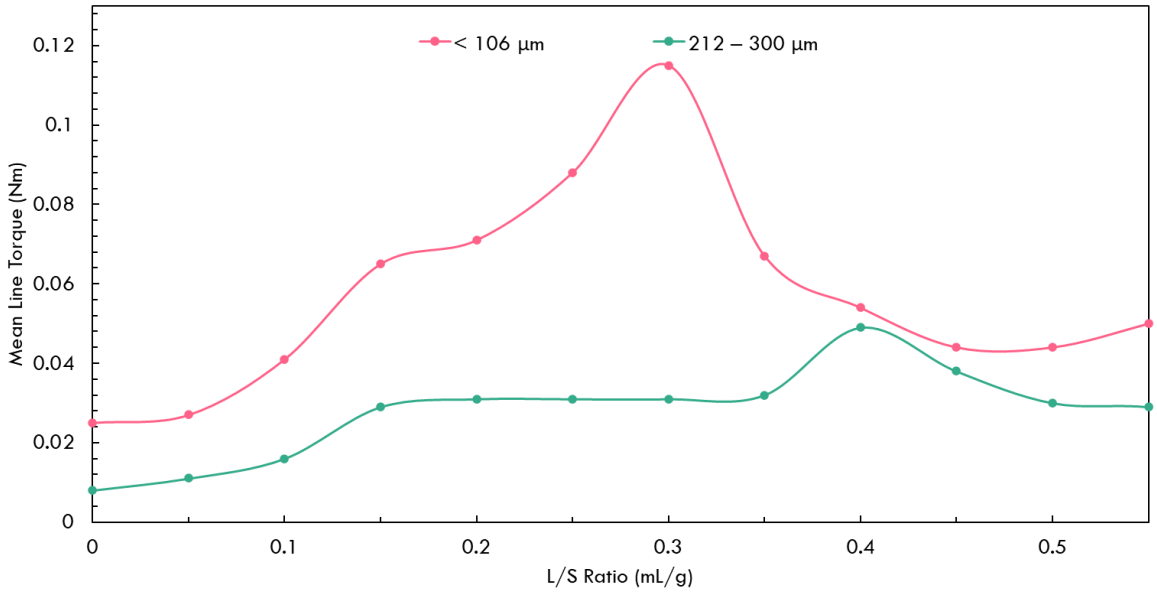

Figure 5.11: MTR curves comparing the relationship between L/S ratio (mL/g) and mean line torque (Nm) for two different size fractions of salicylic acid with water.

The L/S ratio required to reach the capillary state increases when using the 212 – 300 µm size fraction. While the capillary state was reached at a L/S ratio of 0.3 mL/g for the < 106 µm size fraction, a L/S ratio of 0.4 mL/g was required for the 212 – 300 µm size fraction, corresponding to a wet basis MC of 28.6 %. This reflects the reduced surface area available for liquid bridge formation in larger particles, with more solvent being required for particles to be fully saturated. Both the lower torque values and the higher L/S ratio required to reach the capillary state are consistent with experimental observations of reduced agglomeration when using the coarser size fraction of salicylic acid at the same MC.

These MTR results indirectly provide quantitative measurements that reflect the effect of liquid saturation on agglomerate strength by highlighting the different resistances encountered by the blades

when mixing. The data also highlights the effect of changing the primary particle size on agglomeration, with much lower torque values observed for the larger size fraction.

5.2.5 Dimensionless Numbers

Dimensionless numbers are a valuable tool in engineering, as they simplify complex systems to functions of key parameters which enables comparisons between different systems and scales. One example of this is the granule growth regime map introduced in Chapter 2, Section 2.5.1.2. This is used to describe granule growth behaviour as a function of maximum pore saturation (s_{max}) and Stokes deformation number (St_{def}).[37] The x axis represents the maximum pore saturation (s_{max}):

$$s_{max} = \frac{w\rho_s(1 - \varepsilon_{min})}{\rho_l \varepsilon_{min}} \quad 5.5$$

where w is the mass ratio of liquid to solid, ρ_s is the solid particle density, ρ_l is the liquid density and ε_{min} is the minimum porosity of the formulation for specific operating conditions.

The Stokes deformation number (St_{def}) is used to quantify the extent of granule deformation during impact and is calculated as the ratio of the externally applied kinetic energy to the energy required for deformation. The equation for St_{def} is:

$$St_{def} = \frac{\rho_g U_c^2}{2Y_g} \quad 5.6$$

where U_c is collision velocity, ρ_g and Y_g are the granule density and dynamic yield stress, respectively.

Given the similarities between wet granulation and undesired agglomeration in AFDs, these dimensionless numbers are relevant to this work. The Stokes deformation number reflects the balance between externally applied kinetic energy and the energy required for deformation. Investigated parameters such as agitation speed directly affect this balance and also govern whether the agglomerates coalesce, deform or break. The maximum pore saturation reflects the degree of liquid saturation, which directly influences the extent of liquid bridge formation between particles. As the MC determines the amount of liquid in the system, it has been shown to strongly influence the agglomeration behaviour.[40,55]

Due to practical challenges in obtaining agglomerate yield stress values (discussed in Section 5.2.2), torque values from the MTR were used instead to describe the energy required for deformation. These torque measurements represent the resistance of the blades to the wet material, which also reflects the energy required to deform the agglomerates.

The volume was also included in the numerator of the modified Stokes deformation number to account for changes in fill level, as the amount of material agitated can influence the collision energy, collision frequency and, therefore, the resulting agglomeration.

This modified form provides a more suitable approach for analysing agglomeration in AFDs. Despite these adaptations, it remains dimensionless and still captures the fundamental principle of the St_{def} number, which is the ratio of externally applied kinetic energy to the energy required for deformation. Therefore St_{def} hereafter is defined as:

$$St_{def} = \frac{\rho_g U_c^2 V}{\tau} \qquad 5.7$$

where τ is the measured torque required for deformation, and V is the volume of material being agitated.

5.2.6 Developing a Regime Map

The values of s_{max} and St_{def} for the various experimental conditions were calculated and are presented in Table 5.11. These values were used to construct the regime map shown in Figure 5.12, which highlights the different agglomerate growth and breakage dynamics observed under varying conditions.

Table 5.11: Calculated values of the maximum pore saturation (s_{max}) and Stokes deformation (St_{def}) for the various experimental conditions investigated.

Moisture Content (%)	Agitation Speed (rpm)	Primary Material Size Fraction (µm)	Fill Level	s_{max}	St_{def}
0	50	< 106	High	0.00	0.06
5	50	< 106	High	0.08	0.05
	100	< 106		0.08	0.22
20	50	< 106	Low	0.41	0.01
			High	0.41	0.02
	75	< 106	High	0.41	0.05
	100	< 106	Low	0.41	0.05
		< 106	High	0.41	0.09
	50	212-300	Low	0.39	0.05
	100			0.39	0.21

Based on the distribution of data points and the supporting experimental observations, approximate boundaries have been proposed to separate distinct regions corresponding to specific agglomeration behaviours. The demarcations are estimates based on experimental observations, agglomerate characterisation data and torque profiles generated from MTR experiments. Each of the regions in Figure 5.12 is discussed in detail in the following sections.

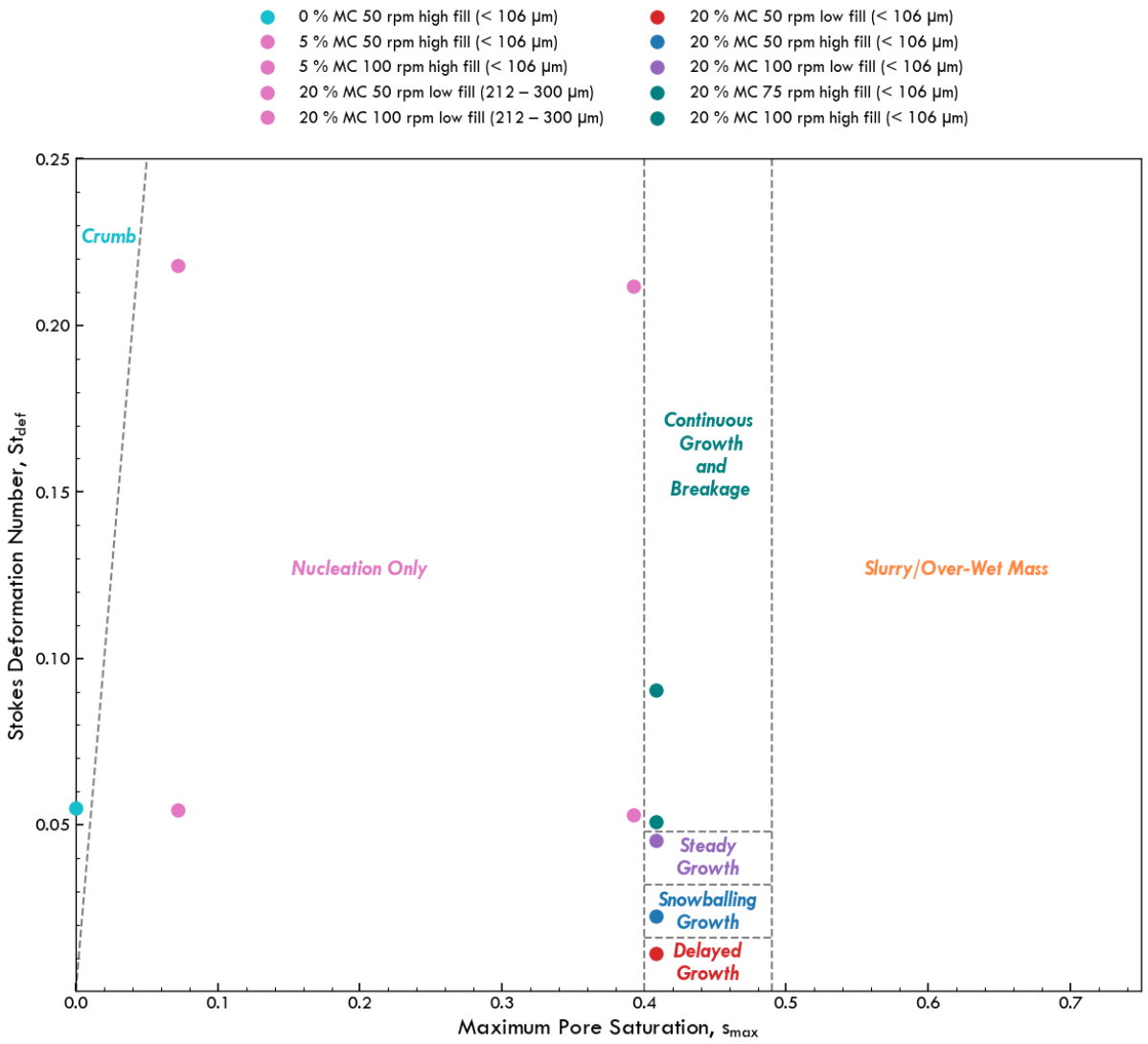

Figure 5.12: Proposed regime map of agglomerate growth and breakage behaviours observed across various experimental conditions in an AFD, using salicylic acid and water.

5.2.6.1 Crumb

Crumb behaviour refers to the formation of small, weak agglomerates that are constantly breaking and reforming.[34] This was observed with the 0 % MC experiment conducted at 50 rpm using the < 106 µm size fraction, with the corresponding d_{50} values over time plotted in Figure 5.13.

As shown in Figure 5.13, there is some initial agglomerate growth, followed by breakage, and some potential regrowth occurring between 30 to 60 minutes of agitation. The lack of moisture prevents the formation of liquid bridges and therefore limits coalescence. As salicylic acid is an inherently cohesive material, some small agglomerates are still able to form from the agitation. However, they are short-lived as they are too weak to withstand the shear forces of agitation.

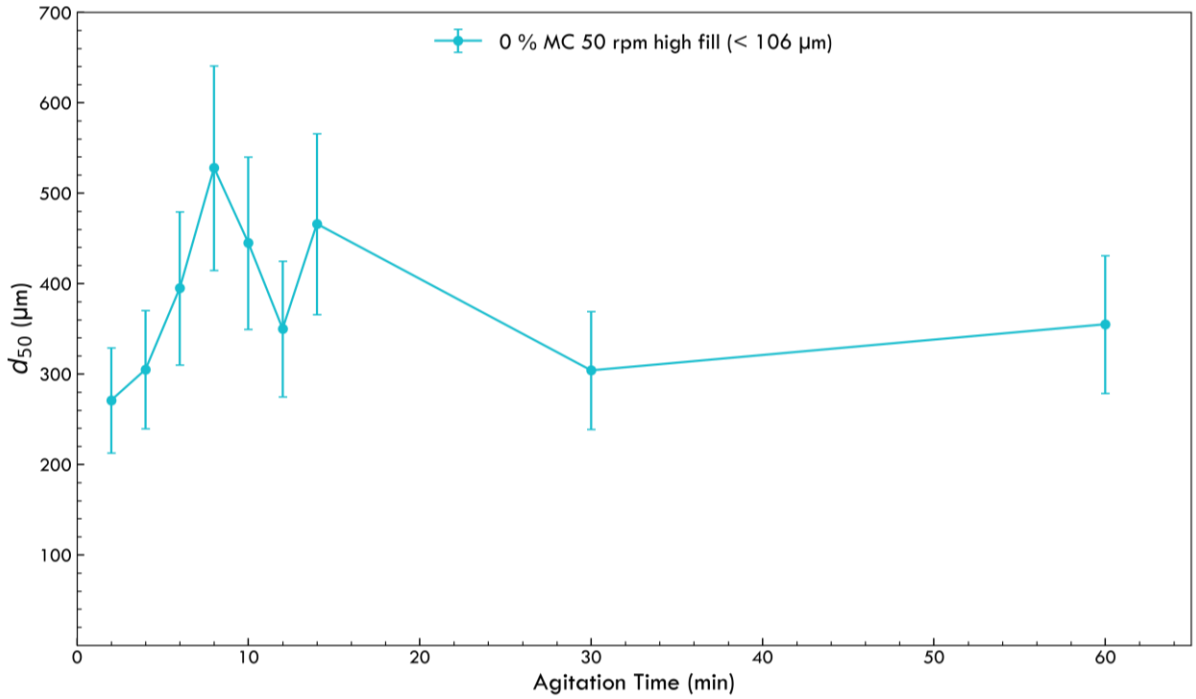

Figure 5.13: d_{50} values of 0 % MC high fill experiments at 50 rpm over time. Error bars represent the minimum and maximum error based on 3 repeat experiments.

This region typically corresponds to systems with low values of s_{max} and a wide range of St_{def} values. These are usually dry systems or systems with minimal moisture. When using moderate to high agitation speeds, any small agglomerates formed continuously break and reform, known as crumb behaviour.

5.2.6.2 Nucleation Only

Nucleation only growth describes the formation of small agglomerates that survive but do not grow any further. This growth behaviour was observed at both agitation speeds for experiments conducted at 5 % MC using the < 106 µm size fraction, as well as 20 % MC experiments using the 212 – 300 µm size fraction. The d_{50} values over time for these datasets are plotted in Figure 5.14.

At 5 % MC, experiments at both speeds formed agglomerates a few millimetres in size, with constant fluctuations in size but no further growth. At this low MC, there is insufficient liquid to promote further agglomerate growth and the rate of coalescence is limited.

Experiments conducted at 20 % MC using the 212 – 300 µm size fraction were previously discussed in Section 5.2.1. As shown in Figure 5.14, small agglomerates form but do not exhibit any further growth. This is likely due to the reduced surface area available for liquid bridge formation when using the coarser grade of salicylic acid. The coarser grade also had fewer particles per unit volume, and hence reduced number of contacts between particles. Having fewer contact points reduces the possibility of liquid bridges forming and hence inhibits agglomerate growth.

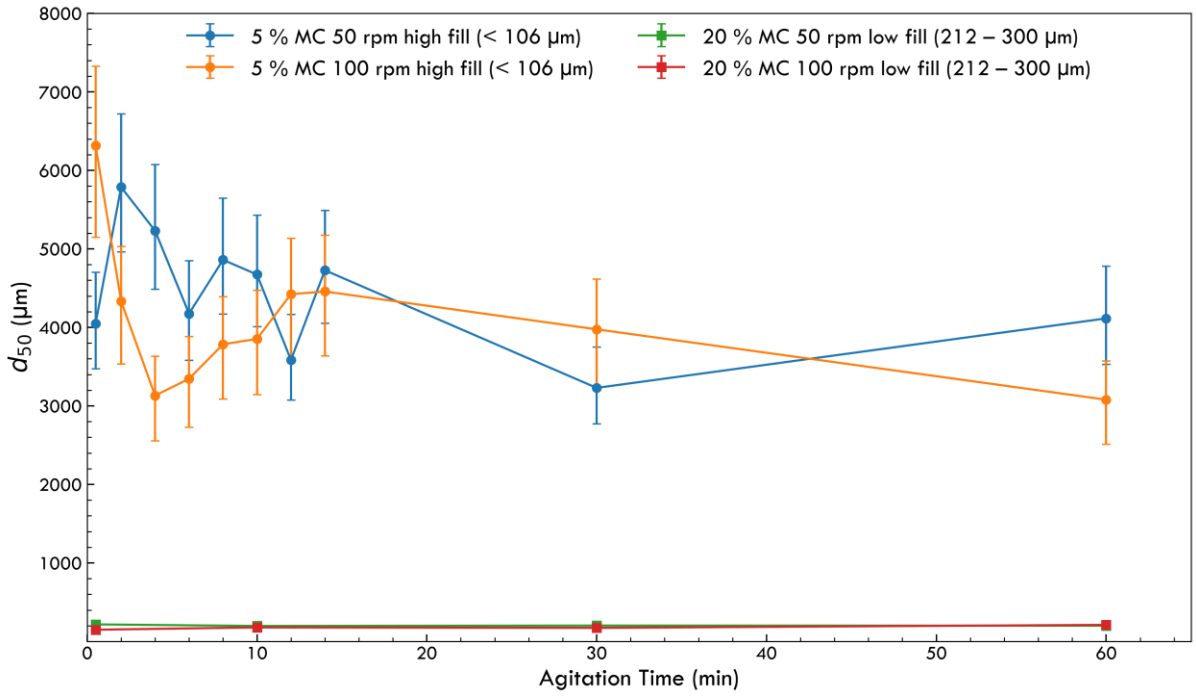

Figure 5.14: d_{50} values over time for experiments conducted at various moisture contents using different size fractions of salicylic acid. Error bars represent the minimum and maximum error based on 3 repeat experiments at 50 rpm for each MC and size fraction.

This region corresponds to systems with low s_{max} values and low to moderate St_{def} values. The coalescence of agglomerates in this study is limited either by low MC which restricts liquid bridge formation, or weaker agglomerates (such as those formed when using the coarser size fraction of salicylic acid). Particles are likely in the pendular or funicular saturation states. Therefore, although small agglomerates will form and persist, there is no further growth which is characteristic of the nucleation only regime.

5.2.6.3 Delayed Growth

In this work, delayed growth is used to describe agglomerate growth that only occurs after extended periods of agitation. This was observed for 20 % MC low fill experiments conducted at 50 rpm using the < 106 µm size fraction of salicylic acid, with the d_{50} values over time plotted in Figure 5.15.

In Figure 5.15, after the initial breakage of the wet cake observed when agitation is started, the d_{50} is stable until the 30 minute mark. After this, some agglomerate growth is observed. This is somewhat analogous to the induction growth regime reported in wet granulation.[34] However, in wet granulation, the induction period is due to insufficient liquid at the granule surface. In this work, the delayed growth is instead driven by the low shear conditions and the reduced collision frequency at a low fill level.

At 50 rpm, there is initially insufficient shear for large agglomerates to form and hence the d_{50} remains stable after the initial breakage of the wet cake, due to a balance between with agglomerate growth and breakage. The lower energy input results in weaker and less consolidated agglomerates. The low fill

level further limits agglomerate growth as the frequency of particle collisions is reduced. However, with continued agitation, the number of collisions increases eventually promoting further agglomerate growth after 30 minutes of agitation.

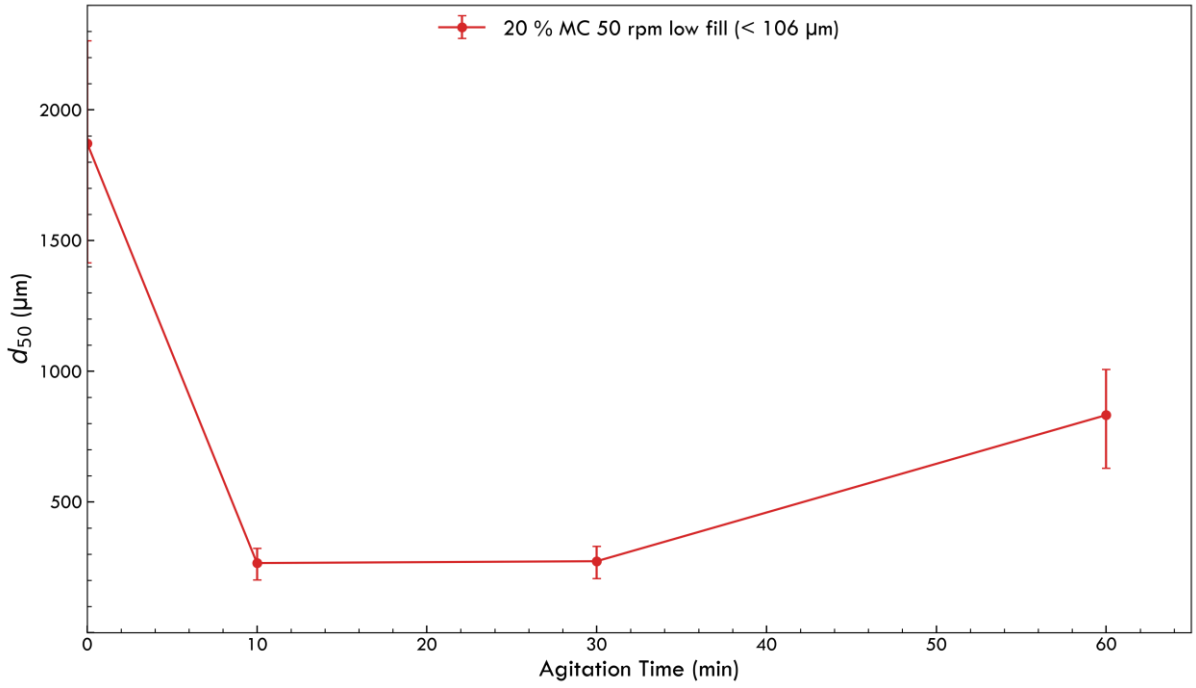

Figure 5.15: d_{50} values of 20 % MC low fill experiments at 50 rpm over time. Error bars represent the minimum and maximum error based on 3 repeat experiments.

This region is observed for moderate values of s_{max}, where the system likely operates in the funicular or capillary saturation states, which is ideal for coalescence. However, the low St_{def} limits the extent of agglomeration. For this particular system, the low St_{def} is due to a combination of low agitation speed (50 rpm) and low fill level. As a result, agglomerate growth only occurs with prolonged agitation, resulting in the term delayed growth.

5.2.6.4 Snowballing Growth

Snowballing growth, as discussed earlier in Chapter 4, Section 4.3, describes the generation of fines from breakage which subsequently layer onto wet agglomerates, promoting agglomerate growth. This growth behaviour was seen for 20 % MC high fill experiments conducted at 50 rpm using the < 106 µm size fraction of salicylic acid. The d_{50} values over time for this dataset are plotted in Figure 5.16.

At this lower agitation speed, the collision energy is insufficient to facilitate the continuous growth and breakage observed at higher speeds, which will be shown later in Section 5.2.6.6. Instead, there is likely some attrition of initial agglomerates which produces fines. These are eventually reincorporated into wet agglomerates, layering over time and resulting in agglomerate growth.

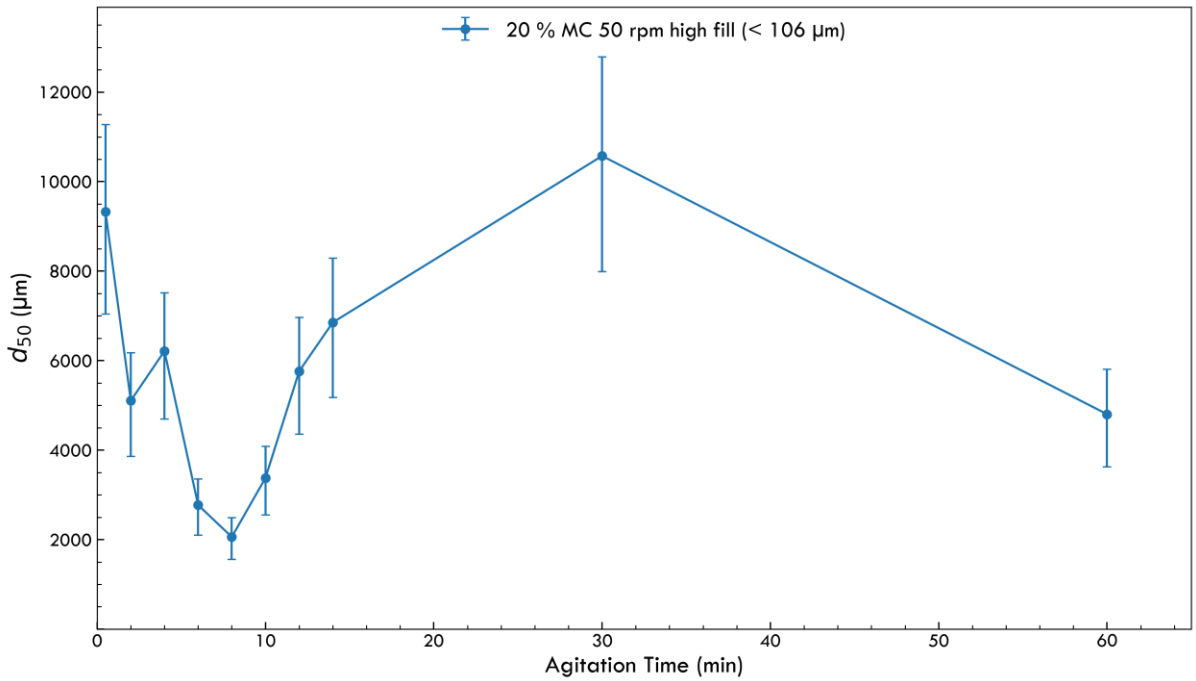

Figure 5.16: d_{50} values of 20 % MC high fill experiments at 50 rpm over time. Error bars represent the minimum and maximum error based on 3 repeat experiments.

This region also corresponds to systems with moderate s_{max} values where particles are likely in the funicular or capillary states. However, the slightly higher values of St_{def} due to a higher fill level results in more frequent collisions and initial breakage of agglomerates. The fines produced from this breakage layer onto wet agglomerates, allowing them to grow via a snowballing mechanism.

5.2.6.5 Steady Growth

Steady growth is used to describe agglomeration behaviour where agglomerates consistently grow over time without any significant breakage occurring. This was observed for 20 % MC low fill experiments conducted at 100 rpm using the < 106 µm size fraction of salicylic acid. The corresponding d_{50} values over time for this dataset are plotted in Figure 5.17.

At 100 rpm, the higher agitation speed results in increased shear, which promotes coalescence and consolidation of agglomerates. While some breakage likely occurs, this is likely to produce fragments which are reincorporated into existing agglomerates. The low fill level also reduces the number of collisions compared to high fill experiments, which likely limits the extent of breakage and enables a steady increase in agglomerate size. The combination of low fill and high agitation speed results in efficient mixing of the wet powder, reducing the likelihood of any stagnant zones and enabling gradual agglomerate growth.

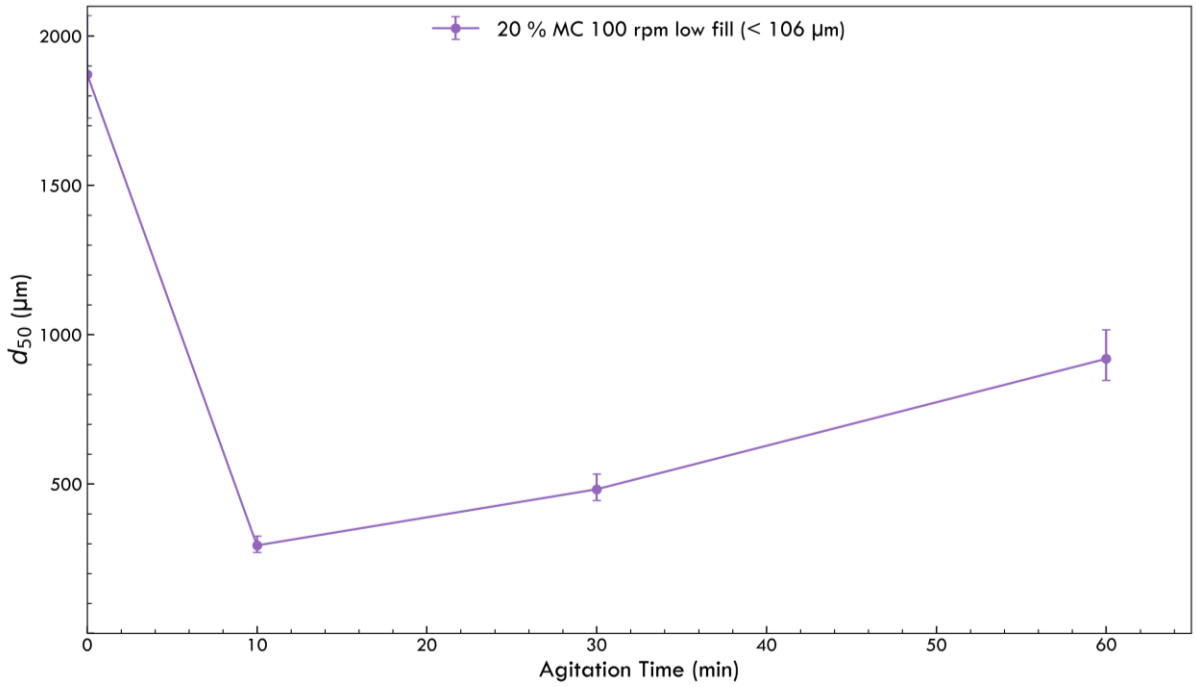

Figure 5.17: d_{50} values of 20 % MC low fill experiments at 100 rpm over time. Error bars represent the minimum and maximum error based on 3 repeat experiments.

This region also corresponds to systems with moderate s_{max} values, but with even higher St_{def} values compared to the snowballing region. The increased St_{def} as a result of higher agitation speeds and increased shear forces facilitates coalescence and consolidation of agglomerates. In this region, the rate of agglomerate growth dominates over the rate of agglomerate breakage, resulting in a steady growth.

5.2.6.6 Continuous Growth and Breakage

The continuous growth and breakage region describes systems where there is a consistent balance between the agglomerate growth and breakage, resulting in stable d_{50} values. This trend was observed for 20 % MC high fill experiments conducted at 75 and 100 rpm using the < 106 µm size fraction of salicylic acid. The d_{50} values over time for both datasets are plotted in Figure 5.18.

This behaviour can partly be attributed to liquid bridge strength. If the liquid bridges are strong enough to withstand the increased shear forces at higher agitation speeds, the more frequent particle collisions will promote agglomerate growth. Higher agitation speeds also tend to form more consolidated agglomerates. The breakage of agglomerates at higher speeds is likely to occur by fragmentation, with the resulting fragments more likely to re-coalesce due to the greater energy of collisions. Overall, this results in a dynamic equilibrium between agglomerate growth and breakage.

This region also corresponds to systems with moderate s_{max} values but with high St_{def} values. The higher St_{def} is a result of both increased fill and higher agitation speeds, which promote more frequent and energetic collisions. This enables the system to achieve a dynamic equilibrium between agglomerate growth and breakage.

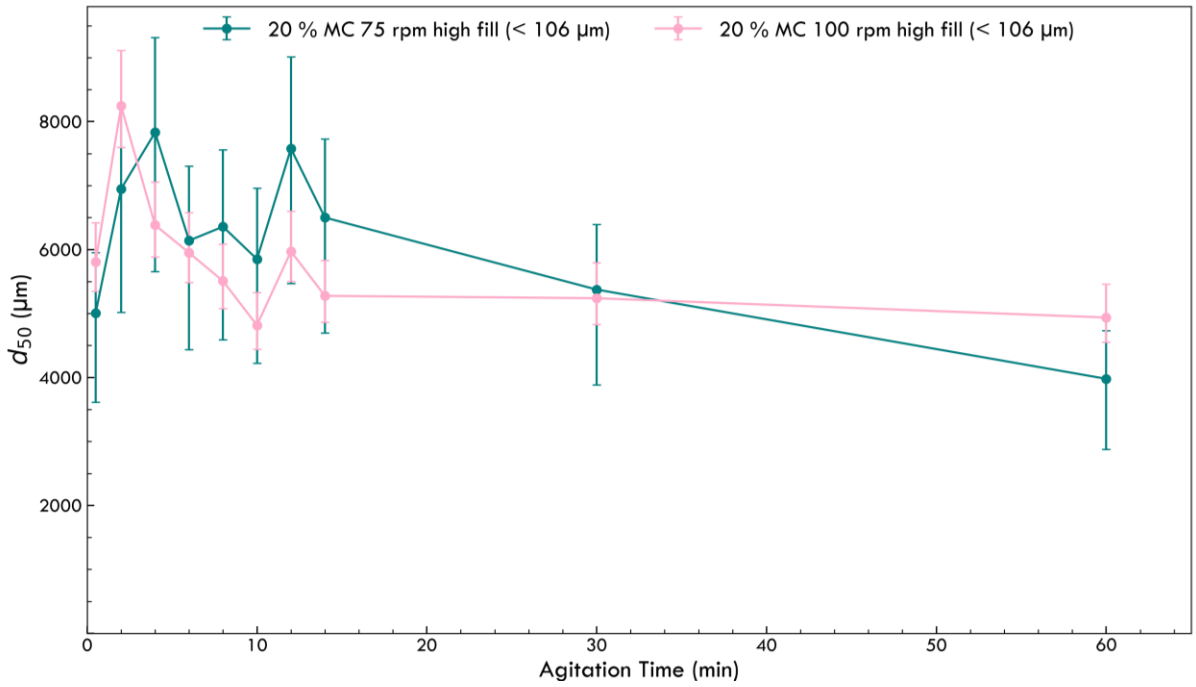

Figure 5.18: d_{50} values of 20 % MC high fill experiments at 75 and 100 rpm over time. Error bars represent the minimum and maximum error based on 3 repeat experiments at each speed.

5.2.6.7 Slurry/ Over-Wet Mass

The slurry or over-wet region describes systems where the liquid saturation has exceeded the capillary state and likely reached the droplet stage. Although the experiments were designed to avoid operating in this region, the boundaries for this region were approximated using MTR results and the L/S ratio corresponding to the droplet state. This region is associated with systems with high values of s_{max} across a range of St_{def} values.

5.2.7 Applicability of Proposed Regime Map

It is important to note that due to the approximation of the demarcation lines between different regimes, this regime map acts as a guide for designing agitated drying processes rather than a tool for quantitative predictions. Further work is required to validate the proposed boundaries and explore their applicability to other material systems, as this study focused specifically on salicylic acid in water.

Drying in AFDs is a dynamic process so as the drying proceeds, the moisture content and, therefore, the s_{max} value decrease. As drying continues, this results in a shift to the left on the regime map. The rate at which this transition occurs will vary depending on the solvent system used and the rate of evaporation.[6] Despite these limitations, this work presents the first regime map proposed for agglomeration in AFDs, highlighting the different agglomerate growth and breakage behaviours observed. It provides a useful framework for qualitatively understanding how various material and process parameters influence agglomeration behaviour but requires further refinement and validation to be used as a predictive tool.

5.3 Conclusions

In this chapter, additional agglomerate growth behaviours beyond those identified in Chapter 4 were investigated by using a coarser size fraction (212 – 300 μm) of salicylic acid. These experiments provided further insight into how the primary particle size influences agglomeration dynamics. To distinguish between agglomerates formed under different experimental conditions, a range of characterisation techniques were explored to assess agglomerate strength and structure.

Using the coarser size fraction in low fill experiments significantly reduced the extent of agglomeration compared to experiments using the < 106 μm size fraction. This was consistent across both agitation speeds for the whole agitation period investigated. The reduced cohesivity and lower surface area to volume ratio of larger particles limits the extent of liquid bridge formation which, thus, reduces the extent of coalescence and consolidation. The difference in the extent of agglomeration was evident even in the initial wet cake prior to agitation, highlighting that the particle size also influences the extent of formation of loosely bound agglomerates in the wet cake.

To characterise and distinguish between agglomerates formed at different MCs and primary particle sizes, various characterisation techniques were assessed. Data from both compression tests and porosity approximations using image analysis did not show statistically significant differences, likely due to imitations from the assumption of spherical agglomerates. Rheometry measurements were used to identify the different saturation states of salicylic acid with increasing water content. The torque measurements were also able to differentiate between systems with different MC and primary particle sizes. The torque directly reflects the resistance experienced by the blades, which is an indication of agglomerate strength.

A regime map was developed using s_{max} and St_{def} as the dimensionless numbers, analogous to the granule growth regime map used in wet granulation. In this context, the St_{def} was calculated using torque measurements instead of dynamic yield stress, and the volume was incorporated to account for the effect of fill level. However, the fundamental principle of St_{def} was preserved and still reflects the ratio of externally applied kinetic energy to the energy required for deformation. The resulting regime map is the first of its kind for AFDs, capturing a range of agglomerate growth and breakage behaviours observed experimentally. Although boundaries were estimated based on experimental observations, agglomerate characterisation and MTR experiments, further work is needed to validate these boundaries and assess their applicability for other material systems.

The agglomerate growth and breakage behaviours observed in this chapter provide insight into how key material and process parameters influence agglomeration. In the following chapter, constant tip speed is used as a scaling index to assess whether the observed agglomeration dynamics are preserved during scale up in a larger AFD and a conical dryer.

Chapter 6 - Agglomeration Behaviour Across Scales: The Role of Tip Speed

In pharmaceutical manufacturing, it is crucial to preserve particle properties during scale up. Increased attrition or agglomeration may impact downstream processing, product quality and final drug product performance. Building on the work presented in Chapter 4, where the effect of agitation input on agglomeration was investigated, this chapter examines how these trends translate to larger scale systems.

Although agglomeration after crystallisation is typically undesirable, a small amount may be acceptable within certain limits. However, significant issues may arise if the extent of agglomeration increases significantly upon scale up, or if the balance shifts in the opposite direction, leading to breakage and attrition. During a three month placement at AstraZeneca (Macclesfield, UK), work was conducted to investigate whether the extent of agglomeration observed in small scale AFD experiments (Chapter 4) can be preserved during scaling up using constant tip speed while maintaining geometric similarity. This was to evaluate the industry standard approach of scaling with constant tip speed, which aims to have similar particle velocities (kinematic similarity) across scales. The influence of dryer geometry on agglomeration behaviour during scale up was also explored to assess whether constant tip speed can account for variations in shear forces and flow patterns. Experiments were conducted in a conical dryer as it is not unusual for products to be transferred between manufacturing facilities and processed using different types of agitated dryers, such as going from an AFD to a conical dryer.[48,142] Characterisation techniques such as micro-CT and SEM were explored to assess their suitability for investigating the morphology of agglomerates. Using micro-CT, the morphological differences between agglomerates in the bulk and heel were also studied.

6.1 Experimental Design and Methodology

6.1.1 Experimental Design

To evaluate the suitability of scaling up using constant tip speed, a set of experiments were designed and conducted with the following aims:

- Assess the similarity in the extent of agglomeration for experiments conducted in a larger scale AFD while maintaining geometric similarity.
- Investigate the effect of modifying dryer geometry on the extent of agglomeration during scale up using a conical dryer.
- Understand the relationship between the mixing screw and orbit arm speed in a conical dryer, and their impact on mixing efficiency and extent of agglomeration.

6.1.2 Materials

Salicylic acid (≥ 98 %) was obtained from VWR Chemicals and sieved to obtain a size fraction below 106 µm to be used as a moisture sensitive model API. The solvent used was distilled water, prepared using a water still.

6.1.3 Scaling Calculations

Scaling is commonly used to achieve the same behaviour and output in vessels of various sizes. Impeller speeds were derived using scaling indices, with constant tip speed being the chosen criterion. This approach is widely used in mixing operations.[143] Other scaling indices, including constant Froude number, power number and shear stress, were considered. However, the calculated agitation speeds for these indices were very similar, making constant tip speed the preferred choice, as it is the most commonly applied in industrial agitated drying processes. Scale up rules were assessed using Equation 6. 1:

$$\frac{N_x}{N_y} = \left(\frac{D_y}{D_x}\right)^n$$

6. 1

where N is the agitation speed of the impeller, D is the impeller diameter, x and y are the different scales of vessels and n is the scaling index.[144] To calculate the tip speed, the following equation is used:

$$Tip\ speed = \pi\ x\ D\ x\ N$$

6. 2

where *N* is the rotation rate. Tip speed is the velocity of an impeller at a selected point on its peripheral. An equal tip speed corresponds to the same maximum shear rate, therefore tip speed is often used for scaling shear dependent processes.[145] For a constant tip speed, $n = 1$, and a sample calculation for determining the agitation speed in the larger scale AFD (FD80) can be seen below:

$$\frac{N_x}{50} = \left(\frac{48}{74}\right)^1 \rightarrow N_x = 32$$

6. 3

Scaling calculations were based on agitation speeds of 50 and 100 rpm in the lab scale AFD, with impeller diameters of 48 mm and 74 mm for the lab scale and larger AFDs, respectively.

6.1.4 Agitated Filter Dryer Experimental Methodology

This section describes the experimental procedure for assessing the use of constant tip speed for scaling up an AFD. Experiments were conducted in a GL Filtration FD80 2L laboratory agitated filter dryer using salicylic acid and water, with the equipment shown in Figure 6.1. The FD80 was connected to a

Julabo unit for heating and cooling, alongside the mains vacuum and nitrogen line for pressurising the vessel. The overall dimensions were 1794 mm (H) x 994 mm (W) x 530 mm (D).

Figure 6.1: Image of FD80 set up.

The FD80 was composed of Hastelloy C22 wetted parts, and SS304L non wetted parts, with a base pivot and a 10 µm sintered filter mesh. The agitator seal was a single mechanical seal with a carbon-on-silicon carbide seal face material. The retractable agitator had a 45° pitch blade geometry and the relative dimensions of the agitator blade and the internal filter basket can be seen in Figure 6.2. Relevant dimensions and properties of the FD80 are listed in Table 6.1.

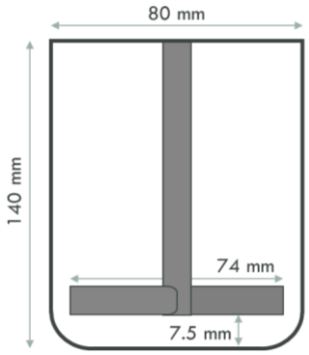

Figure 6.2: 2D schematic of agitator inside the filter basket of the FD80.

Table 6.1: Important properties and dimensions of the FD80.

Filter Mesh Size (µm)	10
Vessel Volume (L)	2
Internal Vessel Diameter (mm)	80
Agitator Diameter (mm)	74
Agitator Geometry	45° pitch blade
Agitator Speed (rpm)	0 - 80
Sweep Ratio D/T	0.93
Vessel Operating Temperature (°C)	-20 - 150

6.1.4.1 Wet cake formation

Salicylic acid primary material (< 106 µm size fraction) and distilled water were charged directly into the vessel in a 1:1 ratio and agitated at 20 rpm for 5 minutes to form a slurry. To maintain the bed height: impeller diameter ratio consistent with the low fill experiments discussed in Chapter 4, Section 4.3, a bed height of 4.6 cm was required. This corresponded to approximately 75 g of salicylic acid. Agitation was started as the impeller moved down the vessel until the required clearance was achieved. The slurry was left to settle for 5 minutes before being filtered at 2 bar under nitrogen pressure until the desired amount of filtrate was obtained to achieve 20 % MC. The balance beneath the filtrate vessel was tared at the start of each experiment to measure the filtrate mass and estimate the filtration endpoint. After filtration, samples were taken via the sight glass to confirm the MC of the wet cake, using a halogen moisture analyser. Samples from multiple regions were combined to minimise sampling error.

6.1.4.2 Agitated drying

Once the target MC was confirmed, the wet cake was agitated at 25 °C at various agitation speeds and times (Table 6.2). Once complete, the agitator was raised above the wet cake before discharging the sample by inverting the filter. The bulk material and heel were separated during discharge. The bulk flowed easily and was primarily removed by inverting the filter, whereas the heel often stuck to the vessel base, requiring manual removal with a spatula. After discharge, both fractions were dried overnight at 40 °C in glass crystallising dishes in a convection drying oven. Due to time constraints during the placement, it was not possible to do repeat runs for all experiments. However, three replicate experiments were conducted at 64 rpm for 14 minutes of agitation and are marked with an * in Table 6.2. The average values from these replicates were used to calculate the minimum and maximum deviations, which are represented as error bars in the data shown in Section 6.2.

Table 6.2: Agitation conditions investigated at 20 % MC in the FD80.

Moisture Content (%)	Agitation Speed (rpm)	Tip Speed (m/s)	Agitation Time (min)
20	0	0	0
	32	0.126	0.5
			8
			14
			30
			60
	64	0.251	0.5
			8
			14*
			30
			60

6.1.5 Conical Dryer Experimental Methodology

This section outlines the experimental procedure for evaluating constant tip speed as a scaling index when transferring from an AFD to a conical dryer. The experiments assess how changes in geometry influence agglomeration behaviour by altering shear forces and flow patterns. Experiments were conducted in a Bolz MiniDRY conical dryer using salicylic acid and water. The equipment was connected to a Julabo unit for temperature control and is shown in Figure 6.3.

Figure 6.3: Image of Bolz miniDRY conical dryer.[146]

The vessel was constructed from SS 316L, and the conical geometry provides a higher surface area to volume ratio compared to an AFD. It was equipped with a mixing screw which lifts particles from the bottom to the top, while the orbit arm rotates the mixing screw around the circumference of the vessel for uniform mixing. The minimal gap between the mixing screw and the vessel maximises material exposed to the heated surface. The screw width at the desired fill height was used to calculate the required agitation speeds for scaling up using constant tip speed. The dimensions of the vessel and mixing screw are shown in Figure 6.4, with relevant properties detailed in Table 6.3.

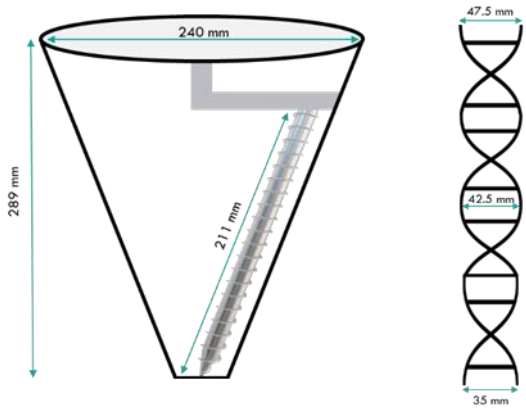

Figure 6.4: 2D schematic of the mixing screw inside the conical dryer.

Table 6.3: Important properties and dimensions of the conical dryer.

Vessel Volume (L)	1.5
Mixing Screw Min Diameter (mm)	35
Mixing Screw Max Diameter (mm)	47.5
Mixing Screw Angle (°)	3.5
Mixing Screw Speed (rpm)	20 - 200
Orbit Arm Speed (rpm)	0.3 - 3
Vessel Operating Temperature (°C)	-20 - 150

6.1.5.1 Bag mix preparation

The wet solids were prepared using a bag mixing method, with salicylic acid primary material and distilled water added in amounts calculated to achieve a 20 % moisture content. A sample was taken from various locations in the bag, and the moisture content was measured using a halogen moisture analyser.

6.1.5.2 Agitated drying

Once validated, the wet solids were charged into the vessel by removing the sight glass and inserting a funnel directly into the conical dryer. The mass of material was kept constant at approximately 94 g, matching the mass of wet cake used in FD80 experiments. This corresponded to a half fill level in the conical dryer. The wet solids were agitated at 25 °C at various agitation speeds and times (Table 6.4). Mixing screw speeds were determined using constant tip speed scaling, while orbit arm speeds were selected based on equipment guidelines and experimental observations. Once complete, material was discharged from the bottom of the dryer by removing the outlet cap and placing a crystallisation dish below to receive the material. This was then dried overnight at 40 °C in a convection drying oven.

Due to time constraints, repeat experiments were not conducted for all conditions. However, three replicates were performed at a specific time point for each mixing screw speed, marked with an * in Table 6.4. Minimum and maximum deviations were calculated and are presented as error bars in Section 6.2. For the marked time points, additional verification experiments were conducted using 20 % MC wet cakes produced in the FD80 to ensure that preparation with bag mixing did not affect agglomeration behaviour. Minimal variation was observed, so bag mixing was used for all conditions tested.

Table 6.4: Agitation conditions investigated at 20 % MC in the conical dryer.

Mixing Screw Speed (rpm)	Orbit Arm Speed (rpm)	Tip Speed (m/s)	Agitation Time (min)
0	0	0	0
58	0.3	0.126	0.5
			8*
			14
			30
			60
116	0.6	0.251	0.5
			8*
			14
			30
			60

6.1.5.3 Influence of orbit arm speed

In previous experiments, the orbit arm speed was doubled alongside the mixing screw speed. However, to better understand the contribution of the orbit arm towards agglomerate breakage, two additional experiments were conducted at 116 rpm with the orbit arm speed maintained at 0.3 rpm (Table 6.5).

Table 6.5: Agitation conditions investigated at 20 % MC with lower orbit arm speed in the conical dryer.

Mixing Screw Speed (rpm)	Orbit Arm Speed (rpm)	Agitation Time (min)
116	0.3	8
		30

6.1.6 Characterisation

The various characterisation methods used for both the starting material and the agglomerates during the placement are outlined in the following sections.

6.1.6.1 Sieving

Samples were sieved using a Fritsch Analysette 3 vibratory sieve shaker. This was used with sieves of mesh sizes from 106 μm to 53 mm (increasing by a magnitude of $\sqrt{2}$ per sieve) in order of decreasing aperture size from top to bottom. Samples were sieved for 2 minutes at an amplitude of 0.2 mm/g. Rationale for the amplitude and sieving time can be found in Chapter 3, Section 3.6.2.

6.1.6.2 Moisture content analysis

The moisture content of agglomerated samples was measured using a Mettler Toledo HX204 Halogen Moisture Analyser, which has a precision up to 0.001 % for moisture content readings. It was operated using the standard drying program in which the sample was heated to 90 °C and held at this temperature. The auto switch off criteria was chosen where the measurement is stopped once there is less than 1 mg loss in weight in 50 seconds.

6.1.6.3 Scanning electron microscopy (SEM)

Images were taken using a Hitachi TM4000 Plus tabletop SEM at an accelerating voltage of 10 kV using the secondary electron (SE) or back scatter electron (BSE) detector. Samples were mounted onto aluminium stubs with adhesive carbon black tape and then sputter coated with a layer of gold using the Quorum Q15ORS plus sputter coater at 20 mA for 2 minutes. Images were taken at a range of magnifications, and this can be seen on each micrograph in Section 6.3, as well as the detector used.

6.1.6.4 Powder X-ray diffraction (PXRD)

Samples of primary material were analysed using a PANalytical Aeris benchtop XRD system. Data were collected over a 10.0 – 100.0° 2θ range at a step size of 0.02°. Results were analysed using DiffractWD, an open-source program used for powder pattern visualisation and comparison. X-ray diffraction methods are the predominant method for determining the crystallinity of the sample, and this depends on the interaction of monochromatic X-ray beams with the crystalline substance. The diffracted X-rays produce both constructive and destructive interference which portray the arrangement of the crystal structure. The atoms within the sample scatter the incident X-rays due to interactions with atoms' electrons, to produce a diffraction pattern.[147] Diffraction patterns show the crystal structure of the compound and are unique to each crystalline form of a compound. PXRD was used to determine the crystallinity of samples. Crystals exhibit long range order and produce sharp diffraction peaks with high intensities whereas amorphous compounds do not have regular arrangements of atoms and result in weak scattering and broader peaks.[148]

The diffraction pattern for salicylic acid was compared against a reference diffraction pattern, which was acquired from the Cambridge Structural Database (CSD). As seen in Figure 6.5, the diffraction pattern exhibits the characteristic peaks of salicylic acid at 2θ = 11 and 17.1°, confirming the identity of the compound.[149]

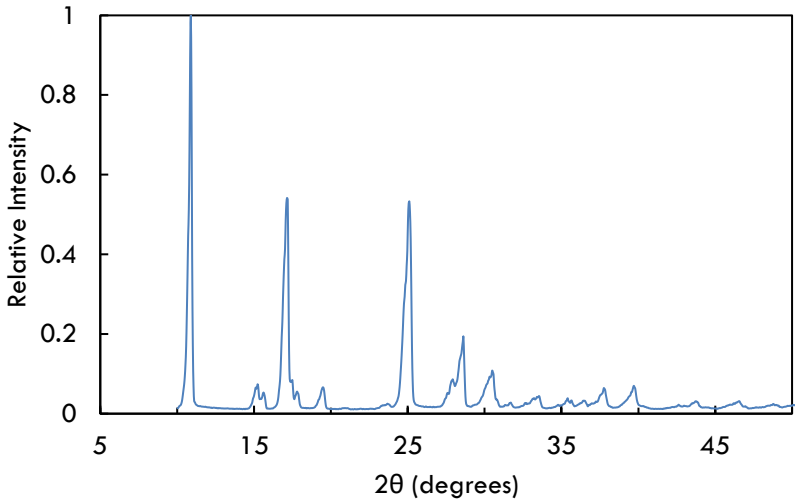

Figure 6.5: PXRD pattern of salicylic acid primary material.

6.1.6.5 Micro-computed tomography (micro-CT)

Agglomerate samples were imaged using a Bruker Skyscan 1272 desktop micro-computed tomography system (micro-CT), with a voxel size of 3 µm and a rotation rate of 0.1° per projection image. The micro-CT scans were conducted by Dr Dean Murphy (Pharmaceutical Technology and Development, AstraZeneca, Macclesfield). The resulting 2D scans were reconstructed using N-Recon software to obtain a 3D representation of the samples.

6.2 Results and Discussion

These experiments were conducted to investigate the suitability of constant tip speed as a scaling index for preserving agglomeration behaviour. The trend in agglomerate size over time is directly compared to the small scale experiments presented in Chapter 4 to assess whether the previously observed agglomeration dynamics are translated on a larger scale. This work examines both scaling up in a larger AFD while maintaining geometric similarity and changing dryer geometry by using a conical dryer. The contributions of the orbit arm and mixing screw to agglomeration is explored with select experiments in the conical dryer. Both SEM and micro-CT were scoped for their potential to study agglomerate structure, and morphology prediction calculations were used to identify dominant crystal growth directions. The data is presented using graphs of d_{50} and d_{90} values over time. To give an in-depth understanding of the agglomerate size distribution (ASD), d values and ASD spans are provided.

6.2.1 Analysis of Agglomeration Rates in Agitated Filter Dryers across Scales

Wet cakes of salicylic acid and water were agitated at two speeds (32 and 64 rpm) in the FD80, scaled up from agitation speeds of 50 and 100 rpm in the smaller AFD, hereafter referred to as the GFD 010. Agitation times were chosen based on time points of interest from the high fill experiments presented in Chapter 4, Section 4.2.1. Experiments were conducted at an average moisture content (MC) of 20.9 ± 1.9 % to minimise differences in agglomeration due to liquid saturation levels. The d_{50} values over time for low and high fill experiments at 50 rpm in the GFD 010 and scaled up experiments at 32 rpm in the FD80 are shown in Figure 6.6. Corresponding d values and ASD spans are provided in Table 6.6.

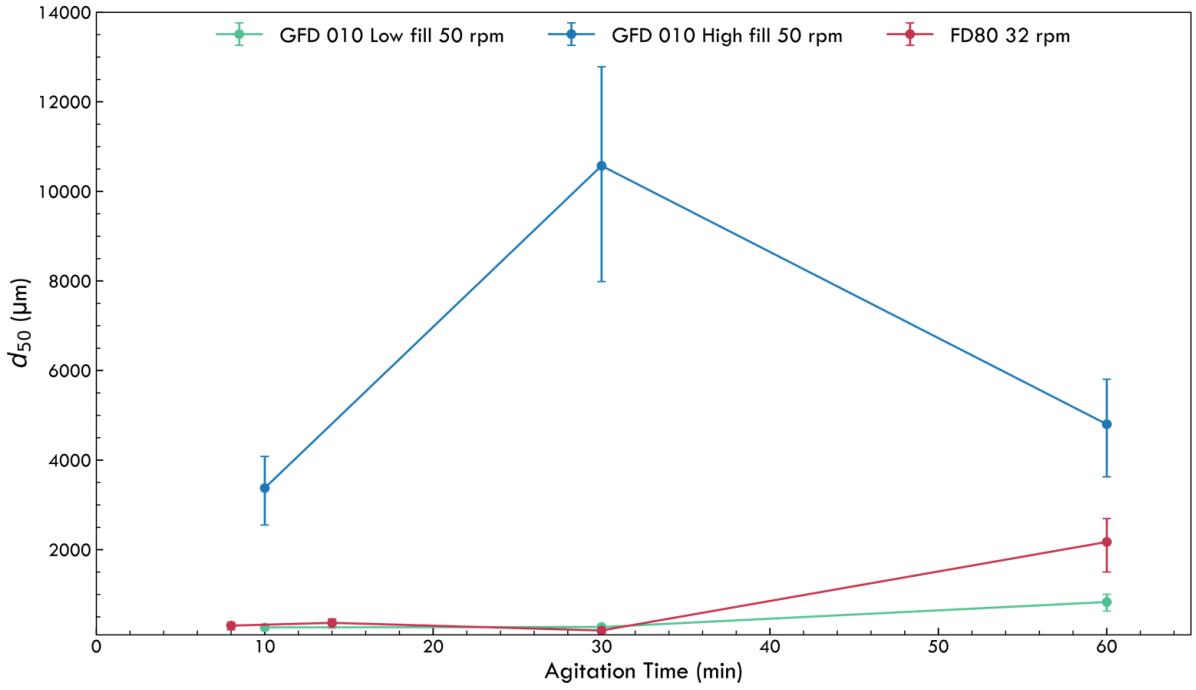

Figure 6.6: d_{50} values at 50 rpm in the GFD 010 and 32 rpm in the FD80 over time. Error bars represent the minimum and maximum error based on 3 repeat experiments at each speed.

Although the experiments were designed to be a scale up of the low fill experiments, the mass of solids used in the FD80 was similar to that used in the high fill experiments in Chapter 4. Therefore, this data is also included for comparison. It is evident from Figure 6.6 that the overall agglomeration trend in the FD80 closely follows that of the low fill experiments conducted in the GFD 010. In both systems, agglomeration and breakage appear to be relatively balanced up to 30 minutes, followed by agglomeration dominating between 30 and 60 minutes. The d_{50} values in both systems remain similar up to 30 minutes, suggesting that scaling using tip speed effectively maintains comparable agitation conditions during the initial agitation period. However, after 30 minutes the d_{50} values diverge, as shown by a d_{50} of 2173 µm in the FD80 at 60 minutes compared to 832 µm in the GFD 010. This indicates that while continued agitation promotes agglomeration in both systems, the rate of consolidation and coalescence seems to be greater in the FD80.

To further investigate these differences, Figure 6.7 presents the d_{90} values over time in both AFDs. Similar trends are observed again between low fill experiments in the GFD 010 and the FD80. As seen with the d_{50} values, the d_{90} values also show a noticeable increase after 30 minutes, reinforcing the observation that agglomeration becomes the dominant mechanism at longer agitation times. This may be attributed to fines generated through breakage being reincorporated into growing agglomerates via the snowballing mechanism. This hypothesis is further supported by the increase in d_{10} from 108 µm at 30 minutes to 298 µm at 60 minutes, indicating an overall shift towards larger granule formation.

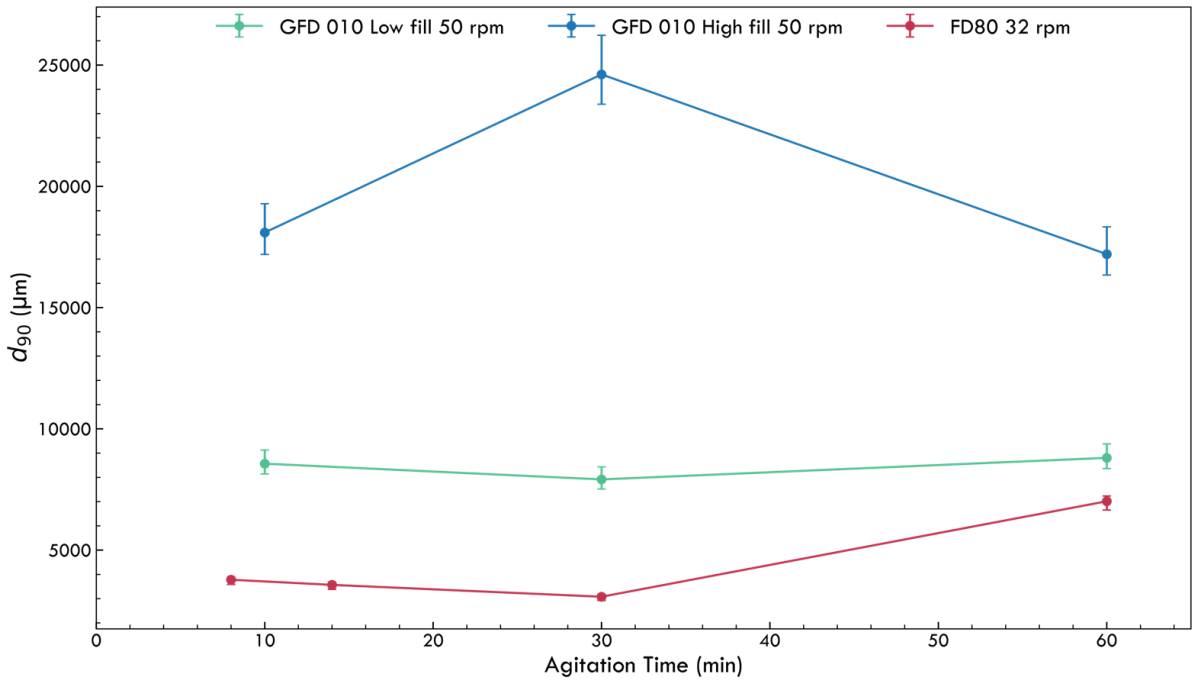

Figure 6.7: d_{90} values at 50 rpm in the GFD 010 and 32 rpm in the FD80 over time. Error bars represent the minimum and maximum error based on 3 repeat experiments at each speed.

Interestingly, despite the d_{50} values in the FD80 exceeding those in the GFD 010 after 30 minutes, the d_{90} values in the FD80 remain consistently lower throughout the agitation period. This suggests that although the larger AFD undergoes a transition to an agglomeration dominated regime after 30 minutes, the largest granules are more prone to breakage in the FD80 than in the GFD 010. Bock *et al*. have previously reported this effect where, despite scaling with constant tip speed, they observed an increase in fines and a shift towards smaller granules when increasing the bowl size.[150] Hibare and Acharya also reported a narrower size distribution skewed towards finer particles when scaling up a high shear mixer using constant tip speed.[151] The increased level of breakage in the FD80 is also highlighted by the effect of initial agitation. The initial wet cake had a d_{50} and d_{90} of 9390 μm and 19196 μm, respectively, which rapidly decreased to 305 μm and 3780 μm after 8 minutes of agitation. In comparison, the initial wet cake for low fill experiments in the GFD 010 had much smaller d_{50} and d_{90} values of 1872 μm and 9834 μm, respectively. Despite the significantly larger wet cake before agitation, the FD80 shows a substantial reduction in agglomerate size during the initial stages of agitation. This suggests the particles in the larger AFD may experience greater shear forces and/or localised areas of increased shear, resulting in breakage. The simultaneous increase in d_{10}, d_{50} and d_{90} values after 30 minutes may indicate delayed growth due to hindered coalescence, potentially caused by the redistribution of fines and a more gradual snowballing mechanism.

Although geometric similarity was maintained across scales, there were likely to be differences in energy distribution between the two AFDs. Larger systems can develop localised regions of high shear near the agitator blades or vessel walls, which may preferentially break larger agglomerates, limiting the upper size range. Despite these differences, the d_{90} values across both scales begin to converge by 60 minutes. Although the dominant mechanisms may differ across the time period, the final d_{90} values are comparable.

The suitability of constant tip speed as a scaling index was also investigated at a higher speed of 64 rpm in the FD80. Figure 6.8a and 6.8b show the d_{50} and d_{90} values over time for low and high fill experiments at 100 rpm in the GFD 010 and the corresponding scale up experiments at 64 rpm in the FD80. All d values and ASD spans are provided in Table 6.6. It is clear from Figure 6.8 that the trends in both d_{50} and d_{90} values over time in the FD80 closely resemble those observed in the low fill experiments in the GFD 010. The d_{50} values generally increase over time, but at a faster rate in the FD80, as indicated by the divergence in d_{50} values by 60 minutes. This behaviour aligns with the trend observed at 32 rpm in Figure 6.6, where d_{50} values remained similar up to 30 minutes, but showed a greater divergence at longer agitation times. The resulting agglomerate sizes from scaling up with constant tip speed across both speeds suggest that this scaling index captures agglomeration dynamics accurately qualitatively, but less so quantitatively.

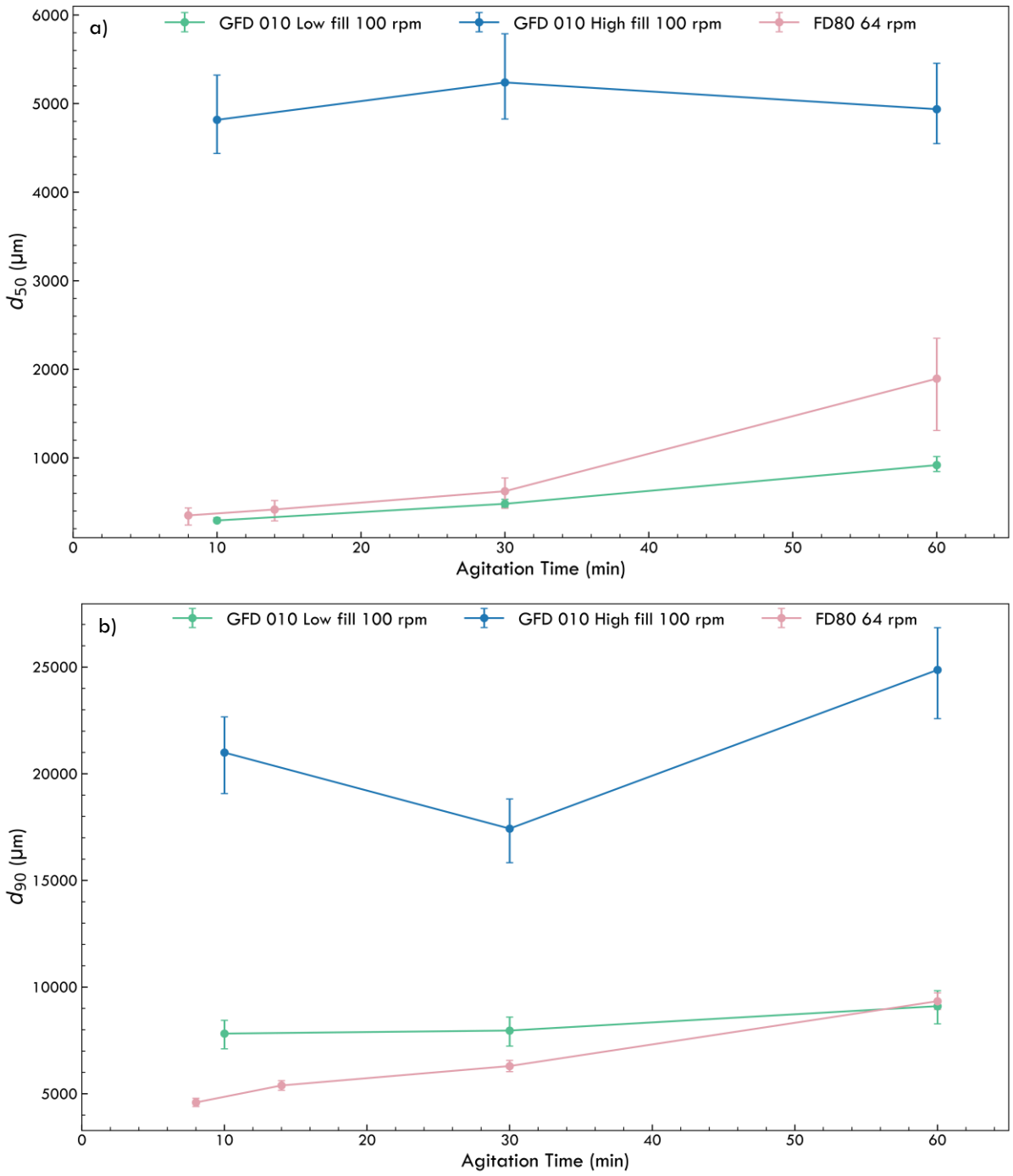

Figure 6.8: a) d_{50} and b) d_{90} values at 50 rpm in the GFD 010 and 64 rpm in the FD80 over time. Error bars represent the minimum and maximum error based on 3 repeat experiments at each speed.

The difference in d_{50} values by 60 minutes is reduced at the higher speed of 64 rpm, with a d_{50} of 1895 µm in the FD80 and 919 µm in the GFD 010. Figure 6.8b also shows that although the d_{90} values in the FD80 are initially lower, they steadily increase and converge with the GFD 010 by 60 minutes. The d_{90} values are 9338 µm and 9105 µm in the FD80 and GFD 010, respectively, with this difference falling within the bounds of error. The generally higher d_{50} values and lower d_{90} values in the FD80 compared to the GFD 010 suggest that despite maintaining geometric similarity and constant tip speed, the larger FD80 likely exhibits a different energy profile. This may promote breakage of larger agglomerates

through fragmentation. A previous study by Tao *et al.* reported similar results where scaling using constant tip speed produced slightly smaller and more porous granules at a larger scale.[152]

Despite these differences in *d* values, agglomeration continues to dominate over breakage as indicated by the steady increase in *d* values over time. Using constant tip speed for scaling demonstrates good agreement in capturing the overall process dynamics. However, despite maintaining geometric similarity, different levels of agglomeration are observed between the scales. This has been previously reported in the literature, where constant tip speed across scales has not resulted in similar mixing patterns or shear stresses.[153,154] The agitation speed is lowered upon scale up to preserve the tip speed but this may result in less effective mixing near the axis.[155] Litster *et al.* reported that powder flow tends to operate under two regimes: bumping and roping.[156] As the impeller speed increases, the powder flow transitions from the bumping regime to roping, where there is good turnover of particles in the powder bed and stable flow patterns. Therefore, the roping regime is favoured as it promotes uniform mixing. However, their work highlighted that constant tip speed may not always preserve the powder flow regimes, and the impeller speed should be adjusted to maintain the roping regime across scales.

Table 6.6: *d* values and ASD spans for all agitation speeds and times investigated at 20 % MC in the FD80.

Agitation Speed (rpm)	Agitation Time (min)	d_{10} (µm)	d_{50} (µm)	d_{90} (µm)	ASD Span
0	0	268	9390	19196	2.0
32	8	119	305	3780	12.0
	14	118	367	3568	9.4
	30	108	196	3079	15.1
	60	298	2173	7015	3.1
64	8	132	351	4591	12.7
	14	118	418	5387	12.6
	30	120	624	6297	9.9
	60	198	1895	9338	4.8

While constant tip speed can maintain a kinematic similarity, the dynamics will vary across scales as the cumulative particle collision energy per time decreases as scale increases. Although particles may have similar collision energies, the particle circulation is reduced in larger vessels. Nakamura *et al.* reported that, since the cumulative particle collision energy depends on both the magnitude and the accumulation rate of these collisions, reduced circulation in larger vessels leads to lower cumulative particle collision energy.[157] To address this, the authors suggested adjusting the granulation time during scale up to preserve the cumulative particle collision energy across scales.

The d_{50} values over time at both 32 rpm and 64 rpm in the FD80 are combined in Figure 6.9. Whilst the primary aim of this work was to assess the suitability of constant tip speed for scale up, it also provides

valuable insight into the material properties and their influence on agglomeration at different speeds. In Chapter 4, experiments conducted at various speeds and fill levels in the GFD 010 demonstrated that higher agitation speeds can promote increased agglomeration during specific periods of agitation. This was attributed to liquid bridge strength and more frequent collisions at higher speeds, which facilitated consolidation and coalescence. This trend is also evident on a larger scale in the FD80, as shown by higher d_{50} values at 64 rpm after 30 minutes of agitation in Figure 6.9. These findings highlight that the effect of agitation speed on agglomeration depends on the timescale.

The results reinforce the conclusions from Chapter 4, demonstrating that the relationship between agitation speed and the rate of consolidation and coalescence remains consistent across scales for this material system of salicylic acid and water. Although the d_{50} values differ in magnitude, the trends are consistent, likely due to the same underlying mechanism. This highlights the importance of considering material properties such as liquid bridge strength relative to the shear forces experienced under different agitation speeds when designing and scaling up agitated drying operations.

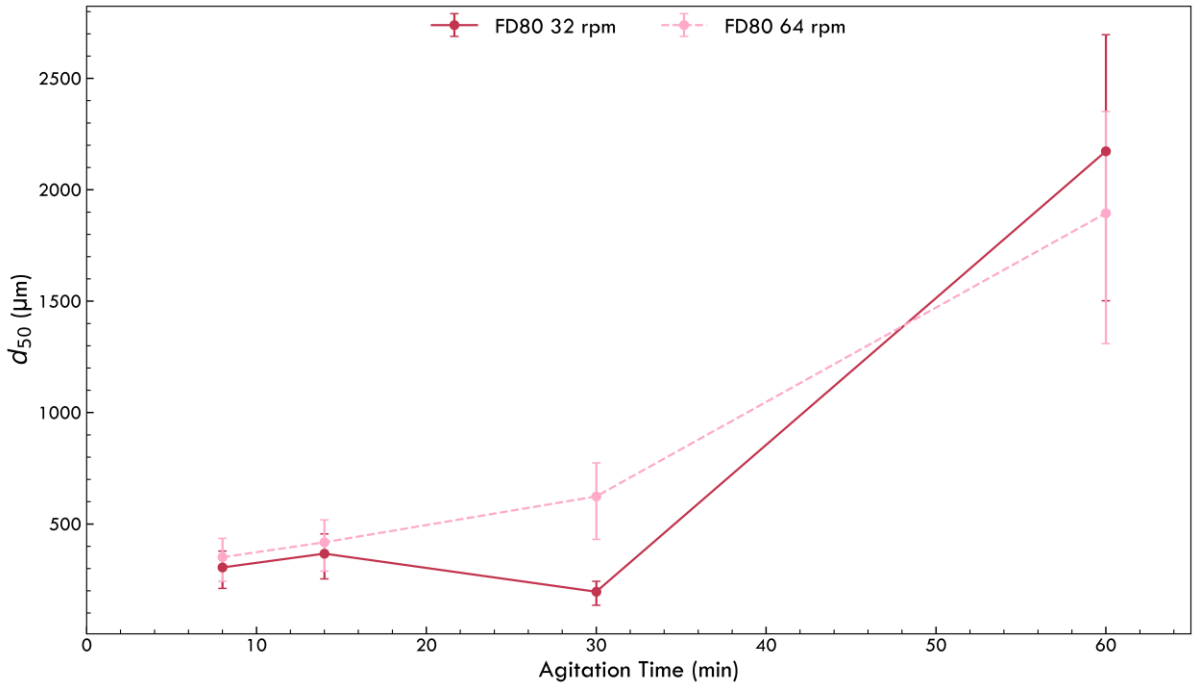

Figure 6.9: d_{50} values at 32 rpm and 64 rpm in the FD80 over time. Error bars represent the minimum and maximum error based on 3 repeat experiments at each speed.

The consistency in agglomeration trends across scales signifies the applicability of constant tip speed for scaling up agitated drying operations where agglomeration occurs. The results highlight that the same mechanisms govern agglomeration across scales. However, as previously discussed, differences in the magnitude of the d values across the two scales suggest that constant tip speed, even while maintaining geometric similarity, does not fully account for differences in particle dynamics at larger scales. Future work on adjusting the agitation times to preserve the cumulative particle collision energy on a larger scale could provide further insight into improving the scale up of agitated drying processes.

6.2.2 Analysis of Agglomeration Rates in a Conical Dryer during Scale Up

To assess the applicability of constant tip speed as a scaling index for preserving agglomeration behaviour when changing dryer geometry, experiments were conducted in a conical dryer. Salicylic acid and water bag mixes were agitated in the conical dryer at mixing screw speeds of 58 and 116 rpm, scaled up from agitation speeds of 50 and 100 rpm in the GFD 010. At a mixing screw speed of 58 rpm, the orbit arm speed was set to be 0.3 rpm and doubled to 0.6 rpm for a mixing screw speed of 116 rpm. The agitation times investigated were kept constant with experiments performed in the FD80. All experiments were conducted at an average MC of 20.1 ± 1 %.

The d_{50} values over time for low and high fill experiments at 50 rpm in the GFD 010 and the scaled up experiments at 58 rpm in the conical dryer are shown in Figure 6.10. All corresponding d values and ASD spans are in Table 6.7. As shown in Figure 6.10, the d_{50} values for the conical dryer are close in magnitude to the low fill experiments conducted in the GFD 010, but the trend over time differs. In the low fill experiments, the d_{50} values remain consistent up to 30 minutes, followed by a gradual increase at 60 minutes. In contrast, the d_{50} values in the conical dryer fluctuate consistently over time. Overall, the d_{50} values in the conical dryer are generally larger than those in the low fill GFD 010 experiments, except at 60 minutes, where the values fall within the bounds of error. This is expected as conical dryers are generally considered to be gentler than AFDs, resulting in lower levels of attrition.[142,158]

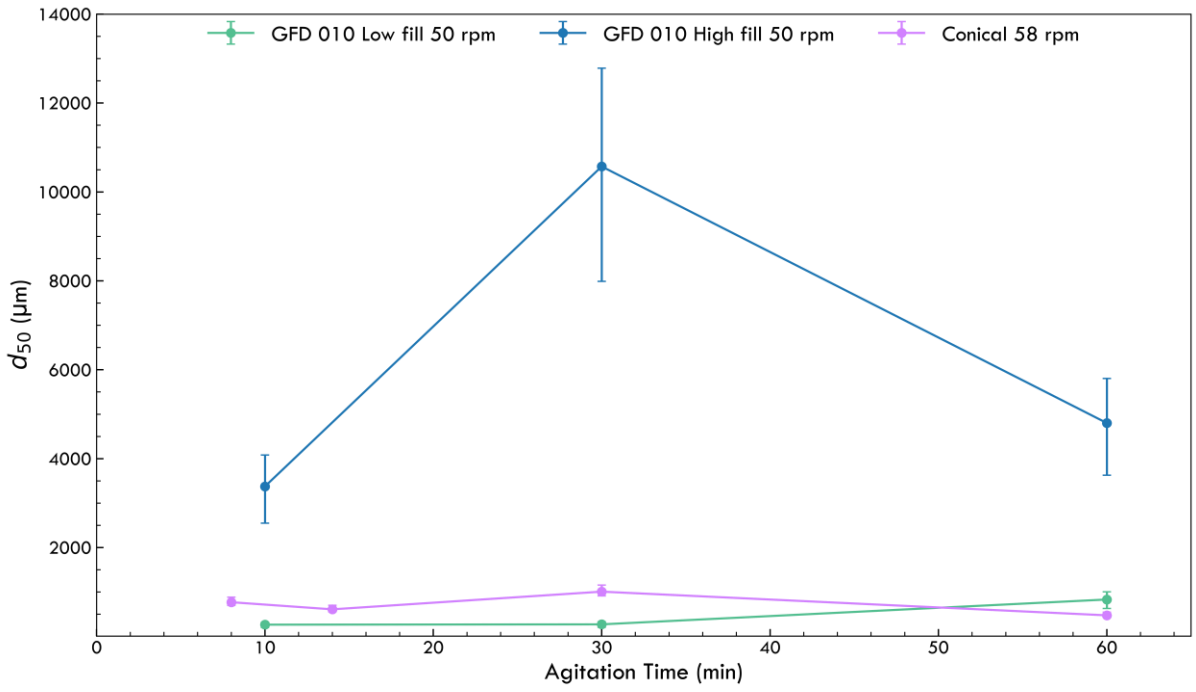

Figure 6.10: d_{50} values at 50 rpm in the GFD 010 and 58 rpm in the conical dryer over time. Error bars represent the minimum and maximum error based on 3 repeat experiments at each speed.

The conical dryer has very different flow patterns compared to an AFD. The mixing screw rotates on its own axis and moves material upwards, while the orbit arm moves the product around the vessel. Any

material outside the influence of the mixing screw flows back down due to gravity and is recirculated. Due to its design, the conical dryer naturally results in a powder bed that consistently includes both a static and an agitated region. As a result, the amount of breakage is reduced in comparison to an AFD where particles have more frequent collisions with the rotating impeller. The fluctuations over time in the conical dryer, although relatively minor, may be a result of the localised mixing inefficiencies, with static areas of the powder bed experiencing less breakage compared to areas within the influence of the mixing screw. This also reduces breakage of any initial agglomerates present in the bag mix prior to agitation. As experiments were conducted at a constant temperature of 25 °C, the particles remained wet throughout the agitation period. Particles residing in the static zones likely experience prolonged periods of contact which may further promote agglomeration.

For further insight into the agglomeration behaviour, the d_{90} values over time are presented in Figure 6.11. Although the d_{50} values in the conical dryer are larger than in the GFD 010 low fill experiments, the d_{90} values remain lower throughout the agitation period. While the d_{90} values are similar in magnitude to low fill GFD 010 experiments, the trend over time is very different, reflecting the same fluctuations seen in the d_{50} values. The lower d_{90} values suggest that the formation of very large agglomerates is hindered in the conical dryer, likely due to the gentle mixing which results in fewer and less energetic collisions, limiting the rate of consolidation and coalescence. Static zones may allow some agglomerates to persist, but without sufficient consolidation, they are more prone to breakage when in contact with the mixing screw. This explains the cyclic trend in d_{50} and d_{90} values over time, with continuous transitions between agglomeration dominated and breakage dominated regimes.

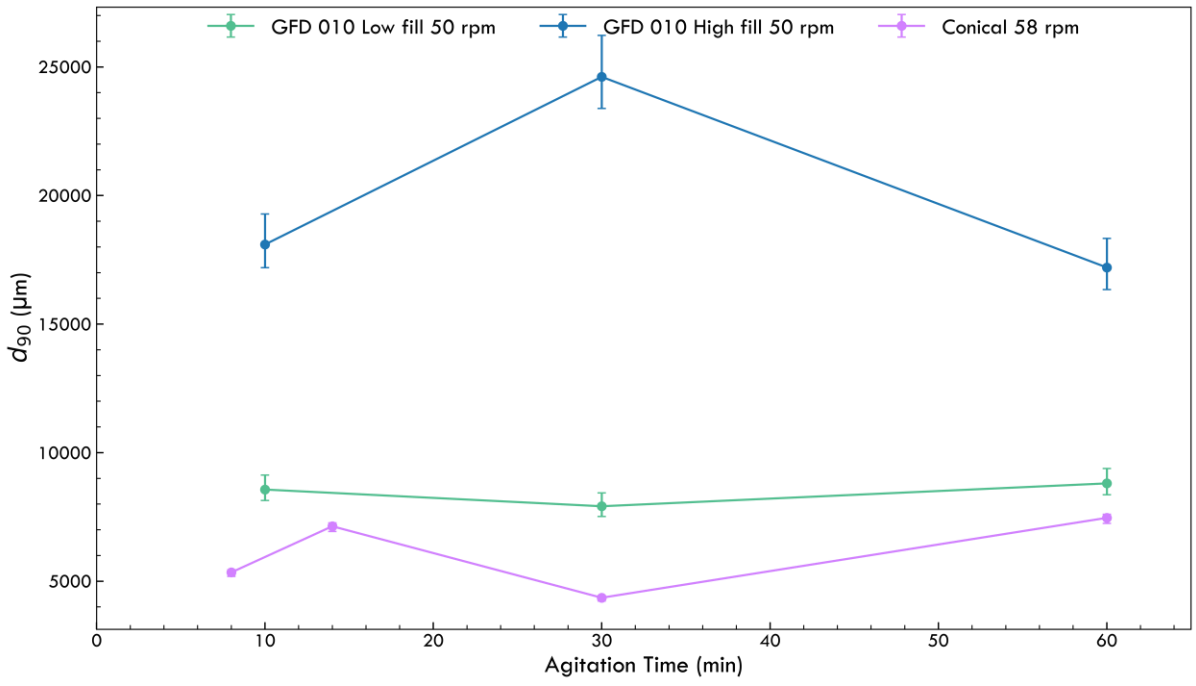

Figure 6.11: d_{90} values at 50 rpm in the GFD 010 and 58 rpm in the conical dryer over time. Error bars represent the minimum and maximum error based on 3 repeat experiments at each speed.

The fluctuations in d_{50} and d_{90} values appear to be inversely related throughout the agitation period, with an increase in d_{50} resulting in a decrease in d_{90} and vice versa. For example, from 14 to 30 minutes of agitation, the d_{50} increased from 611 µm to 1009 µm, whereas the d_{90} decreased from 7138 µm to 4358 µm. This may be due to breakage of larger agglomerates, which would increase the d_{50} while lowering the d_{90}.

This behaviour can be attributed to the mixing dynamics within a conical dryer, where shear intensity varies across different regions of the vessel. Static zones will allow agglomerates to be undisturbed and the prolonged contact between wet agglomerates may further promote agglomerate growth through coalescence. In contrast, regions near the mixing screw will experience higher levels of shear, which can facilitate breakage. The gentle motion characteristic of the conical dryer makes it likely that the dominating breakage mechanism is attrition, with gradual wear of larger agglomerates through low energy impacts, as opposed to fracture. The decrease in d_{90} coupled with the increase in d_{10} and d_{50} suggests that fines produced from breakage of larger agglomerates are reincorporated into smaller agglomerates, likely through the snowballing mechanism.

Overall, this trend reiterates the dynamic nature of agglomeration and breakage occurring simultaneously. This behaviour also aligns with the proposed mechanism introduced in Chapter 4, Section 4.2, where lower speeds resulted in fluctuations between regions dominated by agglomeration and regions dominated by breakage.

The agglomeration behaviour over time was also investigated at a higher mixing screw speed of 116 rpm and an orbit arm speed of 0.6 rpm. Figures 6.12a and 6.12b show the d_{50} and d_{90} values over time for low and high fill experiments at 100 rpm in the GFD 010 and corresponding conical dryer experiments at 116 rpm. All d values and ASD spans are provided in Table 6.7.

Table 6.7: d values and ASD spans for all mixing screw and orbit arm speeds and times investigated at 20 % MC in the conical dryer.

Mixing Screw Speed (rpm)	Orbit Arm Speed (rpm)	Agitation Time (min)	d_{10} (µm)	d_{50} (µm)	d_{90} (µm)	ASD Span
58	0.3	8	194	771	5343	6.7
		14	216	611	7138	11.3
		30	399	1009	4358	3.9
		60	118	476	7465	15.4
116	0.6	8	117	376	2181	5.5
		14	128	285	2369	7.9
		30	360	958	3022	2.8
		60	425	658	2313	2.9

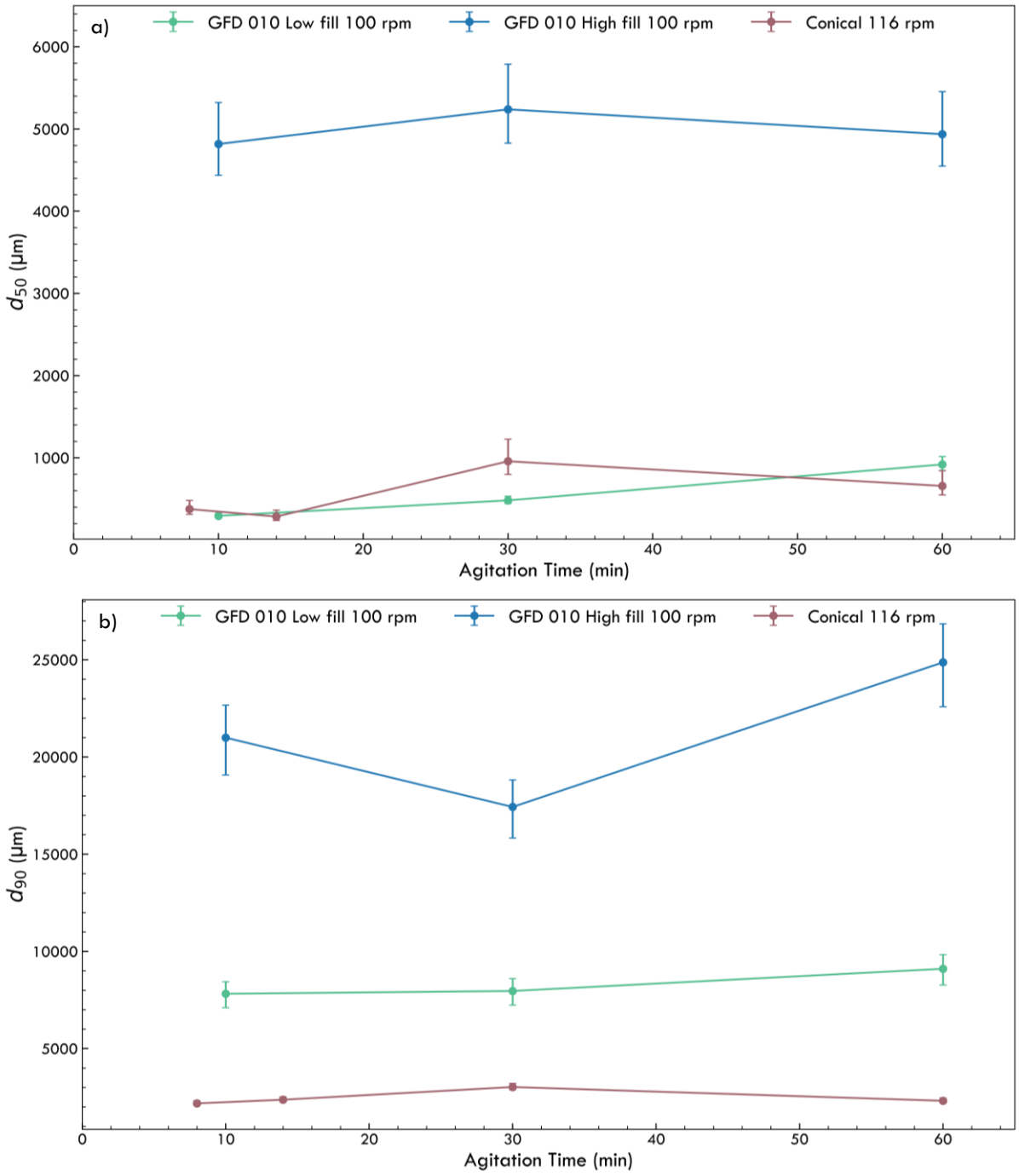

Figure 6.12: a) d_{50} and b) d_{90} values at 100 rpm in the GFD 010 and 116 rpm in the conical dryer over time. Error bars represent the minimum and maximum error based on 3 repeat experiments at each speed.

The trend in d_{50} values over time is consistent even at a higher mixing screw speed of 116 rpm, with values similar in magnitude to low fill experiments in the GFD 010, and constant fluctuations throughout the agitation period. The difference in d_{50} values is greatly minimised at 116 rpm, with the only variation falling outside the bounds of error occurring at 30 minutes, with a d_{50} of 958 µm in the conical dryer and 482 µm in the GFD 010. This increased similarity in d_{50} may be attributed to improved mixing, as both the screw and the orbit arm speeds are doubled, resulting in twice as many rotations around the entire vessel and greater particle circulation.

The d_{90} values over time are still lower in the conical dryer compared to the GFD 010. However, at 116 rpm, the size of the larger agglomerates in the population is more consistent. Compared to the fluctuations seen at 58 rpm in Figure 6.11, the d_{90} values are more stable, indicating a more uniform size distribution. While the gentle mixing in the conical dryer may hinder the rate of consolidation and coalescence, higher screw speeds and orbit arm speeds facilitate more particle interactions. This improves the circulation and reduces static zones within the vessel, promoting a more even balance between breakage and agglomeration.

The d_{50} values as a function of time for both mixing screw speeds of 58 and 116 rpm are combined in Figure 6.13. This figure highlights that the trend in agglomerate growth and breakage remain consistent across speeds. At 116 rpm, d_{50} values tend to be lower, especially for shorter agitation periods. This reinforces that improved mixing and particle circulation at higher screw speeds increases the extent of breakage and reduces agglomeration.

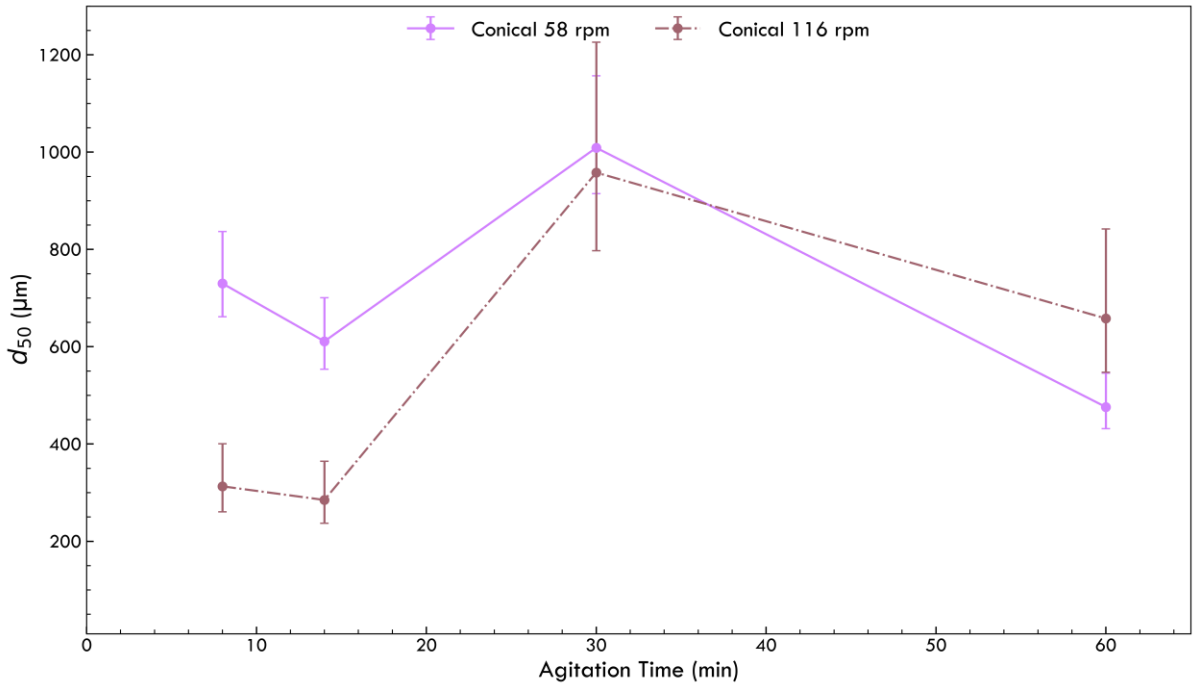

Figure 6.13: d_{50} values at 58 rpm and 116 rpm in the conical dryer over time. Error bars represent the minimum and maximum error based on 3 repeat experiments at each speed.

Despite their widespread use in the pharmaceutical industry, there is minimal literature in the public domain on designing drying processes with conical dryers. Although this work consists of a small data set, it provides valuable insights into the mixing within a conical dryer and how it differs from an AFD. The results demonstrate that scaling up using constant tip speed becomes less reliable when transitioning between dryer geometries, as both the magnitude and trends in d values over time differ significantly. This discrepancy stems from different shear forces and flow patterns in the two dryers. Although such deviations are expected given the significant differences in vessel design, constant tip speed is still commonly used in industry. These findings highlight the need for a more nuanced approach

for scaling up agitated drying processes by considering the flow patterns and shear forces experienced across various dryer types, and how they govern the mechanisms of agglomeration.

For further insight into the contribution of the orbit arm and the mixing screw to the agglomeration observed in the conical dryer, additional experiments were performed at a mixing screw speed of 116 rpm while maintaining the orbit arm speed at 0.3 rpm. The agglomerate size distributions (ASDs) for an 8 minute agitation period with orbit arm speeds of 0.3 and 0.6 rpm are shown in Figure 6.14. The corresponding *d* values and ASD spans are given in Table 6.8.

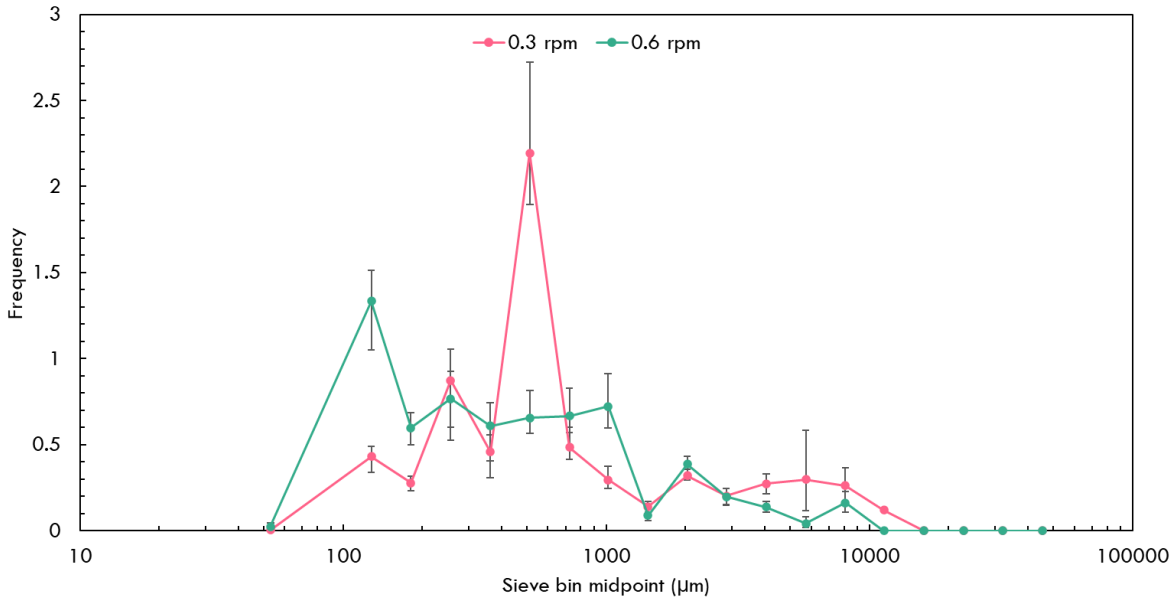

Figure 6.14: Agglomerate size distributions for 116 rpm 8 min runs at orbit arm speeds of 0.3 and 0.6 rpm. Error bars represent the minimum and maximum error based on 3 repeat experiments at 116 rpm.

Table 6.8: *d* values and ASD spans for experiments conducted at 116 rpm at various orbit arm speeds for 8 minutes in the conical dryer.

Mixing Screw Speed (rpm)	Orbit Arm Speed (rpm)	Agitation Time (min)	d_{10} (µm)	d_{50} (µm)	d_{90} (µm)	ASD Span
116	0.3	8	190	523	4790	8.8
	0.6		117	376	2181	5.5

It is evident from Figure 6.14 that reducing the orbit arm speed from 0.6 to 0.3 rpm results in a shift to the right in the ASD, indicating the presence of larger agglomerates. This highlights the importance of the orbit arm in circulating material around the vessel, as the mixing screw speed alone is insufficient to achieve uniform mixing. At a lower orbit arm speed of 0.3 rpm, reduced circulation may lead to less particle contact with the mixing screw, resulting in a broader ASD span with large agglomerates due to decreased breakage. This effect is particularly evident in the d_{90} values which represent the largest agglomerates in the population. Lowering the orbit arm speed from 0.6 rpm to 0.3 rpm leads to an

increase in d_{90} from 2181 µm to 4790 µm, effectively more than doubling its original value. Notably, this d_{90} value of 4790 µm is comparable to that observed at a lower mixing screw speed of 58 rpm, where the d_{90} was 5343 µm for the same agitation time. This shows that the orbit arm speed plays a significant role in agglomerate growth and breakage dynamics within the conical dryer.

The data also highlights the benefit of increasing the screw speed for improving mixing within a conical dryer. At an orbit arm speed of 0.3 rpm, increasing the screw speed from 58 rpm to 116 rpm reduces the d_{50} from 771 µm to 523 µm, demonstrating that higher screw speeds can mitigate agglomeration, even at low orbit arm speeds. However, without sufficient circulation throughout the powder bed, the extent of breakage is limited, and this results in a wider ASD. This data suggests that while higher mixing screw speeds can reduce agglomeration, efficient circulation facilitated by the orbit arm is necessary to promote uniform breakage and prevent the formation and survival of large agglomerates.

The effect of changing orbit arm speed on agglomeration behaviour at a mixing screw speed of 116 rpm was also investigated for a longer agitation period of 30 minutes. The ASDs of experiments conducted for 30 minutes at 116 rpm with orbit arm speeds of 0.3 and 0.6 rpm are shown in Figure 6.15, and the d values and ASD spans can be found in Table 6.9.

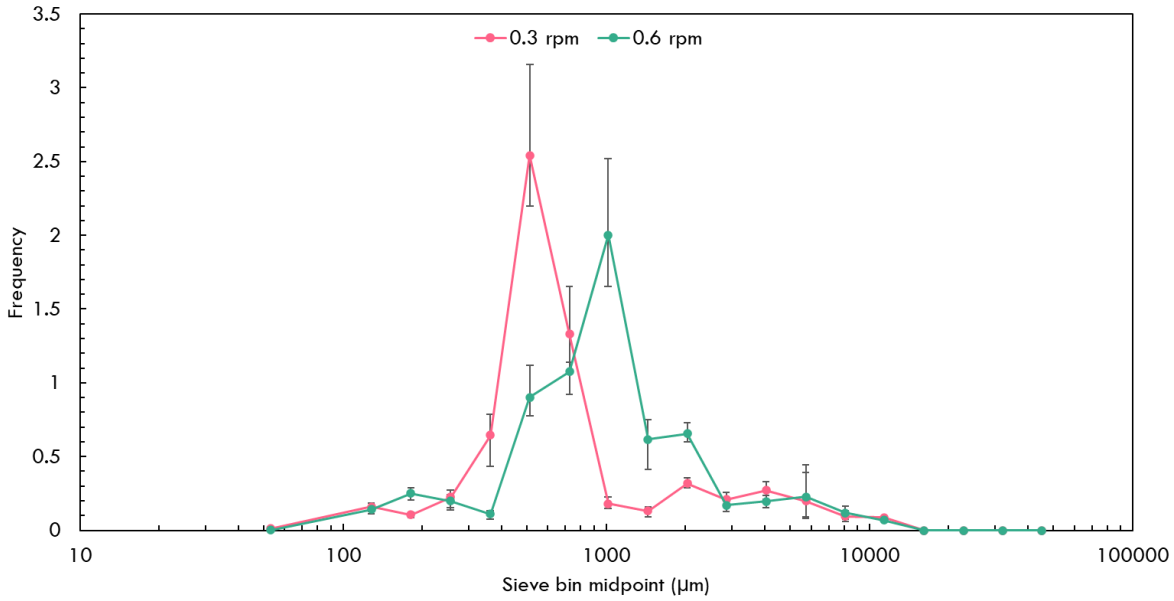

Figure 6.15: Agglomerate size distributions for 116 rpm 30 min runs at orbit arm speeds of 0.3 and 0.6 rpm. Error bars represent the minimum and maximum error based on 3 repeat experiments at 116 rpm.

Table 6.9: d values and ASD spans for experiments conducted at 116 rpm at various orbit arm speeds for 30 minutes in the conical dryer.

Mixing Screw Speed (rpm)	Orbit Arm Speed (rpm)	Agitation Time (min)	d_{10} (µm)	d_{50} (µm)	d_{90} (µm)	ASD Span
116	0.3	30	301	564	3269	5.3
	0.6		360	958	3022	2.8

Interestingly, lowering the orbit arm speed from 0.6 to 0.3 rpm results in a decrease in d_{50} from 958 µm to 564 µm for 30 minutes of agitation. The ASD in Figure 6.15 also shows a small shift to the left when reducing the orbit arm speed. This is the opposite of the trend observed for an 8 minute agitation period, where lower orbit arm speeds initially promoted the formation of larger agglomerates. This suggests that while reduced circulation at 0.3 rpm may initially promote agglomerate growth, continued agitation likely promotes breakage of these agglomerates over time.

Longer agitation times may produce more fines, which can facilitate snowballing growth. At 0.3 rpm, increasing the agitation time from 8 to 30 minutes increases the d_{10} from 190 µm to 301 µm. Further increasing the orbit arm speed to 0.6 rpm results in a slightly larger d_{10} of 360 µm. At 0.6 rpm, the circulation and frequency of particle contact doubles, allowing more fines to adhere to wet agglomerates and further promoting agglomerate growth. The larger d_{50} value of 958 µm may be attributed to this.

Despite the lower d_{50} at 0.3 rpm after 30 minutes, the effect of reduced circulation is reflected in the broader ASD span. At 0.6 rpm, increased circulation and particle contact may create a more dynamic environment, balancing agglomerate growth and breakage more effectively. This is reflected by the decrease in ASD span at 0.6 rpm. At 0.3 rpm, the presence of more static zones may explain why agglomerate growth dominates at shorter agitation times, whereas longer agitation times promote breakage. This behaviour is analogous to the behaviour observed at 50 rpm for high fill experiments reported in Chapter 4, Section 4.3.1, where inefficient mixing led to periods of agglomerate growth or breakage dominating, while higher speeds maintained a continuous balance.

The impact of the mixing screw for controlling agglomerate size is again reflected in this data. Increasing the mixing screw speed from 58 to 116 rpm at an orbit arm speed of 0.3 rpm for 30 minutes of agitation reduces the d_{50} from 1009 µm to 564 µm. This is quite a significant reduction and highlights the improvement in mixing and increased breakage occurring at higher screw speeds.

While this data set on the effect of the orbit arm speed on agglomeration in the conical dryer is limited due to time constraints during the placement, it provides useful insight into the orbit arm's contribution to the overall mixing dynamics. It also highlights the need for further investigation into the relationship between screw speed and orbit arm, with the aim of identifying an optimal ratio for achieving more uniform mixing.

6.2.3 Comparison of Agglomeration Dynamics in AFDs and Conical Dryers during Scale Up

Previously, scale up performance was assessed by comparing large scale data with lab scale AFD results to evaluate the suitability of constant tip speed as a scaling index. To further explore how agglomeration behaviour differs when scaling up in an AFD versus a conical dryer, all d_{50} data sets over time for the speeds investigated in both systems are plotted together in Figure 6.16.

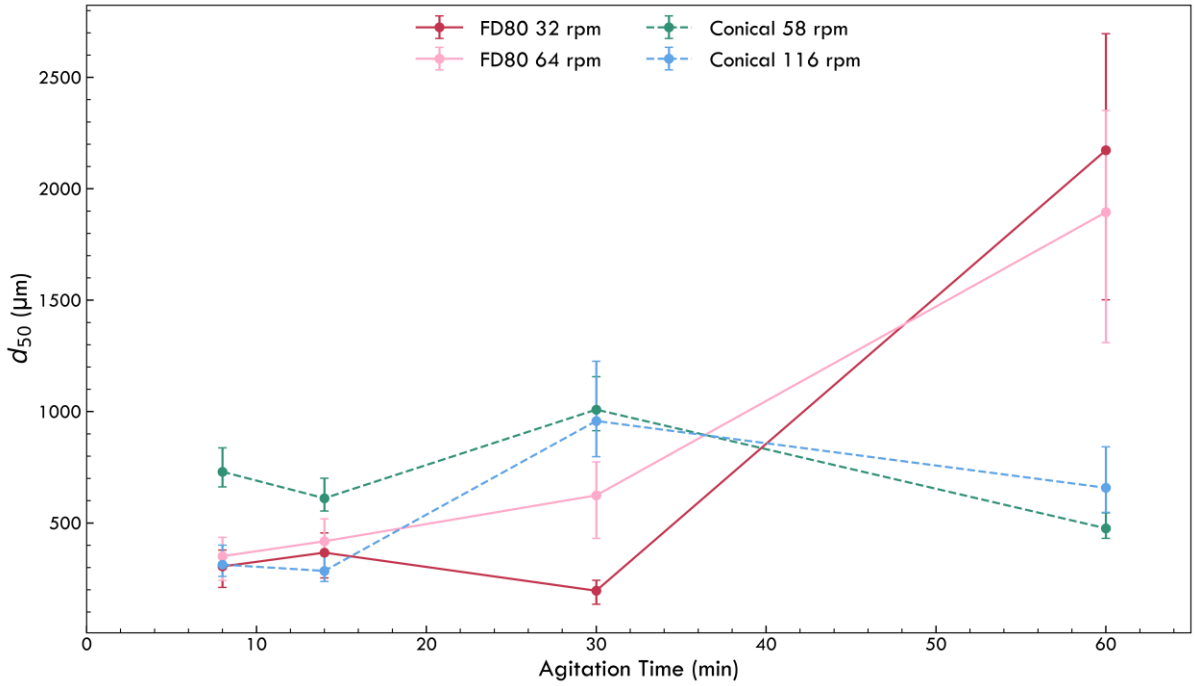

Figure 6.16: d_{50} values at 32 rpm and 64 rpm in the FD80 and 58 rpm and 116 rpm in the conical dryer over time. Error bars represent the minimum and maximum error based on 3 repeat experiments at each speed.

It is clear from Figure 6.16 that agglomeration dynamics are consistent within each dryer type but differ significantly between the FD80 and the conical dryer. During the initial agitation period, the highest d_{50} is observed in the conical dryer at 58 rpm. This is expected due to the gentle mixing action and lower agitation intensity inherent to conical dryers. Similar findings were reported in a previous study, where switching from an AFD to a conical dryer during scale up resulted in an over 50 % reduction in attrition, despite using constant agitation in the conical dryer.[159] As the agitation is continued, the d_{50} values are similar for both speeds in the conical dryer, suggesting that increasing the mixing intensity has a minor impact on the extent of breakage. Although the cyclic nature over time continues, both speeds appear to result in comparable agglomeration dynamics.

The AFD experiments in the FD80 exhibit very different agglomeration behaviour, with a general steady growth over time. This growth occurs at a much faster rate with longer agitation times, as highlighted by the sharp increase in d_{50} from 30 to 60 minutes at both speeds. This is likely due to improved mixing within the AFD with more frequent collisions. This results in increased consolidation and coalescence, as evidenced by the d values.

Overall, this work highlights the importance of accounting for the differences in shear forces and flow patterns across different dryers, as these factors significantly influence agglomeration dynamics. This has important implications for scaling agitated drying processes and suggests that predictive modelling could be beneficial. The following section explores differences in agglomerate structure between the two dryers using SEM and micro-CT analysis.

6.3 Morphological Analysis of Agglomerates within the AFD and Conical Dryer

To investigate how different shear environments influence agglomerate structure, this work involved scoping different imaging techniques to assess their suitability for morphological analysis. Agglomerates from both the AFD and the conical dryer were analysed using SEM and micro-CT. The SEM images were compared with Bravais-Friedel-Donnay-Harker (BFDH) morphology predictions for the dominant crystal growth faces.

It is important to acknowledge that SEM analysis introduces inherent sampling bias, as only agglomerates small and robust enough to remain adhered to the stub are imaged, and only their external surfaces can be examined without destroying the agglomerates. To address this limitation, micro-CT scans were performed on multiple agglomerates from both an AFD experiment and a conical dryer experiment to compare with SEM observations. Additional micro-CT scans were also carried out on samples of the heel from AFD experiments to investigate potential structural differences compared to agglomerates from the bulk.

6.3.1 Analysis of Agglomerates in the AFD

Some SEM images of agglomerates formed in the FD80 are shown in Figure 6.17 from 32 rpm experiments at various agitation times. Both Figure 6.17a and Figure 6.17b appear to show similar consolidation and packing behaviour, with smaller crystals occupying the void spaces between larger crystals. There is likely to be some degree of mechanical interlocking also occurring as a result of the agitation. While the inherent sampling bias of SEM limits the ability to draw conclusions about differences in agglomerate size across runs, the images indicate consolidation may be occurring.

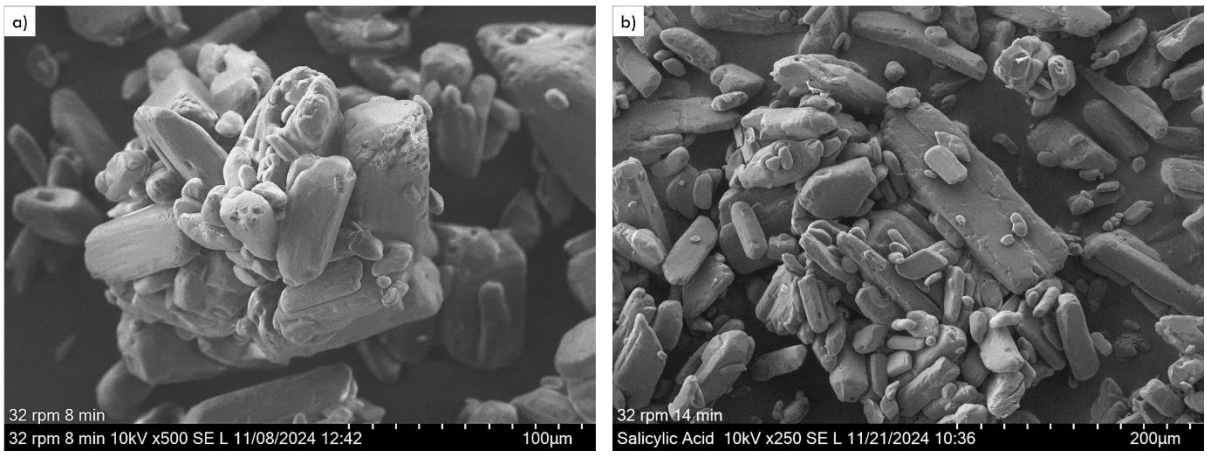

Figure 6.17: SEM images of agglomerates from 32 rpm runs in the FD80 at a) 8 mins and b) 14 mins.

Although SEM is valuable for examining the external morphology of agglomerates, is difficult to analyse the internal structure without breaking them apart. Therefore, micro-CT was used to take scans of agglomerates from FD80 experiments to investigate the 3D structure. Figure 6.18a–d shows cross-sectional images of a specific agglomerate (circled in purple) from a 64 rpm 14 minute run, viewed at

different depths and orientations. This agglomerate was selected to illustrate key features and analyse structural differences across various layers and perspectives.

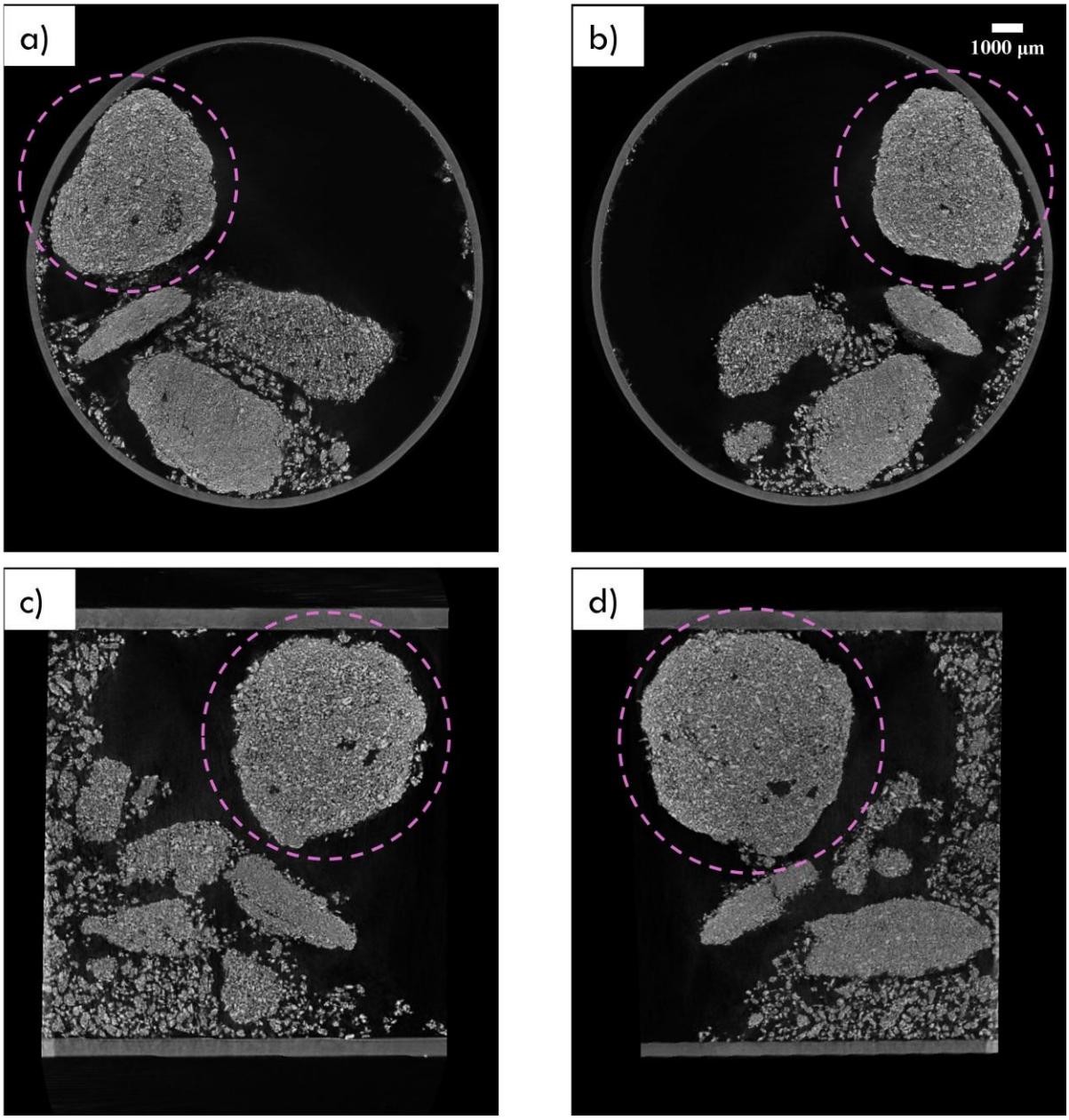

Figure 6.18: Reconstructed micro-CT cross-sectional images of an agglomerate from FD80 experiments at varying depths and orientations showing a) top, b) bottom, c) left, and d) right slices.

Figure 6.18a highlights the initial core of the agglomerate, with potential signs of fines beginning to layer around the exterior. Figure 6.18b also shows this agglomerate core from another angle and there are structural similarities, with voids more present in the core of the agglomerate compared to the outer areas. Figures 6.18c and 6.18d present shallower cross-sections of the agglomerate from a lateral perspective, giving a broader view of the overall agglomerate structure. Again, voids are mainly present in the centre of the agglomerate, with the perimeter appearing to be more packed. This structure may result from the initial agglomerate nucleus growing through the snowballing mechanism, as it is agitated

through the vessel and repeatedly comes into contact with fines that adhere to its surface. The presence of larger voids in Figure 6.18c and Figure 6.18d may also indicate that some coalescence has occurred to enable granule growth, although the relatively low shear environment may have limited the extent of consolidation. Similar structural features have been reported in granules produced in a high shear mixer, where the agglomerates had a porous core surrounded by a shell composed of layered particles. This morphology was attributed to coalescence and layering growth.[160]

These images are useful for trying to further understand the mechanisms of agglomerate growth occurring in the AFD. However, it is difficult to draw definitive conclusions from this limited data, especially with the resolution. Micro-CT is an effective yet costly and time-consuming tool. The voxel size is also critical, as smaller voxels provide higher resolution. However, reducing the voxel size significantly increases the scan acquisition time and size of the data files. Therefore, it is essential to find a balance between the resolution required and the duration of scans. This work is also limited by the use of only one scan, which restricts the extent of analysis. With additional scans, it would be possible to approximate the porosity of agglomerates and provide quantitative data to support the morphological analysis. Despite these limitations, this primary analysis underscores the potential of micro-CT to provide valuable insights into the internal structure of agglomerates.

6.3.2 Analysis of the Heel in the AFD

When agitating the wet cake, it is crucial to maintain a clearance between the bottom of the vessel and the base of the agitator to prevent damage to the filter plate. However, this can lead to the formation of a compressed layer of material, known as the heel. Although the heel consists of agglomerates, the mechanism driving their formation is likely different to the bulk material as the heel is not subjected to direct agitation. Instead, the formation of the heel is likely driven by compaction, with the agitator rotating above it. This will likely result in harder and denser agglomerates compared to the bulk. To investigate this, micro-CT scans were performed on samples of the heel. Although SEM images were obtained, they did not provide insight into the overall structure of the heel and are not included here.

Cross-sectional images of two agglomerates from the heel are shown in Figure 6.19. These images suggest that the heel is highly compacted with minimal porosity and no large voids, unlike the porous bulk agglomerates seen in Figure 6.17. This dense structure appears to support the hypothesis that heel formation is driven primarily by compaction, which differs significantly from the agitation driven formation of agglomerates in the bulk.

In both cross-sections, the internal structure appears homogeneous and consistently consolidated. This is further supported by relatively uniform shading in the images, which suggests a uniform density. These observations reinforce the idea that the heel forms as material settles and compacts beneath the agitator, which rotates above without directly disturbing this region. The mechanical pressure exerted in this static zone likely produces much harder agglomerates, consistent with the lower porosity and

lack of voids. As agglomerate strength typically increases with decreasing porosity, the heel may be more resistant to breakage compared to agglomerates formed in the bulk. Although images from this single scan show clear structural differences between the heel and bulk agglomerates, further scans would be required to estimate porosity and confirm whether this trend is consistent across samples.

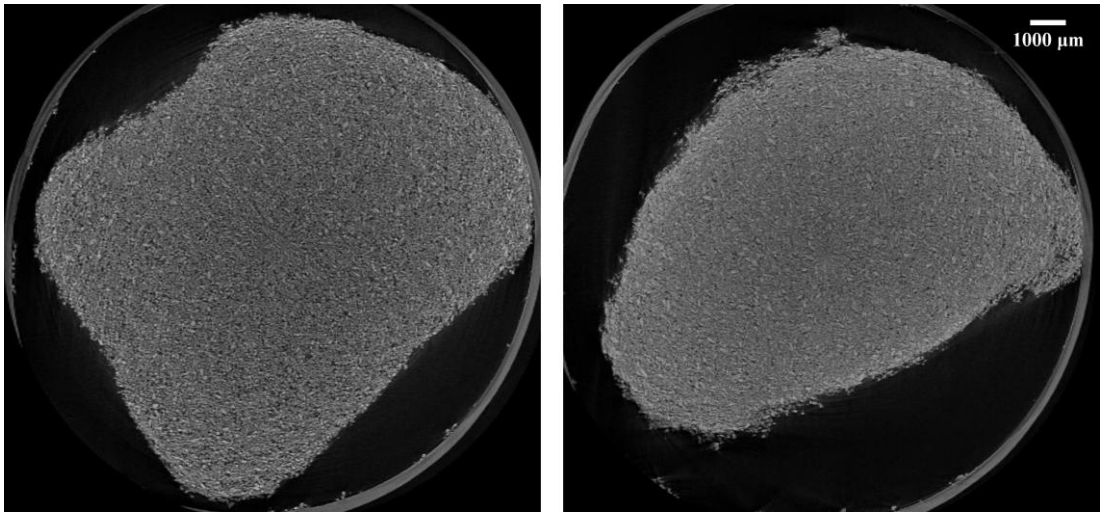

Figure 6.19: Reconstructed micro-CT cross-sectional images of agglomerates from the heel formed in the FD80.

The heel is likely composed of a range of particle sizes, with smaller particles occupying the voids between larger ones. This efficient packing presumably contributes to the minimal porosity observed. However, such packing also results in less channels for the solvent to pass through, increasing the moisture content (MC). Many studies have reported that a broader PSD increases cake resistance and leads to greater solvent retention.[41,44–46]

It is well established that wet cakes are typically inhomogeneous with respect to MC, which is why multiple sampling locations are required for accurate MC analysis. Due to the heel forming at the bottom of the filter cake and experiencing compaction from the agitator above, it is highly likely that this region has a higher MC than the top layers of the cake. This increased MC combined with compaction may contribute to the formation of larger and harder agglomerates within the heel. This difference in MC was also observed experimentally. Although the overall wet cake remained at approximately 20 % MC, as experiments were conducted at a constant temperature of 25 °C to avoid drying, small differences in MC were observed between the bulk and the heel. However, it is difficult to draw conclusions from these measurements due to the nature of separating the bulk and heel, and potential for sample overlap.

6.3.3 Analysis of Agglomerates in the Conical Dryer

The morphology of agglomerates formed in the conical dryer was analysed using SEM and micro-CT. Figure 6.20a and Figure 6.20b present agglomerates from conical dryer experiments conducted at 58 rpm for 60 minutes and 116 rpm for 14 minutes, respectively. Both images appear to show agglomerates composed of crystals of varying sizes and irregular shapes, with some indications of consolidation.

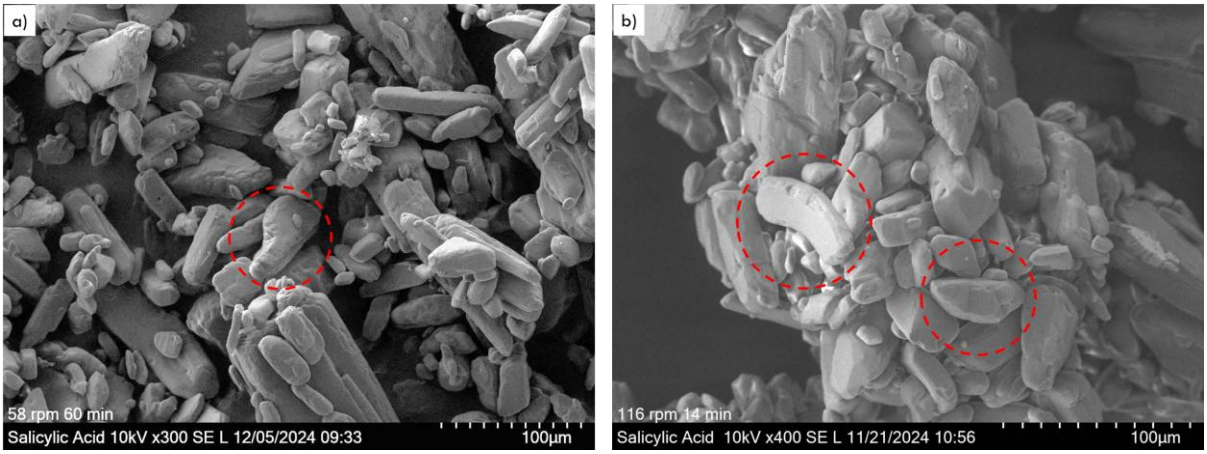

Figure 6.20: SEM images of agglomerates in the conical dryer from a) 58 rpm 60 min and b) 116 rpm 14 min runs.

The crystals on the agglomerate surfaces appear more irregular in shape compared to those observed in the AFD in Figure 6.17, with some examples circled in red. This difference may be due to the geometry of the conical dryer, which could result in some crystals bending if they are trapped in the gap between the mixing screw and the vessel wall. This observation has not previously been reported in the literature but is constrained by the sampling capabilities of SEM and further restricted by the limited number of SEM images obtained. Although direct comparisons between agglomerate morphology in conical dryers and AFDs are limited in the literature, similar trends were reported by Morin and Briens when comparing agglomerates formed in a high shear mixer and a conical fluidised bed.[161] Agglomerates from the fluidised bed were more porous and irregular in shape, likely due to the lower shear forces exerted on the particles compared to a high shear mixer. Other studies have also noted that lower shear conditions in fluidised beds tend to produce porous, irregularly shaped agglomerates.[162,163] Lower shear forces will also inhibit the extent of consolidation occurring.

To complement the SEM analysis, micro-CT was used to study the internal structure of agglomerates formed in the conical dryer. Figure 6.21 shows reconstructed cross-sectional images of agglomerates from an experiment at 116 rpm with a 14 minute agitation period, at different depths. The agglomerates appear to exhibit voids with varying degrees of porosity. This variation is likely due to the inherent nature of the conical dryer where static zones are present. In these regions, particles experience minimal shear, potentially resulting in weaker, less consolidated structures with higher porosity.

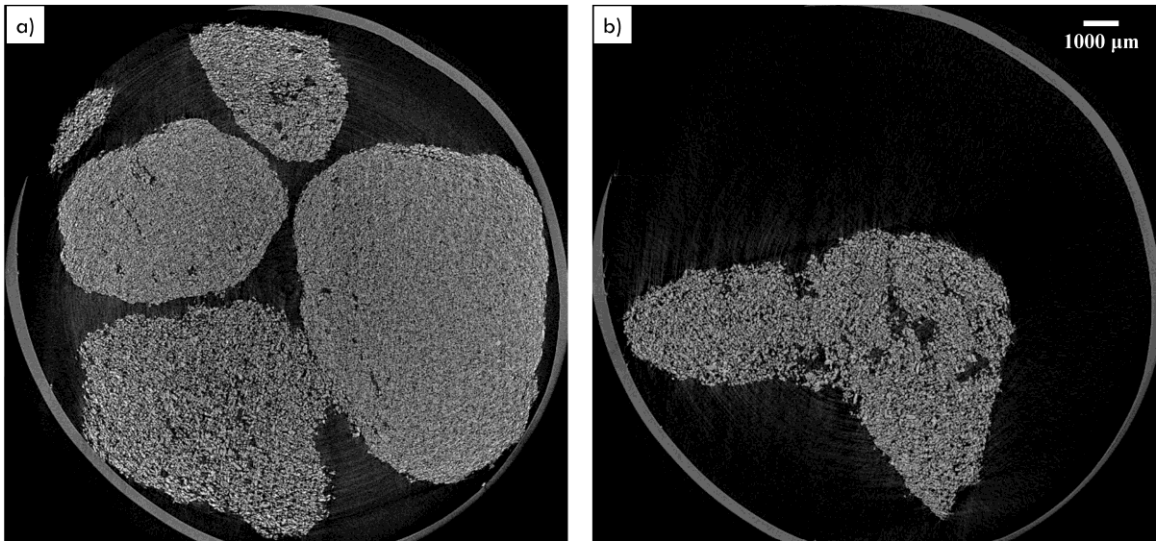

Figure 6.21: Reconstructed micro-CT cross-sectional images of agglomerates in the conical dryer from a 116 rpm 14 min run, shown at two different depths a) and b).

The porosity appears even more pronounced in Figure 6.21b where several large voids are visible. This could further indicate limited consolidation and reduced mechanical stresses in the conical dryer. While the low shear environment may reduce breakage compared to AFDs, the resulting agglomerates are likely mechanically weaker and less likely to withstand continuous shear forces. This may explain the cyclic trend in d_{50} values over time during conical dryer experiments (Figure 6.13). However, additional scans with higher resolution would be required to make any definitive conclusions.

Using both SEM and micro-CT to assess their suitability for understanding agglomerate morphology has highlighted the strengths and limitations of each technique. SEM offers relatively quick analysis of surface features, but it is difficult to use for understanding the internal structure. In contrast, micro-CT enables non-destructive analysis of the internal structure but is very time consuming and constrained by voxel size and scan times. Although this analysis was based on a small data set, it demonstrates the potential for combining both SEM and micro-CT to obtain a comprehensive understanding of both the internal and external structure of agglomerates.

6.3.4 Predicted Growth Mechanism of Salicylic Acid

Information about the crystal structure of salicylic acid was obtained from the Cambridge Structural Database (CSD) and used to predict the dominant growth faces of salicylic acid. The calculations were kindly performed by Dr Helen Blade (Pharmaceutical Technology and Development, AstraZeneca, Macclesfield). These predictions were compared with SEM images to explore potential alignment between predicted and observed morphologies.

The Bravais-Friedel-Donnay-Harker (BFDH) model predicts crystal morphology based on the unit cell shape and symmetry. Using geometrical calculations, the BFDH model predicts the different growth surfaces of the crystal and the relative growth rates of each face. These calculations are based on the assumption that the crystal face growth rate is inversely proportional to the interplanar spacing.[164,165] This provides a rapid method to relate the crystal morphology to the underlying lattice structure. However, the BFDH model does not account for the surface chemistry or intermolecular interactions.

To address this limitation, full interaction maps (FIMs) can be used to estimate the likelihood of interactions occurring on crystal surfaces with a given probe, based on the surface chemistry. Using data from the CSD, the most likely locations for different functional groups can be predicted. This can be compared with a 3D packing diagram to assess if the crystal structure supports the preferential interactions of a given molecular conformation.[166]

In this case, a water probe was used to find the water affinity for the crystal faces of salicylic acid. Figure 6.22 illustrates the different crystal faces of salicylic acid, their corresponding Miller indices and water FIMs density. Miller indices (h, k, l) are used to describe the orientation of planes in a crystal lattice and are the reciprocals of the intercepts on the x, y and z axes.

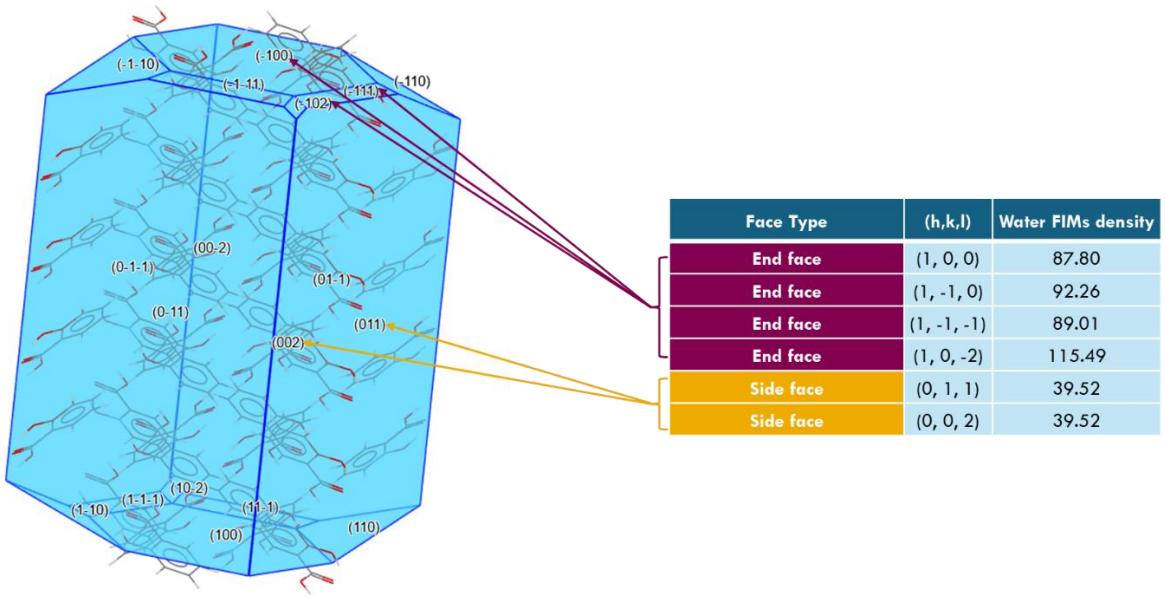

Face Type	(h,k,l)	Water FIMs density
End face	(1, 0, 0)	87.80
End face	(1, -1, 0)	92.26
End face	(1, -1, -1)	89.01
End face	(1, 0, -2)	115.49
Side face	(0, 1, 1)	39.52
Side face	(0, 0, 2)	39.52

Figure 6.22: Crystal morphology of salicylic acid with corresponding Miller indices and water FIMs density for the dominant crystal faces.

The water FIMs density data in Figure 6.22 indicates that the end faces (indicated in purple) have more than twice the affinity for water compared to side faces (indicated in yellow). This implies that end faces are more likely to form liquid bridges in these experiments, where water was used as the solvent.

This prediction was assessed by examining SEM images of agglomerates from both AFDs (GFD010 and FD80) and the conical dryer, as shown in Figure 6.23. Some examples of bridges forming across end faces are circled in blue. Side faces are also positioned together, but it is difficult to visualise if solid bridges formed between them using this technique. However, this work highlights the potential of combining crystal morphology predictions with surface interaction mapping to understand agglomeration at the particle level.

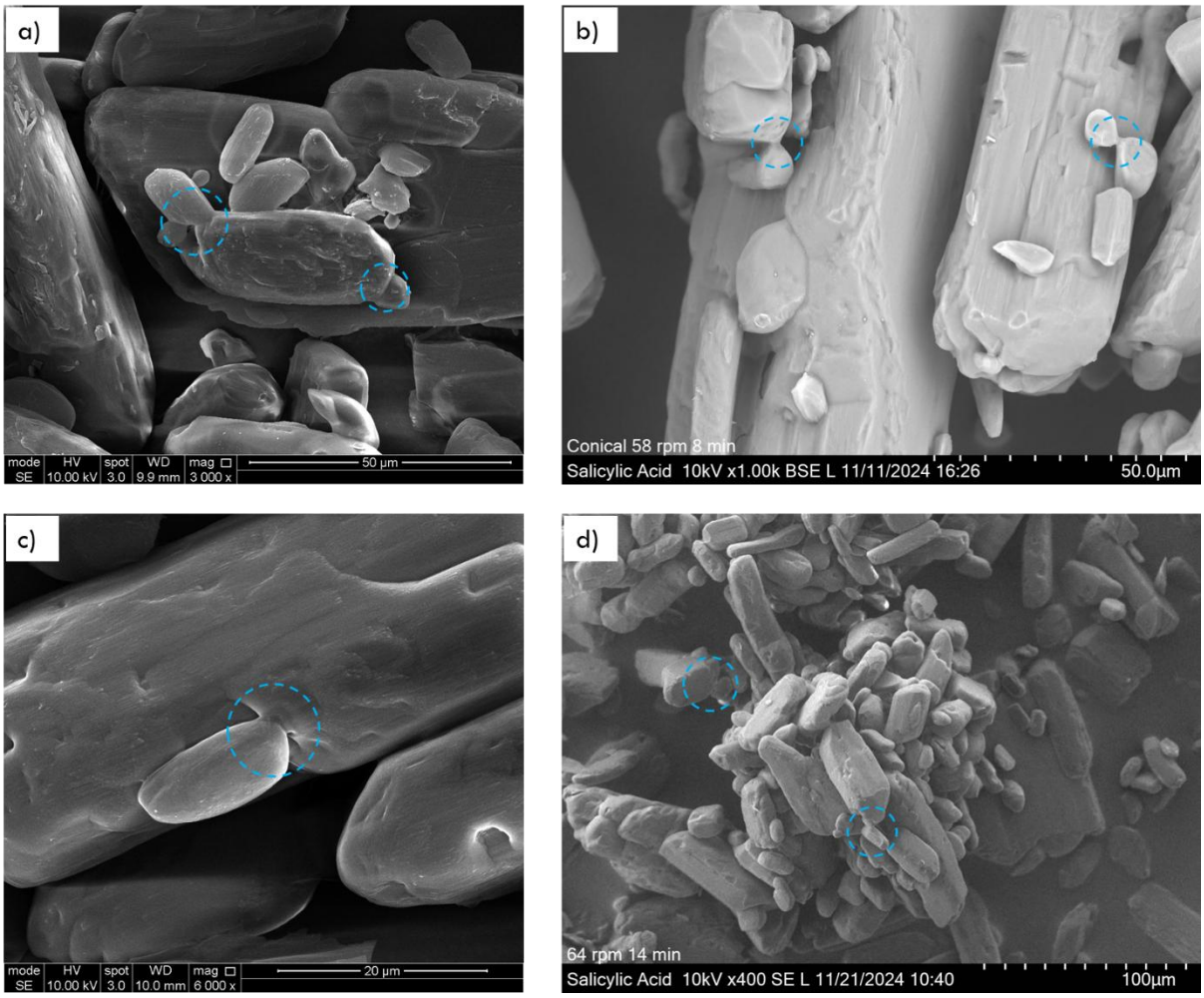

Figure 6.23: SEM images of agglomerates from experiments in the a) GFD010, b) conical dryer, c) GFD010, and d) FD80, with solid bridges circled in blue.

6.4 Conclusions

In this chapter, the scale up of agglomeration behaviour using constant tip speed was investigated in two types of agitated dryers: an AFD and a conical dryer. The contribution of the orbit arm to mixing performance within a conical dryer was also investigated.

In the large scale AFD, scaling up with constant tip speed while maintaining geometric similarity captured the overall trends in agglomeration behaviour qualitatively but not quantitatively. Although the trends were consistent across scales, the d values showed some deviation, particularly at longer agitation times. This was attributed to differences in shear forces acting on particles in the larger AFD.

Agglomeration behaviour in the conical dryer differed significantly from the lab scale AFD, which was expected given different mixing dynamics. The conical dryer generally resulted in a greater extent of agglomeration, likely due to more gentle mixing. However, these agglomerates were mechanically weaker and broke down with continued agitation, likely due to the lower shear forces. The influence of the orbit arm on mixing performance was also explored with select experiments, which indicated that both mixing screw and orbit arm speeds are crucial for uniform mixing. These findings highlight the potential for future work to optimise the speed ratio for improved mixing.

Overall, this work demonstrates the potential of using constant tip speed as a scaling index for agitated drying processes, while also emphasising the need to account for variations in shear forces and flow patterns. These factors significantly impact agglomeration behaviour, and predictive modelling could be a useful tool for simulating different vessels to identify changes in shear and flow patterns. The agglomerate morphology also seemed to differ between the AFD and conical dryer, which is particularly significant as it is not uncommon for changes in dryers during manufacturing. Such changes may impact drug product performance, highlighting the importance of morphology control.

The potential of SEM and micro-CT for understanding agglomerate morphology was explored through preliminary analysis. SEM provided relatively quick analysis of the external structure, while micro-CT offered valuable insights into the internal morphology of agglomerates. Micro-CT confirmed that agglomeration in the heel is driven by a different mechanism, likely compaction, as indicated by the lack of porosity in the samples analysed. Surface interactions using the BFDH model and FIMs have the potential to integrate crystal morphology predictions with imaging techniques to better understand agglomeration mechanisms.

Chapter 7 - Conclusions and Future Work

7.1 Conclusions

The overarching aim of this thesis was to develop a mechanistic understanding of the undesired agglomeration occurring in AFDs. This was achieved by systematically investigating the effect of key material and process parameters on agglomeration. Experimental data, in conjunction with findings from the literature, were used to identify the underlying rate processes driving agglomeration.

A novel mechanism was proposed consisting of three rate processes: the formation of loosely bound agglomerates, consolidation and coalescence, and the solidification of liquid bridges as drying progresses. The drying component was isolated to investigate the effect of agitation input alone on agglomeration. These experiments were used to refine the proposed mechanism and account for the snowballing growth behaviour observed.

Agitation speed and time were shown to significantly influence both the rate and extent of agglomeration. At the lowest speed (50 rpm), a transition from breakage dominated to agglomeration dominated behaviour occurred over time. This was likely due to fines generated from initial breakage of agglomerates driving subsequent agglomerate growth through the snowballing mechanism. At higher speeds (75 and 100 rpm), a dynamic equilibrium between the rate of agglomerate growth and breakage was observed throughout the agitation period. However, regardless of agitation speed, all systems reached a similar d_{50} value by the end of the agitation period. This suggests there is a critical agglomerate size and reinforces the fact that the same underlying mechanisms govern agglomeration, albeit at different rates.

Experimental results also confirmed that moisture content (MC) and fill level strongly influence agglomeration behaviour. The MC played a critical role, with distinct agglomerate growth behaviours observed at 0 %, 5 % and 20 % MC. Significant agglomeration, even at 5 % MC, suggests that the system has a low critical moisture content. The fill level also had a significant impact on the extent of agglomeration. Increased agglomeration was observed at higher fill levels, likely due to more frequent particle contacts and less disruption from the shearing action of the impeller. However, high agitation speeds may be able to offset the reduced mixing efficiency at higher fill levels.

Additional agglomerate growth behaviours were identified by modifying the primary particle size and using a coarser size fraction. Increasing the primary particle size rise resulted in a reduced extent of agglomeration compared to the smaller size fraction across the agitation period at both speeds investigated. These results highlight the reduced surface area available for liquid bridge formation in larger particles, which limits consolidation and coalescence.

Various characterisation techniques were assessed for their ability to distinguish between agglomerates formed under different conditions, primarily MC and primary particle size. Data from compression

testing and porosity approximations using image analysis were limited by the assumption of spherical agglomerates, and the results did not show statistically significant differences between conditions. Mixer torque rheometry (MTR), however, was used to generate torque profiles across a range of MCs using both primary particle size fractions. The torque measurements represent the resistance experienced by the mixing blades, which is analogous to the relative strength of systems at different MC and primary particle sizes.

A regime map was developed to categorise different agglomerate growth and breakage dynamics observed, where agglomerate growth is described as a function of the maximum pore saturation and Stokes deformation number. The Stokes deformation number was calculated using torque measurements instead of dynamic yield stress, and volume was incorporated to account for fill level. Despite the modified equation, the Stokes deformation number remained dimensionless and still represented the ratio of externally applied kinetic energy to the energy required for deformation. This is the first regime map of its kind for describing agglomerate growth behaviours in an AFD.

The use of constant tip speed as a scaling index was assessed when scaling agglomeration behaviour in both an AFD and a conical dryer. In the larger AFD, geometric similarity was maintained and scaling with tip speed reflected the agglomeration dynamics qualitatively but differed quantitatively, likely due to differences in the shear profile. The conical dryer experiments showed distinctly different agglomeration dynamics. This was expected given the significant differences in mixing dynamics in this vessel. The contribution of the orbit arm to mixing dynamics in the conical dryer was investigated through select experiments. The results highlighted that both the mixing arm and orbit arm speeds are crucial for achieving uniform mixing.

Overall, this work advances the current understanding of agglomeration in AFDs and proposes a new mechanism that can serve as a framework for guiding future studies and predictive modelling.

7.2 Future Work

The research in this thesis provides a foundation for several avenues of further investigation. The recommended areas for future work are provided below.

- The relationship between agitation input and the resulting agglomeration behaviour was investigated for a material system of salicylic acid and water. Further work using different solvents or solvent systems would provide insight into the effect of solvent properties on agglomeration dynamics.
- In this work, the drying component was isolated to develop a mechanistic understanding of how the agitation input influences agglomeration. Future work could include experiments conducted with simultaneous agitation and drying to study how changes in moisture content interact with agitation input to drive agglomerate growth or breakage.
- The regime map developed in this thesis could be further developed and the boundaries validated by extending it to other material systems, especially volatile solvents which are commonly used for pharmaceutical manufacturing. This would make the regime map more suitable for the prediction of agglomeration behaviour across a wider range of systems.
- The effect of the agitator clearance from the base of the vessel and the heel on the agglomeration behaviour was investigated in this work. Further work could look at the effect of both the bottom and wall clearances to understand how local shear zones influence the rates of agglomeration and breakage.
- The scale up studies in the larger AFD and conical dryer were limited by time constraints. Continuation of this work to explore how agglomeration dynamics vary with longer agitation periods would provide useful insight into agglomeration trends on a larger scale.
- The use of constant tip speed as a scaling index showed promising results. However, further work to ensure that the systems are still operating under the roping regime and adjusting the agitation speeds accordingly would provide valuable insight. Also, changing the agitation times to ensure the cumulative particle collision energy is preserved may help determine whether improved quantitative similarity can be achieved across scales.
- Computational models such as the discrete element method (DEM) could be used alongside experimental observations to further the mechanistic understanding of agglomeration. Using models such as DEM could also support scale up work by predicting the agglomeration behaviour when scaling up or changing the dryer geometry.

Chapter 8 - References

1 N. K. Nere, K. C. Allen, J. C. Marek and S. V. Bordawekar, *J. Pharm. Sci.*, 2012, **101**, 3886–3895.

2 S. Murugesan, P. K. Sharma and J. E. Tabora, in *Chemical Engineering in the Pharmaceutical Industry: R&D to Manufacturing*, John Wiley & Sons, Ltd, 2010, pp. 315–345.

3 H. L. Lim, K. P. Hapgood and B. Haig, *Powder Technol.*, 2016, **300**, 146–156.

4 E. K. Sahni, R. H. Bogner and B. Chaudhuri, *J. Pharm. Sci.*, 2013, **102**, 2198–2213.

5 T. Kudra and A. S. Mujumdar, in *Advanced Drying Technologies*, CRC Press, 2009, pp. 379–395.

6 A. Tamrakar, A. Gunadi, P. M. Piccione and R. Ramachandran, *Powder Technol.*, 2016, **303**, 109–123.

7 P. K. Sharma, S. Murugesan and J. E. Tabora, in *Chemical Engineering in the Pharmaceutical Industry*, John Wiley & Sons, Ltd, 2019, pp. 799–831.

8 *INTERNATIONAL COUNCIL FOR HARMONISATION OF TECHNICAL REQUIREMENTS FOR PHARMACEUTICALS FOR HUMAN USE IMPURITIES: GUIDELINE FOR RESIDUAL SOLVENTS Q3C(R8)*, 2021.

9 Mujumdar Arun, in *Handbook of Industrial Drying*, ed. A. Mujumdar, CRC Press, 3rd edn., 2006, pp. 14–16.

10 W. Li, PhD Thesis, The University of Leeds, 2014.

11 J. H. Harker, J. R. Backhurst and J. F. Richardson, in *Coulson and Richardson's Chemical Engineering Volume 2 - Particle Technology and Separation Processes*, Elsevier, 5th edn., 2002, vol. 2, pp. 901–913.

12 A. Bahadori, *Essentials of Oil and Gas Utilities*, 2016, 423–488.

13 B. A. Perlmutter, *Process Safety Progress*, 1999, **18**, 161–165.

14 A. Mujumdar, in *Handbook of Industrial Drying*, CRC Press, 2014, pp. 33–60.

15 R. P. Chhabra and J. F. Richardson, *Non-Newtonian Flow and Applied Rheology*, 2008, 376–461.

16 C. Slichter, *Field measurements of the rate of movement of underground waters*, 1905.

17 N. H. Ceaglske and O. A. Hougen, *Ind. Eng. Chem.*, 1937, **29**, 805–813.

18 P. S. H. Henry, *Proc. R. Soc. Lond. A Math. Phys. Sci.*, 1939, **171**, 215–241.

19 C. L. Law and A. Mujumdar, in *Handbook of Industrial Drying*, ed. A. Mujumdar, CRC Press, 3rd edn., 2006, pp. 174–178.

20 M. Guerrero, C. Albet, A. Palomer and A. Guglietta, *Food Science and Technology International*, 2003, **9**, 237–243.

21 S. Devahastin and A. Mujumdar, in *Handbook of Industrial Drying*, ed. A. Mujumdar, CRC Press, Florida, 3rd edn., 2006, pp. 137–148.

22 Agitators in Nutsche Filter / Dryers | De Dietrich Process Systems, https://www.dedietrich.com/en/agitators-nutsche-filter/dryers, (accessed 18 February 2022).

23 Guide to Selecting Filter Media for Nutsche Filter/Dryers, https://www.ddpsinc.com/blog/guide-to-selecting-filter-media-for-nutsche-filter/dryers, (accessed 18 February 2022).

24 D. B. Purchas and K. Sutherland, *Handbook of Filter Media*, 2002, 201–259.

25 L. Svarovsky, *Solid-Liquid Separation*, 2001, 335–348.

26 R. Wolthuis and V. C. Dichiaria, *Handbook of Downstream Processing*, 1997, 20–47.

27 L. Löbnitz, M. Böser and H. Nirschl, *Chemie Ingenieur Technik*, 2018, **90**, 464–471.

28 M. Murru, G. Giorgio, S. Montomoli, F. Ricard and F. Stepanek, *Chem. Eng. Sci.*, 2011, **66**, 5045–5054.

29 S. Huggins, A. Cosbie and J. Gaertner, *Chemical Engineering in the Pharmaceutical Industry*, 2019, 833–845.

30 A. Tamrakar, A. Zheng, P. M. Piccione and R. Ramachandran, *Advanced Powder Technology*, 2020, **31**, 477–492.

31 D. Am Ende, M. Birch, S. J. Brenek and M. T. Maloney, *Org. Process Res. Dev.*, 2013, **17**, 1345–1358.

32 W. Pietsch, in *Agglomeration Processes*, ed. W. Pietsch, John Wiley & Sons Ltd, 2001, pp. 29–132.

33 W. Pietsch, *Handbook of Powder Science & Technology*, 1997, 202–377.

34 S. M. Iveson, J. D. Litster, K. Hapgood and B. J. Ennis, *Powder Technol.*, 2001, **117**, 3–39.

35 S. M. Iveson, P. A. L. Wauters, S. Forrest, J. D. Litster, G. M. H. Meesters and B. Scarlett, *Powder Technol.*, 2001, **117**, 83–97.

36 T. Schæfer and C. Mathiesen, *Int. J. Pharm.*, 1996, **139**, 139–148.

37 S. M. Iveson and J. D. Litster, *AIChE Journal*, 1998, **44**, 1510–1518.

38 M. Butensky and D. Hyman, *Industrial and Engineering Chemistry Fundamentals*, 1971, **10**, 212–219.

39 K. V. S. Sastry and D. W. Fuerstenau, *Powder Technol.*, 1973, **7**, 97–105.

40 D. am Ende, M. Birch, S. J. Brenek and M. T. Maloney, *Org. Process Res. Dev.*, 2013, **17**, 1345–1358.

41 R. Wakeman, *Sep. Purif. Technol.*, 2007, **58**, 234–241.

42 B. A. Perlmutter, in *Solid-Liquid Filtration: Practical Guides in Chemical Engineering*, Elsevier, 2015, pp. 1–122.

43 D. Martynek, J. Němeček, L. Ridvan and M. Šoóš, *Powder Technol.*, 2022, **405**, 117522.

44 K. J. Hwang, Y. S. Wu and W. M. Lu, *Powder Technol.*, 1997, **91**, 105–113.

45 S. Ottoboni, M. Simurda, S. Wilson, A. Irvine, F. Ramsay and C. J. Price, *Powder Technol.*, 2020, **366**, 305–323.

46 D. Wieckhusen and W. Beckmann, *Crystallization: Basic Concepts and Industrial Applications*, 2013, 275–288.

47 J. F. Richardson, J. H. Harker and J. R. Backhurst, in *Chemical Engineering: Particle Technology and Separation Processes: Fifth Edition*, Elsevier Inc., 2013, vol. 2, pp. 372–436.

48 E. W. Conder, A. S. Cosbie, J. Gaertner, W. Hicks, S. Huggins, C. S. MacLeod, B. Remy, B. S. Yang, J. D. Engstrom, D. J. Lamberto and C. D. Papageorgiou, *Org. Process Res. Dev.*, 2017, **21**, 420–429.

49 M. Birch and I. Marziano, *Org. Process Res. Dev.*, 2013, **17**, 1359–1366.

50 M. Shahid, G. Sanxaridou, S. Ottoboni, L. Lue and C. Price, *Org. Process Res. Dev.*, 2021, **25**, 969–981.

51 M. Shahid, C. Faure, S. Ottoboni, L. Lue and C. Price, *Org. Process Res. Dev.*, 2022, **26**, 97–110.

52 B. Perlmutter, 2011.

53 E. W. Conder, A. S. Cosbie, J. Gaertner, W. Hicks, S. Huggins, C. S. MacLeod, B. Remy, B. S. Yang, J. D. Engstrom, D. J. Lamberto and C. D. Papageorgiou, *Org. Process Res. Dev.*, 2017, **21**, 420–429.

54 S. Zhang and D. J. Lamberto, *J. Pharm. Sci.*, 2014, **103**, 152–160.

55 Y. J. Shin, R. Ho, A. Y. Sheikh, P. Kumar, K. Sinha, N. K. Nere and L. Mlinar, *Ind. Eng. Chem. Res.*, 2019, **58**, 10394–10401.

56 L. Kotamarthy, S. Karkala, A. Dan, A. D. Román-Ospino and R. Ramachandran, *Pharmaceutics 2024, Vol. 16, Page 456*, 2024, **16**, 456.

57 A. Lekhal, K. P. Girard, M. A. Brown, S. Kiang, B. J. Glasser and J. G. Khinast, *Powder Technol.*, 2003, **132**, 119–130.

58 A. Herrera-Gómez, G. Velázquez-Cruz and M. O. Martín-Polo, *J. Appl. Phys.*, 2001, **89**, 5431–5437.

59 S. M. Iveson and J. D. Litster, *Powder Technol.*, 1998, **99**, 243–250.

60 C. D. Papageorgiou, M. Langston, F. Hicks, D. Am Ende, E. Martin, S. Rothstein, J. Salan and R. Muir, *Org. Process Res. Dev.*, 2016, **20**, 1500–1508.

61 K. Sinha, E. Murphy, P. Kumar, K. A. Springer, R. Ho and N. K. Nere, *AAPS PharmSciTech 2021 23:1*, 2021, **23**, 1–16.

62 T. Schæfer, *Powder Technol.*, 2001, **117**, 68–82.

63 A. Lekhal, K. P. Girard, M. A. Brown, S. Kiang, J. G. Khinast and B. J. Glasser, *Int. J. Pharm.*, 2004, **270**, 263–277.

64 W. P. Goh, K. Sinha, N. K. Nere, R. Ho, S. Bordawekar, A. Sheikh and M. Ghadiri, *Pharm. Res.*, 2022, **1**, 1–13.

65 I. Ohno, S. Hasegawa, S. Yada, A. Kusai, K. Moribe and K. Yamamoto, *Int. J. Pharm.*, 2007, **338**, 79–86.

66 O. Macho, Ľ. Gabrišová, A. Guštafík, K. Jezso, M. Juriga, J. Kabát and J. Blaško, *Pharmaceutics*, DOI:10.3390/PHARMACEUTICS15082148.

67 S. I. F. Badawy, M. M. Menning, M. A. Gorko and D. L. Gilbert, *Int. J. Pharm.*, 2000, **198**, 51–61.

68 I. C. Kemp and D. E. Oakley, *Drying Technology*, 2007, **20**, 1699–1750.

69 W. B. Pietsch, *Can. J. Chem. Eng.*, 1969, **47**, 403–409.

70 J. Adamson, N. Faiber, A. Gottlieb, L. Hamsmith, F. Hicks, C. Mitchell, B. Mittal, K. Mukai and C. D. Papageorgiou, *Org. Process Res. Dev.*, 2015, **20**, 51–58.

71 S. Lu and S. Song, *Colloids and Surfaces*, 1991, **57**, 49–60.

72 M. S. Kaliszewski and A. H. Heuer, *Journal of the American Ceramic Society*, 1990, **73**, 1504–1509.

73 Z. Q. Yu, R. B. H. Tan and P. S. Chow, *J. Cryst. Growth*, 2005, **279**, 477–488.

74 T. Schæfer, B. Taagegaard, L. J. Thomsen and H. Gjelstrup Kristensen, *European Journal of Pharmaceutical Sciences*, 1993, **1**, 125–131.

75 Y. Kawashima, S. Aoki and H. Takenaka, *Chem. Pharm. Bull. (Tokyo).*, 1982, **30**, 1900–1902.

76 M. Maghsoodi and Z. Yari, *Iran. J. Basic Med. Sci.*, 2014, **17**, 344.

77 F. De Leersnyder, V. Vanhoorne, H. Bekaert, J. Vercruysse, M. Ghijs, N. Bostijn, M. Verstraeten, P. Cappuyns, I. Van Assche, Y. Vander Heyden, E. Ziemons, J. P. Remon, I. Nopens, C. Vervaet and T. De Beer, *European Journal of Pharmaceutical Sciences*, 2018, **115**, 223–232.

78 M. Llusa, K. Sturm, O. Sudah, H. Stamato, D. J. Goldfarb, H. Ramachandruni, S. Hammond, M. R. Smith and F. J. Muzzio, *Ind. Eng. Chem. Res.*, 2009, **48**, 93–101.

79 E. U. Schlünder, *Chemical Engineering and Processing: Process Intensification*, 1984, **18**, 31–53.

80 E. Tsotsas and E. U. Schlünder, *Chemical Engineering and Processing: Process Intensification*, 1986, **20**, 277–285.

81 E. Tsotsas and E. U. Schlünder, *Chemical Engineering and Processing: Process Intensification*, 1987, **21**, 199–208.

82 E. U. Schlünder and N. Mollekopf, *Chemical Engineering and Processing*, DOI:10.1016/0255-2701(84)85012-6.

83 E. Tsotsas, M. Kwapinska and G. Saage, *Drying Technology*, 2007, **25**, 1377–1391.

84 S. Devahastin and A. Mujumdar, in *Handbook of Industrial Drying*, ed. A. Mujumdar, CRC Press, 3rd edn., 2006, pp. 144–148.

85 J. H. Yan, W. Y. Deng, X. D. Li, F. Wang, Y. Chi, S. Y. Lu and K. F. Cen, *Drying Technology*, 2009, **27**, 787–796.

86 E. Tsotsas and E. U. Schlunder, *Chem. Eng. Process.*, 1986, **20**, 339–349.

87 F. Heimann and E. U. Schlünder, *Chemical Engineering and Processing: Process Intensification*, 1988, **24**, 75–91.

88 S. Bin Yeom, E. Ha, M. Kim, S. H. Jeong, S. J. Hwang and D. H. Choi, *Pharmaceutics*, DOI:10.3390/PHARMACEUTICS11080414.

89 M. Marigo and E. H. Stitt, *KONA Powder and Particle Journal*, 2015, **32**, 236–252.

90 S. C. Thakur, J. Y. Ooi and H. Ahmadian, *Powder Technol.*, 2015, **293**, 130–137.

91 H. Chen, Y. G. Xiao, Y. L. Liu and Y. S. Shi, *Powder Technol.*, 2017, **318**, 507–517.

92 S. Lommen, D. Schott and G. Lodewijks, *Particuology*, 2014, **12**, 107–112.

93 M. Kwapinska, G. Saage and E. Tsotsas, *Powder Technol.*, 2008, **181**, 331–342.

94 B. Remy, B. J. Glasser and J. G. Khinast, *AIChE Journal*, 2010, **56**, 336–353.

95 S. Sarkar and B. Chaudhuri, *Asian J. Pharm. Sci.*, 2018, **13**, 220–228.

96 D. Barrasso and R. Ramachandran, *Chemical Engineering Research and Design*, 2015, **93**, 304–317.

97 R. M. Dhenge, K. Washino, J. J. Cartwright, M. J. Hounslow and A. D. Salman, *Powder Technol.*, 2013, **238**, 77–90.

98 M. Börner, M. Michaelis, E. Siegmann, C. Radeke and U. Schmidt, *Powder Technol.*, 2016, **295**, 261–271.

99 P. A. Cundall and O. D. L. Strack, *Geotechnique*, 1979, **29**, 47–65.

100 H. P. Zhu, Z. Y. Zhou, R. Y. Yang and A. B. Yu, *Chem. Eng. Sci.*, 2007, **62**, 3378–3396.

101 C. Hare, M. Ghadiri and R. Dennehy, *Chem. Eng. Sci.*, 2011, **66**, 4757–4770.

102 E. Sahni, J. Hallisey, B. Morgan, J. Strong and B. Chaudhuri, *Advanced Powder Technology*, 2012, **23**, 239–249.

103 E. K. Sahni and B. Chaudhuri, *Chem. Eng. Sci.*, 2013, **97**, 34–49.

104 P. Chaksmithanont, G. McEntee, C. Hartmanshenn, C. Leung, J. G. Khinast, C. D. Papageorgiou, C. Mitchell, J. L. Quon and B. J. Glasser, *Powder Technol.*, 2023, **422**, 118459.

105 C. S. Campbell, *J. Fluid Mech.*, 2002, **465**, 261–291.

106 B. Remy, J. G. Khinast and B. J. Glasser, *AIChE Journal*, 2009, **55**, 2035–2048.

107 B. J. Ennis, J. Li, T. Gabriel I. and P. Robert, *Chem. Eng. Sci.*, 1990, **45**, 3071–3088.

108 C. A. Radeke, B. J. Glasser and J. G. Khinast, *Chem. Eng. Sci.*, 2010, **65**, 6435–6442.

109 S. Ravjee, S. W. Jacobsz, D. N. Wilke and N. Govender, *Granul. Matter*, 2018, **20**, 1–14.

110 S. Watano, T. Morikawa and K. Miyanami, *Chem. Pharm. Bull. (Tokyo).*, 1996, **44**, 409–415.

111 T. Tanaka and N. Ouchiyama, *Industrial and Engineering Chemistry Process Design and Development*, 1974, **13**, 383–389.

112 H. Liu, T. O'Connor, S. Lee and S. Yoon, *Powder Technol.*, 2018, **327**, 188–200.

113 J. A. Gantt and E. P. Gatzke, *Powder Technol.*, 2005, **156**, 195–212.

114 D. Barrasso and R. Ramachandran, *J. Pharm. Innov.*, 2016, **11**, 231–249.

115 K. Hayashi, H. Nakamura and S. Watano, *Powder Technol.*, 2020, **360**, 1321–1336.

116 J. A. Gantt, I. T. Cameron, J. D. Litster and E. P. Gatzke, *Powder Technol.*, 2006, **170**, 53–63.

117 L. X. Liu and J. D. Litster, *Chem. Eng. Sci.*, 2002, **57**, 2183–2191.

118 S. A. L. de Koster, L. X. Liu, J. D. Litster and R. M. Smith, *Advanced Powder Technology*, 2021, **32**, 1390–1398.

119 Laser Diffraction Particle Size Analysis | Malvern Panalytical, https://www.malvernpanalytical.com/en/products/technology/light-scattering/laser-diffraction, (accessed 20 June 2022).

120 R. G. Holdich, *Fundamentals of Particle Technology*, 2002, 5–17.

121 H. G. Merkus, *Particle Size Measurements*, 2009, 13–42.

122 K. L. Dishman, *Encyclopedia of Analytical Chemistry*, DOI:10.1002/9780470027318.A1514.

123 T. Allen, in *Particle Size Measurement*, Springer, Boston, MA, 3rd edn., 1981, pp. 122–133.

124 M. J. O'Neil, *The Merck index: an encyclopedia of chemicals, drugs, and biologicals.*, Whitehouse Station, 14th edn., 2006.

125 Z. Q. Yu, R. B. H. Tan and P. S. Chow, *J. Cryst. Growth*, 2005, **279**, 477–488.

126 A. Shalmashi and A. Eliassi, *J. Chem. Eng. Data*, 2008, **53**, 199–200.

127 G. Madras and B. J. McCoy, *J. Cryst. Growth*, 2007, **305**, 211–217.

128 H. G. Kristensen, P. Holm and T. Schaefer, *Powder Technol.*, 1985, **44**, 227–237.

129 B. Gielen, J. Jordens, L. C. J. Thomassen, L. Braeken and T. Van Gerven, *Crystals 2017, Vol. 7, Page 40*, 2017, **7**, 40.

130 R. F. Nascimento, M. F. Ávila, A. G. P. da Silva, O. P. Taranto and L. E. Kurozawa, *Powder Technol.*, 2023, **420**, 118377.

131 C. E. Capes, *Powder Technol.*, 1972, **5**, 119–125.

132 M. Schröter, S. Ulrich, J. Kreft, J. B. Swift and H. L. Swinney, *Phys. Rev. E Stat. Nonlin. Soft Matter Phys.*, 2006, **74**, 011307.

133 J. B. Wade, G. P. Martin and D. F. Long, *Pharm. Dev. Technol.*, 2015, **20**, 257–265.

134 S. I. Farag Badawy and M. A. Hussain, *AAPS PharmSciTech 2004 5:3*, 2004, **5**, 16–22.

135 S. I. Farag Badawy, T. J. Lee and M. M. Menning, *AAPS PharmSciTech*, 2000, **1**, 7.

136 E. Atanaskova, N. Anevska Stojanovska and S. Ugarkovic, *Macedonian Pharmaceutical Bulletin*, 2020, **66**, 129–130.

137 T. Schæfer, D. Johnsen and A. Johansen, *European Journal of Pharmaceutical Sciences*, 2004, **21**, 525–531.

138 S. M. Iveson and J. D. Litster, *Powder Technol.*, 1998, **99**, 234–242.

139 W. F. Sakr, M. A. Ibrahim, F. K. Alanazi and A. A. Sakr, *Saudi Pharmaceutical Journal*, 2012, **20**, 9–19.

140 R. C. Rowe and G. R. Sadeghnejad, *Int. J. Pharm.*, 1987, **38**, 227–229.

141 M. Landín, R. C. Rowe and P. York, *J. Pharm. Sci.*, 1995, **84**, 557–560.

142 I. C. Kemp, *Drying Technology*, 2024, **42**, 2057–2069.

143 P. R. Mort and G. I. Tardos, *KONA Powder and Particle Journal*, 1999, **17**, 64–75.

144 N. Rahmanian, B. H. Ng, A. Hassanpour, Y. L. Ding, J. Antony, X. D. Jia, M. Ghadiri, P. G. J. van der Wel, A. Krug-Polman, D. York, A. Bayly and H. S. Tan, *Kona Powder and Particle Journal*, 2008, **26**, 190–204.

145 F. X. McConville and S. B. Kessler, in *Chemical Engineering in the Pharmaceutical Industry: R&D to Manufacturing*, ed. D. J. am Ende, John Wiley & Sons, Ltd, 2010, pp. 249–267.

146 Laboratory System BS-miniDRY® - HEINKEL Drying & Separation Group, https://www.heinkel.com/product/laboratory-system-bs-minidry/, (accessed 12 February 2025).

147 L. M. D. Cranswick, in *Principles and Applications of Powder Diffraction*, eds. A. Clearfield, J. H. Reibenspies and N. Bhuvanesh, John Wiley & Sons, Ltd, 2009, pp. 1–72.

148 R. S. H. Mansour, P. K. Deb and R. K. Tekade, *Dosage Form Design Parameters*, 2018, **2**, 105–154.

149 M. A. Elbagerma, H. G. M. Edwards, T. Munshi, M. D. Hargreaves, P. Matousek and I. J. Scowen, *Cryst. Growth Des.*, 2010, **10**, 2360–2371.

150 T. K. Bock and U. Kraas, *European Journal of Pharmaceutics and Biopharmaceutics*, 2001, **52**, 297–303.

151 S. Hibare and K. Acharya, *Powder Technol.*, 2014, **254**, 265–273.

152 J. Tao, P. Pandey, D. S. Bindra, J. Z. Gao and A. S. Narang, *J. Pharm. Sci.*, 2015, **104**, 2323–2333.

153 G. I. Tardos, K. P. Hapgood, O. O. Ipadeola and J. N. Michaels, *Powder Technol.*, 2004, **140**, 217–227.

154 R. Plank, B. Diehl, H. Grinstead and J. Zega, *Powder Technol.*, 2003, **134**, 223–234.

155 I. C. Kemp, *Drying Technology*, DOI:10.1080/07373937.2024.2364256.

156 J. D. Litster, K. P. Hapgood, J. N. Michaels, A. Sims, M. Roberts and S. K. Kameneni, *Powder Technol.*, 2002, **124**, 272–280.

157 H. Nakamura, H. Fujii and S. Watano, *Powder Technol.*, 2013, **236**, 149–156.

158 S. Kim, B. Lotz, M. Lindrud, K. Girard, T. Moore, K. Nagarajan, M. Alvarez, T. Lee, F. Nikfar, M. Davidovich, S. Srivastava and S. Kiang, *Org. Process Res. Dev.*, 2005, **9**, 894–901.

159 J. Gaertner, N. K. Nere, J. C. Marek, S. Bordawekar, L. Mlinar, M. Diwan and L. Cao, *Chemical Engineering in the Pharmaceutical Industry*, 2019, 848–853.

160 S. A. L. de Koster, K. Pitt, J. D. Litster and R. M. Smith, *Powder Technol.*, 2019, **355**, 514–525.

161 G. Morin and L. Briens, *AAPS PharmSciTech*, 2014, **15**, 1039–1048.

162 K. Flore, M. Schoenherr and H. Feise, *Powder Technol.*, 2009, **189**, 327–331.

163 J. Z. H. Gao, A. Jain, R. Motheram, D. B. Gray and M. A. Hussain, *Int. J. Pharm.*, 2002, **237**, 1–14.

164 J. Donnay and D. Harker, *American Mineralogist*, 1937, **22**, 446–467.

165 A. Bond, *Pharmaceutical Crystallography: A Guide to Structure and Analysis*, 2019, 68–81.

166 P. A. Wood, T. S. G. Olsson, J. C. Cole, S. J. Cottrell, N. Feeder, P. T. A. Galek, C. R. Groom and E. Pidcock, *CrystEngComm*, 2012, **15**, 65–72.